THE LARGE SCALE STRUCTURE IN TWO-DIMENSIONAL VORTICITY LAYERS AND THE CENTRE-TO-CENTRE POINT-VORTEX APPROXIMATION

by

Bernard A. Delcourt

Ingénieur Civil Physicien
(Université de Liège, Belgium)

A thesis presented to the Faculty
of Engineering of the University of Adelaide
for the Degree of Doctor of Philosophy

Department of Mechanical Engineering,
University of Adelaide.

April 1980.

TABLE OF CONTENTS

SUMMARY

The large-scale structure which emerges spontaneously from random periodic vorticity layers is studied by a novel discrete vortex element method.

The validity of the point-vortex approximation is examined in terms of its ability to represent the integral invariants of two-dimensional continuous vorticity distributions. The method is retained to study the large-scale motions in rotational flows where the exact behaviour of individual vortices is largely irrelevant ("cloud discretization" approach). A new, simple and computationally economical point-vortex tracing scheme is presented. The properties of the "centre-to-centre" method, which preserves notably the invariance of the energy of the vortex system, are established in reference to two exact test flows: the disk of uniform vorticity (Rankine's vortex) and the roll up of a vortex sheet (Westwater's problem).

With this understanding of the numerical procedure, the method is applied to the study of periodic vorticity layers. A vortex sheet is modelled by a "thick" line of 750 vortices repeated periodically to infinity to avoid boundary conditions. Layers with uniform and random circulation per unit length are considered; in both flow families, the finite thickness of the layer is obtained by a random lateral positioning of the vortices. Computed flows show in all cases the spontaneous emergence of large vortical structures and their subsequent amalgamation interactions. The relevance of these large-scale, strictly two-dimensional unsteady motions as a model of the coherent structure in the turbulent mixing layer is discussed. Uniform layers are found to exhibit a strong similitude (growth rates,

similarity characteristics of the structure) with laboratory flows; the behaviour of random layers is reminiscent of that of externally forced mixing layers. The model establishes the importance of the initial conditions in determining the flow behaviour over very large times. The sensitivity of the structures to molecular and "turbular" diffusion (i.e. that which arises from a secondary small-scale motion acting as an enhanced viscosity) is investigated and appears to be remarkably weak. Low Reynolds number layers are found to grow by viscous diffusion and not by interactions between vorticity structures.

The point-vortex model is extended to the general case of non circulation-preserving motions. The effects of (large) density ratios upon the large-scale structure are investigated for a simple flow geometry (i.e. for a sinusoidal vorticity layer). The computations, based on an original discretized form of Bjerknes theorem, fully demonstrate the distortion of the structure in non-uniform incompressible layers. The response of the layer to the action of gravity (Froude number effects) is briefly illustrated by some additional examples.

To the best of the candidate's knowledge and belief, this thesis contains no material which has been accepted for the award of any degree or diploma in any University, and contains no material previously published or written by another person, except where due reference is made in the text.

B.A.G. Delcourt.

ACKNOWLEDGMENTS

Il m'est extrêmement agréable, alors que je termine la rédaction de cette thèse, de pouvoir remercier ici toutes les personnes qui, de près ou de loin, m'ont permis de mener à bien ce travail.

Je tiens tout spécialement à remercier M. le Professeur G.L. Brown pour les heures consacrées à de nombreuses discussions, souvent passionnantes et toujours amicales, et pour les conseils et encouragements qu'il m'a constamment prodigués au cours de ces dernières années ; qu'il trouve ici l'expression de ma gratitude et de ma sincère admiration.

Je suis particulièrement reconnaissant à M. le Professeur R.E. Luxton de m'avoir permis d'entreprendre ce doctorat sous sa supervision, dans une atmosphère de travail à la fois stimulante et agréable.

Par ailleurs, je remercie M. le Professeur R. Narasimha de son hospitalité lors d'un court séjour à l'Institut Indien des Sciences et de l'intérêt qu'il a porté à cette thèse.

Je remercierai finalement M. C.J. Abell pour son aide et ses suggestions dans la correction d'une première version de ce mémoire.

Ce travail n'a pu être réalisé que grâce au support financier de l'Université d'Adelaide (URG Scholarship).

GENERAL INTRODUCTION

The properties and effects of the large-scale organized motions observed in various turbulent shear flows have recently attracted a great deal of interest in fundamental fluid mechanics research. The existence of identifiable large structures, the interactions of which appear to control much of the development of the flow, suggests a refreshed attitude toward turbulence problems. A new point of view is currently emerging, which favors a quasi-deterministic description of real turbulence, and suggests that knowledge of the properties of the organized motions is a prerequisite to the understanding of the complex physical processes (growth, transport, entrainment, mixing, noise generation, etc...) in turbulent flows (Roshko, 1976; Kovasznay, 1977).

There is increasingly convincing evidence that characteristic organized structures exist in turbulent flows as diverse as jets (Moore, 1977), wakes (Papailiou & Lykoudis, 1974) and boundary layers (Laufer, 1975). It is in plane turbulent mixing layers, however, that the visual identification of a large-scale structure has been the most striking (Brown & Roshko, 1971; 1974). The mixing layer structure appears as a train of "breaking waves" or "rollers" which develop from the Kelvin-Helmholtz instability of the free shear layer that separates from the splitter plate; it is essentially two-dimensional (Browand, 1978; Wygnanski et al, 1978).

That the coherent structure plays a central role in the mechanics of the mixing layer is now firmly established (Brown & Roshko, 1974; Bernal et al, 1979; Dimotakis & Brown, 1976). In particular, the response to external forcing (Oster et al, 1978), the sensitivity to initial conditions

(Batt, 1975), the role of feedback (Dimotakis & Brown, 1976), the strong effect of density ratio on entrainment (Brown, 1974) in mixing layers, and more general acoustic coupling and resonances in other turbulent flows appear all explicable in terms of the large structure and its dynamics. Salient features of these structures are their very weak sensitivity to viscous action and their marked two-dimensional nature; in this respect, their response to three-dimensional disturbances remains poorly understood (Roshko, 1976).

There is therefore a strong suggestion that many features of turbulent mixing layers arise from the properties of a rotational, essentially two-dimensional inviscid flow. It is interesting to compare these features with those computed in a model which follows, by a strictly two-dimensional calculation, the development of the large-scale motion associated with an initial distribution of vorticity. The present work is primarily concerned with the development of such a model and its application to several flows in the general context of their possible relevance to the turbulent mixing layer.

In all these problems, there is no pretension that an unsteady, two-dimensional calculation could do more than shed light on the dynamics of the mixing layer large-scale structure. One of the distinctive properties of turbulent flows is their ability, under suitable conditions, in increasing their total vorticity contents by extension of their vortex lines. This mechanism of vortex-stretching is characteristic of three-dimensional kinematics and has no equivalent in two dimensions. A second intrinsic characteristic of real turbulence is the existence, at the smallest scales of motion, of a viscous dissipation which operates at a rate independent of viscosity (as $\nu \to 0$). In two-dimensional models, the dissipation rate

vanishes as the Reynolds number tends to infinity, and the turbulent dissipation of energy is grossly underestimated (Saffman, 1977). Although clearly not modelling turbulence, two-dimensional calculations appear nevertheless useful to appreciate the importance of physical mechanisms in real flows.

Problems that relate to two-dimensional rotational motions of an inviscid fluid are conveniently tackled by the method of discrete vortex elements. This method has been applied, with various degrees of success, to a wide range of problems (Clements & Maull, 1975). Simplicity, flexibility and ability in providing direct visualizations of the vorticity field appeared as immediate advantages of point-vortex calculations. Indiscriminate use of the point-vortex approximation, which suffers from some drawbacks (Baker & Saffman, 1979), was avoided by applying it in an original form. An important part of this work is consequently dedicated to the presentation of a novel point-vortex tracing scheme and a full discussion of its properties. The new algorithm is shown to be well suited for economically computing the evolution of clouds of vortices. The proposed numerical procedure, which provides an accurate description of the large scales of the motion, is confidently applied to the study of various hydrodynamical problems.

The material presented in this thesis is distributed in four chapters which are organized as follows.

Various aspects of the mathematical foundations of the point-vortex approximation are presented in the first chapter. The concept of vortex filament leads naturally, in the study of vorticity kinematics, to the notion of point-vortex; the velocity field associated with a point-vortex is easily derived from the law of Biot-Savart (Section I.2). The existence of kinematical invariants of two-dimensional vorticity fields has been

valuable in developing an accurate vortex-tracing scheme; these invariants are examined in Section I.3. Most equations of interest in point-vortex computations are elegantly derived with the formalism of complex variables; they are summarized in Section I.4 for convenient reference.

The bulk of the second chapter is allocated to the presentation of a new point-vortex tracing scheme, the centre-to-centre (CTC) method. The reasons that led to the development of the CTC tracing scheme are exposed in Section II.2, which details the salient features of the point-vortex approximation. Arguments that advocate the suitability of the approximation for depicting the large-scale behaviour of the rotational region are given in Section II.3. The CTC algorithm is then presented (Section II.4) and its properties established in the rest of the chapter on the basis of three known reference problems: the motion of a disk of uniform vorticity (Section II.5), the viscous decay of a vorticity disk (Section II.6) and the rolling up of a vortex sheet (Section II.7).

The core of the third chapter is the general study of the large-scale motions of two-dimensional, uniform-density vorticity layers. Various CTC computations are described and their results discussed with in mind, their possible relevance as a model of the turbulent mixing layer, the essential features of which are recalled in Section III.2. The model follows the temporal evolution of periodic vorticity layers. The relationship between flows which grow in time and those which spread in space, the type of initial conditions used and the choice of parameter values for accurate CTC calculations are considered in Section III.3; this section closes on an ultimate accuracy check of the numerical procedure by applying it to Acton's flow, the thick sinusoidal vortex sheet (Acton, 1976). All results pertaining to inviscid layers are collected in Section III.4. Flow visualizations are presented which show the spontaneous emergence of a

large-scale structure from an initially random layer of point-vortices (§ III.4.1); the analysis of the growth histories of the layers reveals interesting features and suggests strong similitudes between computed and experimental flows (§ III.4.2); the coherence and the similarity properties of the structures are investigated in terms of the autocorrelation functions of the fluctuating velocity field (§ III.4.3). The possibility of including viscous effects exists in point-vortex models; it relies on the simulation of diffusion by the addition of a Gaussian random walk to the hydrodynamic motion of the vortices (Milinazzo & Saffman, 1977). Section III.5 explores the response of the large structure to molecular and "turbular" diffusion effects (i.e. one which arises from a secondary small-scale motion that acts like an enhanced viscosity). An example of the evolution of a very low Reynolds number layer is also presented.

Chapter four is essentially concerned with the extension of the point-vortex approximation to non circulation-preserving flows, in connection with the modelling of mixing layers between fluids of different densities. The circulation around a material contour convected by the flow may be modified in the presence of density gradients; the mechanism responsible for these changes is analyzed in Section IV.2. It is shown in Section IV.3 that the point-vortex approximation may be generalized to non circulation-preserving flows of an incompressible fluid; a novel technique is presented which allows to compute the rate of change of the strength of point-vortices that belong to a cloud. The generalized point-vortex method is then applied to the study of large density ratios on the large-scale structure of a thick sinusoidal vorticity layer (Section IV.4); the correspondence between temporal and spatial problems is reexamined in some detail. Mention is made of the effects of Froude number on the development of the structure.

CHAPTER I : INTRODUCING THE THEORY OF POINT-VORTICES

CHAPTER I

INTRODUCING THE THEORY OF POINT VORTICES

I.1 INTRODUCTION

This chapter summarizes the basic ideas that constitute the theoretical foundation of the point-vortex approximation employed in this thesis to compute (two-dimensional) free rotational flows at large Reynolds numbers.

The notion of a point-vortex arises naturally in the study of two-dimensional, rotational flow fields of an incompressible fluid. Section I.2 sketches the logical connection between such flows and the "generalized law of Biot-Savart", which governs the kinematics of three-dimensional vorticity distributions. The derivation given here presents illustrative arguments that should not be regarded as a substitute for a complete mathematical treatment such as may be found in Batchelor (1967) and various other texts.

The existence of integral invariants is an important feature of two-dimensional vorticity distributions in flow fields extending to infinity; this property is equally shared by analogous point-vortex systems. The expression and significance of these (five) kinematical invariants are examined in section I.3, for both the continuous and the discrete cases. Further aspects of these invariance properties are outlined in Appendix A.

The theory of point-vortices is elegantly cast using the formalism of complex variables. This approach clarifies the mathematical nature of point-vortices, which are in this context introduced as

allowable singularities in an otherwise analytic velocity field. A number of results pertaining to the complex theory of point-vortices are given in section I.4 to provide the convenience of a succinct mathematical summary of all equations fundamental to the point-vortex computation method. This section is essentially inspired from Friedrichs (1966).

I.2 ROTATIONAL FLOW FIELDS OF INCOMPRESSIBLE FLUIDS

An important result in the analysis of rotational motions of a uniform, incompressible fluid is the "generalized Biot-Savart law"

$$\underset{\sim}{u}_{\omega}(P) = \underset{\sim}{u}_{BC}(P) - \frac{1}{4\pi}\int_V \frac{[\underset{\sim}{e}_{QP}(Q) \times \underset{\sim}{e}_{\omega}(Q)]}{R_{PQ}^2}\,\underset{\sim}{\omega}(Q)\,dV(Q) \qquad [1.1]$$

which gives the velocity field $\underset{\sim}{u}_{\omega}(P)$ at any point P in the fluid associated with a vorticy distribution $\underset{\sim}{\omega} = \underset{\sim}{\nabla} \times \underset{\sim}{u}_{\omega}$ specified over part - or the whole - of the domain V occupied by the fluid. The notation $\underset{\sim}{e}$ is used to indicate unit vectors, i.e.

$$\underset{\sim}{e}_{\omega} = \frac{\underset{\sim}{\omega}}{|\underset{\sim}{\omega}|} \quad ; \quad \underset{\sim}{e}_{QP} = \frac{\underset{\sim}{r}(P) - \underset{\sim}{r}(Q)}{R_{PQ}}$$

with $$R_{PQ} = |\underset{\sim}{r}(P) - \underset{\sim}{r}(Q)|$$

The vector field $\underset{\sim}{u}_{BC}$ is simultaneously irrotational and solenoidal and is chosen so that the conditions imposed on the flow at the boundaries are satisfied by the resultant velocity field $\underset{\sim}{u}_{\omega}$. The assumption is made that the flow field extends to infinity.

In flow fields without interior boundaries - of particular interest in this work - expression [1.1] reduces to

$$\underset{\sim}{u}_{\omega}(P) = -\frac{1}{4\pi}\int_{V}\frac{[\underset{\sim}{e}_{QP}(Q)\times\underset{\sim}{e}_{\omega}(Q)]}{R_{PQ}^{2}}\,\underset{\sim}{\omega}(Q)\,dV(Q) \qquad [1.2]$$

The velocity at any point P in the fluid appears as the superposition of contributions from volume elements $\delta V(Q)$, each amounting to

$$\delta\underset{\sim}{u}_{\omega}(P) = \frac{1}{4\pi R_{PQ}^{2}}\,\omega(Q)\;\delta V(Q)\;(\underset{\sim}{e}_{\omega}\times\underset{\sim}{e}_{QP}) \qquad [1.3]$$

as illustrated in Figure 1. The magnitude of this contribution is usually written as

$$\delta u_{\omega}(P) = \frac{\omega(Q)\;\delta V(Q)}{4\pi R_{PQ}^{2}}\sin\chi \qquad [1.4]$$

where χ is the angle between the unit direction vectors $\underset{\sim}{e}_{\omega}(Q)$ and $\underset{\sim}{e}_{QP}(Q)$.

The vector lines of $\underset{\sim}{\omega}$ that pass through a closed contour ℓ drawn in the fluid define a vortex-tube. It is readily shown, using Stokes theorem, that the flux of vorticity through a cross-section of the tube has a value independent of the location of the section along the tube; the characteristic quantity

$$\kappa = \int_{A}\underset{\sim}{\omega}\cdot d\underset{\sim}{A} = \int_{\ell}\underset{\sim}{u}\cdot d\underset{\sim}{s} \qquad [1.5]$$

defines accordingly the strength (circulation) of the vortex tube. It

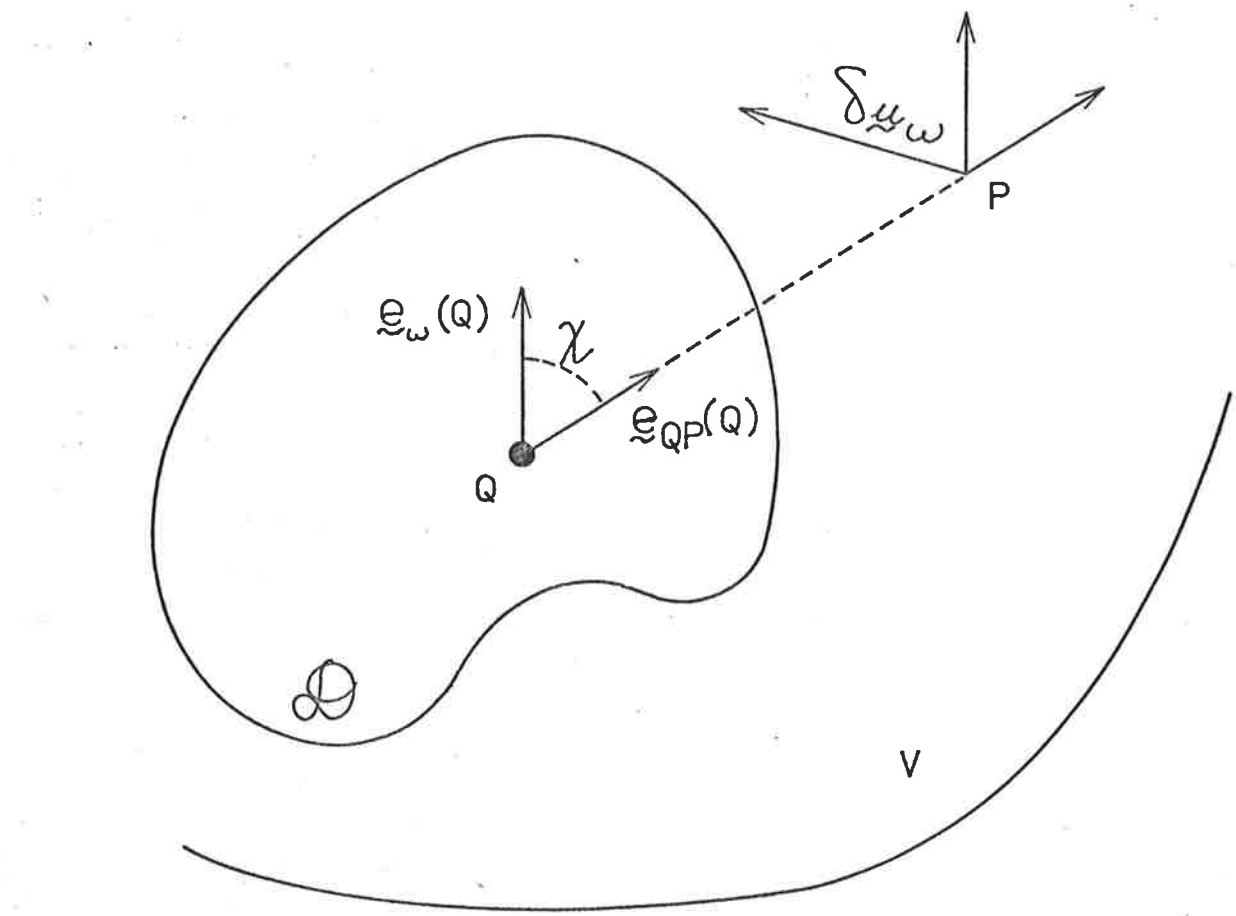

Figure 1. Geometry and notations for the BIOT-SAVART law.

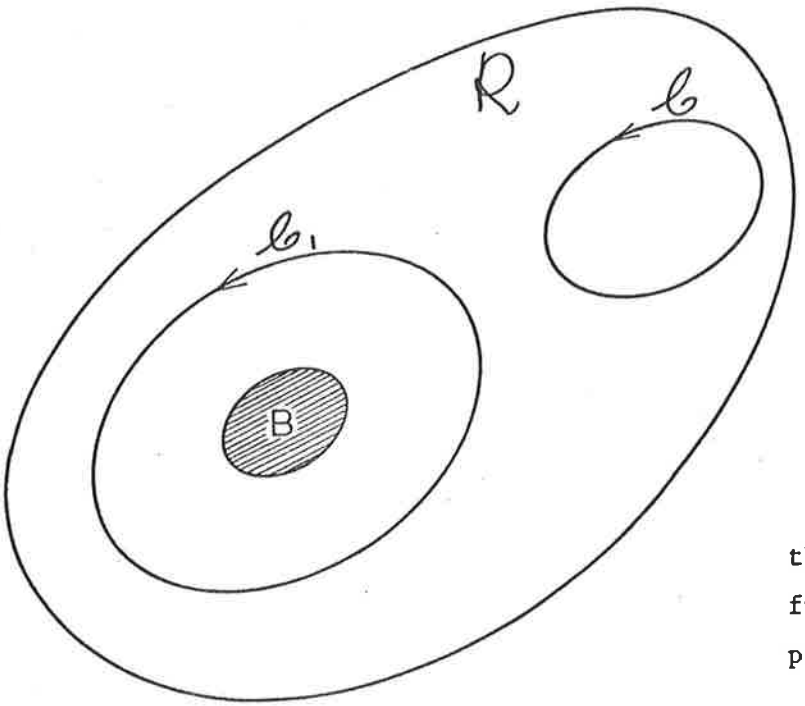

Figure 2. Cauchy's theorem for analytic functions: integration paths.

is clear that the cross-section of a tube cannot contract to zero without the vorticity becoming infinite; vortex-tubes must therefore form finite closed loops, end or begin on boundaries, or extend to infinity.

A vortex-filament of strength κ is a vortex-tube of infinitesimal cross section; it may be visualized as a set of contiguous cylindrical vorticity elements, of length δL and section σ with

$$\underset{\sim}{\omega}\ (Q)\quad \delta V\ (Q) = \omega\ (Q)\ \sigma\ (Q)\ \delta \underset{\sim}{L}\ (Q)$$
$$= \kappa\ \delta \underset{\sim}{L}\ (Q) \qquad [1.6]$$

aligned along a given curve L drawn in the fluid. The velocity field "induced" by a vortex-filament is given by equation

$$\underset{\sim}{u}_{\kappa}\ (P) = \frac{\kappa}{4\pi} \int_{L} \frac{d\underset{\sim}{L}(Q) \times \underset{\sim}{e}_{QP}\ (Q)}{R_{PQ}^{2}} \qquad [1.7]$$

which is a particular form of [1.2].

Two-dimensional flow fields correspond to configurations where all vortex-tubes are parallel cylinders extending to infinity; the plane of flow is clearly normal to the direction of their generating lines.

Denoting δA the element of area in the plane of flow, and δz the element of length normal to that plane, one transforms [1.2] by writing

$$\delta V\ (Q) = \delta A\ (Q)\ \delta z\quad (Q)$$

and carrying out the integration with respect to the variable z.
The velocity components are now given by the expressions

$$u(P) = -\frac{1}{2\pi} \int_A \frac{[y(P) - y(Q)]}{R_{PQ}^2} \omega(Q)\, dA(Q)$$

and

$$v(P) = \frac{1}{2\pi} \int_A \frac{[x(P) - x(Q)]}{R_{PQ}^2} \omega(Q)\, dA(Q) \,. \qquad [1.8]$$

The velocity field is known to be solenoidal and hence is derivable from a stream function which has the form

$$\psi(P) = \frac{-1}{4\pi} \int_A \omega(Q) \log R_{PQ}^2\, dA(Q) \qquad [1.9]$$

in view of [1.8].

The two-dimensional velocity field induced by an infinite, rectilinear vortex-filament is obtained from [1.7] :

$$u(P) = -\frac{\kappa}{2\pi} \frac{[y(P) - y(Q)]}{R_{PQ}^2}$$

$$v(P) = \frac{\kappa}{2\pi} \frac{[x(P) - x(Q)]}{R_{PQ}^2} \,. \qquad [1.10]$$

The point Q represents the trace of the filament in the plane of analysis, and represents a point-vortex of strength κ. The corresponding stream function is

$$\psi(P) = -\frac{\kappa}{4\pi} \log R_{PQ}^2 \,. \qquad [1.11]$$

The above results may be obtained if a slightly different point of view is adopted. The point-vortex approximation (PVA) generates a discretized form of equations [1.8] , [1.9] according to the following procedure. The vortical area A is broken up into a number NV of small elements δA that satisfy the requirement.

$$A = \sum_{\alpha}^{NV} \delta A\ (Q_\alpha) \ ,$$

Q_α being the "centre" of element "α". The assumption that each element $\delta A\ (Q_\alpha)$ contracts into a point-vortex of strength

$$\kappa\ (Q_\alpha) = \int_{\delta A} \omega\ (Q_\alpha)\ \delta A(Q_\alpha) = \kappa_\alpha \qquad [1.12]$$

leads to the fundamental formulae

$$\psi\ (P) = -\frac{1}{4\pi} \sum_{\alpha}^{NV} \kappa_\alpha \log R_{P\alpha}^2 \qquad [1.13]$$

$$u\ (P) = -\frac{1}{2\pi} \sum_{\alpha}^{NV} [y\ (P) - y_\alpha] / R_{P\alpha}^2$$

$$v\ (P) = +\frac{1}{2\pi} \sum_{\alpha}^{NV} [x\ (P) - x_\alpha] / R_{P\alpha}^2 \ , \qquad [1.14]$$

with $Q_\alpha = (x_\alpha, y_\alpha)$

and $R_{P\alpha}^2 = [x\ (P) - x_\alpha]^2 + [y\ (P) - y_\alpha]^2 .$

It is interesting to point out that the vorticity concept, which is central to the theory of *incompressible* fluid motion, is complemented by the notion of expansion in the general case of *compressible* fluid motion.

The "Cauchy-Stokes decomposition theorem" asserts that "an arbitrary instantaneous state of motion may be resolved at each point into a uniform translation, a dilatation along three mutually orthogonal axes and a rigid rotation of these axes" (Truesdell, 1954). This theorem shows clearly that the vorticity $\underset{\sim}{\omega} = \underset{\sim}{\nabla} \times \underset{\sim}{u}$ - representative of the fluid rotation - and the expansion $\theta = \underset{\sim}{\nabla} \cdot \underset{\sim}{u}$ - giving the fractional rate of change in the volume of a material element - appear naturally as dual variables in the analysis of the kinematics of continuous media.

The essential significance of the distributions of vorticity and expansion may be otherwise appreciated by considering the Stokes potentials of the velocity field. It is a well-known result of vector analysis that any vector field $\underset{\sim}{c}$, enjoying suitable differentiability properties, may be globally represented as the sum of an irrotational field and a solenoidal field

$$\underset{\sim}{c} = \underset{\sim}{\nabla}\,\Phi + \underset{\sim}{\nabla} \times \underset{\sim}{A} \ .$$

The scalar function Φ and the vector field $\underset{\sim}{A}$ - known as the Stokes potentials of the field $\underset{\sim}{c}$ - are not uniquely determined: the addition of a harmonic function ϕ to the scalar potential Φ and that of a gradient term $\underset{\sim}{\nabla} a$ to the vector potential A leave the above representation unaltered. One possible pair of potentials is given by the expressions

$$\Phi = -\frac{1}{4\pi} \int_V \frac{(\underset{\sim}{\nabla} \cdot \underset{\sim}{c})}{r}\, dV \quad ; \quad A = \frac{1}{4\pi} \int_V \frac{(\underset{\sim}{\nabla} \times \underset{\sim}{c})}{r}\, dV \ .$$

The double indetermination can be raised by selecting a so that $\underset{\sim}{A}$ is solenoidal, whilst choosing ϕ so that boundary conditions imposed on $\underset{\sim}{c}$ are satisfied.

One can therefore broadly assert that in general, the velocity field may be represented under the form

$$4\pi\, \underset{\sim}{u}\,(P) = -\,\underset{\sim}{\nabla} \int_V \frac{\theta(Q)\,dV(Q)}{R_{PQ}} + \underset{\sim}{\nabla} \times \int_V \frac{\underset{\sim}{\omega}(Q)\,dV(Q)}{R_{PQ}}$$

(of which [1.1] is a particular example).

Vortices and sources are singularities of the vorticity field and expansion field respectively; any (instantaneous) motion may be induced by an unstable configuration of sources and vortices. The source-vortex analogy breaks down however when dynamical considerations are included in the analysis: vortices are essentially Lagrangian in character, while sources are an Eulerian feature of the flow. The difficulties met in

attempts to generalize the point-vortex approximation to include compressibility effects stem essentially from this distinguishing property, which leads to complex evolution equations for the coupled vorticity and expansion distributions.

I.3 INTEGRAL INVARIANTS OF TWO-DIMENSIONAL VORTICITY DISTRIBUTIONS

All results presented in Section I.1 are essentially kinematical in nature: they refer to instantaneous configurations of the velocity field and apply at any given instant, irrespective of the dynamical aspects of the flow. Dynamical considerations are, however, necessary to establish that the temporal evolution of (two-dimensional) vorticity distributions takes place in a manner which conserves several integral quantities. These invariants and their physical significance are examined below.

Kelvin's circulation theorem asserts that the circulation $\Gamma = \oint_L \underset{\sim}{u} \cdot d\underset{\sim}{L}$ round a material line in an inviscid, incompressible fluid of uniform density is invariant:

$$\dot{\Gamma} = \frac{d\Gamma}{dt} = 0 \ , \qquad [1.15]$$

provided the body force is derivable from a single-valued potential.

A direct consequence of this theorem for the case of a two-dimensional vorticity distribution extending over a bounded region A is that the total circulation

$$\Gamma = \oint_L \underset{\sim}{u} \cdot d\underset{\sim}{L} = \int_A \omega \, dA \qquad [1.16]$$

around a closed contour fully containing A is invariant. This invariance

condition is locally expressed as

$$\frac{d}{dt}(\omega \delta A) = 0 \qquad [1.17]$$

for a material element of area δA.

Consider now the time rate of change of the expression

$$M_y = \int_A x\, \omega\, dA \qquad [1.18]$$

which is the first moment of the vorticity distribution with respect to the y axis.

One computes

$$\dot{M}_y = \int_A \frac{d}{dt}(x\, dA) = \int_A \dot{x}\, (\omega dA) + \int_A x \frac{d}{dt}(\omega dA)$$

$$= \int_A u(P)\, \omega(P) dA(P) \text{ in view of } [1.17].$$

Introducing the expression of u (P) from equation [1.8] one obtains

$$\dot{M}_y = -\frac{1}{2\pi} \int_A dA(P) \int_A \frac{\omega(Q)\omega(P)y(P) - \omega(P)\omega(Q)y(Q)}{R_{PQ}^2} dA(Q)$$

an expression which vanishes identically. The quantity M_y is therefore an invariant of the motion; it is obvious that the moment

$$M_x = \int_A y\, \omega\, dA \qquad [1.19]$$

is also invariant.

The position of the centre of vorticity of the distribution is defined in terms of Γ, M_x and M_y by the relations

$$X = \frac{M_y}{\Gamma} = \frac{\int_A x\,\omega\,dA}{\int_A \omega\,dA}$$

$$Y = \frac{M_x}{\Gamma} = \frac{\int_A y\,\omega\,dA}{\int_A \omega\,dA} \qquad [1.20]$$

provided that Γ differs from zero. One can also consider that the vorticity centre is situated at infinity when the total circulation vanishes.

It is easy to show that the rate of change of the quantity

$$J = \int_A (x^2 + y^2)\,\omega\,dA \qquad [1.21]$$

is zero. Indeed, one has, using [1.17],

$$\dot{J} = \int_A 2(xu + yv)\,dA$$

and substitution of the explicit expressions of u(P) and v(P) (equations [1.8]) into the above identity yields

$$\dot{J} = \frac{1}{\pi} \iint_A \omega(P)\omega(Q)[x(P)y(Q) - y(P)x(Q)]\,dA(P)\,dA(Q)\ ,$$

and finally $\dot{J} = 0$.

The invariant quantity J is identified with the "moment of inertia" of

the vorticity distribution. It is convenient to introduce a "radius of gyration" (or "dispersion length") I by the relationship

$$I^2 = \frac{\int_A [(x-X)^2+(y-Y)^2]\,\omega\, dA}{\int_A \omega dA} \qquad [1.22]$$

i.e. $$I^2 = \frac{J}{\Gamma} - (X^2+Y^2).$$

The integral giving the kinetic energy of the fluid occupying the whole plane is not finite. It is however possible to derive an invariant associated with the kinetic energy by examining the manner in which the energy integral over a bounded region Ω diverges when letting Ω tend to infinity. Consider the kinetic energy of the fluid (*) within the region Ω, taken as a circle of large radius R totally covering the vorticity domain A:

$$T = \tfrac{1}{2} \int_\Omega (u^2+v^2)\, d\Omega \quad .$$

One transforms T as follows with the use of Stokes theorem:

$$T = \tfrac{1}{2} \int_\Omega \left(u\frac{\partial\psi}{\partial y} - v\frac{\partial\psi}{\partial X}\right) d\Omega$$

$$= \tfrac{1}{2} \int_A \psi\omega\, dA - \tfrac{1}{2} \int_\Omega \left[\frac{\partial}{\partial X}(v\psi) - \frac{\partial}{\partial y}(u\psi) \right] d\Omega$$

$$= \tfrac{1}{2} \int_A \psi\omega\, dA - \tfrac{1}{2} \oint_{\partial\Omega} \psi\, \underset{\sim}{u}.\underset{\sim}{ds} \quad , \qquad [1.23]$$

(*) Assuming unit density for simplicity, i.e. using the kinematical description.

where $\partial\Omega$ is the circumference of radius R limiting the region Ω. Letting R tend to infinity, one computes the contribution from the line integral as

$$\oint \psi \, \underset{\sim}{u}.d\underset{\sim}{s} = \int_0^{2\pi} \psi(R) u_\theta \, R d\theta$$

$$= \oint_0^{2\pi} \frac{\Gamma}{2\pi} \log\left(\frac{1}{R}\right) \frac{\Gamma}{2\pi R} \, R d\theta$$

$$= \frac{\Gamma^2}{2\pi} \log\left(\frac{1}{R}\right) \qquad (R \to \infty).$$

The asymptotic form of expression [1.23] for $R \to \infty$ may be written

$$T + \frac{\Gamma^2}{4\pi} \log\left(\frac{1}{R}\right) = \tfrac{1}{2} \int_A \psi\omega \, dA \, . \qquad [1.24]$$

The kinetic energy of the fluid is conserved in the absence of dissipation; the left hand side of [1.24] is therefore independent of time, a property which establishes the invariance of the quantity

$$H = \tfrac{1}{2} \int_A \psi\omega \, dA \, . \qquad [1.25]$$

An alternative expression for H - called the Hamiltonian of the vorticity distribution, for reasons exposed in section I.4 - is obtained by substitution of equation [1.9] into equation [1.25], yielding

$$H = -\frac{1}{8\pi} \int_A \int_A \omega(P)\omega(Q) \log R_{PQ}^2 \, dA(P) dA(Q) \, . \; (*) \qquad [1.26]$$

(*) H is also called the "Kirchhoff function" of the system of vortices; both names will be used in this work.

There are several ways of establishing the expressions for the invariant quantities associated with the motion of a collection of isolated point-vortices. Inspection of the definition integrals for Γ, X, Y and I^2 suggests, in view of relation [1.12], that the discrete counterparts of expressions [1.16], [1.20] and [1.22] are respectively

$$\Gamma = \sum_{\alpha}^{NV} \kappa_\alpha \qquad [1.27]$$

$$X = \sum_{\alpha}^{NV} \kappa_\alpha x_\alpha / \Gamma \qquad [1.28]$$

$$Y = \sum_{\alpha}^{NV} \kappa_\alpha y_\alpha / \Gamma$$

$$\Gamma I^2 = \sum_{\alpha}^{NV} \kappa_\alpha [(x_\alpha - X)^2 + (y_\alpha - Y)^2] \; . \qquad [1.29]$$

The expression for the discrete Hamiltonian must be determined somewhat more carefully due to the singular character of the kinetic energy of a point-vortex. It is necessary to consider, as for the continuous case, the kinetic energy T of the fluid within a circle of large radius R, and outside small circles of radius ε centered on each point-vortex. One shows that the following relationship holds asymptotically as $R \to \infty$ and $\varepsilon \to 0$:

$$T + \frac{1}{4\pi} \left(\sum_{\alpha}^{NV} \kappa_\alpha^2 \right) \log \varepsilon - \frac{1}{4\pi} \left(\sum_{\alpha}^{NV} \kappa_\alpha \right)^2 \log R$$

$$\to - \frac{1}{4\pi} \sum_{\alpha} \sum_{\beta \neq \alpha} \kappa_\alpha \kappa_\beta \log R_{\alpha\beta} \qquad [1.30]$$

This identity, analogous to equation [1.24], establishes on similar

arguments the invariance property of

$$H = -\frac{1}{4\pi} \sum_{\alpha} \sum_{\beta \neq \alpha} \kappa_\alpha \kappa_\beta \log R_{\alpha\beta} \qquad [1.31]$$

($R_{\alpha\beta}$ represents the distance between vortex "α" and vortex "β").
Table 1 summarizes the expressions for the five invariants for continuous vorticity distributions and systems of point-vortices.

A more rigorous derivation of the invariance of expressions [1.27] to [1.31] is presented in paragraph I.4.5, based on some fundamental properties of the Hamiltonian of systems of point-vortices. Another aspect of the invariance properties of continuous distributions of vorticity is proposed in Appendix A, which examines them in the Fourier transform space.

I.4 COMPLEX THEORY OF POINT VORTICES

I.4.1 The concept of the point vortex

Consider the two-dimensional motion of an incompressible fluid, having an everywhere irrotational velocity field, except possibly on certain lines or at certain points where singularities, the character of which is to be specified, are allowed. The velocity field $\underset{\sim}{u} = (u,v)$ can be described simultaneously in terms of a stream function ψ - effectively the only non-zero component of a potential vector $\underset{\sim}{\psi}$ - and a velocity potential ϕ, according to the relations

$$\underset{\sim}{u} = \underset{\sim}{\nabla} \times \underset{\sim}{\psi} = \underset{\sim}{\nabla} \times (0,0,\psi)$$

$$\underset{\sim}{u} = \underset{\sim}{\nabla}\phi \qquad [1.32]$$

TABLE 1: Invariants of two-dimensional vorticity fields.

CONTINUOUS DISTRIBUTIONS		POINT VORTEX DISTRIBUTIONS
	CIRCULATION (Γ)	
$\Gamma = \int_A \omega dA$		$\Gamma = \sum_\alpha \kappa_\alpha$
	VORTICITY CENTRE (X,Y)	
$X = \frac{1}{\Gamma} \int_A \omega x \, dA$		$X = \frac{1}{\Gamma} \sum_\alpha \kappa_\alpha x_\alpha$
$Y = \frac{1}{\Gamma} \int_A \omega y \, dA$		$Y = \frac{1}{\Gamma} \sum_\alpha \kappa_\alpha y_\alpha$
	RADIUS OF GYRATION (I)	
$I^2 = \frac{1}{\Gamma} \int_A [(x-X)^2+(y-Y)^2] \omega dA$		$I^2 = \frac{1}{\Gamma} \sum_\alpha [(x_\alpha-X)^2+(y_\alpha-Y)^2] \kappa_\alpha$
	HAMILTONIAN (H)	
$H = -\frac{1}{8\pi} \int_A \int_A \omega_P \omega_Q \log R_{PQ}^2 \, dA_P dA_Q$		$H = -\frac{1}{2\pi} \sum_{\alpha>\beta} \kappa_\alpha \kappa_\beta \log R_{\alpha\beta}$

The scalar functions ϕ and ψ are related by equations of the Cauchy-Riemann type:

$$\frac{\partial \psi}{\partial y} = \frac{\partial \phi}{\partial x} \quad ; \quad \frac{\partial \psi}{\partial x} = - \frac{\partial \phi}{\partial y} \quad , \qquad [1.33]$$

allowing the analysis to be pursued in terms of the analytic function

$$\chi(z) = \phi + i\psi \qquad [1.34]$$

of the complex variable $z = x + iy$; $\chi(z)$ is the complex potential of the flow. The complex velocity field

$$w(z) = u + iv \qquad [1.35]$$

is obtained by differentiating $\chi(z)$ with respect to its argument:

$$\chi'(z) = u - iv = \frac{\partial \phi}{\partial x} + i \frac{\partial \psi}{\partial x} = w^*(z) \qquad [1.36]$$

(starred quantities represent complex conjugates). Cauchy's theorem for analytic functions states that

$$\oint_C f(z)dz = 0$$

for any function $f(z)$ analytic in a domain $\mathcal{R}$ and any simple closed contour C completely within $\mathcal{R}$. The complex velocity $w(z)$ is clearly not analytic in a domain $\mathcal{R}$ that contains bodies (see Figure 2). The complex circulation

$$Z = \oint_C w^*(z)dz \qquad [1.37]$$

around any closed curve encircling a body does not vanish and one has generally

$$Z = \oint_C w^*(z)dz = \kappa + i\Lambda \ ,$$

where

$$\kappa = \oint_C (udx + vdy) = \oint_C d\phi$$

and

$$\Lambda = \oint_C (udy - vdx) = \oint_C d\psi \ .$$

The complex circulation reduces to its real part if no sources (sinks) are present within the region limited by the contour C; it will be assumed hereafter that this condition is realized (i.e. $\Lambda = 0$).

Suppose now that the cross-section of the body is made to shrink to an infinitesimally small circle, all other flow conditions remaining unaltered. The body becomes a punctual singularity of the flow field, such that

$$Z = \oint_C w^*(z)dz = \kappa \qquad [1.38]$$

for any closed contour drawn around it: the singularity defined by this limit process is a point-vortex of strength κ. Any velocity field of the form

$$w^*(z) = \frac{\kappa}{2i\pi(z-\zeta)} + w_R^*(z) \qquad [1.39]$$

(κ real)

where $w_R^*(z)$ is analytic at $z = \zeta$, comprises a point-vortex of strength κ at $z = \zeta$, as shown by a direct application of the residue theorem when evaluating the corresponding circulation around a curve enclosing the point $z = \zeta$. The complex potential associated with [1.39] has the form

$$\chi(z) = \frac{\kappa}{2i\pi} \log(z-\zeta) + \chi_R(z) \ , \qquad [1.40]$$

where $\chi_R(z)$ is regular at $z = \zeta$.

The point-vortex has been introduced as the trace in the plane of analysis of a thin, infinite, straight cylindrical body; it can also be visualized as the trace of a thin, infinite straight cylinder of rotating fluid. In the former case, the filament is capable of sustaining the force exerted by the surrounding fluid, and one speaks of a *bound vortex*; in the latter case, the filament cannot sustain this force, and behaves as a *free vortex*. Point-vortices are usually understood to represent free vortices.

I.4.2 The motion of point-vortices

The condition that a point-vortex cannot sustain any force (exerted on it by the surrounding fluid) leads directly to the determination of its equation of motion. The force experienced by a body immersed in an inviscid fluid of negligible weight is known to be

$$\underset{\sim}{F} = \oint_C [\, q^2 \underset{\sim}{n} - 2\underset{\sim}{u}(\underset{\sim}{u}.\underset{\sim}{n})]\, ds$$

where $\underset{\sim}{n}$ is the outward normal to the contour enclosing the body, and $q = (\underset{\sim}{u}.\underset{\sim}{u})^{\frac{1}{2}}$ is the velocity magnitude. This result (a two-dimensional form of one of Blasius' theorems) is recast in terms of complex quantities as

$$F_x + i\, F_y = \oint_C w^2\, dz^* \qquad [1.41]$$

(cf. Lamb, 1932, art. 726). Using expression [1.39] for the velocity field, one rewrites [1.41] as

$$F_x - i\, F_y = \frac{\kappa}{2\pi} \oint_C \frac{w_R^*}{(z-\zeta)}\, dz$$

since the only contribution arises from the cross-product term. Cauchy's integral formula yields immediately

$$F_x + i\, F_y = - i \kappa\, w_R(\zeta), \qquad [1.42]$$

which represents the force on a point-vortex at rest at $z = \zeta$, in a fluid moving with a velocity $w(z)$.

The formula remains valid in a frame of reference attached to the moving vortex, if the relative flow velocity is adequately introduced. Calling $\dot{\zeta}$ the vortex velocity, one obtains

$$F_x + i\, F_y = - i\, \kappa[w_R(\zeta) - \dot{\zeta}].$$

A free vortex, by definition unable to sustain any force, must necessarily move according to the differential equation

$$\dot{\zeta} = w_R(\zeta) \qquad [1.43]$$

which is the law of motion required. It is remarkable to note that vortex motion obeys a first-order differential equation.

I.4.3 The isolated cloud of point-vortices

Consider the situation where NV point-vortices are present in a fluid filling the whole plane and at rest at infinity. The flow field is completely determined by specifying the locations ζ_α and the strengths κ_α of all vortices ($\alpha = 1,2,\ldots,NV$). The complex potential describing the cloud of vortices is obtained by adding elementary potentials of the form [1.40], leading to

$$\chi(z) = \frac{1}{2i\pi} \sum_\beta \kappa_\beta \log(z-\zeta_\beta) \qquad [1.44]$$

(the upper summation limit NV and the time dependence $\zeta_\beta(t)$ being implied).

The corresponding velocity field is clearly

$$w^*(z) = \frac{1}{2i\pi} \sum_\beta \kappa_\beta/(z-\zeta_\beta) \ . \qquad [1.45]$$

The equation of motion of vortex α ($\alpha = 1,2,\ldots,NV$) is readily obtained by extracting the regular part of [1.45] at $z = \zeta_\alpha$; according to [1.43] one has therefore

$$\dot{\zeta}_\alpha = w_R(\zeta_\alpha) = \frac{1}{2\pi i} \sum_{\beta(\alpha)} \kappa_\beta/(\zeta^*_\alpha - \zeta^*_\beta) \ . \qquad [1.46]$$

The notation $\sum_{(\alpha)}$ will be used to indicate a sum over all elements of the cloud, excepting element α that must be omitted.

The equation of motion for vortex α can be rewritten in terms of real variables in the form

$$\begin{aligned} \dot{x}_\alpha &= -\frac{1}{2\pi} \sum_{(\alpha)} \kappa_\beta \, Y_{\alpha\beta}/R^2_{\alpha\beta} \\ \dot{y}_\alpha &= \frac{1}{2\pi} \sum_{(\alpha)} \kappa_\beta \, X_{\alpha\beta}/R^2_{\alpha\beta} \end{aligned} \qquad [1.47]$$

with

$$\begin{aligned} \zeta_\alpha &= x_\alpha + i\, y_\alpha \\ X_\alpha &= x_\alpha - x_\beta \\ Y_{\alpha\beta} &= y_\alpha - y_\beta \end{aligned} \qquad [1.48]$$

and $$R^2_{\alpha\beta} = X^2_{\alpha\beta} + Y^2_{\alpha\beta} \ .$$

I.4.4 The periodic cloud of point-vortices

Consider now the particular spatial arrangement where equistrength point-vortices are aligned along the $\dot{x}$-axis at the positions $x_n = \pm na$ ($n = 0,1,2,...$) (a real). The complex potential for this row of point-vortices is given by the expression

$$\chi(z) = \frac{\kappa}{2i\pi} \{\log z + \log(z-a) + \log(z+a) + \log(z-2a) + \log(z+2a)...\}$$

$$= \frac{\kappa}{2i\pi} \log \{z + \prod_{n=1}^{\infty} (z^2-n^2a^2)\}$$

$$= \frac{i\kappa}{2\pi} \log \sin \frac{\pi z}{a} \quad . \qquad [1.49]$$

The point vortex corresponding to $n = 0$ is the representative element of the row; it is convenient to say that a "row-vortex" of strength κ and period a is located at $z = \zeta$ whenever the complex potential takes the form

$$\chi(z) = \frac{i\kappa}{2\pi} \log \sin \frac{\pi}{a} (z-\zeta) \quad . \qquad [1.50]$$

Direct differentiation leads to the expression for the velocity field

$$w^*(z) = \frac{i\kappa}{2a} \operatorname{cotg} \frac{\pi}{a} (z-\zeta) \quad , \qquad [1.51]$$

which is singular at $z = \zeta$. It is clear that a row-vortex does not move in its own induced velocity field.

Far from the row, the velocity field is found to behave as

$$\lim_{y\to\pm\infty} u = \mp \frac{\kappa}{2a} = \pm u_\infty$$

$$\lim_{y\to\pm\infty} v = 0. \qquad [1.52]$$

The flow associated with a *cloud* of NV row-vortices located at $\zeta_\beta = (x_\beta, y_\beta)$ $(\beta = 1,2,\ldots,NV)$ is described by the complex potential

$$\chi(z) = \frac{i}{2\pi} \sum_\beta \kappa_\beta \log \sin \frac{\pi}{a} (z-\zeta_\beta) \ . \qquad [1.53]$$

The velocity field induced by the vortices at any regular point of the plane is given by

$$w^*(z) = \frac{i}{2a} \sum_\beta \kappa_\beta \operatorname{cotg} \frac{\pi}{a} (z-\zeta_\beta) \ . \qquad [1.54]$$

Far away from the vortices, one has

$$\begin{aligned} &\lim_{y\to\pm\infty} u = \mp \frac{1}{2a} \sum_\beta \kappa_\beta = \mp \frac{\Gamma}{2a} = \pm u_\infty \\ &\lim_{y\to\pm\infty} v = 0 \ . \end{aligned} \qquad [1.55]$$

The velocity of row-vortex α corresponds to the regular part of expression [1.54] at the vortex location $z = \zeta_\alpha = (x_\alpha, y_\alpha)$. Reverting to real variables, the equations of motion of vortex α are written:

$$\begin{aligned} \dot{x}_\alpha &= \frac{1}{2a} \sum_{(\alpha)} \kappa_\beta \sinh\left(\frac{2\pi}{a} Y_{\alpha\beta}\right)/D_{\alpha\beta} \\ \dot{y}_\alpha &= -\frac{1}{2a} \sum_{(\alpha)} \kappa_\beta \sin\left(\frac{2\pi}{a} X_{\alpha\beta}\right)/D_{\alpha\beta} \end{aligned} \qquad [1.56]$$

with

$$D_{\alpha\beta} = D_{\beta\alpha} = \cosh\left(\frac{2\pi}{a} Y_{\alpha\beta}\right) - \cos\left(\frac{2\pi}{a} X_{\alpha\beta}\right) . \qquad [1.57]$$

I.4.5 Hamiltonian formulation

The motion of a cloud of NV point-vortices is governed by a set of 2 NV differential equations of the first order (see equations [1.47]).

Consider the function $H = H(\zeta_\alpha, \zeta_\alpha^*)$ given by the expression

$$H = \frac{1}{2\pi} \sum_{\alpha>\beta} \kappa_\alpha \kappa_\beta \log (\zeta_\alpha - \zeta_\beta)(\zeta_\alpha^* - \zeta_\beta^*) \qquad [1.58]$$

where $\sum_{\alpha>\beta}$ denotes a double summation, over all pairs (α,β), each pair being taken once only and the pair $\alpha = \beta$ being excluded $\left(\sum_{\alpha>\beta} = \frac{1}{2} \sum_{\alpha} \sum_{\beta(\alpha)} \right)$.

Kirchhoff noted that the equations of motion [1.47] can be concisely written in terms of H under the form

$$\kappa_\alpha \dot{\zeta}_\alpha^* = -2i \frac{\partial H}{\partial \zeta_\alpha} \quad . \qquad [1.59]$$

This equation is readily expressed in terms of real variables; recalling that

$$x_\alpha = \tfrac{1}{2}(\zeta_\alpha + \zeta_\alpha^*) \qquad y_\alpha = \frac{1}{2i} (\zeta_\alpha - \zeta_\alpha^*) \ ,$$

one obtains the equivalent differential system

$$\kappa_\alpha \dot{x}_\alpha = -\frac{\partial H}{\partial y_\alpha} \quad ; \quad \kappa_\alpha \dot{y}_\alpha = +\frac{\partial H}{\partial x_\alpha} \quad . \qquad [1.60]$$

The form of these equations is identical to that of the canonical equations of motion in the theory of Hamiltonian mechanics. The quantities $x_\alpha \sqrt{\kappa_\alpha}$ and $y_\alpha \sqrt{\kappa_\alpha}$ can be identified respectively as the generalized coordinates and momenta of the system of vortices. The Kirchhoff function H is the Hamiltonian of the system and is defined by expression [1.58] for the case of the isolated cloud of point-vortices. It is easily shown that the Hamiltonian for a cloud of row-vortices is defined by the equivalent expressions

$$H = \tfrac{1}{2} \sum_{\alpha>\beta} \kappa_\alpha \kappa_\beta \log\left[\sin \frac{\pi}{a} (\zeta_\alpha - \zeta_\beta) \sin \frac{\pi}{a} (\zeta_\alpha^* - \zeta_\beta^*)\right]$$

$$= \tfrac{1}{2} \sum_{\alpha>\beta} \kappa_\alpha \kappa_\beta \log\left[\sin^2 X_{\alpha\beta} + \sinh^2 Y_{\alpha\beta}\right]$$

$$= -\tfrac{1}{2} \sum_{\alpha>\beta} \kappa_\alpha \kappa_\beta \log \frac{D_{\alpha\beta}}{2} , \qquad [1.61]$$

with $D_{\alpha\beta}$ defined by [1.57].

An important question, which arises naturally in the context of Hamiltonian mechanics, concerns the existence of invariants associated with the motion of the vortices. The existence of the Hamiltonian makes the invariance analysis particularly simple.

The Hamiltonian itself may be regarded as the basic invariant of the system; indeed, one computes

$$\dot{H} = \frac{d}{dt} H(x_\alpha, y_\alpha) = \sum_\alpha \left(\frac{\partial H}{\partial x_\alpha} \dot{x}_\alpha + \frac{\partial H}{\partial y_\alpha} \dot{y}_\alpha \right)$$

$$= \sum_\alpha \left[\dot{x}_\alpha \kappa_\alpha y_\alpha + \dot{y}_\alpha (-\kappa_\alpha x_\alpha) \right] = 0$$

using the equations of motion [1.60], so that

$$H(x_\alpha, y_\alpha) = \text{CONSTANT} = H_0 . \qquad [1.62]$$

The Hamiltonian is completely determined by the relative positions of the vortices - for a given distribution of strengths. Its value remains unaltered for any arbitrary translation of rotation of the coordinate axes; the relationships

$$H(\zeta_\alpha, \zeta_\alpha^*) = H(\zeta_\alpha + \xi, \zeta_\alpha^* + \xi^*)$$

$$H(\zeta_\alpha, \zeta_\alpha^*) = H(\zeta_\alpha e^{i\theta}, \zeta_\alpha^* e^{-i\theta})$$

hold for arbitrary values of the constants $\xi = \alpha + i\beta$ and θ.

These identities are equivalent to the three conditions

$$\left.\frac{\partial H}{\partial \alpha}\right|_{\xi=0} = 0 \quad ; \quad \left.\frac{\partial H}{\partial \beta}\right|_{\xi=0} = 0 \quad ; \quad \left.\frac{\partial H}{\partial \theta}\right|_{\theta=0} = 0 \quad ,$$

alternatively expressed as

$$\sum_\alpha \frac{\partial H}{\partial x_\alpha} = 0 \quad ; \quad \sum_\alpha \frac{\partial H}{\partial y_\alpha} = 0 \quad ; \quad \sum_\alpha \left(\zeta_\alpha \frac{\partial H}{\partial \zeta_\alpha} - \zeta_\alpha^* \frac{\partial H}{\partial \zeta_\alpha^*}\right) = 0$$

Consideration of the equations of motion [1.59] or [1.60] discloses immediately the invariance property of the quantities

$$M = \sum_\alpha \kappa_\alpha \zeta_\alpha \qquad [1.63]$$

and

$$\Gamma J^2 = \sum_\alpha \kappa_\alpha \zeta_\alpha \zeta_\alpha^* \, . \qquad [1.64]$$

The invariants H, M and J^2 may be considered respectively as the energy, the moment of mass and the moment of inertia of the system of vortices. Another invariant quantity is obviously the total strength of the cloud,

$$\Gamma = \sum_\alpha \kappa_\alpha \qquad [1.65]$$

It is clear that the real quantities X,Y and J^2 introduced through the relationships

$$X = \mathcal{R}e[M/\Gamma] \qquad [1.66]$$

$$Y = Im[M/\Gamma] \qquad [1.67]$$

$$\Gamma I^2 = J - \Gamma|M|^2 \qquad [1.68]$$

are those previously defined in Section I.3 (Equations [1.28] , [1.29]).

I.5 SUMMARY

Chapter I is intended as an "aide-mémoire" that covers succinctly several aspects of point-vortex theory. It emphasizes the kinematical significance of point-vortices, outlines the important invariance properties of two-dimensional vorticity distributions and enumerates most of the equations that are needed in the point-vortex approximation method.

Applications of the method of point-vortices are considered in the following chapters.

CHAPTER II: THE CENTRE-TO-CENTRE POINT VORTEX APPROXIMATION

CHAPTER II

THE CENTRE TO CENTRE POINT-VORTEX APPROXIMATION

II.1 INTRODUCTION

The purpose of this chapter is to introduce the computation method developed for the numerical studies of two-dimensional, rotational flows presented in this thesis. The method is an original implementation of the point-vortex approximation detailed in Chapter I.

The properties of the proposed vortex-tracing algorithm are carefully examined by comparing computed flows with two simple, exact reference flows. Rankine's combined vortex (the disk of uniform vorticity) is first considered in order to determine the limitations and accuracy of the method used here and the nature of the "viscous" effects inherent in the computation procedure. The rolling-up of an elliptically loaded vortex sheet (Westwater's problem) is then investigated to further assess the capabilities of the method, and to vindicate its use when information about large-scale aspects of the flow is sought.

Throughout this chapter, attention is focused on the behaviour of the invariants that characterize the motion of a two-dimensional inviscid vorticity field. It is found that the invariants - in particular the Hamiltonian or Kirchhoff function - can be used to monitor the accuracy of the computation; this is in contrast with most applications of the point-vortex approximation reported in the literature, in which various arbitrary numerical restraints have been applied without assessment of their effects on the invariants of the motion and on the consequent accuracy.

It is argued that the method is therefore capable of providing

adequate "statistical" information about two-dimensional, rotational inviscid flows - which is proposed to be relevant to high Reynolds number, free turbulent flows - in terms of quantitative estimates of parameters associated with the large scale motions.

The bearing of the present results on some implementations of the point-vortex approximation reported in the literature is briefly discussed. It is felt that the information obtained here gives additional insight into the somewhat controversial point-vortex method, whilst suggesting a new attitude towards further developments of the technique.

II.2 THE POINT-VORTEX APPROXIMATION

II.2.1 Outline of the method

Two-dimensional motions of inviscid, incompressible and homogeneous fluids are governed, when analysed in terms of the vorticity field $\omega(x,y,t)$, by the non-linear equations

$$\nabla^2\psi = -\omega \quad ; \qquad \frac{D\omega}{Dt} = 0 \qquad [2.1]$$

where $\psi(x,y,t)$ represents the stream function and $\frac{D}{Dt}$ denotes differentiation following the motion. These equations are satisfied in some domain $\mathcal{R}$ of the plane, limited by a contour $\partial\mathcal{R}$, where appropriate boundary conditions apply.

The structure of the differential system [2.1] reveals the central role played by the vorticity distribution in the dynamics of the flows under consideration. Clearly, knowledge of the vorticity distribution at some instant determines completely the current and subsequent configurations of the velocity field (subject to the constraints imposed at the boundary $\partial\mathcal{R}$). Furthermore, and in contrast to its active part as "source" of the

motion, the vorticity remains attached to the fluid particles and is transported during the motion as a passive, scalar quantity.

Several discretization schemes are available to the numerical analyst in order to solve the differential problem [2.1]. Among possible alternatives, the point-vortex approximation (PVA) remains particularly appealing due to its simplicity, its suitability for computer analysis, and its flexibility in providing direct visualization of flow patterns. For the reasons given below, a new implementation of the PVA has been developed and used throughout this work to conduct a number of numerical experiments.

In essence, the PVA replaces the continuous vorticity distribution by a system of discrete, interacting point-vortices. The principle of the discretization may be represented as follows. The rotational region of the flow is divided into a large number of small elements (the fluid "particles"), each of which carries a certain amount of vorticity. The circulation around each element boundary has therefore a non-zero value that is readily evaluated. Each element is then assumed to shrink about its vorticity centre, whilst retaining the value of its circulation. This limit process defines clearly the location and strength of the point-vortex that represents the element in the final discretized system. The flow evolution is then depicted by the motion of the set of point-vortices. Each point-vortex interacts instantaneously with every other vortex by a simple action-at-a-distance law; it moves according to the local value of the velocity field whilst simultaneously contributing to the motion of all other vortices. The tracking of the vortices requires in principle the numerical integration of a system of ordinary, non-linear differential equations that present the remarkable property of forming a Hamiltonian

system. The system is known to possess kinematical invariants which can be used to monitor the accuracy of the numerical computation.

The simplicity of the PVA is, however, deceptive and masks partially unresolved questions, some of which will be briefly outlined in the following paragraphs; tentative solutions will be proposed later in the analysis.

Most problems in the PVA arise from the elimination of the notion of material area physically associated with each point-vortex. With this geometrical element removed from the analysis, some flow aspects can no longer be accounted for, nor represented adequately; for example, the relationship between distribution of vortices and vorticity field is not uniquely determined.

Finite-area vorticity elements which are far apart (their separation being gauged in terms of a length representative of their linear dimensions) interact almost as pointwise elements. As they approach one another, their interactions become more complex with the increasing influence of finite area effects; local distortions of the velocity field, leading to deformations of the cores, cannot be ignored for neighbouring elements and must be included in a rigorous analysis. Self-induced deformations may naturally occur and should also be considered. One must therefore note that the inability of the PVA method to cope with such phenomena may lead to physical inconsistencies (*). The importance of these flow features, and the magnitude of the error made in ignoring them have not previously been adequately estimated.

Additional difficulties arise from the singular character of the velocity field at the point-vortex itself. For numerical reasons, this

---

(*) for example, material lines initially formed of distinct fluid particles may occasionally cross - a physical impossibility.

singular behaviour is usually removed by some ad-hoc method, which often consists in approximating the velocity field in the vicinity of the vortex by that due to a vortex with a finite (circular) cross section. This artifice of computation, which relies on numerical intuition for determining a suitable core dimension, does not restore the original concept of the material vorticity element, and ignores the additional problems caused by the introduction of finite-area vortices.

It is here appropriate to place these problems within their historical perspective. The following section presents a brief chronological survey of the evolution of the point-vortex method, provides a comparative background for the present method and discusses some of the solutions to the questions raised previously.

II.2.2 The development and substance of the Point-Vortex Approximation

The idea of representing a continuous vortex sheet by a number of discrete, "elemental" vortices, the temporal motion of which is followed by a numerical, step by step procedure, was first proposed by Rosenhead (1931), in his study of the progressive deformation of the unstable interface between two parallel streams of fluid moving in opposite directions. Rosenhead considered an initial sinusoidal disturbance $y(x) = A_0\, a \sin(2\pi x/a)$, discretized by NV row-vortices of equal strength $\kappa = a\Delta U/NV$, uniformly distributed over one wavelength. Although the number of vortices used was very limited (NV = 12), Rosenhead was able to demonstrate the *smooth* rolling up of the vortex sheet, accompanied by the periodic concentration of vortices at intervals equal to the wavelength of the original perturbation. The smallest time step used in this calculation had the magnitude $\Delta T = 0.25a/\Delta U$; the integration scheme used Euler's method.

Among naturally occuring vortex systems, the trailing vortex sheet produced by an aerofoil is of obvious importance. The PVA was employed in this context by Westwater (1935), to study the rolling up of a vortex sheet of finite breadth, the two-dimensional idealization of the wing-tip vortex system. The sheet was found to roll-up *smoothly*, at a predictable rate, in accordance with the spiral structure predicted analytically by Kaden (1931).

However, it was not until the advent of modern computers that the full capabilities and difficulties of the method were to be extensively explored, by allowing a finer discretization of the vortex sheet and the use of higher-order integration schemes, together with much smaller time steps.

The possibility of a *smooth* roll up of the sheet, in the absence of viscosity, was first questioned by Birkhoff & Fisher (1959). Their refined version of Rosenhead's calculations revealed a *random* trend in the motion of the vortices, and the development of an irregular, contorted and physically unrealistic geometry of the interface, in total conflict with the smooth, regular pattern of the original calculations. However, vortices were found to cluster, which, according to Birkhoff, does not necessarily reflect a genuine concentration of vorticity: the Hamiltonian associated with a system of vortices is a suitable measure of the concentration and is an invariant of the motion. The ultimate randomness of the distribution of the vortices was also advocated by appealing to the applicability of the ergodic theorem for Hamiltonian systems (Birkhoff, 1962).

The calculations of Westwater were reconsidered by Takami (1964) and Moore (1971) who were both unable to reproduce the original results: the smooth spiral structure was again destroyed by the same chaotic motion of the vortices as that showed by Birkhoff and Fisher. The possibility

that this chaotic motion was due to the numerical method failing to integrate the equations of motion correctly was ruled out by the findings of Moore: if the time step is chosen to be much smaller than the orbital period of the two closest vortices, the equations of motion are integrated correctly. One is therefore led to conclude that the exact solution in the PVA does not converge to the solution corresponding to the continuous vortex sheet; increasing the number of vortices worsens the situation. A satisfactory explanation for the emergence of a chaotic motion in the rolled-up portion of the spiral is provided by the possibility that vortices belonging to distinct turns of the spiral, may come very close together and generate unrealistically large interactions that eventually disrupt the smooth evolution of the system (Moore, 1974). The correctness of this explanation is supported by the success met by several techniques in eliminating this random behaviour of the vortices, all of which prevent any two vortices from approaching one another too closely, hence suppressing the occurence of excessive induced velocities. The methods used differ from author to author. Nielsen & Schwind (1971) substitute, for two vortices closer than some threshold distance, a single equivalent vortex located at the vorticity centre of the critical pair. Chorin & Bernard (1972) introduce point-vortices having a small, finite radius core which ensures the boundedness of the velocity field everywhere in the plane. A similar technique is adopted by Milinazzo & Saffman (1977) and by Acton (1976). Kuwahara & Takami (1973) employ the velocity field associated with a diffusing line vortex to the same effect. They also note that the coefficient of viscosity appearing in their equations characterizes an artificial viscosity rather than a genuine, molecular viscosity.

Another, more rigorous, explanation for the development of a random motion of the vortices is given by Fink & Soh (1974), who show that

the PVA of a periodic, continuous vortex sheet neglects the self-induced velocity of vortex-sheet segments that must be included in a correct discretization of the Biot-Savart integral. Inclusion of higher-order terms in the approximation of the integral equation for the elliptically loaded vortex sheet is shown to lead to calculations which converge as the discretization is refined, and which predict a smooth rolling up of the sheet into the expected spiral structure (Fink & Soh, 1978).

Many other applications of the PVA have been reported in the literature, but are not discussed in detail here; they include studies of the temporal interactions between periodic vortex sheets of opposite vorticity - a simple model for the formation of a wake behind bluff bodies (see Abernathy & Kronauer, 1962) and analyses of the spatio-temporal development of shear layers shed from bodies placed in transverse flows. Problems belonging to the second category involve the additional complexity of boundaries. An extensive and excellent survey of related work can be found in Clements & Maull (1975).

Some authors have been primarily concerned with the computational aspects of the PVA. The easiest numerical implementation of the method consists of a direct evaluation of the velocity of each vortex by summing the separate contributions of all other vortices present in the flow. Clearly then, tracing the motion of the whole population requires, at each time step, a computing effort that scales with the square of the population size, NV^2. It is clear that this summation algorithm rapidly becomes expensive in terms of computing cost, even for a moderate number of vortices. The situation worsens if higher-order numerical schemes are employed for the integration of the equations of motion.

An alternative method evaluates the velocities of the vortices via the stream function, and the velocity field. A fast Poisson-solver is

used to determine the values of the stream function at the nodes of a rectangular mesh defined over the spatial area of interest. The vorticity field is prescribed as a set of discrete mesh-point values, obtained by redistributing the contributions of the vortices within a cell to its four nodal points. The velocity field is then computed from the stream function field values, leading in turn to the velocities of the vortices. This approach constitutes the basis of the cloud-in-cell (CIC), particle-in-cell (PIC) or vortex-in-cell method (VIC). The technique was pioneered in the context of plasma physics, and extensively applied to hydrodynamical problems by Christiansen (1973). The ability to rapidly solve Poisson's equation originates from numerical algorithms akin to Fast Fourier Transform methods. These methods present, however, additional uncertainties linked with the variety of possible choices in mesh sizes and interpolation procedures required to switch back and forth from an essentially Lagrangian description to the Eulerian description over the computation mesh. The necessity of solving Poisson's equation implies that boundary conditions be imposed over all domain boundaries; conditions "at infinity" must necessarily be imposed at finite distances, leading to possible limitations of the method. Different codes must also be developed to allow for various types of boundary conditions (Dirichlet or Neumann; periodic or non-periodic).

The possibility of using the summation algorithm in the PVA is often subordinate to the availability of low cost computing resources. A new vortex tracing scheme, based on a fast version of this algorithm, was developed, with the intention of applying it to the study of two-dimensional vorticity layers, using a "cloud discretization" approach. The simplicity of the method limits the number of parameters required for the understanding of its properties; these are described in detail in Section II.5 and II.6.

The concept of "cloud discretization" is introduced in the next section.

II.3 THE CLOUD DISCRETIZATION APPROACH

The question of whether the point-vortex approximation generates a suitable discretization of the continuous vorticity distribution has not been convincingly resolved. In the absence of a rigorous mathematical analysis establishing that the point-vortex flow converges to the continuous flow for increasingly refined discretizations, the assertion that "... concentrations of vorticity in two-dimensional flow can safely be approximated analytically by point vortices" (Batchelor, 1967, p.527) must be considered with some caution.

The point-vortex discretization is a first-order approximation to the integro-differential system that governs the motion of two-dimensional vorticity regions. An analysis similar to that used by Fink & Soh (1978) for the vortex-sheet roll up problem is required to establish the order of magnitude of all terms in higher-order approximations of the integrals

$$u(P) = -\frac{1}{2\pi}\int_A \frac{y(P)-y(Q)}{R_{PQ}^2}\,\omega(Q)\,dA(Q)$$

$$v(P) = \frac{1}{2\pi}\int_A \frac{x(P)-x(Q)}{R_{PQ}^2}\,\omega(Q)\,dA(Q). \qquad [2.2]$$

All applications of the PVA implicitly assume that the terms omitted are effectively negligible; it is now clear that for the particular case of the vortex *sheet*, this assumption cannot be justified.

The situation appears to be somewhat more favourable in the case of surface (i.e. two-dimensional) vorticity distributions. This may be understood on the basis of the following simple argument. Refer to

Figure 3. Assume that a segment of length ℓ of a *line* distribution of vorticity must be discretized by point vortices. Be Γ the value of the circulation around that segment. A measure of the difficulties associated with the point-vortex discretization is given by considering the induced velocity between two neighbouring vortices. Clearly, for N vortices of equal strength $\gamma = \Gamma/N$, this velocity is of the order

$$\Delta u \sim \frac{\gamma}{d} = \frac{\Gamma}{N \frac{\ell}{N}} = \frac{\Gamma}{\ell} = \text{constant}$$

and does not decrease when the discretization is refined (i.e. when $N \to \infty$). The same quantity, evaluated for a surface element of area A in a *two-dimensional* distribution of vorticity, has the value

$$\Delta u \sim \frac{\gamma}{d} = \frac{\Gamma/N}{\sqrt{A/N}} = \frac{\Gamma}{\sqrt{A}} \frac{1}{\sqrt{N}} ,$$

and is seen to decrease as $N \to \infty$. This suggests that the effect of small errors in the position of a nearest neighbour can be made small in the case of the cloud of vortices, i.e. for two-dimensional vorticity distributions.

The validity of the PVA in the two-dimensional case is further supported by noting that the value of all invariants of the continuous motion is approached by that of their discretized counterparts as the number of vortices N is increased indefinitely; indeed, it can be shown that convergence is achieved in the limit $N \to \infty$. (*) The equations of motion of the discretized system approximate, to first order, those that govern the evolution of the continuous system. In principle, these equations can

---

(*) For the Kirchhoff function, the point-vortices must be assumed to have some small but finite core and to have a strength equal to the integral of the vorticity over the area they represent.

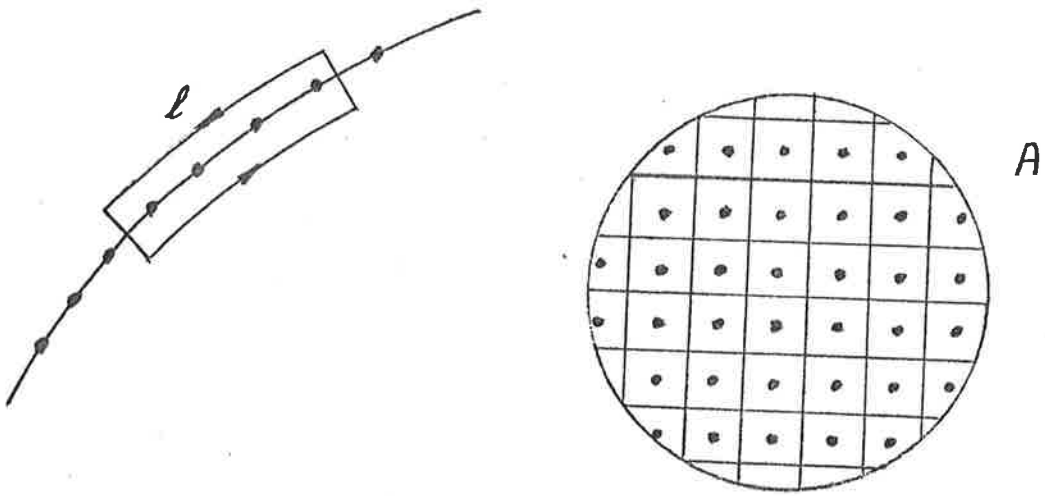

Figure 3: Point Vortex Approximation for a line and a surface distribution of vorticity.

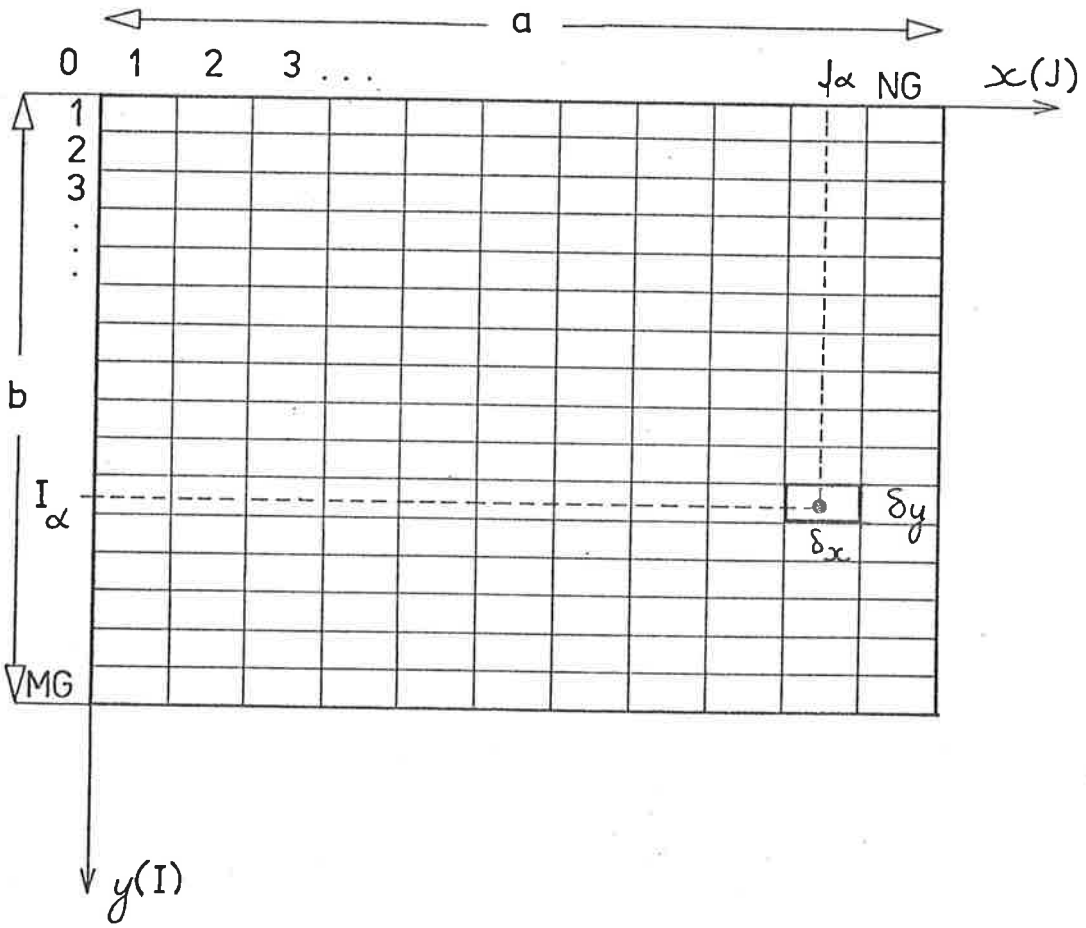

Figure 4a: Definition of the computation grid in the CTC method.

be solved exactly; in practice, the accuracy of the computation may be checked by monitoring the conservation of the invariants.

These arguments seemed a justification to proceed with the point-vortex approximation, largely in the spirit of an experiment. In a "cloud discretization" calculation, vortices are not tracked exactly, and one does not expect the phenomena determined by local flow conditions to be described faithfully. Integral expressions - that is, expressions computed over the whole population of vortices - are however computed accurately, in the limits indicated by the flow invariants. Flow features are determined statistically, as resulting from several computations with varying initial conditions. Each particular discretization can be regarded as one realization from a statistical ensemble. In this statistical interpretation, it is conjectured that an ensemble average over random discretizations defines a solution of the continuous problem (Milinazzo of Saffman, 1977).

A new vortex-tracing algorithm, the centre-to-centre (CTC) method, well suited to the cloud discretization spirit, was developed and used in all PVA calculations presented in this work. The remainder of this chapter is dedicated to the presentation of the CTC method.

II.4 THE CENTRE-TO-CENTRE METHOD

The motion of the vortices is followed over a fixed computation grid, which paves the interval of interest with a large number of rectangular cells, as illustrated in Figures 4a & b. No *a priori* attempt is made to track the vortices exactly. At all stages of the computation, the coordinates of all vortices are deliberately identified with those of the centre of the cell in which they happen to lie. Vortices move, therefore, from cell-centre to cell-centre over the computation grid. This tracing

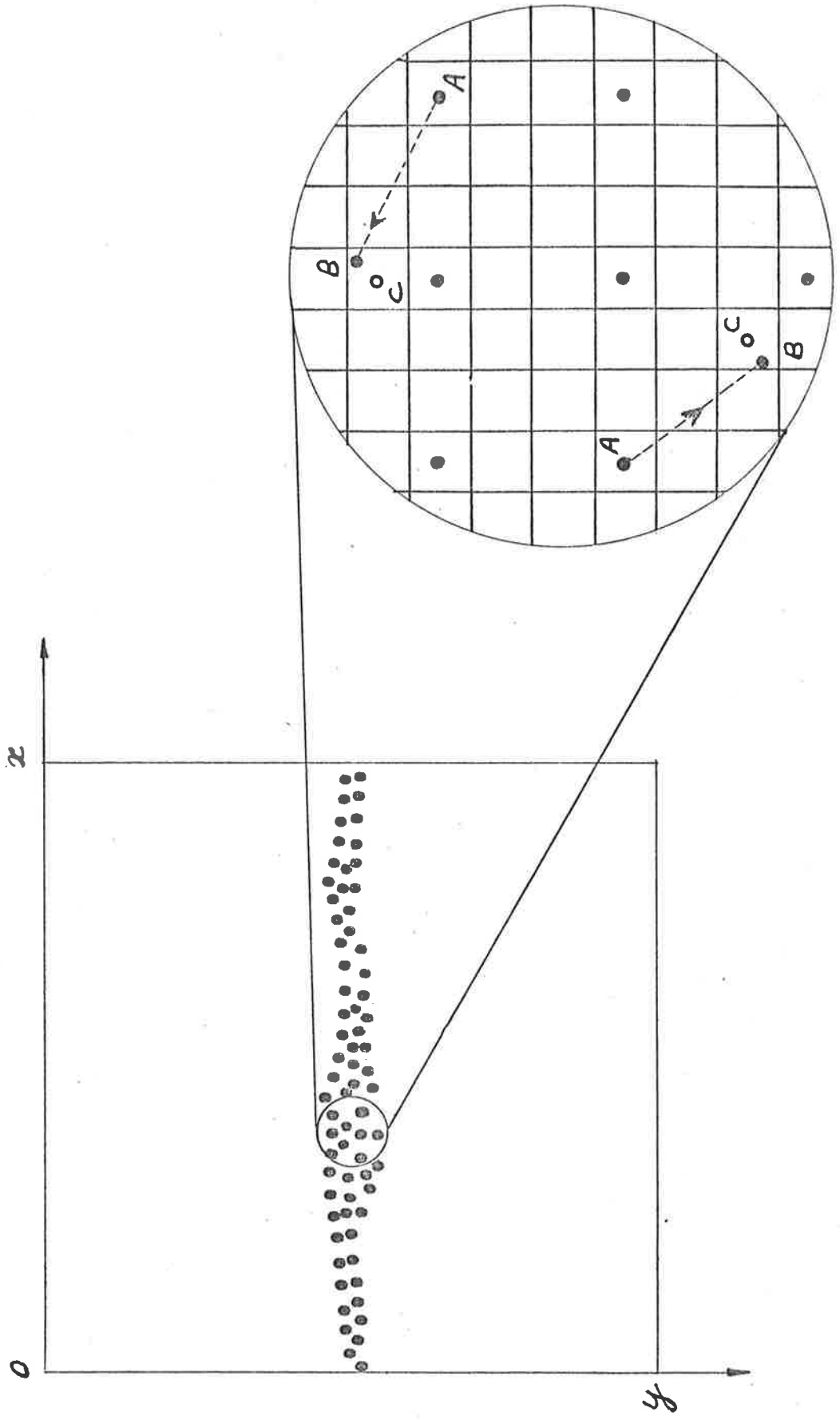

Figure 4b: Sketch of the computation grid in the CTC method. Point-vortices moving from A to B are relocated at point C. The configuration sketched represents a vorticity layer (periodicity in the x direction).

algorithm is accordingly called the centre-to-centre (CTC) method, and will be shown to possess properties that make it a valid alternative to many vortex-tracing schemes reported in the literature.

A one-to-one correspondence can be established between the elements of a matrix having MG rows and NG columns and the cells of a computation grid with the same dimensions. That is, one can introduce, in order to locate the centre of each cell, a pair of integral coordinates (J,I) related to the exact coordinates (x,y) of the cell centre by the relations

$$x = \frac{\delta x}{2} \ (2J-1) \quad \text{and} \quad y = \frac{\delta y}{2} \ (2I-1),$$

in the coordinate system defined in Figure 4a; $\delta x = a/NG$ and $\delta y = b/MG$ are the cell dimensions.

Consider the motion of a set of NV point vortices over the computation grid: vortices start at some initial instant from cell centres, and are followed in their motion during a suitably small time interval Δt. Note here that vortices do not necessarily occupy all cells, i.e. that many computation cells may span the average distance between vortices if so required. If after the time step Δt, the exact coordinates of vortex α are (x_α, y_α), then its integral coordinates (J_α, I_α) are computed from the formulae

$$J_\alpha = \| \left[\frac{x_\alpha}{\delta x} \right] \| + 1 \quad ; \quad I_\alpha = \| \left[\frac{y_\alpha}{\delta y} \right] \| + 1 \ ,$$

where $\| [A] \|$ denotes the largest integer smaller than or equal to the number A.

A population of NV vortices is completely described, over a given grid, by the set of triplets $\{(J_\alpha, I_\alpha, \kappa_\alpha); \ \alpha = 1,2,\ldots,NV\}$, where

κ_α denotes the strength of vortex α. The initial flow configuration is prescribed as the set of values $\{(J^\circ_\alpha, I^\circ_\alpha, \kappa^\circ_\alpha);\ \alpha = 1,2,\ldots,NV\}$. The velocity of each vortex can be computed from the interaction law and the new positions of the vortices determined by integration of the equations of motion.

A few preliminary comments are warranted. The CTC method removes the possibility of occurrence of high-induced velocities by effectively preventing vortices from approaching one another too closely. The cell dimensions act as a critical approach distance: if two or more vortices happen to lie within the same cell at the end of a time step, they are thereafter regarded as a single vortex, the strength of which is the sum of all individual vortices. The component vortices remain, however, identifiable, since they retain their label in the set of triplets describing the configurations.

The introduction of integral coordinates significantly improves the computational aspect of the summation algorithm. Distances between vortices are necessarily integral multiples of cell dimensions; many operations can be carried out using integer arithmetic when evaluating the interaction summations. This is of particular interest on smaller computers where floating-point arithmetic operations are especially time-consuming. In the special case where row-vortices are tracked, the hyperbolic and circular functions appearing in the "influence coefficients" of the interaction summations (see equations [1.56] and [1.57]) can be tabulated once and for all; the velocity of each vortex is then readily computed from table "look-ups" and simple arithmetic operations. Adoption of this technique substantially reduces the amount of computing time (by approximately one order of magnitude). Vortex coordinates are integer numbers

which are easily packed/unpacked for efficient internal and external storage. Again, this feature may be appealing when working with machine configurations where available memory space is limited; it is even more effective when equi-strength vortices are employed, each configuration requiring only the specification of NV pairs of coordinates $\{(J_\alpha, I_\alpha);\ \alpha = 1,2,\ldots,NV\}$ for its complete description.

The tracing algorithm must now be completed by the choice of a numerical scheme for the integration of the equations of motion. Many options are available; the choice is however limited by practical considerations of cost versus precision. The simplest and most economical scheme is the one-step forward algorithm known as Euler's method, which relies on the first-term of a Taylor series expansion. This method has been used by many authors (Rosenhead, 1931; Kuwahara & Takami, 1973; Acton, 1976). Higher-order schemes have also been employed, usually belonging to the family of Runge-Kutta formulae (Moore, 1974 ; Zalosh, 1976); they are prohibitively expensive, however, when the number of vortices becomes relatively large (a few hundred).

The properties of the CTC algorithm, coupled with the effects of the integration scheme, have been systematically investigated by comparing computed flows with an exact reference flow, the disk of uniform vorticity; this investigation is described in detail in Sections II.5 & II.6.

II.5 EFFECTS OF INTEGRATION PROCEDURE, TIME STEP AND CELL SIZE IN THE CTC METHOD

The purpose of this section is to present the first series of tests carried out to quantify the performance and to understand the fundamental properties of the CTC method. If the method is applied to compute the

exact motion of the vortices, one can identify, *a priori*, two sources of inaccuracy:

(a) the exact locations of the vortices are assimilated to the coordinates of the cell centres; the spatial resolution of the method is therefore limited to the computation cell. The magnitude of this "grid error" depends clearly on some characteristic dimension δ of the cell;

(b) the numerical integration of the equations of motion induces necessarily an "integration error", essentially dependent on the size of the time step Δt.

In the limit where the cell dimensions becomes infinitesimally small, the CTC method traces the vortices in a conventional manner, its accuracy being limited by that of the numerical integration scheme.

The combined effects of grid and integration errors for small but finite cell sizes were investigated by applying the method to a simple, known, exact reference flow. A formal solution exists for describing the velocity field associated with any two-dimensional distribution of vorticity over some bounded region of the plane (see equations [2.2]). Explicit analytical solutions are, however, difficult to obtain from these integrals, even for uniform vorticity distributions and simple geometries; the choice of possible test problems is then practically limited to the case of the isolated circular disk of uniform vorticity, generally known as Rankine's vortex. The problem is briefly discussed in the following paragraph.

II.5.1 Rankine's vortex

Consider a disk $\mathcal{D}$ of radius a and uniform vorticity ω_0 in an otherwise irrotational flow extending to infinity. The problem is conveniently solved in its differential form; the integral formulation is given

in Appendix B.

The stream function ψ must satisfy the equations

$$\nabla^2\psi = -\omega \quad \text{inside} \quad \mathcal{D}$$
$$\nabla^2\psi = 0 \quad \text{outside} \quad \mathcal{D}\,. \qquad [2.3]$$

The circular symmetry is preserved when ω and ψ are functions of the radial distance only; steady motion is possible if ω is an arbitrary function of ψ. For ω constant$(= \omega_0)$, one has

$$\frac{d^2\psi}{dr^2} + \frac{1}{r}\frac{d\psi}{dr} + \omega_0 = 0 \text{ in } \mathcal{D}$$

and [2.4]

$$\frac{d^2\psi}{dr^2} + \frac{1}{r}\frac{d\psi}{dr} = 0 \quad \text{outside} \quad \mathcal{D}.$$

The general integral of this equation is $\psi(r) = A \log r + B$; a particular solution of the nonhomogeneous forms is $\psi(r) = -\omega_0 r^2/4$. Therefore, the internal and external solutions are, respectively,

$$\psi_i = A_i \log r + B_i - \omega_0 r^2/4$$

and [2.5]

$$\psi_e = A_e \log r + B_e\,.$$

The requirements that ψ be finite at $r = 0$ and that ψ and $\frac{d\psi}{dr}$ be continuous at the disk boundary lead to

$$\psi_i(r) = \frac{\omega_0}{4}\,(a^2 - r^2) - \frac{\omega_0 a^2}{2}\,\log a$$

and [2.6]

$$\psi_e(r) = -\frac{\omega_0 a^2}{2}\,\log r,$$

where the additive constant B_e has been omitted. The velocity potential

outside the disk is found to be

$$\phi_e(x,y) = \frac{\omega_0 a^2}{2} \tan^{-1}(y,x) \; ; \qquad [2.7]$$

ψ_e is a multiple-valued function with cyclic constant $\Gamma = 2\pi \frac{\omega_0 a^2}{2} = \pi a^2 \omega_0$. The velocity field is derived from

$$u_r = \frac{1}{r} \frac{\partial \psi}{\partial \theta} \qquad u_\theta = - \frac{\partial \psi}{\partial r} \qquad [2.8]$$

and is found to be

$$u_\theta(r) = \frac{\omega_0}{2} r \quad \text{within } \mathcal{D} \, ,$$
$$[2.9]$$
$$u_\theta(r) = \frac{\omega_0 a^2}{2r} \quad \text{outside } \mathcal{D} \, .$$

The disk rotates about its axis as a rigid body with angular velocity $\Omega = \omega_0/2$, corresponding to a period of rotation $T = 4\pi/\omega_0$.

For the sake of completeness, let us mention that the pressure field is determined from Euler's equation of motion inside $\mathcal{D}$ and Bernoulli's relation outside $\mathcal{D}$. One obtains:

$$\frac{u_\theta^2}{r} = \frac{1}{\rho} \frac{dp}{dr} \text{ giving } p(r) = \frac{\omega_0^2}{4} \rho \frac{r}{2} + p(0) \text{ inside } \mathcal{D} \, ,$$

$$p(r) = p_\infty - \rho \frac{u_\theta^2}{2} \text{ outside } \mathcal{D}.$$

Continuity of the pressure field at $r = a$ leads to the results

$$p(r) = p_\infty - \rho \frac{\gamma 2}{a^2} \quad 1 - \frac{r^2}{2a^2} \quad \text{inside } \mathcal{D}$$

and $$[2.10]$$

$$p(r) = p_\infty - \frac{\gamma^2 \rho}{2r^2} \qquad \text{outside } \mathcal{D} \, .$$

$$\left(\gamma = \frac{\Gamma}{2\pi} = \frac{\omega_0 a^2}{2} \right) .$$

The five invariants for the uniform vorticity disk are obtained by direct evaluation of the definition integrals,

$$\Gamma = \int_{\mathcal{D}} \omega \, d\mathcal{D} \qquad [2.11]$$

$$\Gamma X = \int_{\mathcal{D}} \omega \, x \, d\mathcal{D} \qquad [2.12]$$

$$\Gamma Y = \int_{\mathcal{D}} \omega \, y \, d\mathcal{D} \qquad [2.13]$$

$$\Gamma G = \Gamma I^2 = \int_{\mathcal{D}} \omega[(x-X)^2 + (y-Y)^2] \, d\mathcal{D} \qquad [2.14]$$

$$H = \frac{1}{2}\int_{\mathcal{D}} \psi\omega \, d\mathcal{D} \qquad [2.15]$$

with

$$\psi(P) = -\frac{1}{4\pi}\int_{\mathcal{D}} \omega' \log[(x(P)-x')^2 + (y(P)-y')^2] \, dx'dy' \qquad [2.16]$$

Their values are obtained as

$$\Gamma = \pi \, a^2 \, \omega_0 \qquad [2.17]$$

$$X = Y = 0 \qquad [2.18]$$

$$G = I^2 = a^2/2 \qquad [2.19]$$

$$H = \frac{\omega_0 a^2 \pi^4}{16} \, (1 - 4 \log a) \, . \qquad [2.20]$$

(See Appendix B).

II.5.2 The Point-Vortex Approximation of Rankine's vortex

The continuous vorticity distribution over the disk is discretized into a number of equi-strength point-vortices uniformly distributed over the disk area, according to the following procedure. The square circumscribing the disk is covered with a grid of (N×N) cells; point vortices

are then placed at the centres of all cells which belong to the interior of the disk. The number of vortices retained is approximately equal to $NV = 0.8\ N^2$. This discretization procedure is clearly symmetrical and ensures that the resulting point-vortex distribution approaches uniformity, for NV large. Boundary effects, however, cannot be fully eliminated and are reflected in the values of the invariants G and H (Γ, X and Y achieve their theoretical value) (see Table 2).

The smallest distance between adjacent vortices is $\Delta = 2a/N$. The motion is usually computed over a fine mesh computation grid of cell size δ. It is convenient to select the ratio $\Delta/\delta = N_\delta$ as an odd integer, in order to keep the initial configuration unaltered by the redefinition of the grid (Figure 5).

The influence of the two basic parameters δ (cell size) and Δt (time step) was investigated on the basis of a comprehensive number of computer runs. For reasons previously exposed (see section II.3), it seemed crucial to evaluate the invariants of the flow, particularly the Hamiltonian or Kirchhoff function of the system: it appears important to ensure that in its final state, the system possesses the same total energy as that of its initial configuration. If this energy were not conserved, the mechanisms responsible for the loss of invariance had to be identified and the magnitude of their effects appreciated. The behaviour of the three other invariants X, Y and G was also considered. In all computations, covering a wide range of values for cell size and time step, the centre of vorticity (X, Y) of the cloud was found to remain fixed with a high degree of accuracy. Results presented concern almost exclusively the behaviour of the Kirchhoff function H of the system. The behaviour of the radius of gyration $I = \sqrt{G}$ was however monitored in order to confirm the conclusions drawn from the function H; in all cases, conclusions drawn independently

NV	I/a_0	$H/\frac{a_0^4\omega_0^2}{4}$
52	.7156	.58648
137	.7175	.66702
256	.7087	.73535
421	.7116	.73771
616	.7071	.76529
861	.7094	.76025
1124	.7039	.78787
1457	.7082	.77093
1804	.7060	.78250
2217	.7088	.77136

I/a_0 theor = .707107

$H/\frac{a_0^4\omega_0^2}{4}$ theor = .7853982

Table 2: PVA of Rankine's vortex: invariants of the discretized system (effect of NV on values of I and H).

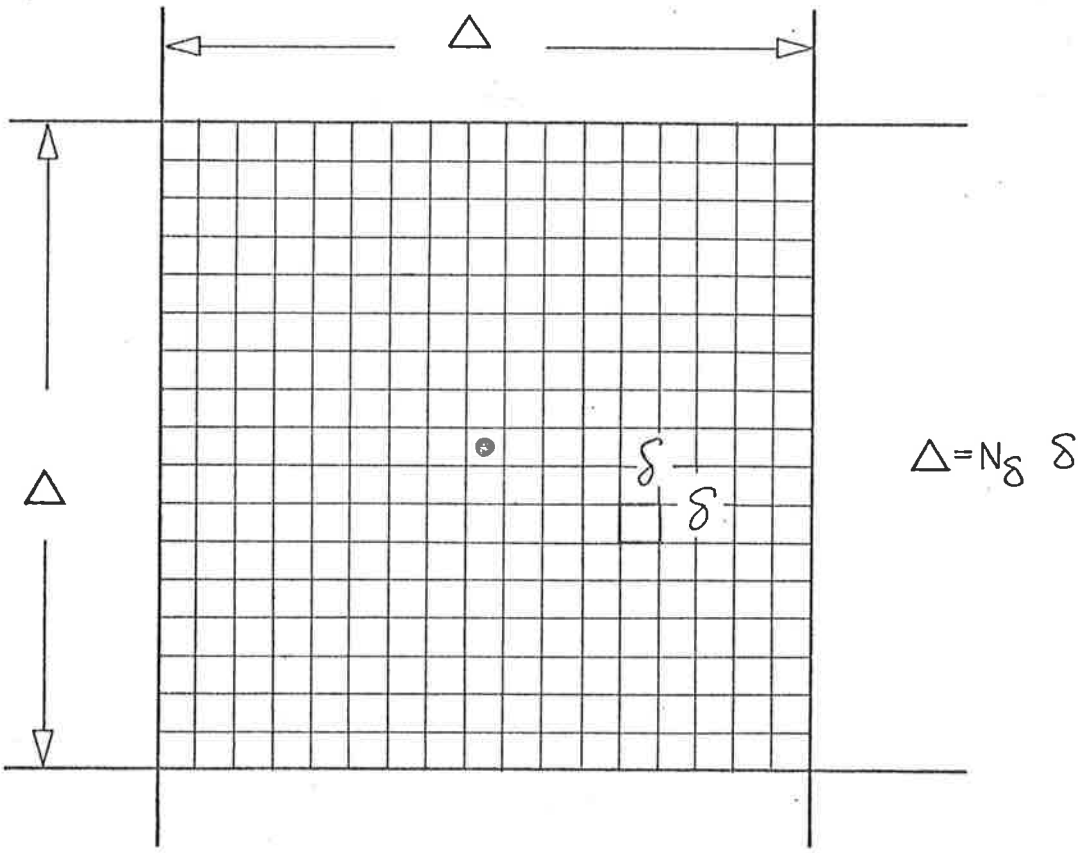

Figure 5: definition of computation grid in relation to average distance Δ between vortices (Rankine's vortex).

were in full agreement. Sections II.5.3, II.5.4 et II.6 present and discuss the interesting sensitivity of the Kirchhoff function to the values chosen for the parameters δ and Δt. In several cases, it was found convenient to use N_δ as a measure of the cell size. The number of vortices used in the computations was close to 200, although on some occasions, up to 500 vortices were tracked.

II.5.3 Euler's integration method

In a preliminary approach, and following in this choice several authors (Acton, 1976; Kuwamara and Takami, 1973), the equations of motion [1.47] of the vortices were integrated using Euler's method. The coordinates of vortex α at time $t + \Delta t$ are obtained from those at time t by the relations

$$x_\alpha(t + \Delta t) = x_\alpha(t) + u_\alpha(t)\ \Delta t$$
$$y_\alpha(t + \Delta t) = y_\alpha(t) + v_\alpha(t)\ \Delta t, \qquad [2.21]$$

expressed in integer coordinates (J_α, I_α).

For a fixed time step, it was found that changing the cell size by three orders of magnitude had no effect whatever on the *change* in H observed (Figures 6a, 6b and 6c). For a time step $\Delta t\ \omega_0 = .2$, the Hamiltonian H changed by 40 % in a quarter of rotation of the vorticity disk. Note that $\omega_0\ \Delta t$ may be interpreted as the time step Δt scaled by the characteristic time of rotation of two neighbouring vortices a distance $\bar{d}$ apart: $\omega_0\ \Delta t = \Delta t/(\bar{d}^2/\gamma)$. A value of $\omega_0\ \Delta t$ of the order .075 is commonly used in several studies (e.g. Acton, 1976). Figure 6a shows that the decrease of H with time is issentially linear. Decreasing the time step (see figure 6b, where $\omega_0\ \Delta t = .1$) reduces the rate of decrease of H

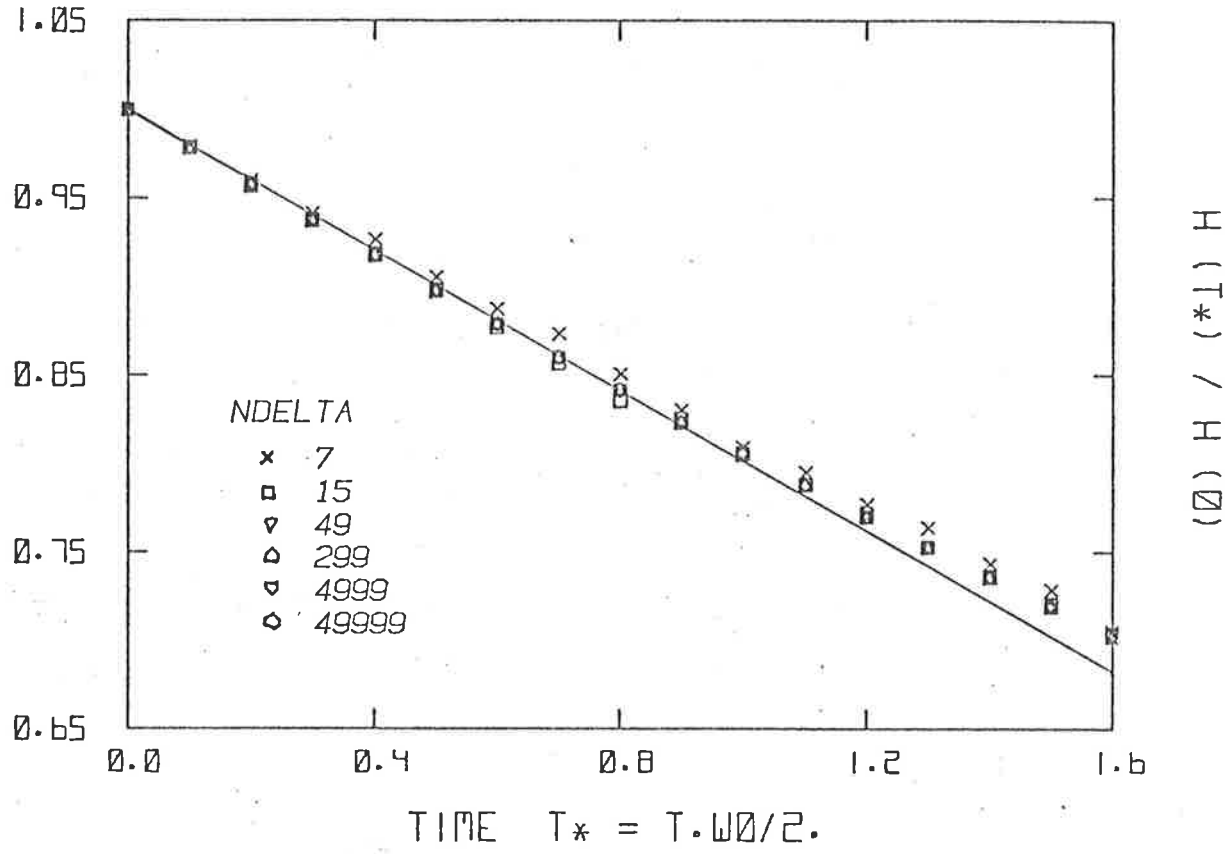

Figure 6a: effect of cell size on Hamiltonian (Euler method; $\Delta t^* = 0.1$)

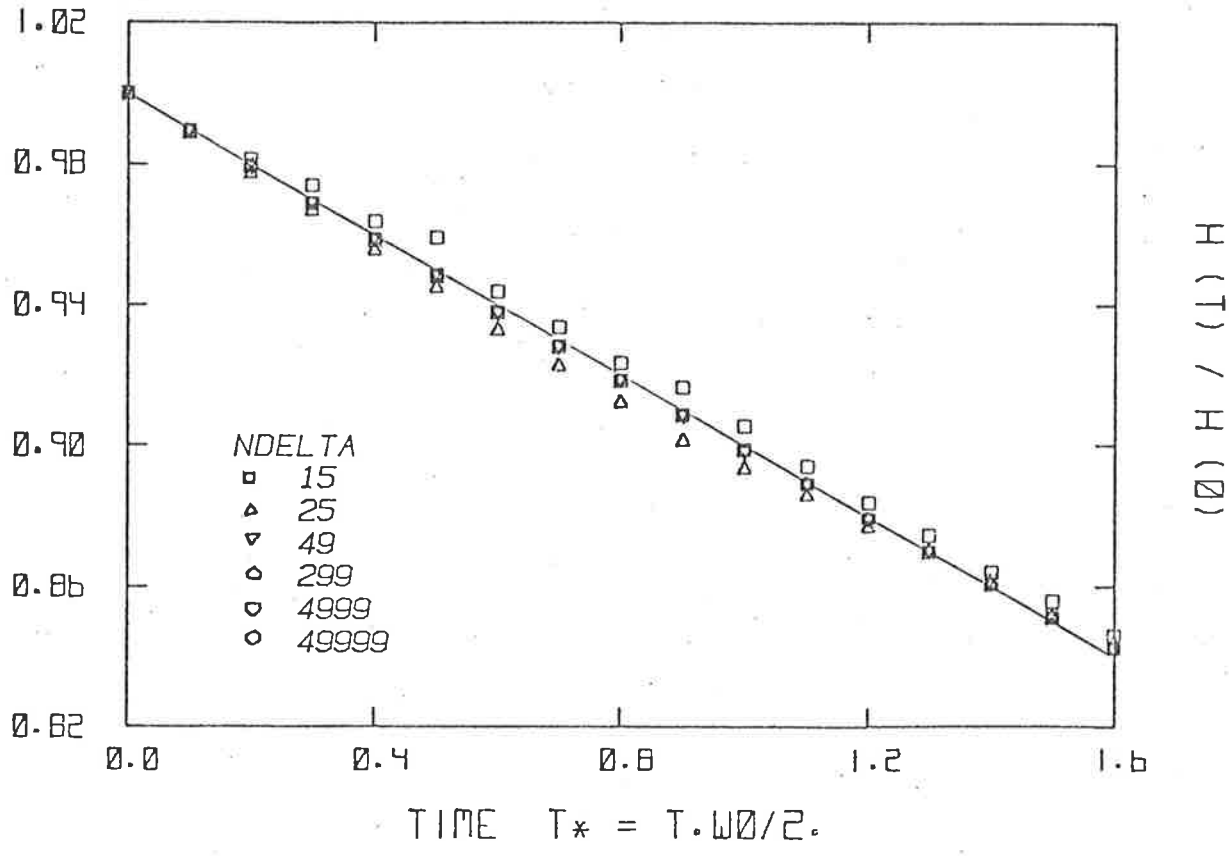

Figure 6b: effect of cell size on Hamiltonian (Euler method; $\Delta t^* = 0.05$)

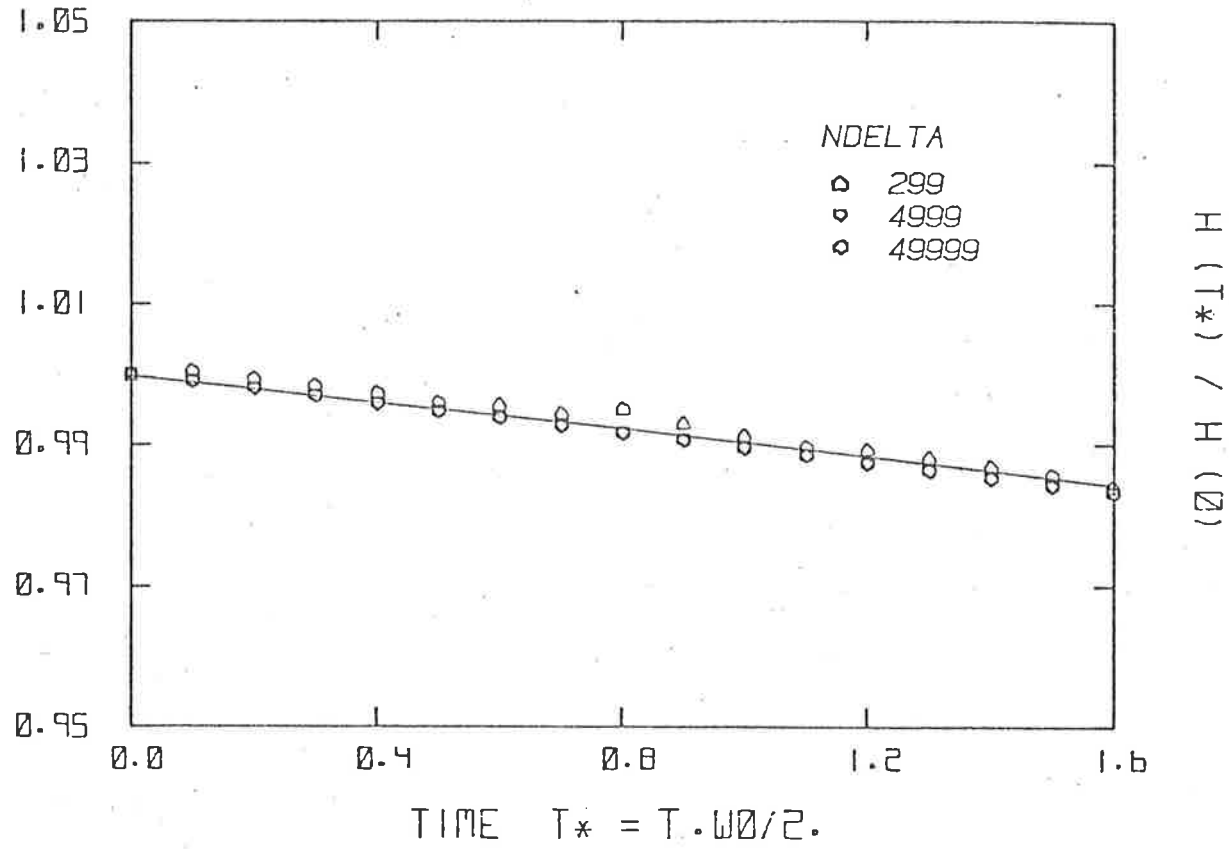

Figure 6c: Effect of cell size on Hamiltonian (Euler's method; $\Delta t^* = 0.005$)

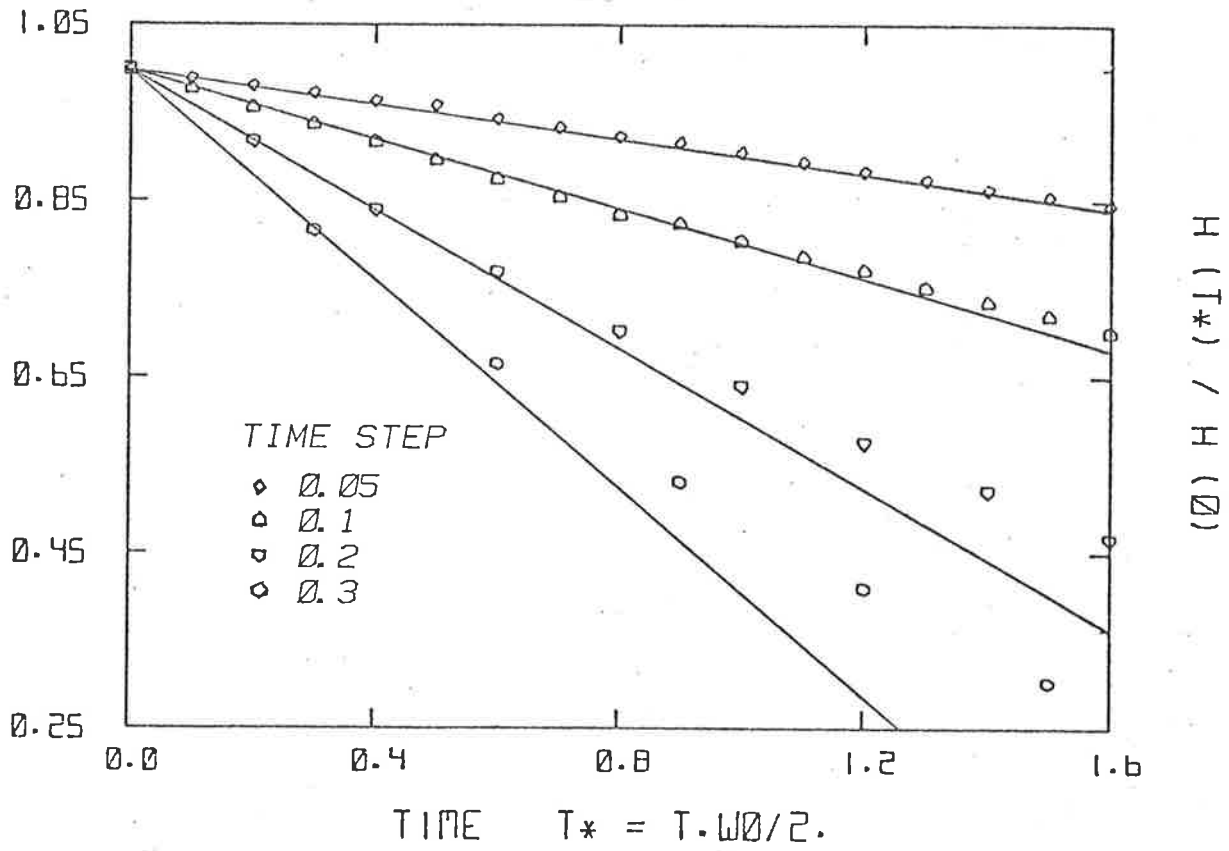

Figure 7a: Effect of time step on Hamiltonian (Euler's method; $N_\delta = 15$)

without altering the linear trend of the behaviour. A decrease in Δt of an order of magnitude (see Figure 6c, $\omega_0 \Delta t = .01$) resulted in a change in H of approximately 10% for one rotation (about 650 time steps). Again, changing the cell size by several orders of magnitude had no discernible effect on the results; this is illustrated on figures 7a, 7b & 7c, which show the evolution of the Kirchhoff function in time with $\Delta t^* = \Delta t \, \omega_0/2$ as a parameter, δ (N_δ) being kept fixed.

The explanation of this dependence is straightforward. The grid error is essentially random whereas the integration error is fundamentally one-sided. When tracking vortices of the same sign, the integration procedure introduces errors largely of one sign which, when summed over all vortices and time steps, lead to a "bulk" diffusion of the cloud of vortices. This accumulation of errors has an effect on the invariants H and G which appears to swamp any other source of random error. The magnitude of this effect is easily predicted. Refer to figure 8. A point vortex ideally moving on a circumference of radius r about the disk centre is followed, during each time interval Δt, tangentially to its true trajectory. The computed path of each vortex is then a spiral. The resulting relative error is given by

$$\frac{\varepsilon}{r} = \frac{\tilde{BB}}{OA} = \frac{1 - \cos(\omega_0 \Delta t/2)}{\cos(\omega_0 \Delta t/2)} = \frac{1 - \cos \Delta t^*}{\cos \Delta t^*}$$

i.e. $$\frac{\varepsilon}{r} = \frac{1}{2} \Delta t^{*2} \quad \text{for} \quad \Delta t^* \ll 1 \; . \qquad [2.22]$$

For the disk of radius a and of circulation Γ, one has

$$H = \frac{\Gamma^2}{16\pi} (1 - 4 \log a)$$

and allowing the radius to be a function of time, one computes

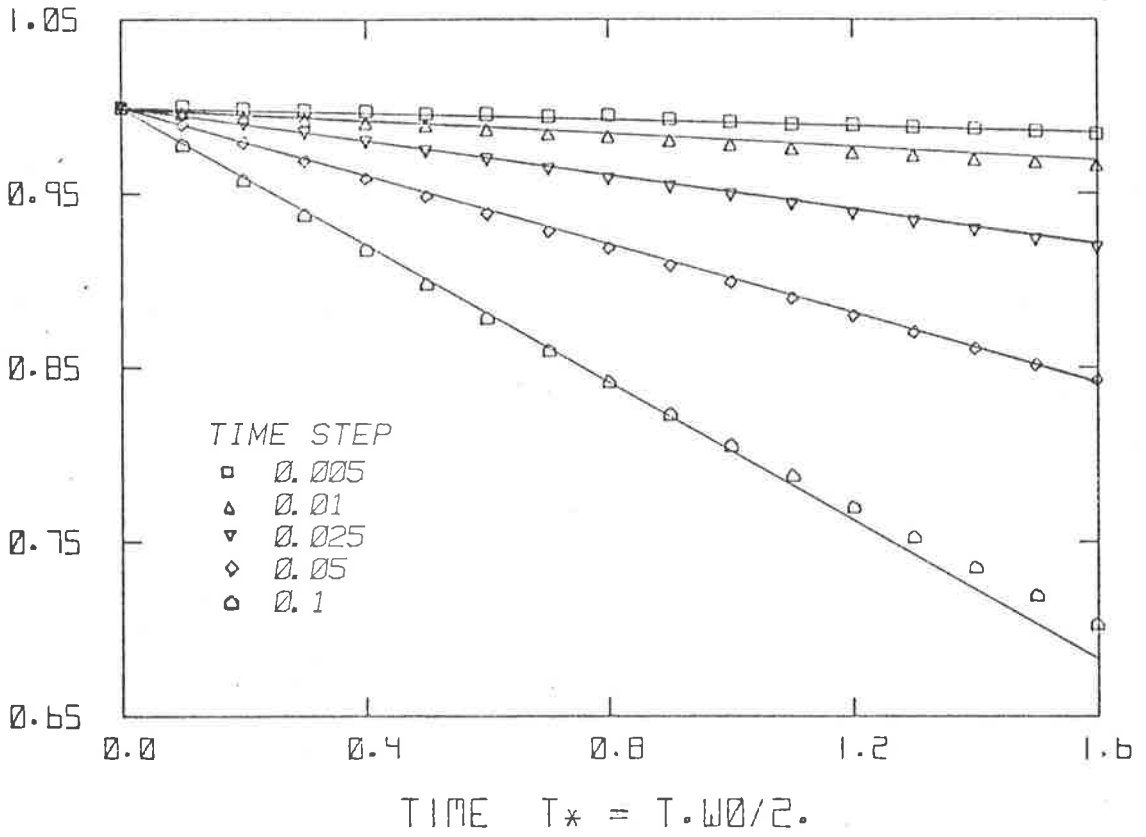

Figure 7b: Effect of time step on Hamiltonian (Euler's method; N_δ = 299)

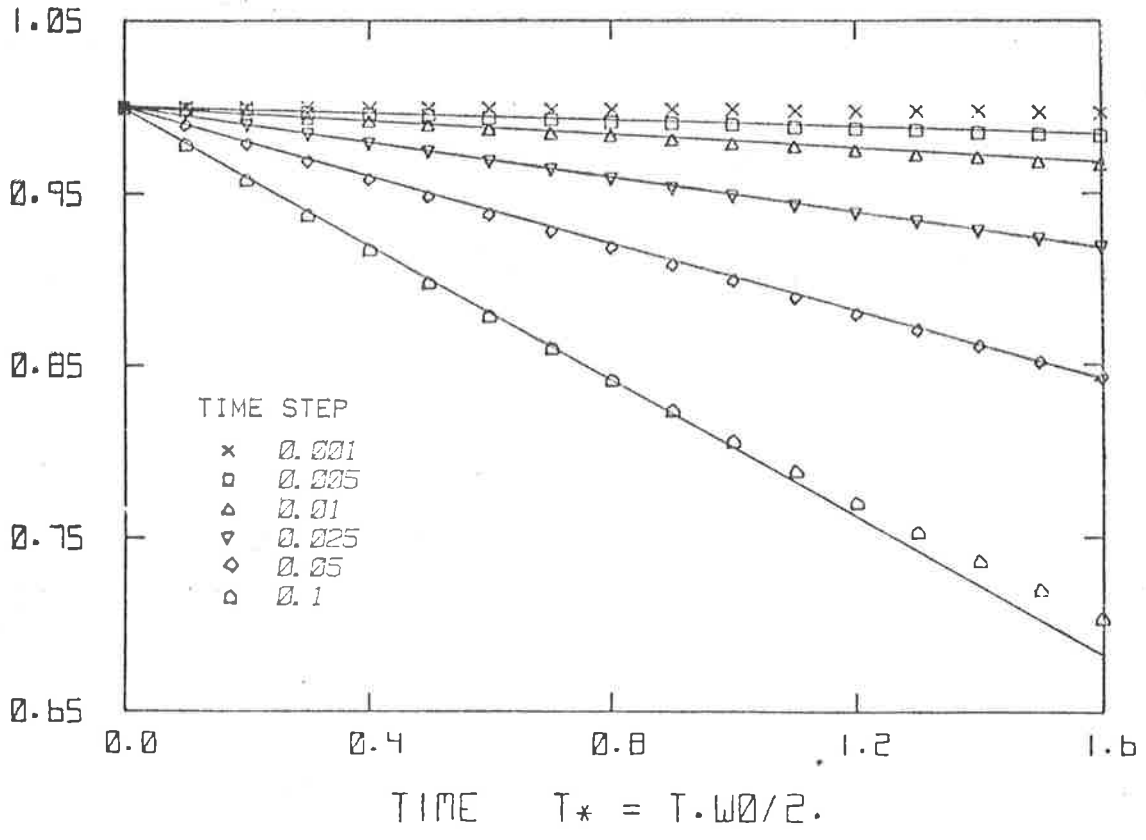

Figure 7c: Effect of time step on Hamiltonian (Euler's method; N_δ = 49999)

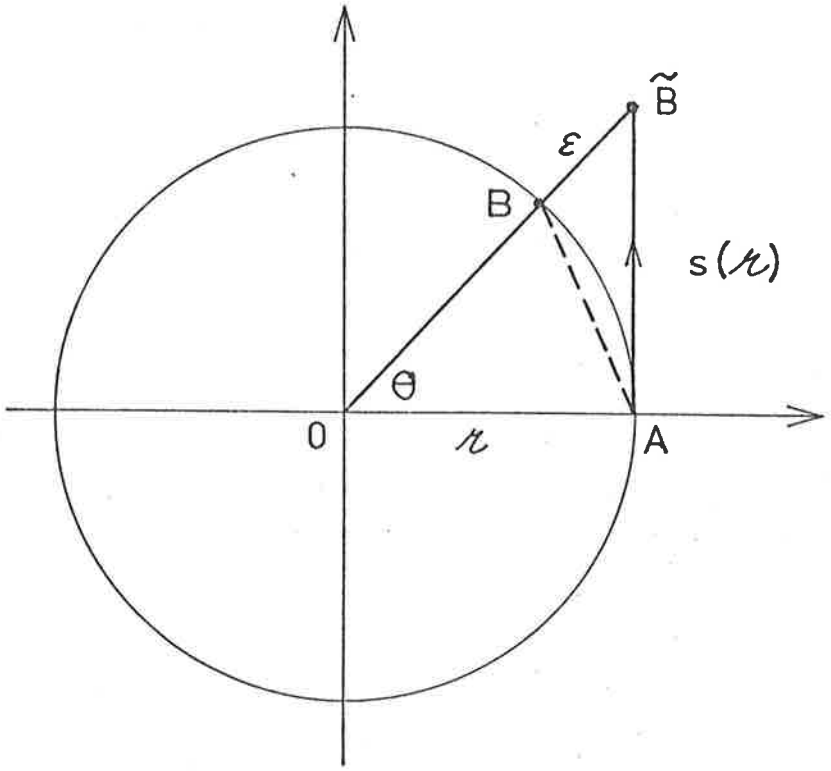

Figure 8: integration error in Euler's method.

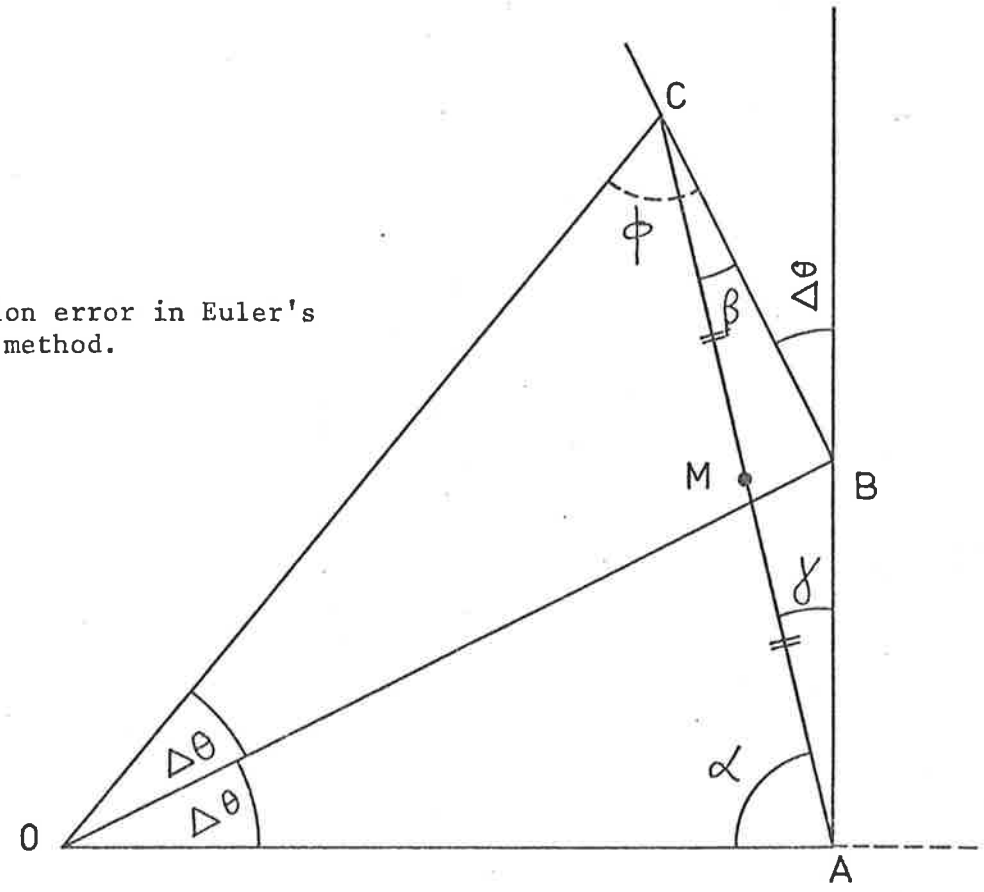

Figure 9: integration error in Euler's modified method.

$$\Delta H = H(t^*+\Delta t^*) - H(t^*) = -\frac{\Gamma^2}{4\pi} \log\left(1 + \frac{\Delta a}{a}\right)$$

i.e. $$\Delta H \approx -\frac{\Gamma^2}{4\pi} \frac{\Delta a}{a}$$

This leads to the following estimate for the decay rate m_H of the Kirchhoff function:

$$m_H = \frac{d}{dt^*} \frac{H(t^*)}{H(0)} = -2\,\Delta t^* \qquad [2.23]$$

for $a(0) = 1$.

The prediction $$\frac{H(t^*)}{H(0)} = 1 - (2\,\Delta t^*)\, t^* \qquad [2.24]$$

accounts completely for the computed time dependence of the Kirchhoff function and is represented by plain lines on Figures 6 and 7. Note that the time rate of change m_I of the radius of gyration I is readily obtained as

$$m_I = \frac{d}{dt^*} \frac{I(t^*)}{I(0)} = \frac{\Delta t^*}{2} \qquad [2.25]$$

a result which agreed fully with the numerical data (not shown on the figures).

It appears therefore that the use of Euler's method in conjunction with point-vortices is not to be recommended, and indeed should be avoided whenever the trajectories of the vortices all have positive (or negative) curvatures. In this case, elaborate schemes to prevent vortices from coming close together or to compute the "accurate" positioning of the vortices appear totally unwarranted. Euler's method was abandoned in this study for a higher-order integration method. It is interesting to note that the relocation mechanism of the CTC method does not accumulate one-sided errors, and that the nett grid-error effect tends to average out,

even for values of $\Delta t^* \bar{d}/\delta$ as small as 5. This balancing mechanism is effective for reasonably fine computation grids ($\Delta t^* \bar{d}/\delta > 10$).

II.5.4 Huen's (Euler's modified) integration method

Results of the preceding section stress the importance of the integration technique used in vortex-tracing algorithms. The cumulative nature of the one-sided integration error can lead to important bulk diffusion effects which rapidly distort the flow picture. This distorsion, quantified in terms of the invariants of the motion, seems unacceptable in the case of Euler's method.

Many higher-order integration schemes are in principle available as an improvement of Euler's method; in practice, however, any scheme of order higher than two results in prohibitive computing costs. This led to the choice of Euler's modified second-order scheme, a predictor-corrector method also known as Huen's method (*).

Euler's modified method is based on the equations

$$\underset{\sim}{r}(t+\Delta t) = \underset{\sim}{r}(t) + \Delta t\ \hat{\underset{\sim}{u}}(t)$$

and [2.26]

$$\hat{\underset{\sim}{u}}(t) = \frac{1}{2}\left[\underset{\sim}{u}(t) + \underset{\sim}{u}(t+\Delta t)\right]$$

where $\underset{\sim}{u}(t)$ is the velocity corresponding to the current vortex configuration and $\underset{\sim}{u}(t+\Delta t)$ is the velocity corresponding to the predicted configuration.

(*) Furthermore, any prediction scheme used in conjunction with the CTC method gives a relocation of the vortex to the cell centre at the end of each intermediate step. This involves an error of order $\delta/v\Delta t_i$, where v is a characteristic vortex velocity and Δt_i is the intermediate time step. Hence the modified Euler scheme seems preferable to any predictor scheme where the intermediate time step is a fraction of the nominal time step, since $\Delta t_i = \Delta t_{nominal}$ in Euler's modified method.

An analysis similar to that made in the case of Euler's method discloses the expected dependence of the Hamiltonian on the time step. Refer to Figure 9. The point vortex initially at A is now traced by the algorithm to point M, the mid-point of line segment AC. The radial error $\varepsilon = OM - OA$ is found from the following geometric relations:

(a) $OA = OB \cos \Delta\theta$

$OB = OC \cos \Delta\theta \quad ; \quad OA = r$

(b) $\dfrac{AC}{\sin 2\Delta\theta} = \dfrac{OC}{\sin \alpha} \quad ; \; AC = 2\, AM$

(c) $\alpha = \dfrac{\pi}{2} - \gamma$

(d) $\dfrac{BC}{\sin \gamma} = \dfrac{AB}{\sin \beta} \quad ; \quad \gamma + \beta = \Delta\theta$

(e) $OM^2 = OA^2 + AM^2 - 2\, OA\, AM \sin \gamma \; ; \; OM = \tilde{r}$.

All quantities in the right-hand side of (e) can be expressed in terms of r and $\Delta\theta$ if relations (a) - (d) are employed; one finds that

$$\tilde{r}^2 = r^2\left(1 + \frac{1}{4}\tan^4\Delta\theta\right) \qquad [2.27]$$

i.e. $$\tilde{r} = r\left(1 + \frac{\Delta\theta^4}{8}\right) \quad ; \quad \Delta\theta << 1 \; .$$

The radial error is

$$\frac{\varepsilon}{r} = \frac{\tilde{r}-r}{r} = \frac{\Delta\theta^4}{8} = \frac{\Delta t^{*4}}{8}$$

since $\Delta t^* = \dfrac{\omega_0}{2}\, \Delta t = \Delta\theta$ by definition.

The decay rate m_H' of the Hamiltonian should now scale with t^* according to:

$$m'_H = -\frac{1}{H(0)}\frac{dH}{dt^*} = \frac{\Delta t^{*3}}{2(1-4\log a_0)}$$

i.e. $$m'_H = \Delta t^{*3}/2 \quad \text{for } a_0 = 1. \qquad [2.28]$$

It can be similarly shown that the growth rate of the radius of gyration is given by

$$m'_I = \Delta t^{*3}/8 \qquad [2.29]$$

Figures 10a to 10d illustrate for increasing cell sizes the degree of improvement achieved in conserving the Hamiltonian when Euler's modified method is employed. Note that the time interval here is about thirty times that used to illustrate effects of similar magnitude with Euler's method. The full lines indicate the expected behaviour of H, as predicted by equation [2.28]. This prediction is clearly followed for relatively large time steps, as seen on Figures 10. For smaller time steps and relatively large cell sizes, however, departures from the linear behaviour are apparent (see details on Figures 10c and 10d). Following an idea of Moore (see Milinazzo and Saffman, 1977), one is led to speculate as to whether the finite cell size introduces a calculable viscosity ν_{CTC} (of magnitude proportional to $\delta^2/\Delta t$) in the nominally inviscid computation. This possibility is examined in the following section.

II.6 VISCOUS EFFECTS IN THE CTC METHOD

Moore's argument is based on the observation that molecular diffusion in fluids emerges as the averaged effect of the random motion of the molecules, superimposed on the mean motion of the fluid as a whole. One may then expect that the random relocation of the vortices in the CTC method is, under certain circumstances (large δ and small Δt^*), capable of generating an observable action of viscosity.

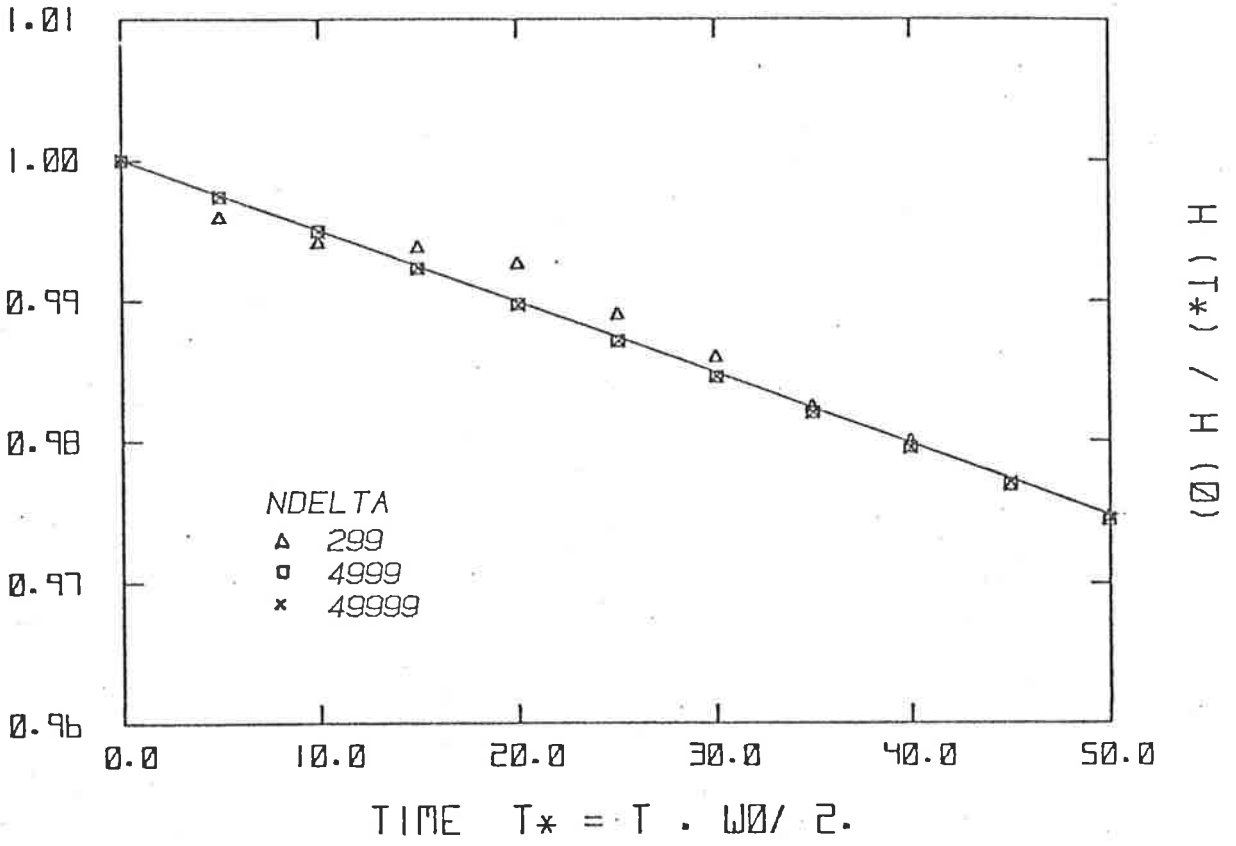

Figure 10a: Effect of cell size on Hamiltonian (Huen's method; $\Delta t^* = 0.1$)

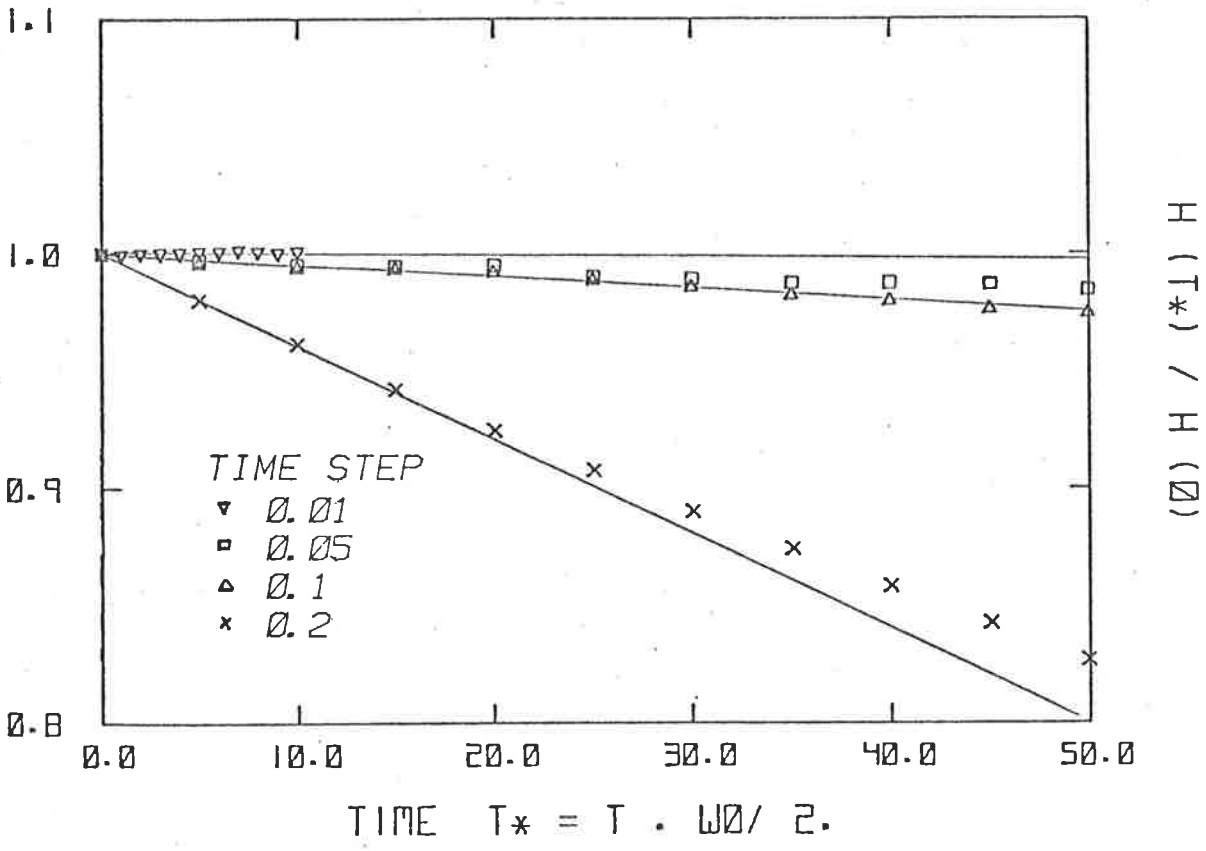

Figure 10b: Effect on time step on Hamiltonian (Huen's method; $N\delta = 299$).

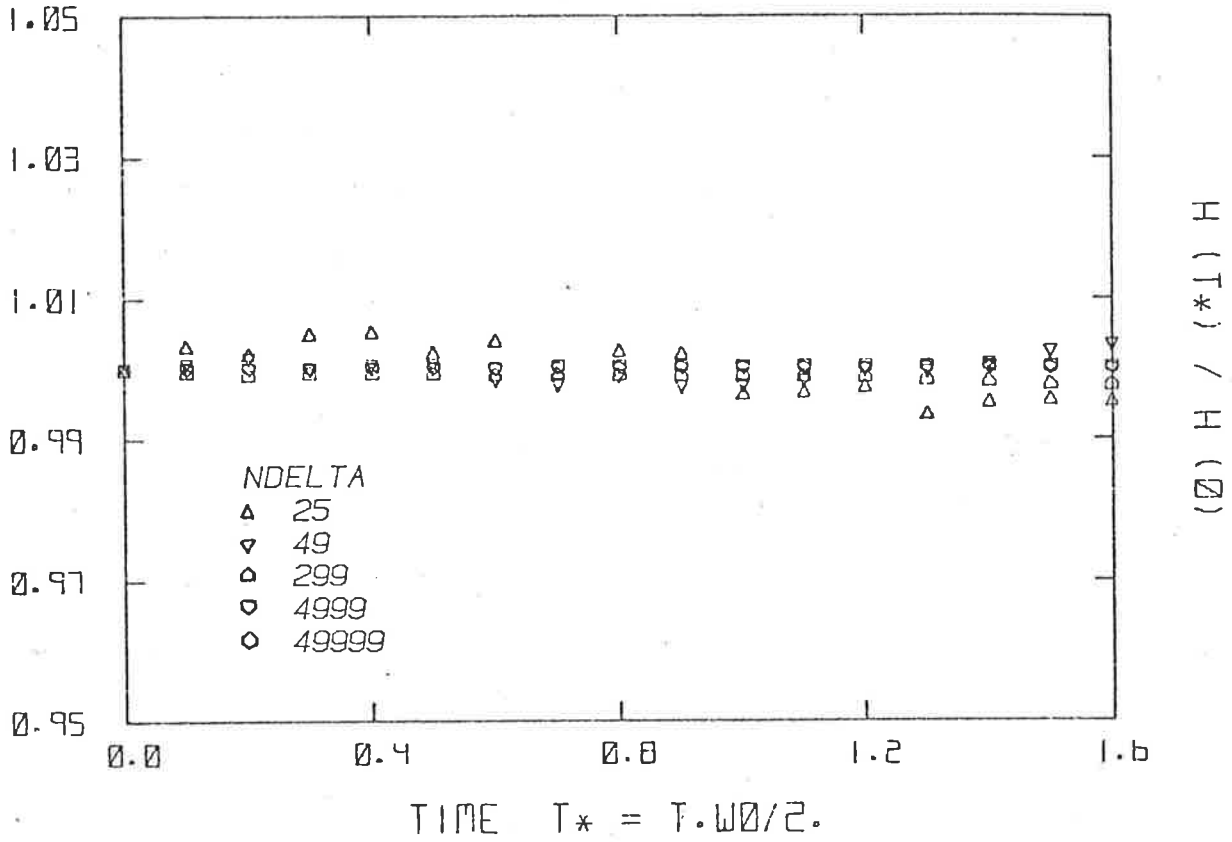

Figure 10c: Effect of cell size on Hamiltonian (Huen's method; $\Delta t^* = .025$)

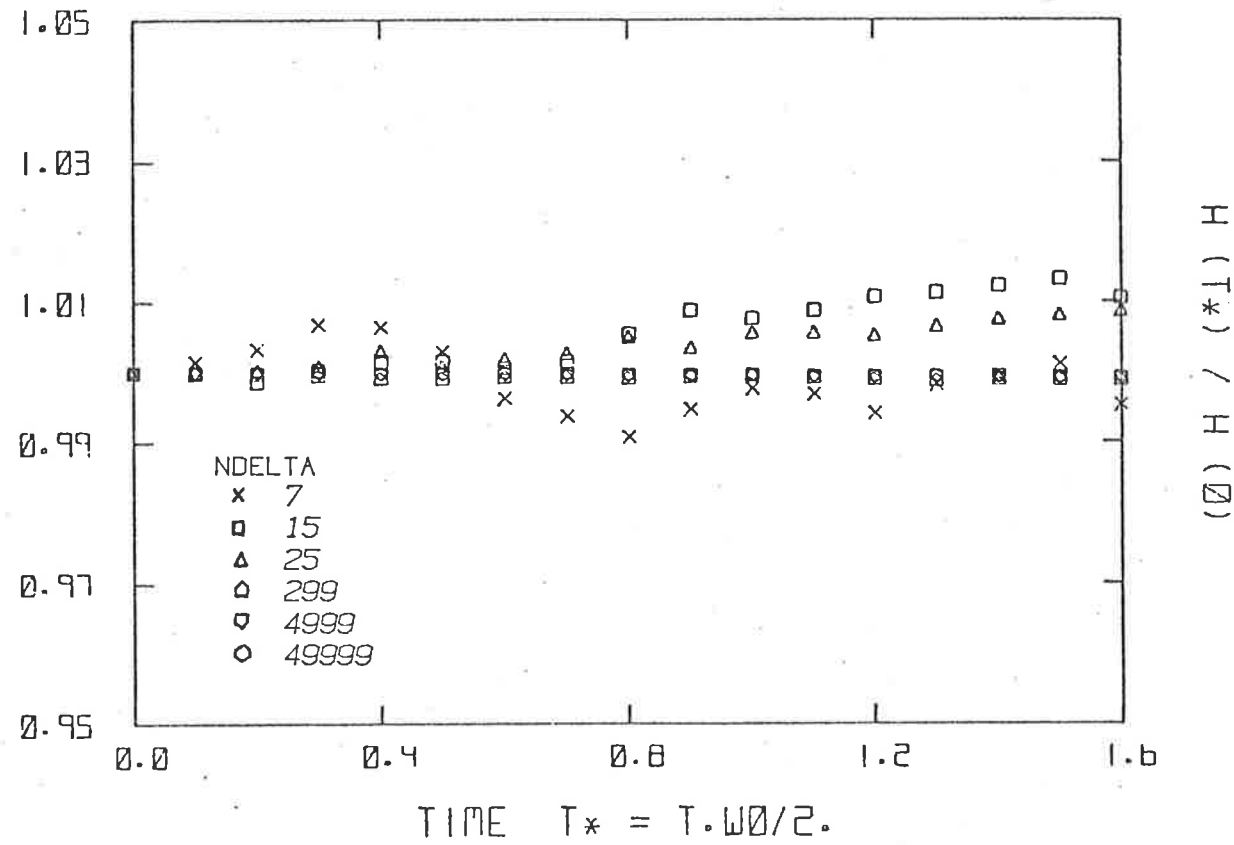

Figure 10d: Effect of cell size on Hamiltonian (Huen's method; $\Delta t^* = .1$)

In an attempt to confirm this possibility, calculations were pursued over many disk revolutions, using the relevant ranges of cell size and time step. This analysis parallels that of Milinazzo and Saffman (1977), who examine the accuracy of a "viscous" computation based on the addition of Gaussianly distributed random displacements to the hydrodynamical motion of the vortices. For Gaussian displacements with zero mean and r.m.s. amplitude σ_G, the diffusion effects correspond to a molecular viscosity of magnitude

$$\nu_G = \frac{\sigma_G^2}{2\ \Delta t} \qquad [2.30]$$

(to the first order in $(NV)^{-1}$, where NV is the number of vortices). In their study, numerical results and analytical arguments support the view that an accurate simulation of viscous effects requires the number of vortices used in the discretization to be large compared with the characteristic Reynolds number

$$Re = \Gamma/\nu \qquad [2.31]$$

of the problem. In their numerical experiments, Milinazzo and Saffman used Huen's integration method to follow vortices with a finite core, chosen such that the maximum (hydrodynamical) displacements of the vortices during the elementary time interval is of the order of their average separation.

Although similar in spirit, the present study must be distinguished from that of Milinazzo & Saffman on several points. Firstly, the CTC method cannot differentiate between vortex core size and amplitude of the random displacements: both are determined by the cell dimensions, and cannot be selected separately. Secondly, the probability distribution of the random fluctuations differ markedly from normality in the CTC method. Finally,

the existence of a random motion is subordinate to that of the hydrodynamical motion pure diffusion effects cannot be directly modelled by the CTC method.

With these restrictions in mind, one can estimate the values of an equivalent core size and r.m.s. amplitude as follows. The square cell of dimension δ is assimilated to a circular core of radius $\sigma = \delta/\sqrt{\pi}$. The actual probability distribution of the relocation displacements is approximated by a uniform distribution over the cell, yielding a mean square value

$$\langle d^2 \rangle = \int_{-\frac{\delta}{2}}^{\frac{\delta}{2}} \int_{-\frac{\delta}{2}}^{\frac{\delta}{2}} (x^2+y^2)\, dx\, dy = \frac{\delta^2}{6} .$$

The calculated viscosity in the CTC method is therefore

$$\nu_{CTC} = \frac{\delta^2}{12\Delta t} \qquad [2.32]$$

The validity of this prediction may be tested by comparing the outcome of the numerical computations with the analytical solution for the decay of a uniform vorticity disk in a viscous fluid. It is possible to predict the change with time of the Hamiltonian resulting purely from diffusion at the boundary of the disk; comparison with the behaviour of H in the numerical computations allows to infer the actual value of the viscosity in the CTC method and a check on expression [2.32]. Before presenting the results of these calculations, it is necessary to consider the problem of the uniform disk of vorticity in a viscous fluid and several related expressions; this is the object of Sections II.6.1 and II.6.2.

II.6.1 Viscous decay of a vorticity disk

Consider a vorticity disk of radius a and uniform vorticity ω_o and its motion in an otherwise initially irrotational viscous fluid

extending to infinity. Viscous action at the disk boundary tends to smooth out the step discontinuity in the vorticity distribution, leading to the spreading of the rotational region of the flow by a process of gradient diffusion.

In all generality, the two-dimensional vorticity distribution in a viscous, incompressible fluid is governed by the scalar equation

$$\dot{\omega} = \nu \nabla^2 \omega \qquad [2.33]$$

where $\omega = \frac{\partial v}{\partial x} - \frac{\partial u}{\partial y}$; ν is the kinematic viscosity of the fluid. In polar coordinates (r,θ), the above equation is rewritten

$$\frac{\partial \omega}{\partial t} + u_r \frac{\partial \omega}{\partial r} + \frac{u_\theta}{r} \frac{\partial \omega}{\partial \theta} = \nu \left[\frac{1}{r} \frac{\partial}{\partial r} \left(r \frac{\partial \omega}{\partial r} \right) + \frac{1}{r^2} \frac{\partial^2 \omega}{\partial \theta^2} \right] \qquad [2.34]$$

where

$$\omega(r,\theta) = \frac{1}{r} \left[\frac{\partial}{\partial r} (r u_\theta) - \frac{\partial u_r}{\partial \theta} \right] . \qquad [2.35]$$

In view of the azimutal symmetry of the problem of the disk, one needs only consider functions which do not depend on θ ; furthermore, it is clear that the velocity field has no radial component $(u_r = o)$. With these simplifications, the differential equations of the problem reduce to

$$\frac{\partial \omega}{\partial t} = \frac{\nu}{r} \frac{\partial}{\partial r} \left(r \frac{\partial \omega}{\partial r} \right) \qquad [2.36]$$

$$\omega = \frac{1}{r} \frac{\partial}{\partial r} (ru) \qquad [2.37]$$

where u has been written for u_θ. The boundary and initial conditions to be satisfied by $\omega(r,t)$ are the following:

$$\begin{aligned} &\omega(r,o) = \omega_o \qquad o \leqslant r \leqslant a \\ &\omega(r,o) = o \qquad a < r < \infty \\ &\lim_{r \to \infty} \omega(r,t) = o \qquad \text{for all } t > o \end{aligned} \qquad [2.38]$$

The solution of the differential problem [2.36] - [2.38] may be obtained as the superposition of solutions of the "source" type. Observe first that the function

$$\omega_s\ (r,t) = \frac{C}{t}\ e^{-r^2/4\nu t} \qquad [2.39]$$

where C is a constant, is a solution of equation [2.36]; this is readily checked by direct substitution. It is easy to verify that this solution is singular at the origin at the initial instant $t = o$, in the sense that

$$\begin{aligned} &\lim_{t\to o} \quad \omega_s(r,t) = o \qquad r \neq o \\ &\lim_{t\to o} \quad \omega_s(o,t) = \infty \qquad r = o \ . \end{aligned} \qquad [2.40]$$

However, for all $t>o$, the quantity $\int_A \omega_s(r,t)\ dA$ remains finite and indeed constant. One computes easily the value of this integral:

$$\int_A \omega_s(r,t)dA = 4\pi\nu C = \Gamma \qquad [2.41]$$

(the integration being extended to the whole plane).

The solution ω_s represents a point-vortex of strength Γ located at the origin and diffusing into the surrounding fluid by viscous action. If the vortex is located at the point (r_o,θ_o) - see Figure 11a -, the solution becomes

$$\omega_s(r,t) = \frac{\Gamma}{4\pi\nu t}\ e^{-R^2/4\nu t} \qquad [2.42]$$

where R represents the distance between the vortex and the point $P\ (r)$ where the vorticity is evaluated; explicitely, one has

$$R^2 = (x-x_o)^2 + (y-y_o)^2$$

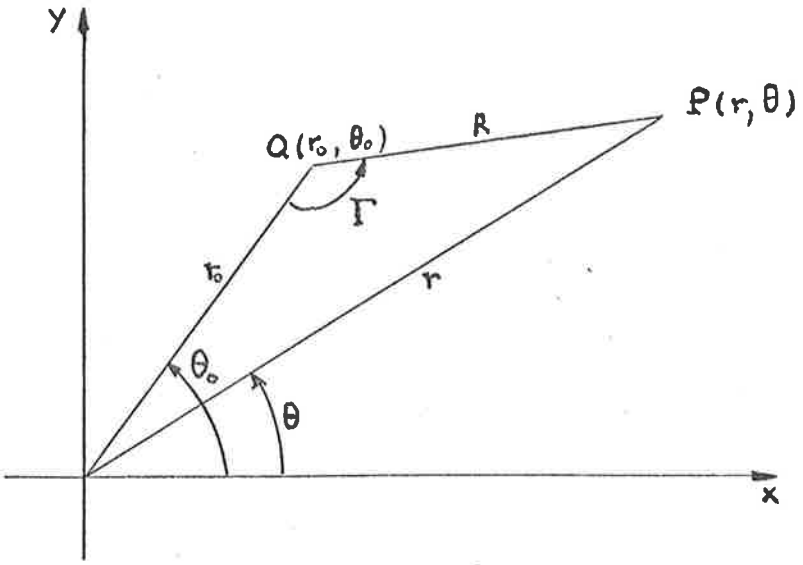

Figure 11a

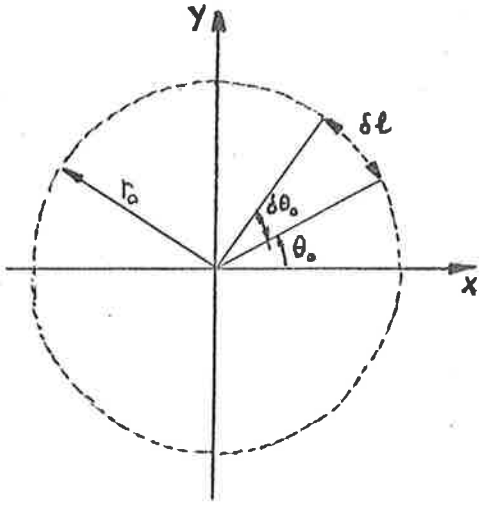

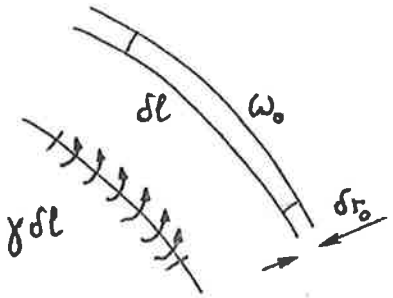

Figure 11b

Figures 11: Construction of the solution to the problem of the viscous decay of a disk of vorticity.

or $$R^2 = r^2 + r_o^2 - 2rr_o \cos(\theta-\theta_o) \ . \qquad [2.43]$$

Consider now a continuous line-distribution of circulation, defined such that the amount of circulation "carried" by a line-element $\delta\ell$ has the value $\delta\Gamma = \gamma\delta\ell$. Assume in addition that this line of circulation is a circumference of radius r_o centered at the origin ; clearly then $\delta\ell = r_o d\theta$. The viscous diffusion of a uniform "vorticity ring" is described by the function

$$\omega_c(r,t) = \oint_C \omega_s(r,t)\, dC$$

$$= \frac{\gamma r_o}{4\pi\nu t} \int_0^{2\pi} e^{-R^2/4\nu t}\, d\theta_o$$

$$\text{i.e. } \omega_c(r,t) = \frac{\gamma r_o}{4\pi\nu t} e^{-(r^2+r_o^2)/4\nu t} \int_0^{2\pi} e^{rr_o \cos\Delta\theta/2\nu t}\, d\theta_o \ . \qquad [2.44]$$

The integral may be expressed in terms of the solution I_o of the modified Bessel equation of order zero (see Watson, 1922, 3.7). One rewrites the ring solution under the form

$$\omega_c(r,t) = \frac{\gamma r_o}{2\nu t} e^{-(r^2+r_o^2)/4\nu t} I_o\left(\frac{rr_o}{2\nu t}\right) \ . \qquad [2.45]$$

Note that the circulation per unit length γ may be related to the local value of the vorticity ω_o as follows. Consider the ring of circulation as an annulus of radius r_o and width δr_o (see Figure 11b); clearly one has

$$\gamma\delta\ell = \omega_o \delta A = \omega_o\, \delta\ell\delta r_o$$

$$\text{i.e.} \qquad \gamma = \omega_o\, \delta r_o \ .$$

It is now easy to obtain the solution for the problem of the uniform disk of vorticity, by superposing the contributions of concentric rings of

vorticity. One writes therefore

$$\omega_\nu(r,t) = \iint \omega_c(r,t)\, dA$$

$$\text{i.e.} \quad \omega_\nu(r,t) = \frac{\omega_o}{2\nu t}\, e^{-r^2/4\nu t} \int_0^a e^{-r_o^2/4\nu t}\, I_o\left(\frac{r r_o}{2\nu t}\right) r_o\, dr_o \,, \quad [2.46]$$

a solution which will be considered under the form

$$\Omega_\nu(\rho,\xi) = \frac{\omega_\nu(r,t)}{\omega_o} = \frac{1}{2\xi}\, e^{-\rho^2/4\xi} \int_0^1 e^{-\lambda^2/4\xi}\, \lambda\, I_o\left(\frac{\rho\lambda}{2\xi}\right) d\lambda \,, \quad [2.47]$$

where the adimensional variables $\rho = \frac{r}{a}$ and $\xi = \nu t/a^2$ have been introduced. The integral in [2.47] cannot be evaluated analytically, except at $\rho = o$ where the solution becomes

$$\Omega_\nu(o,\xi) = 1 - e^{-1/4\xi} \,. \quad [2.48]$$

Figure 12 shows the evolution of $\Omega_\nu(\rho,\xi)$ for values of the parameter ξ in the range 0.15 to 3; the radial distance represented here covers three times the initial radius ($\rho_{max} = 3.$) Details about the numerical evaluation of $\Omega_\nu(\rho,\xi)$ may be found in Appendix C.

II.6.2 The evaluation of $H_\nu(t)$ and of $dH_\nu(t)/dt$

The solution [2.46] of the viscous decay problem may now be used to compute a quantity of interest in the present analysis, the Kirchhoff function of the system:

$$H_\nu(t) = \frac{\rho}{2} \int \psi\omega dA$$

$$= -\frac{\rho}{8\pi} \iint \omega(P)\, \omega(Q)\, \log R_{PQ}^2\, dA(P)\, dA(Q) \quad [2.49]$$

(R_{PQ} represents the distance between the vorticity elements at the points

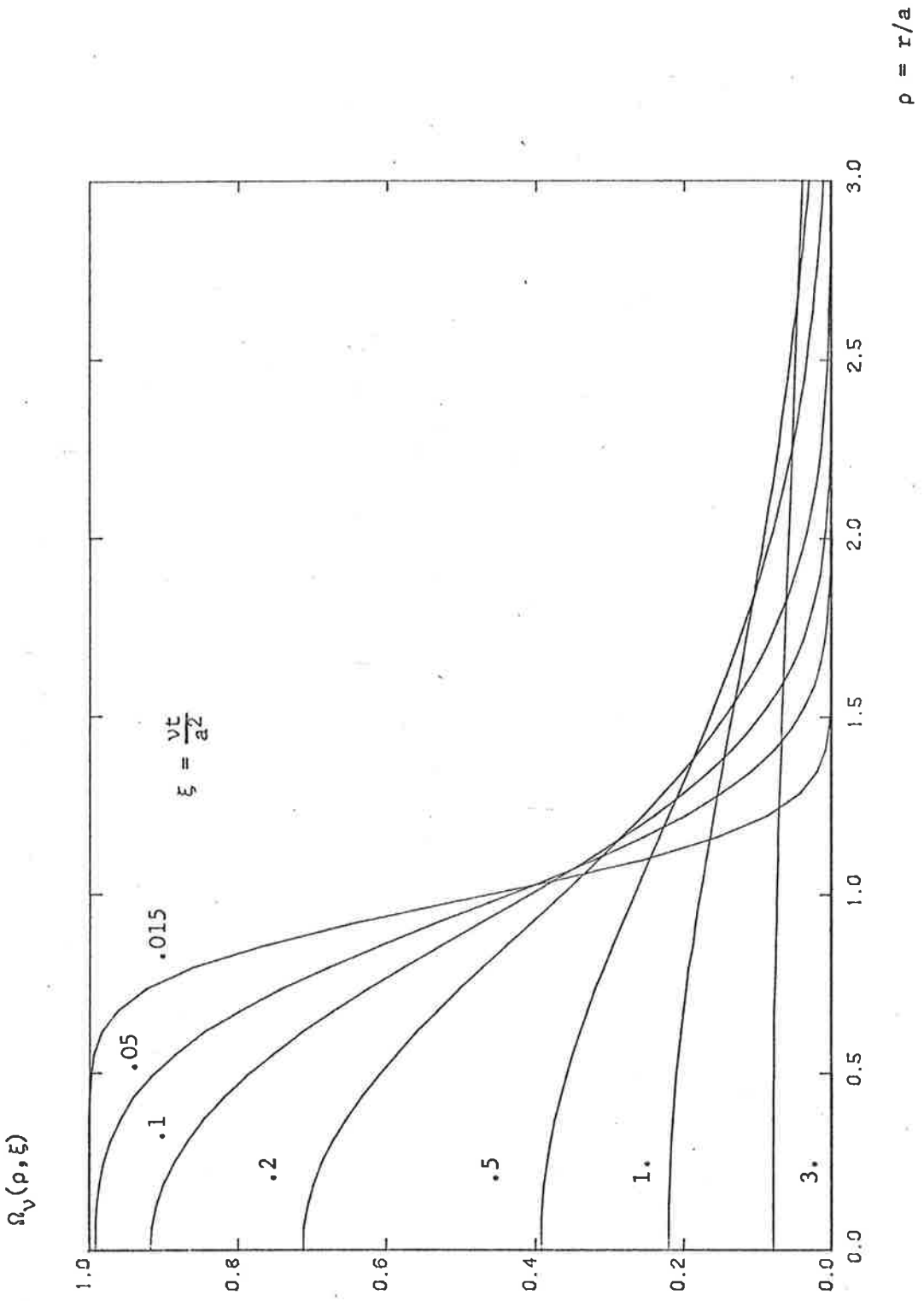

Figure 12: Evolution with time ($\xi = \nu t/a^2$) of vorticity distribution $\Omega_\nu(\rho,\xi)$ in viscous decay of disk.

P and Q). Introducing polar coordinates (r_o,θ_o) and (r,θ) - refer to Figure 11a -, one obtains the Kirchhoff function under the form

$$H_\nu = -\frac{\rho}{8\pi} \int_0^{2\pi} d\theta_o \int_0^{2\pi} d\theta \int_0^{\infty} r\omega_\nu(r)\, dr \int_0^{\infty} r_o\omega_\nu(r_o) \log R_{PQ}^2\, dr_o,$$

with $R_{PQ}^2 = r^2 + r_o^2 - 2rr_o \cos(\theta-\theta_o)$.

The integration with respect to the angles may be carried out in a manner similar to that used in Appendix B; one obtains the expression

$$H_\nu = -\pi \left\{ \int_0^{\infty} \rho\omega_\nu(\rho) \log\rho\, d\rho \int_0^{\rho} r\omega_\nu(r)\, dr + \int_0^{\infty} \rho\omega_\nu(\rho)\, d\rho \int_\rho^{\infty} r\, \omega_\nu(r) \log r\, dr \right\}. \qquad [2.50]$$

Noting that the expression for the stream function

$$\psi_\nu(P,t) = \frac{-1}{4\pi} \int_A \omega_\nu(Q) \log R_{PQ}^2\, dA(Q),$$

considered at the origin, writes

$$\psi_\nu(o,t) = -\int_0^{\infty} r\, \omega_\nu(r) \log r\, dr, \qquad [2.51]$$

one transforms [2.50] into

$$H_\nu(t) = \frac{\Gamma}{2} \psi_\nu(o,t) + \pi \int_0^{\infty} \rho\omega(\rho)\, d\rho \int_\rho^{\infty} r\omega(r) \log \left(\frac{r}{\rho}\right) dr. \qquad [2.52]$$

Expression [2.52] may be used to evaluate numerically the value of the Kirchhoff function at any instant of time. The behaviour of H_ν as a function of the variable ξ is shown in Figure 13. In order to check the accuracy of the numerical procedure used to evaluate H_ν, the total

circulation (Γ) and the moment of inertia (G_ν) were also computed as functions of ξ; their behaviour with time is known (relevant details may be found in Appendix C). The circulation is seen to remain constant; the moment of inertia grows linearly with the expected rate, as predicted analytically. (see Appendix D).

The value of the Hamiltonian is no longer conserved in the presence of viscosity; this is to be expected in view of the relationship, examined in the following paragraph, between H_ν and the kinetic energy E of the fluid: viscous action leads necessarily to energy dissipation. The existence of this relation between H_ν and E, and knowledge of the expression giving the rate of change with time of the kinetic energy in terms of the viscosity, will be exploited to infer a value for the viscosity coefficient inherent in CTC computations. These relationships are established hereafter.

II.6.2.1 The relationship between H_ν and E

Consider the kinetic energy E_R of the fluid within a circle A of (large) radius R centered at the origin. The expression for E_R is

$$E_R = \frac{\rho}{2} \int_A u^2 dA \qquad [2.53]$$

and simplifies, for the case $u = u(r)$, to

$$E_R = -\rho\pi \int_0^R u\, r\, \frac{\partial \psi}{\partial r}\, dr \quad . \qquad [2.54]$$

A stream function $\psi(r)$ may be introduced since the fluid is incompressible. Recall that $u(r)$ stands for $u_\theta(r)$ and that

$$u_\theta(r) = -\frac{\partial \psi}{\partial r} \quad . \qquad [2.55]$$

Integration by parts yields the following expression for E_R:

$$E_R = \pi\rho \int_0^R \psi\, \omega\, r\, dr - \pi\rho\, [u\, r\, \psi]_0^R \quad ; \qquad [2.56]$$

use has been made of the fact that

$$r\omega_\nu = \frac{d}{dr}\,(ur). \qquad [2.57]$$

The Kirchhoff function H_ν^R is defined similarly to E_R:

$$H_\nu^R = \frac{\rho}{2} \int_A \psi\omega_\nu dA \qquad [2.58]$$

i.e.
$$H_\nu^R = \pi\rho \int_0^R \psi\omega_\nu r\, dr \quad ; \qquad [2.59]$$

equation [2.56] reads therefore

$$E_R = H_\nu^R - \pi\rho\, [r\, u\, \psi]_0^R \quad . \qquad [2.60]$$

For finite values of u and ψ at the origin, and observing that the factor of the integrated term at $r = R$ may be related to the circulation round the circumference of radius R, one rewrites [2.60] under the form

$$E_R = H_\nu^R - \frac{\rho}{2}\, \Gamma_R\, \psi\,(R) \qquad [2.61]$$

This expression, considered in the limit $R \to \infty$, shows that the kinetic energy and the Hamiltonian function of the whole fluid differ by a constant value; clearly then

$$\frac{dH_\nu}{dt} = \frac{dE}{dt} \qquad [2.62]$$

where $E = \lim_{R\to\infty} E_R$ and $H_\nu = \lim_{R\to\infty} H_\nu^R$.

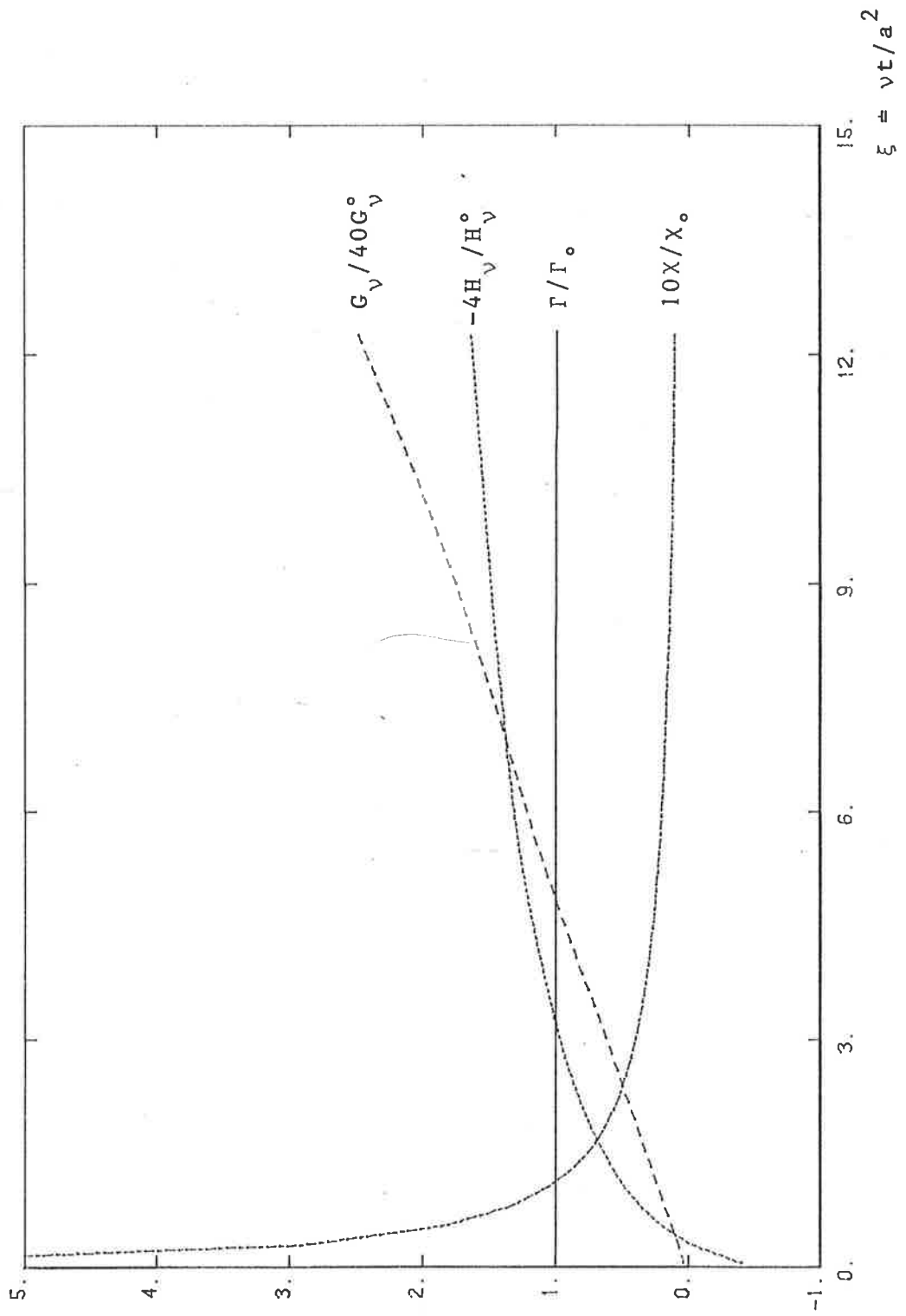

Figure 13 : Behaviour with time of circulation, Kirchhoff function, dissipation and moment of inertia during viscous decay of vorticity disk

Direct evaluation of dE/dt yields therefore the value of the time rate of change of the Hamiltonian.

II.6.2.2 The evaluation of dE/dt

An expression for dE/dt may be derived directly from equations [2.36] and [2.37] as follows. Multiplying [2.36] by r and subtituting into the resulting equation the value of $r\omega_\nu$ drawn from [2.37] lead to the evolution equation for u:

$$\frac{\partial u}{\partial t} = \nu \left(\frac{\partial^2 u}{\partial r^2} + \frac{1}{r} \frac{\partial u}{\partial r} - \frac{u}{r^2} \right) . \qquad [2.63]$$

Multiplying the above expression by ρu yields

$$\frac{\partial}{\partial t} \frac{\rho u^2}{2} = \mu \left(u \frac{\partial^2 u}{\partial r^2} + \frac{u}{r} \frac{\partial u}{\partial r} - \frac{u^2}{r^2} \right)$$

and successively:

$$\frac{\partial}{\partial t} \frac{\rho u^2}{2} = \mu\, u \frac{\partial}{\partial r} \left(\frac{\partial}{\partial r} + \frac{u}{r} \right)$$

$$= \mu\, u \frac{\partial}{\partial r} \left(\frac{1}{r} \frac{\partial}{\partial r} (ur) \right)$$

$$= \mu\, u \frac{\partial \omega_\nu}{\partial r} \qquad [2.64]$$

in view of [2.37]. Integrating over a circle of radius R leads to the expression

$$\frac{dE_R}{dt} = 2\pi\mu \int_0^R r\, u \frac{\partial \omega_\nu}{\partial r}\, dr$$

$$= \mu\, \Gamma(R)\omega_\nu(R) - 2\pi\mu \int_0^R r\, \omega_\nu^2\, dr$$

Taking the limit for $R \to \infty$ and noting that the vorticity distribution

vanishes at infinity, one obtains the required expression

$$\frac{dE}{dt} = - 2\pi\mu \int_0^\infty \omega_\nu^2 \; r \; dr \qquad [2.65]$$

This may be rewritten, in view of [2.62],

$$\frac{dH_\nu}{dt} = - \mu\chi \qquad [2.66]$$

where $$\chi = 2\pi \int_0^\infty r \; \omega_\nu^2 \; dr \qquad [2.67]$$

represents the dissipation function. This dissipation function is not constant in time, as seen on Figure 13. One notes that χ appears to vanish for large values of ξ, a result consistent with the behaviour of $H_\nu(\xi)$ which asymptotes a constant value at large times. The functions in Figure 13 have been plotted under the form $\Gamma/\Gamma_\circ$, $- 4\ H_\nu/H_\nu^\circ$, $10\ \chi/\chi_\circ$ and $G_\nu/40\ G_\nu^\circ$; scaling factors have been introduced to improve the legibility of the figure.

II.6.3 Viscosity estimates

Relation [2.66] provides a simple means of determining the magnitude of the viscosity associated with a CTC computation: at any instant of time, the viscosity coefficient is given by

$$\nu = - \frac{dH_\nu/dt}{\chi} \; , \qquad [2.68]$$

where H_ν is the computed Kirchhoff function (*). Alternatively, the viscosity coefficient may be inferred from the behaviour of the moment of inertia G_ν of the vorticity distribution by the expression

---

(*) the computer calculations are carried out for a fluid of unit density, i.e. consider the function H_ν/ρ.

$$\nu = \frac{1}{4} \frac{dG_\nu}{dt} \; ; \qquad [2.69]$$

Indeed, it is readily shown (see Appendix D) that $G_\nu(t)$ exhibits the exact time dependence

$$G_\nu(t) = G_\nu(o) + 4\nu t \; . \qquad [2.70]$$

Practically, estimates of ν based on H_ν are obtained at early times by observing that for $\nu t/a^2 = \xi << 1$, one may write

$$H_\nu(\xi) = H_\nu(o) + \xi \left(\frac{\partial H_\nu}{\partial \xi}\right)_0$$

$$= H_\nu(o) - a^2 \xi \, \chi_o \; , \qquad [2.71]$$

where

$$\chi_o = 2\pi \int_0^\infty \omega_\nu^2 (r,o) \; r \; dr$$

$$= 2\pi \; \omega_o^2 \int_0^a r \; dr = \pi \omega_o^2 a^2$$

is the initial value of the dissipation. One writes [2.71] as:

$$\frac{H_\nu(\xi)}{H_\nu(o)} = 1 - \frac{16 \, \xi}{(1-4 \log a)}$$

i.e.

$$\frac{H_\nu(\xi)}{H_\nu(o)} = 1 - 16\xi/C \qquad [2.72]$$

where $C = 1-4 \log a$ is a constant.

Equation [2.70] may be rewritten

$$\frac{G_\nu(\xi)}{G_\nu(o)} = 1 + 8 \, \xi \qquad \text{(all } \xi\text{)}. \qquad [2.73]$$

Two separate estimates of the viscosity may then be obtained from [2.72] and [2.73] from the expressions

$$\nu_H = - \frac{Ca^2}{16} \frac{d}{dt} \frac{H_\nu(t)}{H_\nu(o)} \qquad [2.74]$$

and

$$\nu_G = \frac{a^2}{8} \frac{d}{dt} \frac{G_\nu(t)}{G_\nu(o)} \quad . \qquad [2.75]$$

II.6.4 Discussion of results

The results of the computer runs are plotted in Figure 14, which shows the behaviour of the ratios ν_H/ν_{CTC} (crosses) and ν_G/ν_{CTC} (squares), as a function of the parameters δ and Δt^* (the choice of the independent variable, $\bar{d}\Delta t^{*2}/\delta$, $\bar{d}$ being the average distance between vortices, is clarified by the following argument). It is known (see section II.5.4) that for relatively large time steps and small cell sizes, the time rate of change of H_ν is given by

$$\frac{d}{dt^*} \frac{H_\nu(t^*)}{H_\nu(o)} = - \Delta t^{*3}/2 \quad . \qquad [2.76]$$

Equation [2.74] indicates that the rate of change is also given by

$$\frac{d}{dt^*} \frac{H_\nu(t^*)}{H_\nu(o)} = - \frac{32}{C} \frac{\nu_H}{\omega_o a^2} \quad . \qquad [2.77]$$

Now the expected viscosity, as given by [2.32], is known to be

$$\nu_{CTC} = \frac{\delta^2}{12\ \Delta t} = \frac{\delta^2\ \omega_o}{24\ \Delta t^*} \quad . \qquad [2.78]$$

Substitution of [2.78] into [2.77] yields

$$\frac{d}{dt^*} \frac{H_\nu(t^*)}{H_\nu(o)} = - \frac{4}{3C} \frac{\delta^2}{\Delta t^* a^2} \quad . \qquad [2.79]$$

As predicted by results [2.76] and [2.79], the ratio of the "viscosity" ν_H inferred from [2.77] to the expected viscosity ν_{CTC} must be unity when

$$\frac{\Delta t^{*4}}{\delta^2} << \frac{8}{3C} \frac{1}{a^2} \quad , \qquad [2.80]$$

while it must behave like

$$\frac{\nu_H}{\nu_{CTC}} = \frac{3C}{8} \; a^2 \; \frac{\Delta t^{*4}}{\delta^2} \qquad [2.81]$$

when the inequality [2.80] is reversed.

Identical predictions may be drawn for the estimate ν_G, using equation [2.75] and replacing [2.76] by

$$\frac{d}{dt^*} \; \frac{G_\nu(t^*)}{G_\nu(o)} = \Delta t^{*3}/4 \; .$$

Equation [2.81] may be rewritten in terms of the average distance $\bar{d}$ between vortices, using the estimate drawn from the relation $\pi a^2 = NV \, \bar{d}^2$. Figure 14 uses logarithmic scales, for which one has

$$\log \left(\frac{\nu}{\nu_{CTC}} \right) = \log \left(\frac{3C}{8} \; \frac{NV}{\pi} \right) + 2 \log \left(\frac{\bar{d} \; \Delta t^{*2}}{\delta} \right) \qquad [2.82]$$

everywhere, except for values of the independent variable satisfying

$$\log \left(\frac{\Delta t^{*2}}{\delta} \right) << \frac{1}{2} \log \left(\frac{8}{3Ca^2} \right) \qquad [2.83]$$

where $\log (\nu/\nu_{CTC})$ must vanish.
Some of the scatter in the results is due to the difficulty in estimating the slopes of the functions $H_\nu(t^*)$ and $G_\nu(t^*)$ which tended to fluctuate about the linear trend. In addition, the criterion [2.31] of Milinazzo & Saffman could not be met given the imposed constraint that all vortices be able to move at least one half a cell length in the time step Δt^*. Basically, however, results corroborate the validity of the arguments developed above.

The essential conclusion from this analysis is that the combined effects of the choice of cell size and time step are completely understood.

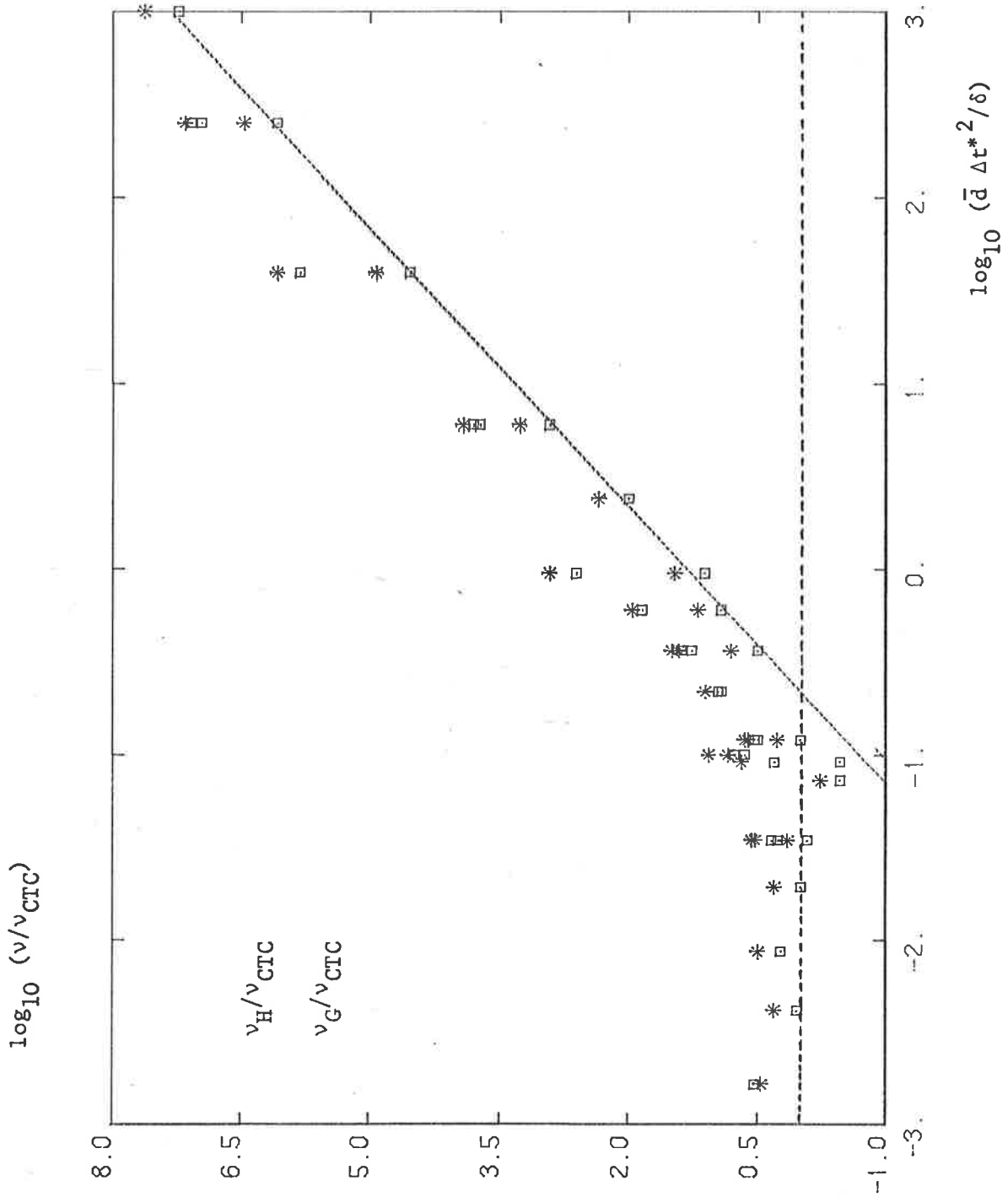

Figure 14: Viscous effects in the CTC method: dependence of estimated viscosities with time step and cell size. Predictions [2.80] and [2.81] are shown by dashed lines.

Unless the time step is very small, the one-sided integration error dominates the overall accuracy of the computation: the random relocation errors are comparatively insignificant. For sufficiently small time steps, however, the grid errors introduce a diffusion of the gradient type, for which the coefficient of viscosity is predictable. Varying the magnitude of the viscosity by adding a further random component of velocity appears therefore a simple possibility.

II.7 THE ROLLING-UP OF A VORTEX SHEET

Previous results indicate that the CTC method, coupled with Euler's modified method for the integration of the equations of motion, is a satisfactory device for the computation of flows of point-vortices. Intrinsic viscous effects are non-existent in comparison with integration error effects, when realistically large time steps and reasonably small cell sizes are employed. The criterion [2.80] is useful as an indication of the type of behaviour that may be expected for a particular choice of the parameters, although the connection between the problem at hand and the problem of the disk may not be a direct one.

The problem of the rolling-up of a vortex sheet (Westwater's problem) was finally considered, with two purposes in mind: firstly, to apply the CTC method to a geometrically-different problem presenting the added complexity of vortices of different strengths and, secondly, to assess the potential of the cloud discretization approach, as opposed to the classical "line" discretization used by Westwater.

II.7.1 Westwater's roll-up problem

The trailing vortex sheet that develops behind an elliptically-loaded lifting surface may be considered as essentially two-dimensional far

enough downstream. The problem reduces to the computation of the self-induced motion of an initially straight vortex segment along which the vorticity is distributed according to the relation

$$\omega(x) = 2Ux(\ell^2-x^2)^{-\frac{1}{2}} \qquad [2.84]$$

in a reference frame where the segment lies on the axis $y = 0$, over the interval $-\ell \leqslant x \leqslant \ell$. U is the constant speed of the wing that generates the vortex sheet.

In a conventional PVA approach, the continuous sheet is divided into an even number of equal intervals; equivalent point vortices are then placed at all interval mid-points, and their subsequent motion followed. The geometrical line that connects the successive vortices is regarded as a suitable marker for following the deformation of the vortex sheet. The circulation of the vortex located at $x = x_\alpha$ is computed as

$$\kappa(x_\alpha) = \int_{x_\alpha-\Delta/2}^{x_\alpha+\Delta/2} \frac{2U\xi\, d\xi}{(\ell^2-\xi^2)^{\frac{1}{2}}} , \qquad [2.85]$$

Δ being the distance between adjacent vortices. This integral is evaluated explicitly to yield

$$\kappa(x_\alpha) = 2U\ell(\cos\theta^+ - \cos\theta^-) , \qquad [2.86]$$

where θ^+ and θ^- are given by the relations

$$\begin{aligned} \ell \sin\theta^+ &= x_\alpha + \Delta/2 \\ \ell \sin\theta^- &= x_\alpha - \Delta/2 . \end{aligned} \qquad [2.87]$$

This discretization scheme was employed to define the initial configuration of the vortices in the following CTC analysis. Five calculations were

carried out with the values of the parameters NV (number of vortices), N_δ (cell size parameter) and Δt^* (adimensional time step) given in the table below.

Run	NV	N_δ	Δt^*
1	120	15	.001
2	120	149	.001
3	120	1499	.001
4	240	14999	.001
5	120	14999	.0005

The computation cell size was chosen here as $\delta = \Delta/N_\delta$ and the time made dimensionless using the velocity U and length ℓ. All runs were conducted with $U = \ell = 1$. Results are presented in Figures 15a to 15c. All observed flow features agree fully with those obtained by Moore (1971). A chaotic trend in the motion of the vortices emerges rapidly, accompanied by physically unacceptable distortions of the geometrical - and supposedly material - line that joins the vortices. There is evidence of the development of a "Kelvin Helmholtz" instability by which neighbouring vortices tend to agglomerate and henceforth evolve as "twin" vortices. This instability originates in the rolled-up portion of the sheet and propagates rapidly towards its centre. The behaviours of the Hamiltonian and of the quantity $\Gamma G = \sum_{\alpha}^{NV} \kappa_\alpha (x_\alpha^2 + y_\alpha^2)$, depicted in Figures 16a and 16b, confirm that the accuracy of the method is easily controlled. The Hamiltonian is seen to be more sensitive to change in values of the parameters than the other invariant; this justifies the choice of Hamiltonian as a suitable indicator for the accuracy of the computation.

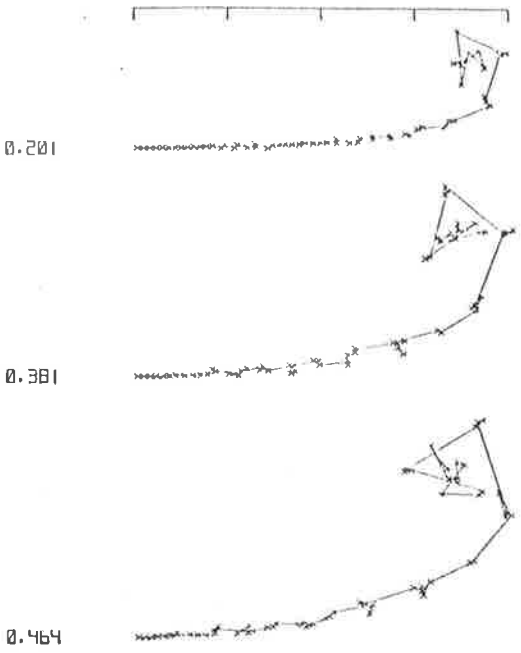

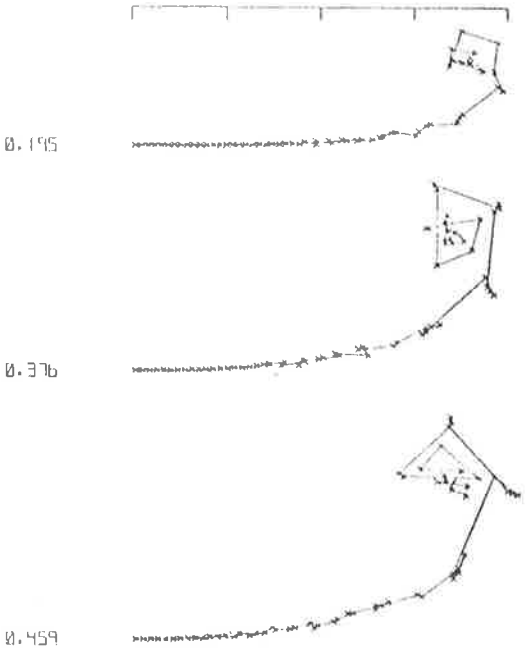

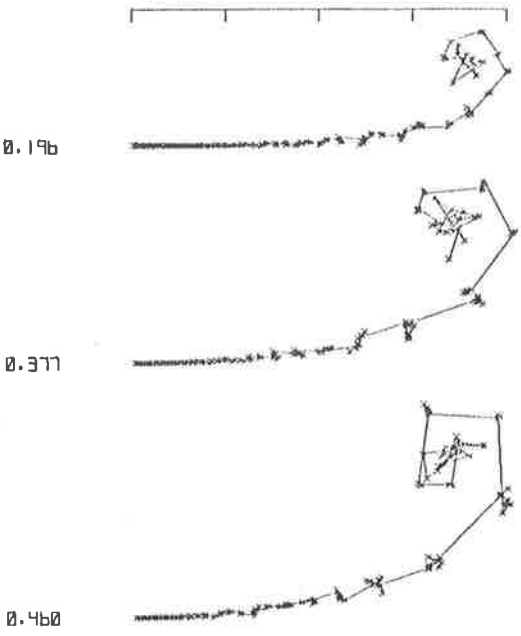

Figures 15a, b & c

Rolling-up of a vortex sheet, discretized as a single row of vortices

Runs

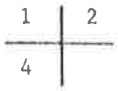

Figures

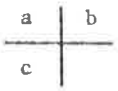

The displacement of the sheet is given for each configuration.

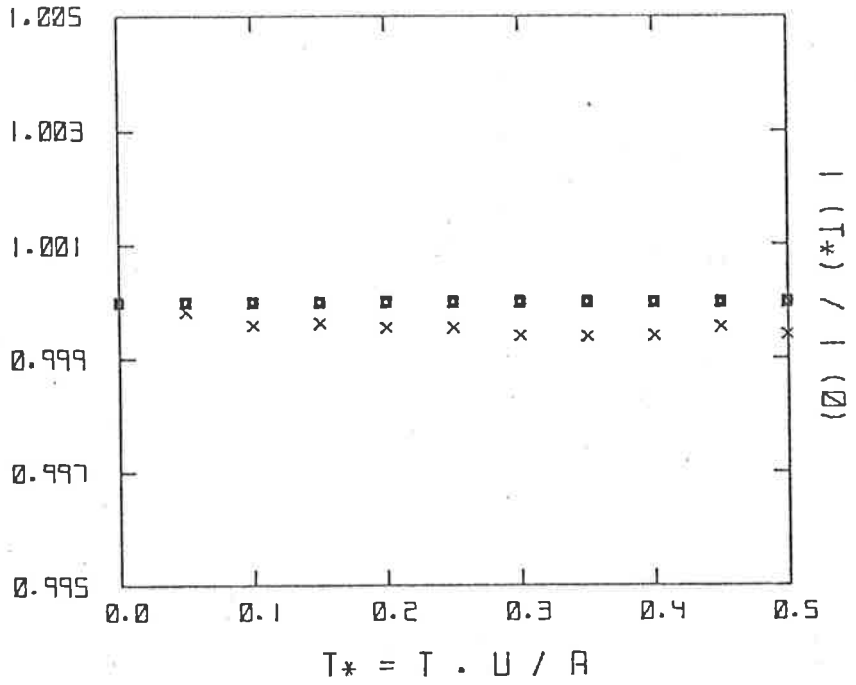

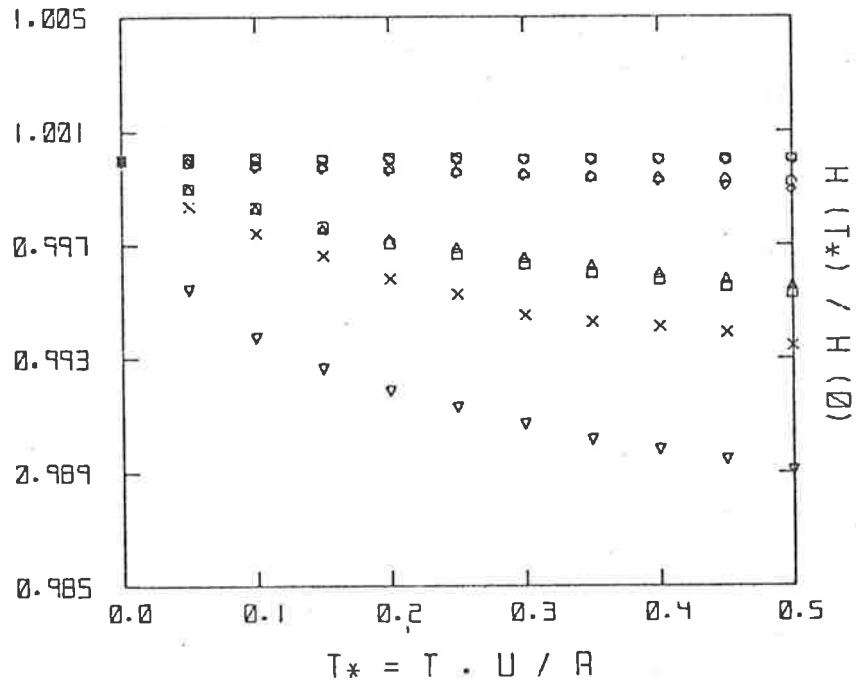

Symbol	Run
×	1
□	2
△	3
▽	4
◇	5
⌂	6
▽	7
◇	8

Figures 16a & 16b. Invariants Γ(0) and H as a function of time for the roll up of a vortex sheet. (Refer to tables pages 68 & 70 for definition of runs).

Failure to model the continuous flow stems not from the computing method; indeed, it is known from Moore's study that the discretization itself is responsible for the anomalies observed. In a recent work, Fink & Soh (1978) have convincingly demonstrated that the PVA, as anticipated by Moore, does not yield a complete discretized form of the integral equation that describes the motion of the continuous vortex sheet. Additional terms that become necessarily large must be taken into account, and radically affect the flow pattern. One is led to conclude that the conventional PVA used in the vortex sheet roll-up problem is clearly inadequate. The idea of adopting another type of discretization, based on the cloud discretization concept, is explored in the next section.

II.7.2 The Cloud Discretization Approach

Westwater's analysis, in its classical formulation, bears little relation to the physical problem. The wing-tip vortex system generated by a moving aircraft has necessarily a finite thickness; furthermore, the action of viscosity diffuses the vortex sheet which soon loses the sharpness of its initial definition. These physical arguments suggest that the sheet may be validly discretized using several superimposed layers of vortex filaments that confer a small, but finite thickness to the discretized system. The evolution of the configuration of vortices describes the motion of the sheet in a cloud-like manner, and must be interpreted in the appropriate, average sense (see Section II.3). In this coarser description of the flow, the question of determining the exact geometrical deformation of the vortex sheet cannot be clearly answered; other global flow features, however, like the speed of the sheet mid-point, or the rate at which vorticity enters the spiral, are likely to be well approximated.

The cloud discretization idea was tested on the roll-up problem as

follows. The sheet was discretized as the superposition of several layers of equidistant vortices. Three cases were considered, as shown in the table, where h represents the distance between layers.

Run	NV	N_δ	Δt^*	h/Δ	Layers
6	120	14999	$5\ 10^{-4}$	0.5	2
7	120	14999	$5\ 10^{-4}$	1.5	2
8	120	14999	$5\ 10^{-4}$	0.5	3

The value of the circulation at a given abscissa was computed according to [2.86] & [2.87] and divided evenly between all vortices located at that abscissa. Runs 6 and 7 were conducted with two layers differently spaced and run 8 with three layers.

Figures 17a to 17c present several configurations of the vortex system. The geometrical line linking successive vortices has been deliberately omitted to convey the impression of a cloud that must prevail when interpreting these figures. The occurence of an orbital "Kelvin-Helmholtz" instability is still visible in the elongated parts of the spiral, where vortices issuing from different layers show a clear tendency to pairing. The instability is less pronounced for the higher ratio h/Δ, and is hardly noticeable for the triple-layer discretization. This improvement can be attributed to the fact that vortices are being fed into the spiral from each layer alternatively, more uniformly in the three-layer case than in the two-layer one. This leads to an increased definition of the outside arc of the spiral and the inhibition of the tendency toward "vortex satellisation" by the improved balancing action of the local

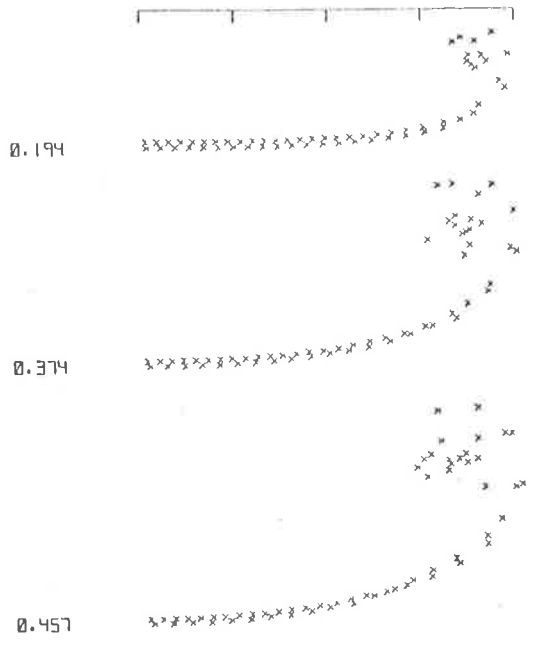

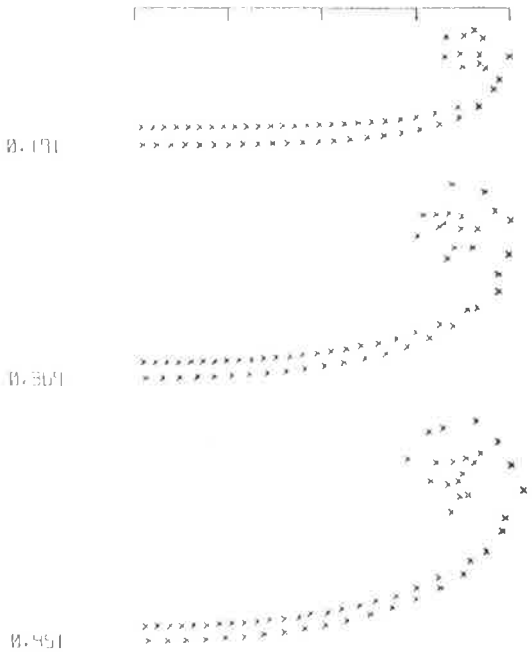

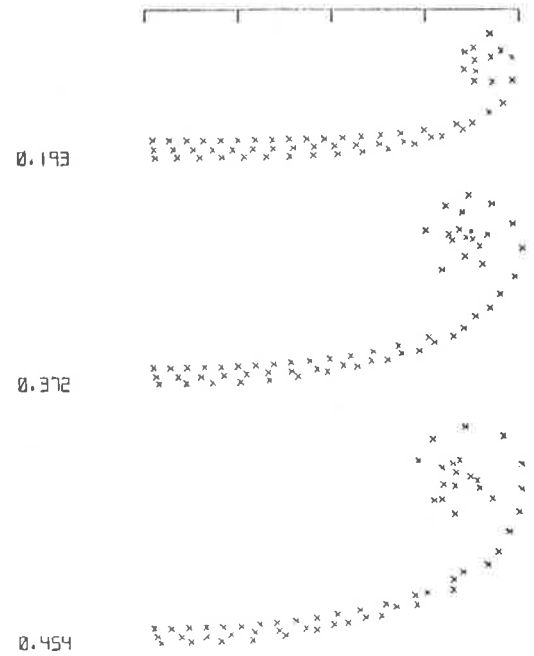

Figures 17a, b & c
Rolling up of a vortex sheet
discretized as several rows of vortices.

Runs 6 | 7
8

Figures a | b
c

influences. Examination of the behaviour of the two invariants (Figures 16a and 16b) confirms that the accuracy of the computation is better than that of the most accurate single layer discretization (i.e. runs 4 and 5).

The behaviour of the sheet was followed over a longer period in the case of the triple layer discretization. Figures 18a and 18b depict flow configurations after 3200 and 5200 time steps respectively ($t^* = 1.6$ and $t^* = 2.6$). It is interesting to note how accurately the invariance is preserved by the CTC computation after long time intervals; after 5200 time steps, one recorded the ratio values

$$\frac{G}{G_o} = 1.000021 \quad ; \quad \frac{H}{H_o} = 1.000256.$$

II.8 SUMMARY

The central purpose of Chapter II is to present the numerical method used in this work to compute the temporal evolution of two-dimensional, rotational flow fields; this method is an application of the point-vortex approximation.

A novel point-vortex tracing algorithm has been developed, in which the flow field is subdivided into a grid and vortices are always located at the centres of the cells. In the spirit of "centre-to-centre" (CTC) calculations, no attempt is made to try and track vortices exactly; flow features are determined in a statistical sense, as averages over varying initial conditions, that is, over several "realizations" of the corresponding continuous problem. This point of view has been termed the "cloud discretization approach". Attention is drawn on the existence of invariants in two-dimensional vorticity fields, and to their utility for monitoring the accuracy of point-vortex calculations. In particular, the evaluation of the

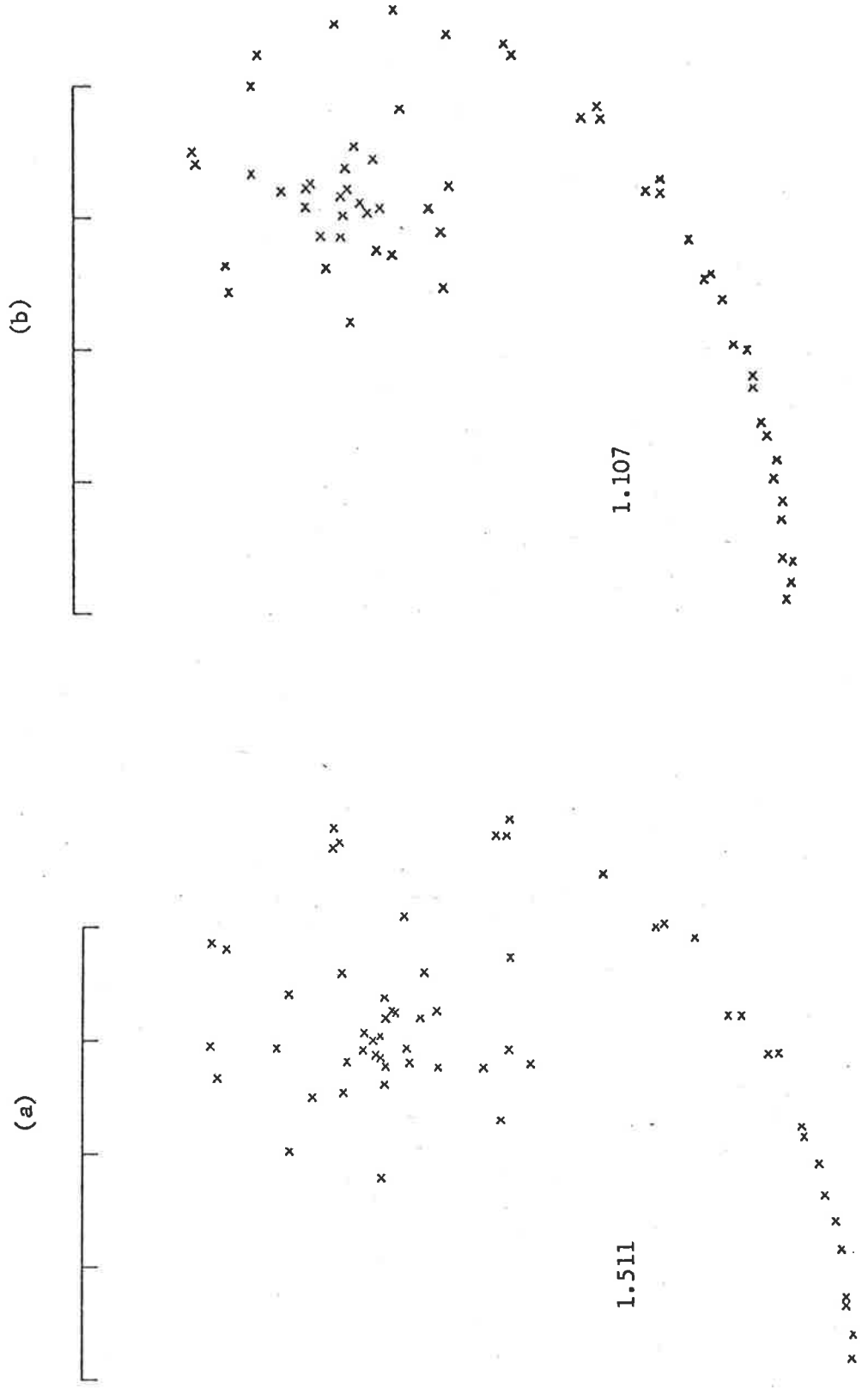

Figures 18a & b: Large time configurations of vortex sheet
(Run 8: triple layer discretization)
(a): $t^* = 1.6$ (3200 time steps)
(b): $t^* = 2.6$ (5200 time steps)

numerical effects on the energy invariant (the Kirchhoff function or Hamiltonian of the system) appears as a crucial aspect of the CTC method.

The properties of the CTC method have been thoroughly investigated on the basis of the problem known as Rankine's vortex. The essential conclusion from the results obtained is that the combined effects of the basic characteristic parameters (cell size and time step) are fully understood; these effects may be quantitatively predicted in terms of their influence on the energy invariant. The importance of the choice of the numerical integration procedure is also demonstrated. The performance of the CTC algorithm and the relevance of the cloud discretization approach are illustrated on the problem of Westwater, the rolling-up of an elliptically loaded vortex sheet. An attractive feature of the CTC scheme is without doubt its simplicity, which allows the nature of the errors resulting from the various approximations to be explored relatively easily. The centre-to-centre method may well constitute a simple answer to many problems connected with the point-vortex approximation. The remarkable lack of sensitivity of integral flow quantities to large changes in cell size - of itself an intriguing property - strongly suggests that the use of complicated stratagems to remove the singular character of the point-vortex velocity field (e.g. locally diffusing vortices, Kuwahara & Takami, 1973) cannot be seriously justified in comparison with the simple vortex-relocation technique of the CTC method. On the other hand, the necessity of employing an accurate scheme for the integration of the equations of motion has implications that must be considered in any point-vortex tracing scheme.

Finally, the ability of the CTC method to preserve all invariants of the motion presents advantages that cannot be claimed by other available techniques, in particular with all methods where arbitrary amalgamations are forced upon the vortices, leading to unavoidable discontinuities in the

value of the invariants. The removal of any ad-hoc mechanism that controls the amalgamations of vortices is without doubt another satisfactory aspect of the method.

The proposed computation method allows a very significant saving in computing time, since the velocity of any one vortex becomes a function of the integer number of x and y - spacings; the function values may be tabulated prior to any computation. Although the resulting algorithm is faster than most other "summation algorithm" methods, it does not match the computing speed of Fast Poisson Solvers. It is likely, however, that a combination of the CTC method and a Fast Poisson Solver or a Fast Fourier Transform technique would provide an even more efficient computing code.

CHAPTER III : THE LARGE-SCALE STRUCTURE IN PERIODIC, TWO-DIMENSIONAL VORTICITY LAYERS

III.1 INTRODUCTION

In many free turbulent flows there is a suggestion that some features arise from the properties of a *rotational* but *inviscid* flow. This is the case for vortex shedding at high Reynolds number, and probably for the plane mixing layer which appears to be dominated by a quasi-*two-dimensional*, large-scale structure (Brown & Roshko, 1974). Recent results (Browand, 1978; Wygnanski et al, 1978) confirm the large transverse correlation scales of these structures.

The motion pictures of the mixing layer (Brown & Roshko, 1974) leave little doubt that the mechanics of the mixing layer is dominated by the development and interactions of roller-like structures which originate from the Kelvin-Helmholtz instability of the initial vortex sheet. This impression is supported by various experimental observations. Browand & Weidman (1976) find, at moderate Reynolds number, an essentially two-dimensional flow, in which the mixing layer grows by the pairing of large structures; the flow, whilst not having the three-dimensional velocity fluctuations distribution of the higher Reynolds-number flow (i.e. $\overline{v'^2} \approx \overline{w'^2}$), exhibits a Reynolds-stress similarity. Konrad (1979) determined a critical threshold Reynolds number beyond which the small-scale turbulent energy experiences an increase of at least one order of magnitude, without significant changes in the estimated growth rate of the layer.

Thus, through in many turbulent flows one deduces from the mean profiles that the flow is relatively viscous to account for the stress, it is of interest to ask how much of this stress results from a large-scale unsteady motion of either an *inviscid* rotational fluid, or a "turbular" fluid (after the terminology of Liepmann), i.e. one in which a secondary small-scale motion can be considered to act like an enhanced viscosity, yet

of much smaller value than the eddy viscosity deduced from the mean profile. The mixing layer is the simplest flow in which to test this idea, and possibly the one where, if at all, it is likely to be true. It is worth noting that sub-grid scale models of turbulence rely on this possibility (Clark et al, 1977).

In any case, and whatever its connection to conventional turbulence, it seems very likely that the sensitivity of normally turbulent flows to external forcing - observed in jets (Moore, 1977; Acton, 1977) and mixing layers (Oster et al, 1978; Abell, 1977) - is related to the rotational inviscid behaviour of such a flow. Similarly, the sensitivity to initial conditions (Batt, 1975), the role of feedback (Dimotakis & Brown, 1976), the resonances in turbulent flows past a cavity and more general acoustic couplings and resonances of turbulent flows (Ho & Nosseir, 1978) appear to be explicable in terms of large structures and their dynamics. Furthermore, the strong effects of density ratio on the entrainment ratio (Brown, 1974) or the effects of streamline curvature in the mean flow (Bradshaw, 1973) seem likely to arise through their action on the large-scale motion.

There arguments appeared sufficient to motivate a study of the dynamics of the large-scale structure in mixing layers, using an unsteady, two-dimensional calculation. In all problems considered in this work, there is no suggestion that such a model could do more than shed light on some properties of the large-scale structure. There is obviously no vortex stretching and, for an inviscid fluid, no dissipation, both of which are crucial in the usual energy cascade argument. The intriguing question is, *how important* are vortex stretching and dissipation in the evolution of the structure, in the generation of the stress, and in the response of the layer to perturbations. The usefulness of a model without these two physical mechanisms does not seem a priori impaired; their absence may

indeed prove as illuminating as the inclusion and complex interactions of several effects of unknown relative significance.

The two-dimensional evolutions of inviscid and viscous vortex sheets were modelled by following the positions in time of 750 point vortices initially distributed in a thin layer; the vortices were tracked using the CTC method. The essential aim of this chapter is to present the results that were obtained in these calculations.

III.2 THE TURBULENT MIXING LAYER IN THE LABORATORY

It is appropriate to begin this chapter by a brief description of the turbulent mixing layer as it is observed in experimental facilities, such as the one described by Brown & Roshko (1974). The arrangement used in the laboratory to generate nominally two-dimensional turbulent mixing layers has the idealized geometry sketched on Figure 19. Two parallel, plane streams of respective uniform velocities U_1 and U_2 are separated by a rigid, semi-infinite plane aligned in the direction of the flow. The streams come into contact at the edge of the plane and are then allowed to mix freely. The fluids may or may not be different; in the former case, the fluid densities are denoted by the symbols ρ_1 and ρ_2 .

The major events in the evolution of "conventional" turbulent mixing layers may be summarized as follows. The vortex sheet emanating from the splitter plate suffers an instability associated with the inflection point in the velocity profile. This instability is essentially inviscid and in its early stages, is well predicted by linear stability theory. As the instability amplifies, non-linear interactions develop and the vortex sheet rolls up into classical "Kelvin-Helmholtz" billows, loosely interpreted on the basis of visualizations as "concentrations of vorticity". These

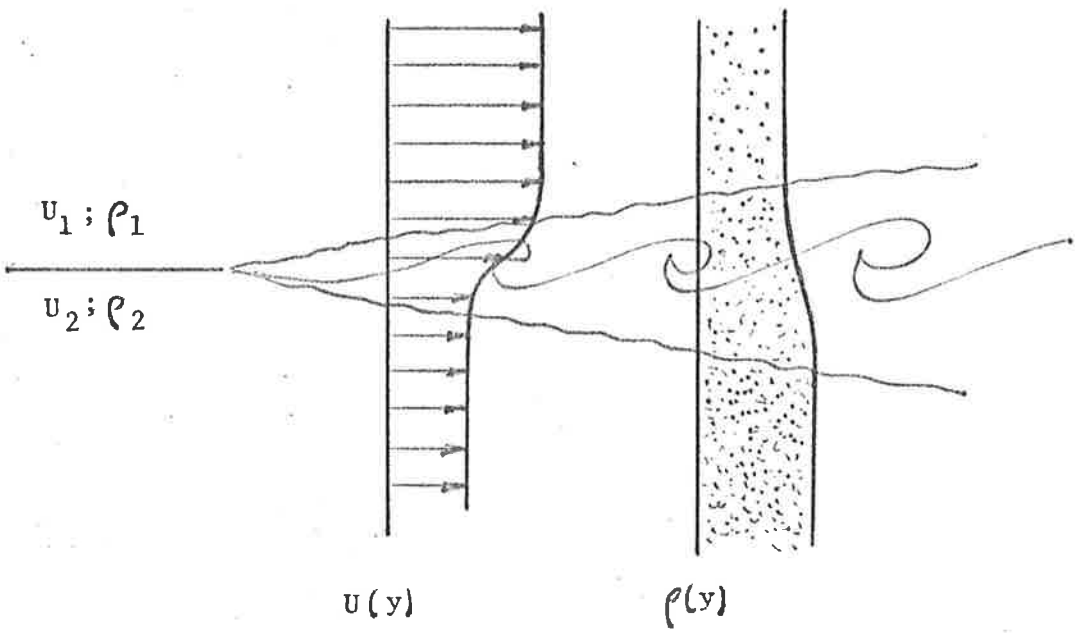

Figure 19. Idealized "spatial" mixing layer.

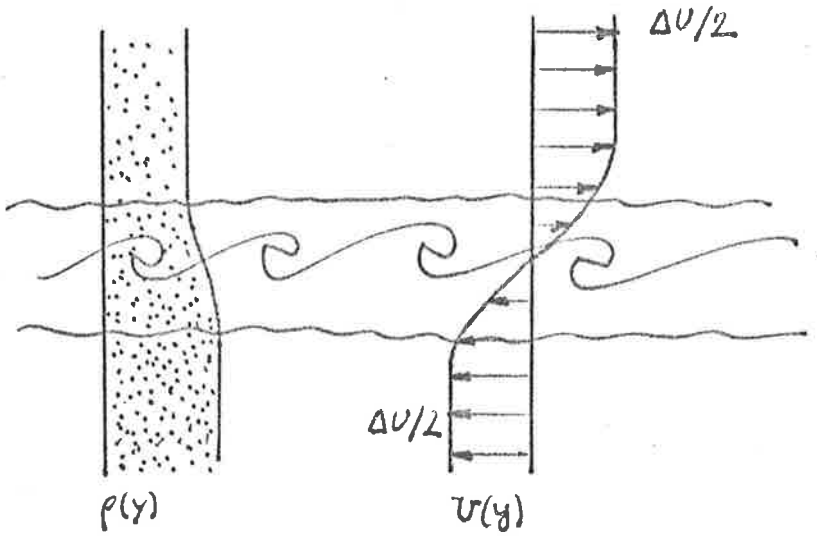

Figure 20. Idealized "temporal" mixing layer.

billows interact and are themselves subject to internal instabilities, viscous diffusion and external perturbations. These mechanisms are central to the transition process to a fully turbulent state characterized by three-dimensional velocity fluctuations. That this "turbulent chaos" may be, under certain conditions, replaced by (or indeed constituted of) a coherent essentially organized, two-dimensional structure is demonstrated (suggested) by the shadowgraphs of Brown & Roshko (1974), taken in high Reynolds-number mixing layers. However, whilst several investigations (Dimotakis & Brown, 1976; Oster et al, 1978; Wygnanski et al, 1978) have reported the existence of the structure - and confirmed its large transverse correlation scales (Browand, 1978) - the structure has not been identified in a number of studies (refer to Chandrsuda et al, 1978). These apparent discrepancies bring about essential, partly unanswered questions. Should the large-scale structure be regarded as a relic of the instability mode of a laminar shear layer, which has persisted due to favourable conditions? Does the structure develop if the initial boundary layer is transitional or fully turbulent? More precisely, what is the importance of the initial conditions, specifically on the existence of the structure, and, generally, on the development of the layer? Similarity considerations and the occurence and uniqueness of an asymptotic state must also be reexamined in terms of the existence of a persistent, apparently deterministic, large structure.

These fundamental issues have triggered a renewal of interest for the turbulent mixing layer, as witnessed by the numerous contributions recently published on the subject in the literature (see for example the proceedings of the conference on the "Structure and Mechanisms of Turbulence", Berlin 1977; Springer-Verlag, Fiedler editor, 1978). Despite these efforts, the problem of turbulence in the mixing layer - an apparently "simple" flow - remains theoretically unresolved; this reflects the general inability

of present analytical theories of turbulence to cope with real flow situations. A study of the evolution of vorticity layers, in which the essential characteristics of the large-scale structure, two-dimensionality and Reynolds-number independence, are imbedded, appears therefore well worth while in the context depicted above. The following sections show how the problem was tackled in the scope of the point-vortex approximation.

III.3 POINT-VORTEX MODELLING OF TURBULENT MIXING LAYERS

III.3.1 Periodic Vorticity Layers

The "turbulent" character of the mixing layer in an inviscid, two-dimensional fluid was first recognized by Kadomtsev & Kostomarov (1972). Their numerical, point-vortex study of the spatial problem was, however, unable to uncover the existence of a large-scale structure. (It is in fact interesting to note that they identify the turbulent character of the layer by referring to the absence of a "regular chain of vortices" in the computed flow configurations.) The lack of evidence of an organized vortex structure in their computations may be attributed to various factors. There is, first, the poor resolution in the definition of the vorticity field connected with the limited number (100) of vortices used in the discretization of the free shear layer. The presence of an absorbing wall - normal to the direction of flow and placed some distance downstream of the "splitter plate" edge, necessary to limit the extent of the computation interval, introduces boundary effects of unknown importance. Finally, and more importantly, there is the possibility that the technique employed for the shedding of vortices at the partition trailing edge was critical to the subsequent layer development (see Clements & Maull, 1975). These uncertainties illustrate the intrinsic difficulties associated with

the modelling of the spatial problem. In order to avoid the complexities brought about by the presence of boundaries, consider the following problem (refer to Figure 20).

Imagine an observer attached to a Galilean reference frame moving downstream with a convection velocity $U_M = \frac{1}{2}(U_1+U_2)$. This observer sees the growth with time of a turbulent shear layer driven by a velocity difference $\Delta U = U_1 - U_2$. The mixing layer flow, viewed in this different perspective, can be idealized as follows. Two half-planes, filled with the same fluid or with fluids of different densities, are separated by a membrane set on the axis $y = 0$. In both half-spaces, motion is taking place with uniform velocities, $U_1 = \Delta U/2$ in the upper half plane, $U_2 = -\Delta U/2$ in the lower half-plane. At some initial instant, the membrane is suddenly removed, creating an unstable interface, effectively a vortex sheet of strength ΔU per unit length, which will deform and eventually become turbulent, for any small initial perturbation in the case $\rho_1 = \rho_2$ or spontaneously for $\rho_1 \neq \rho_2$. This idealization defines the *temporal problem*. The modelling of the temporal problem amounts, therefore, to the computation of the self-induced motion of an infinite, perturbed vortex sheet.

Computations of finite-length vorticity layers suffer from a major disadvantage: the ends of the vortex sheet roll up, resulting in strong tip vortices that induce rapidly unacceptable distortions of the whole velocity field. It is more satisfactory to consider infinitely-periodic vorticity layers, generated by the cyclic repetition of a layer of finite length. Periodic vorticity distributions $\omega_p(x,y,t)$ satisfy the requirement that

$$\omega_p(x,y,t) = \omega_p(x \pm nL,y,t) \quad (n = 1,2,3,\ldots) , \qquad [3.1]$$

L being the length of the basic definition interval.

It is clear, in view of [3.1] and [1.54] - [1.55], that row-vortices provide a suitable means of discretizing periodic vorticity fields. The motion of a cloud of NV row-vortices initially at rest in a given configuration ($(x^\circ_\alpha, y^\circ_\alpha; \kappa^\circ_\alpha)$ specified) is obtained by numerical integration of equations [1.56].

The simplicity of the summation algorithm for row-vortices is, in conventional tracing methods, heavily penalized by the computation load that arises from the (costly) evaluation of the hyperbolic- and circular-function terms in formulae [1.56]. The CTC method drastically reduces the computing effort by allowing the pretabulation of these terms. Distances between vortices in the CTC method are necessarily multiples of the cell size, so that

$$X_{\alpha\beta} = \delta x(J_\alpha - J_\beta) = \delta x\, J_{\alpha\beta}$$

$$Y_{\alpha\beta} = \delta y(I_\alpha - I_\beta) = \delta y\, I_{\alpha\beta} \,. \qquad [3.2]$$

The integer $J_{\alpha\beta}$ ($I_{\alpha\beta}$) takes any of the possible values 0,1,2,...,NG-1 (MG-1), if the computation grid has NG columns and MG rows. The functions $\sin \frac{2\pi}{a} X_{\alpha\beta}$ ($\cos \frac{2\pi}{a} X_{\alpha\beta}$) and $\sinh \frac{2\pi}{a} Y_{\alpha\beta}$ ($\cosh \frac{2\pi}{a} Y_{\alpha\beta}$) take accordingly any of NG(MG) possible values, which need be computed only once and stored in a table for further, quick reference (typically NG & MG ~ 5000). This procedure reduces the central processing time by a factor of the order of 10 (CDC 6400 computer).

III.3.2 The initial flow configurations

Two of the serious criticisms that have been made about vortex modelling studies of turbulent flows refer to the lack of "predictive ability" of the method, and to the questionable validity of its "post-

dictions" in view of the arbitrary choices for the vortex interaction law and for the method of simulating diffusion effects (Saffman, 1977). A constant concern in this study has been not only to reduce the arbitrariness and uncertainties of the method by avoiding the use of ad hoc computation stratagems, but also to try and assess the predictive ability of the PVA by minimizing the amount of information fed into the model about the phenomenon to be investigated. The choice of appropriate, realistic initial flow configurations is an important step of the modelling process and was guided by the following considerations.

It is argued in linear stability theory that arbitrary perturbations (of a basic flow configuration) may be viewed as the superposition of "normal modes" and that stability characteristics are, consequently, suitably analyzed in terms of elementary Fourier components (see for example Chandrasekhar, 1961). This approach has prevailed in most point-vortex studies of the infinite vortex sheet problem, where the initial configuration consists of a sinusoidal perturbation (Rosenhead, 1931; Zalosh, 1976; Acton, 1976). An alternative point of view has been adopted here. Initial configurations are obtained by randomizing the positions of the vortices within a narrow strip along the interface, as shown on Figure 21. The random element in the initial conditions is introduced at two distinct levels. Initializations of the first type - "type-I flows" - are characterized by a uniform circulation per unit length: the randomization only affects the lateral positioning of the vortices. Initial conditions of the second type - "type-II flows" - are fully random : they present non-uniformities in circulation per unit length as well as in the lateral positioning of the vortices.

Randomized vorticity distributions provide a reasonably unbiased starting point to investigate the possible universal character of vortical

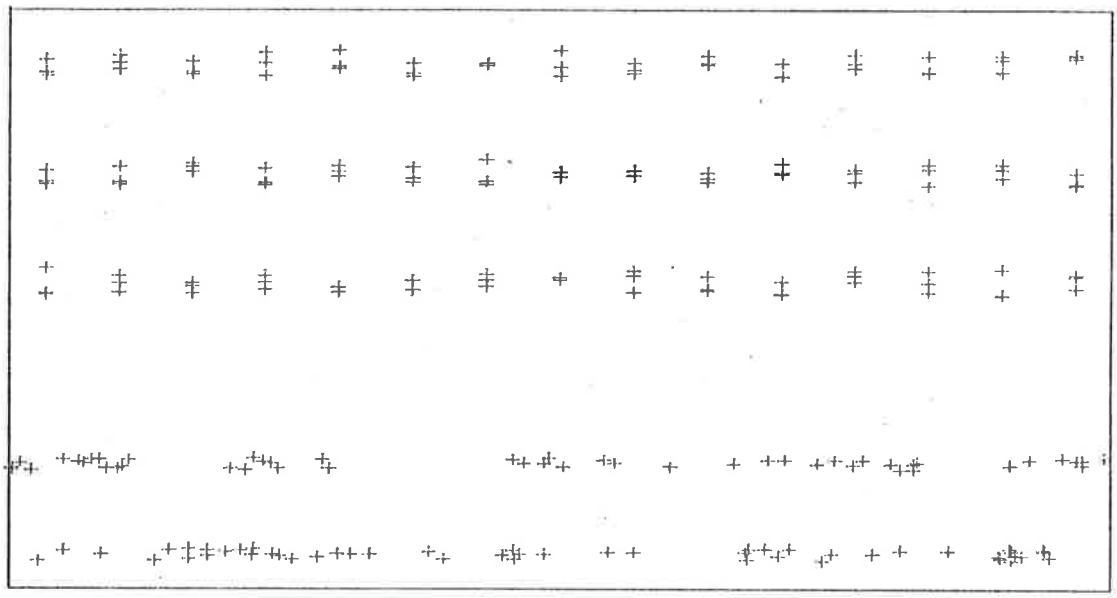

Figure 21: Typical random initializations of vorticity layers, showing 15 segments out of the 250 that are distributed over the interval L. The top three layers are of the first type; two type -II are shown at the bottom.

large structures: the Fourier components of the perturbation fields at flow initiation cover, in principle, an extended range of wavenumbers. It is therefore interesting to consider the outcome of the instability mechanism in the light of linear instability theory. A further justification for the choice of initial conditions is found in the observation that random distributions of vorticity emerge spontaneously from initially uniform, unperturbed vortex sheets under the action of viscosity (this action being equivalent to random displacements of vortices in the discretized system).

In selecting these initial conditions, it also seemed important to have very large aspect ratios (length of cyclic interval L : initial vorticity thickness δ_ω°) to try and avoid substantial effects due to the periodic interval. The use of a large number of vortices was necessary to achieve a reasonable visualization of the vorticity regions. Specific type -I and type -II flows were generated as follows. The cyclic interval was divided into 250 equal lengths. In type -I flows, three vortices were placed at the middle of each of the 250 segments (to give the uniform circulation per unit length); their vertical positions were chosen from 14 possible locations in a total height equal to approximately one-half of the segment length. In type -II flows, the 750 vortices were allocated in a fully random way over the 250 segments and within a height of 1/4 of a segment length. A standard random number generator was used to obtain the uniformly distributed random numbers. Two type -I and three type -II flows were studied; the layers were followed until their aspect ratio dropped at the most to a value of 3 (typically, not less than 10).

III.3.3 Selecting time step and cell size

The choice of time step was guided by considerations about allowable changes in the energy invariant of the system of vortices during a complete calculation. Order of magnitude estimates for $\Delta H/H_o$ may be obtained from a generalization of the results obtained for the test case of Rankine's vortex. This required interpreting the adimensional time previously used, $t^* = t\omega_o/2$ (see section II.5.3), in terms of the characteristic rotation period $\tau = d^2/\gamma$ of neighbouring vortices (d is the average distance between the vortices; γ is the vortex strength); clearly $t^* = t/2\tau$. Observing that the calculations are to follow the layer development over a range of aspect ratios going from an initial value $L/\delta_\omega^\circ \sim 200$ to a final value $L/\delta_\omega^f \sim 20$, and anticipating a temporal growth for the vorticity thickness of the order of

$$\frac{\delta_\omega}{\Delta H} \approx \frac{t}{10} = \frac{t^*\tau}{5}, \qquad [3.3]$$

one may estimate the duration T^* of a complete computer run to be approximately

$$T^* \approx (\delta_\omega^f - \delta_\omega^\circ)\frac{5}{\tau\Delta U} \approx \frac{5\delta_\omega^f}{\tau\Delta U}. \qquad [3.4]$$

Using the two relationships

$$NV\, d^2 = \delta_\omega^\circ L \quad ; \quad \gamma = L\Delta U / NV, \qquad [3.5]$$

one obtains the estimate

$$T^* \approx 5\, \delta_\omega^f / \delta_\omega^\circ \; ; \qquad [3.6]$$

typically, using the representative figures given above, one obtains $T^* \approx 50$. The time rate of change of the Kirchhoff function may reasonably

be expected to be of the order $\Delta t^{*3}/2$; over the time interval T^*, the total change in H is approximated by

$$\frac{\Delta H}{H_o} \approx N \, \Delta t^{*4}/2 \, , \qquad [3.7]$$

where N is the number of time steps. Limiting the number of time steps to 1500 by choosing $\Delta t^* = 1/30$ leads to a total variation in H of the order of $2\ 10^{-3}$; this choice of Δt^* was retained as an adequate compromise between accuracy and computation cost.

The choice of cell size is to some extent arbitrary; it affects only the size of the arrays for the tabulated circular and hyperbolic functions, and the magnitude of the implicit viscosity ν_{CTC}. From [2.30] and [3.5], the expression for ν_{CTC} is readily found to be $\nu_{CTC} = \delta^2 \, \Delta U \, / \, 24 \, \delta_\omega^\circ \, \Delta t^*$. A characteristic Reynolds number may be formed:

$$Re = \frac{\Delta U \, \delta_\omega}{\nu_{CTC}} = 24 \, \delta_\omega \, \delta_\omega^\circ \, \Delta t^*/\delta^2 \, , \qquad [3.8a]$$

and rewritten, using $\delta = L/NG$, as

$$Re = 24 \, \Delta t^* \, NG^2 \left(\frac{\delta_\omega^\circ}{L} \right) \left(\frac{\delta_\omega}{L} \right) . \qquad [3.8b]$$

Selecting a typical value $NG = 8250$ (and using $\Delta t^* = 1/30$), one estimates the initial and final Reynolds numbers to be

$$\mathring{Re} \approx 1360 \quad ; \quad \overset{f}{Re} = 13600 \, . \qquad [3.9]$$

Reynolds numbers recorded in the actual computations ranged from $\mathring{Re} \approx 1500$ to $\overset{f}{Re} \approx 75{,}000$. With this value of the viscosity, the diffusion contribution to the total growth of the layer compared with that of the inviscid processes is estimated to be 1% only; in fact, changes in the Kirchhoff function were of the order of 6% after 1200 time steps, a variation

that can be attributed to viscous diffusion, although not readily predicted from the results for Rankine's vortex.

Before discussing various aspects of the computed flows, it is opportune to examine the relation of the present study with that of Acton (1976), and to outline, in particular, the divergences that stem from two, essentially distinct approaches of the same fundamental idea.

III.3.4 Acton's mixing layer model

Initial steps in the modelling of the (turbulent) shear layer large eddies were taken by Acton (1976) - work hereafter referred to as "reference A" - who proposed a direct extension of Rosenhead's approach to the problem of the sinusoidal vortex sheet (1931; see section II.2.2). The initial configuration analyzed by Acton consists of two sinusoidal wavelengths, represented by 96 equi-strength vortices evenly distributed in four layers along the waveform (see Figure 22a). The geometrical parameters of the arrangement are the layer local thickness Δ, the wave amplitude A and a length δ that corresponds to a vertical offset distance between the two wavelengths. The study examines the influence of the parameters Δ/L, A/L and δ/L on the flow development ($L = 2\lambda$ is the length of the cyclic interval).

It is interesting to consider the significance of that approach in the light of the present work, not only in view of the differences in the numerical schemes used for the tracing of the vortices (see below), but also in terms of the types of initializations chosen to model the two-dimensional shear layer. The numerical scheme employed in reference A to trace the vortices combines Euler's integration method with the stratagem of finite core vortices, which removes the singular character of the

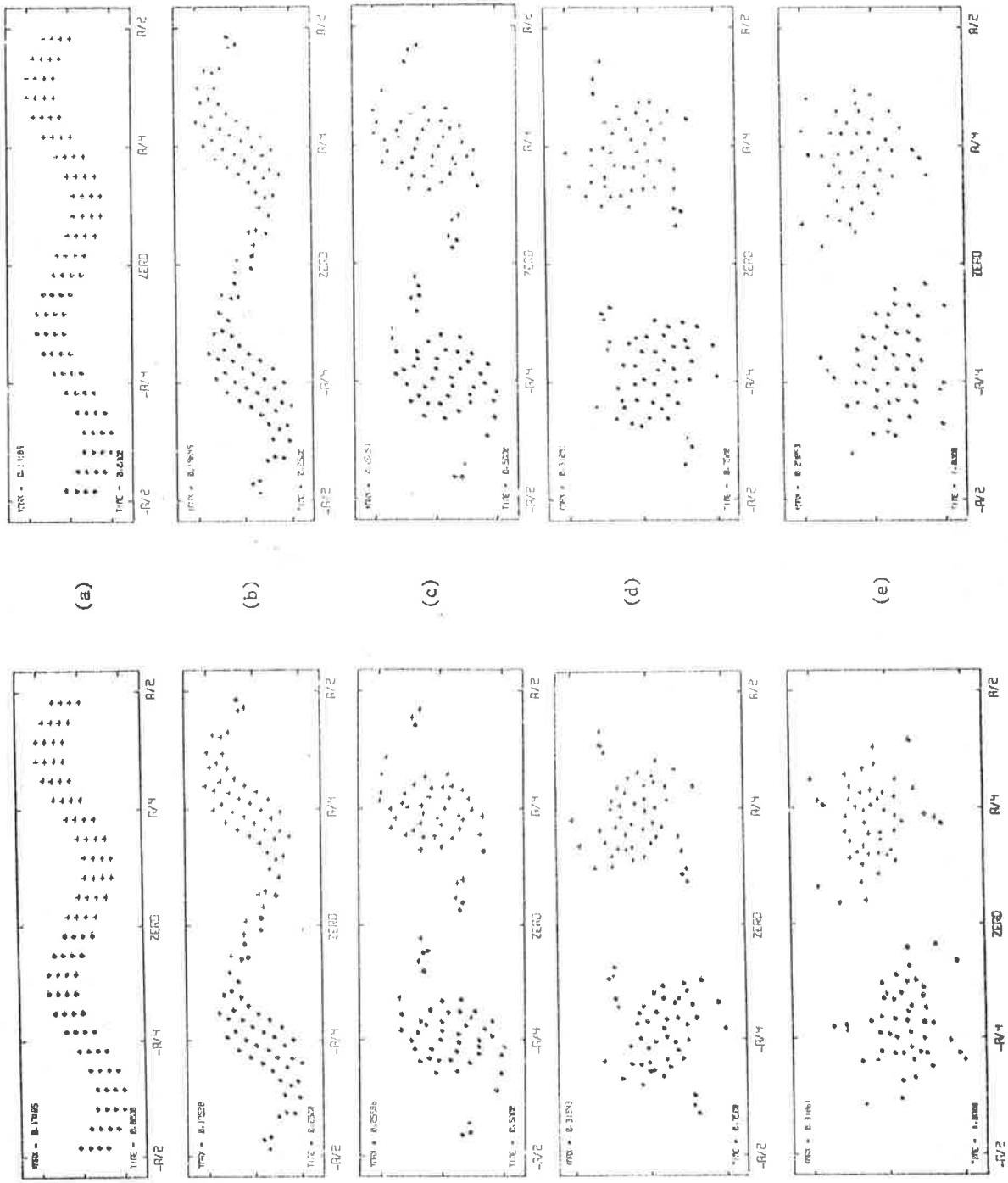

Figure 22 (a)-(e). Flow patterns resulting from CTC computation (left) and computation analogous to Acton's method (right).

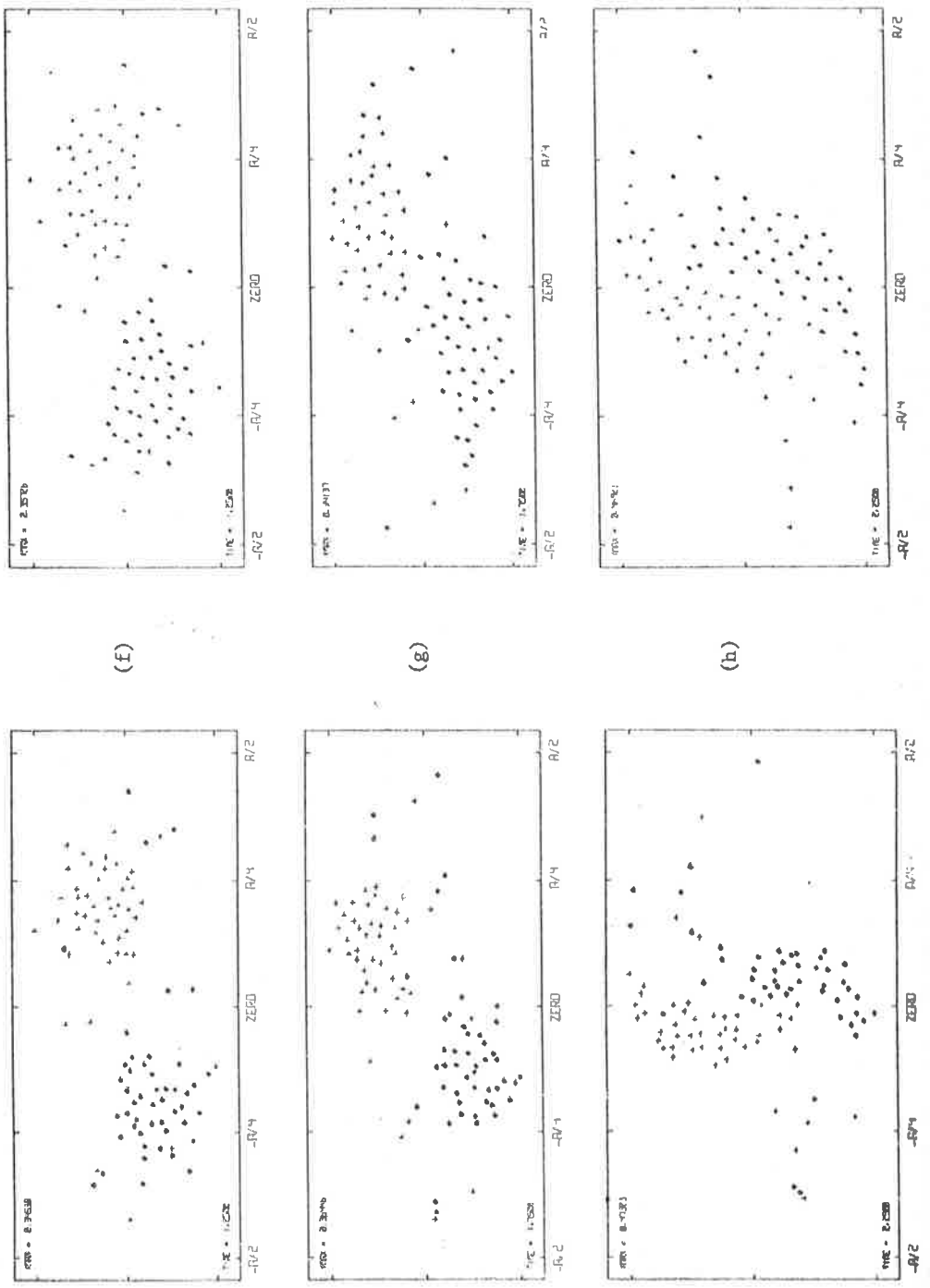

Figure 22 (f)-(h). Flow patterns comparison (continuation).

discretization (proposed by Chorin & Bernard, 1972; see section II.2.2).

It is particularly illuminating to compare the outcome of a CTC analysis (using Euler's modified method and no explicit numerical artifice) of the sinusoidal, two-wavelength problem with that of the method of reference A (*). A typical example of comparative runs is proposed in Figure 22. The flow configurations in the right-hand side column correspond to run 1 of reference A ($\Delta/\lambda = 0.15$; $A/\lambda = 0.10$; $\delta/\lambda = 0.0375$; $\Delta t^* = \frac{\Delta t\ U_\infty}{\lambda} = 0.0125$). The left-hand side flow patterns were obtained by a CTC analysis using a square cell ($\delta/\lambda = 5\ 10^{-4}$) and keeping the same value for the time step Δt^*. The obvious discrepancies that emerge, as the computations proceed, lead rapidly to fundamentally dissimilar flows (see patterns (h)). The accuracies of the numerical procedures are compared in Figure 23 in terms of Hamiltonian conservation. The pronounced loss of invariance (80% over the time interval considered), imputable to the numerical method used in reference A, is clearly reflected in the diminishing compactness of the vortex clouds and is a direct consequence of the "bulk diffusion" effect characteristic of Euler's integration method. One is therefore led to conclude that the validity of Acton's modelling appears questionable, and that some of the results given in reference A may require a careful reassessment.

The choice of a simple sinusoidal initialization appears justifiable in an attempt to isolate the basic parameters that influence the rolling-up process: one may, however, anticipate that periodicity (i.e. boundary)

(*) The flow configurations of reference A were used to choose the parameters of a CTC computation *based on Euler's method*. This procedure was found to give results in close agreement with those of reference A, and was consequently retained as a satisfactory substitute for Acton's calculation method. Acton's method could not be duplicated exactly due to a lack of knowledge of the core radius value used.

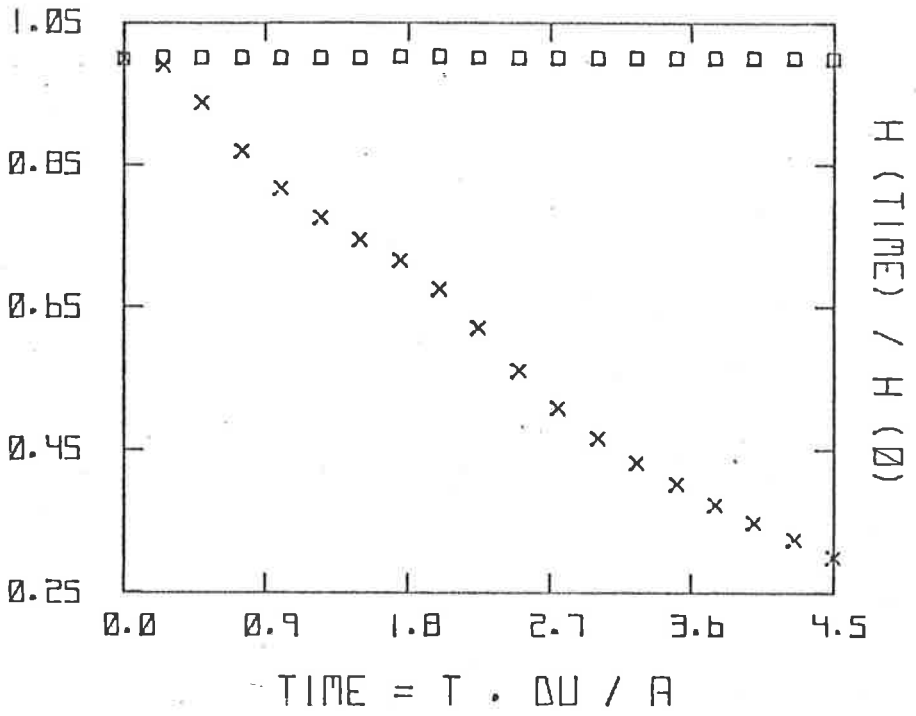

Figure 23: Comparison of invariance of Kirchhoff function for computation method used in reference A (x) and CTC calculation (□).

effects become non-negligible as soon as the two vortex clouds that emerge from the sine waves amalgamate into a single central structure: this is likely to seriously restrict the time interval over which the computation may be taken as being "realistic". This argument is supported by the anomalous behaviour of the growth of the layers at the late stages of the computations (see reference A, Figure 17). In this respect, it is significant to point out that, in the present study:

(a) all layers possess an extremely large initial aspect ratio ($L/\delta_\omega^\circ \sim 250$);

(b) all computations *terminate* when the flow patterns consist of only a few structures or, equivalently, when the layer aspect ratio drops down to values in the range of 10 to 3. This order of magnitude is, in contrast, typical of the *initial* configurations examined in Reference A;

(c) the ability of witnessing as many interaction events as possible is an essential feature of the present investigation; this capability is not included in the computations of Acton, which concentrate on a single, particular pairing event.

III.4 THE INVISCID VORTICITY LAYERS

III.4.1 Computed Flow Patterns

Qualitatively, the five separate inviscid flows developed similarly. The striking similarities between the computed flow patterns and the experimental flow visualizations of turbulent mixing layers (see Winant & Browand, 1974) leave little doubt that the large-scale structure is fundamentally a two-dimensional, inviscid phenomenon. The comparison with the largely two-dimensional flow of Winant & Browand must naturally allow

for differences in initial conditions and the minor dissimilarity between the spatial and temporal problems.

A typical sequence of vorticity configurations can be seen in Figure 24; it includes 13 frames extracted from the evolution history of a random layer with initially-uniform circulation per unit length (type -I flow). The emergence of clusters of point-vortices is manifest in the very early stages of the evolution of the layer. Once established, these formations evolve as distinct entities that eventually interact to generate larger vortex formations; the interaction pattern that results may be described as follows. The most frequent interaction events consists of a *pairing process*, by which two neighbouring vortex clouds amalgamate, giving birth to a similar, identifiable structure of larger dimensions; it is easy to recognize several such pairing events by inspection of Figures 24. The pairing originates as a motion of two neighbouring structures toward each other, indicating a tendency to "reciprocal satellization". This orbiting motion, reminiscent of the basic behaviour of two vortices - both of which possess a positive (negative) circulation - is, however, impaired by a stronger propensity to amalgamate, whenever the structures become sufficiently close; these structures subsequently lose their separate identities and merge into a larger vortical cloud. Moore & Saffman (1975) have suggested that the interaction event may take the form of the tearing of a structure "trapped" into the straining field of two neighbouring ones; this "amalgamation by disintegration", occurring with no evidence of orbital motion, does not appear as a fundamental interaction mode in the layers considered here. The reason for this has been attributed by Saffman (1977) to the inadequacy of the two-dimensional model which decreases *a priori* the level of turbulent

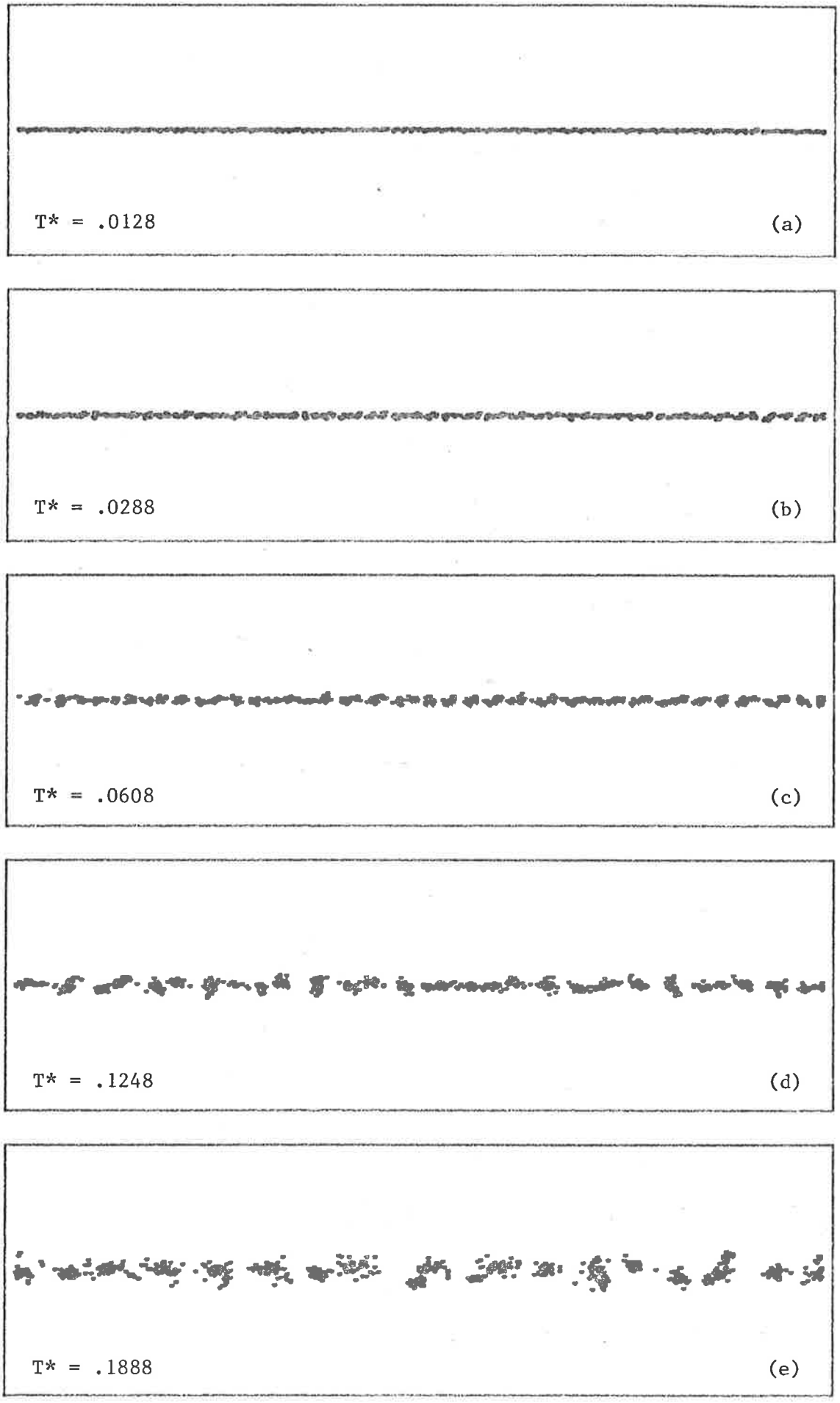

Figure 24: Flow patterns of inviscid, type -I vorticity layer (a)-(e).

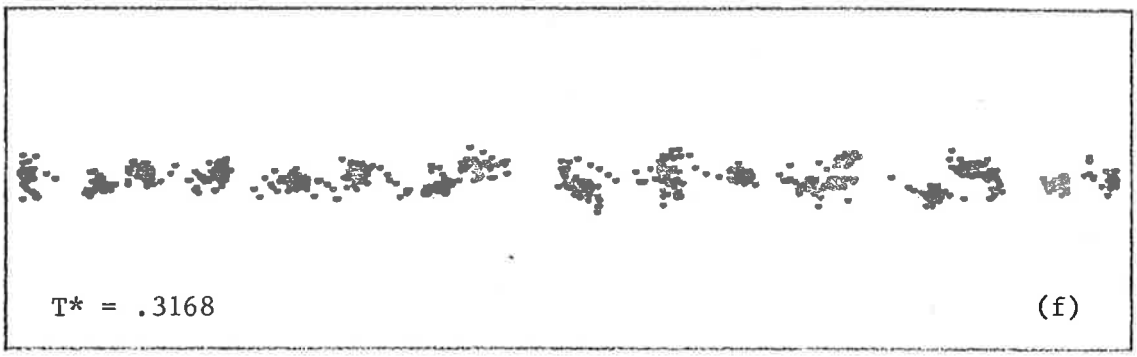

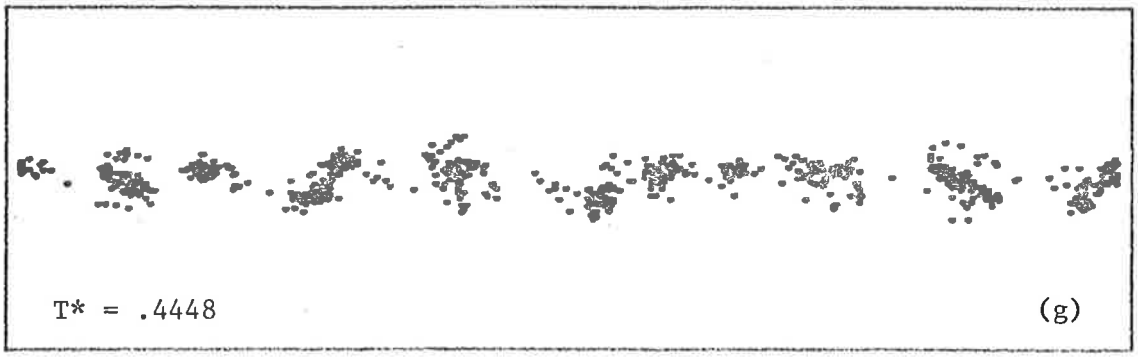

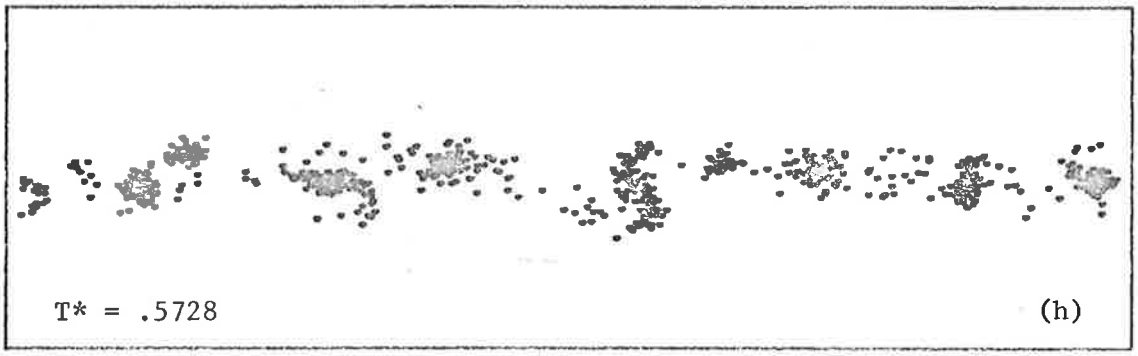

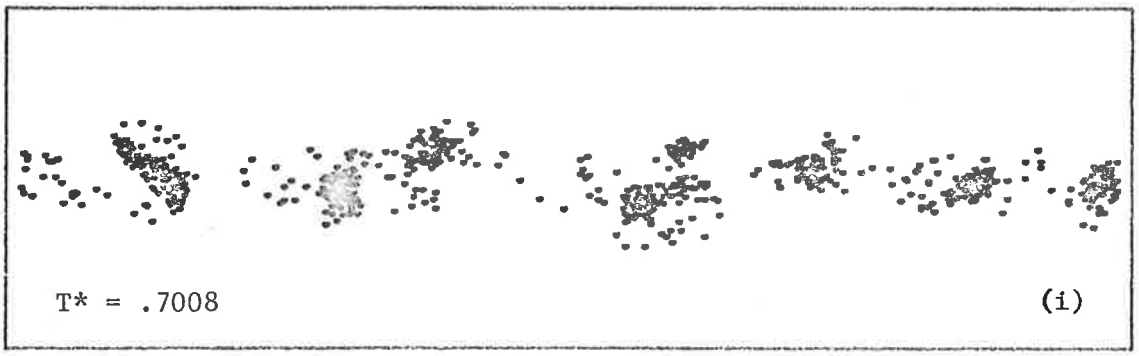

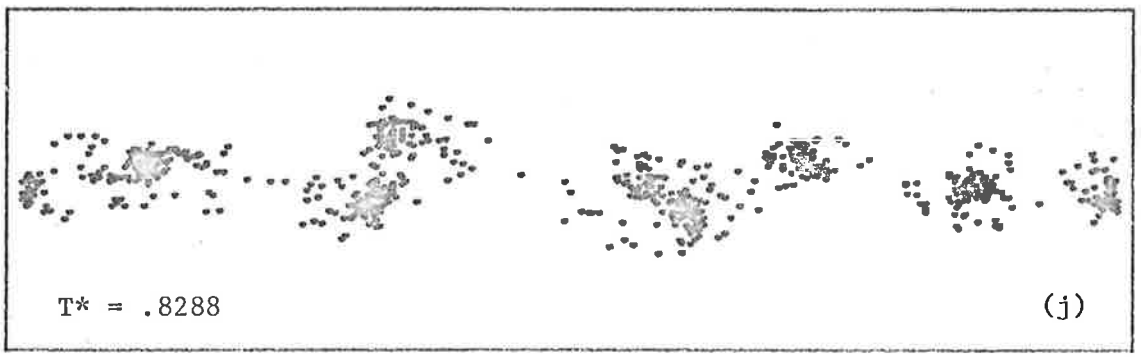

Figure 24: Evolution of type -I vorticity layer (continuation) (f)-(j).

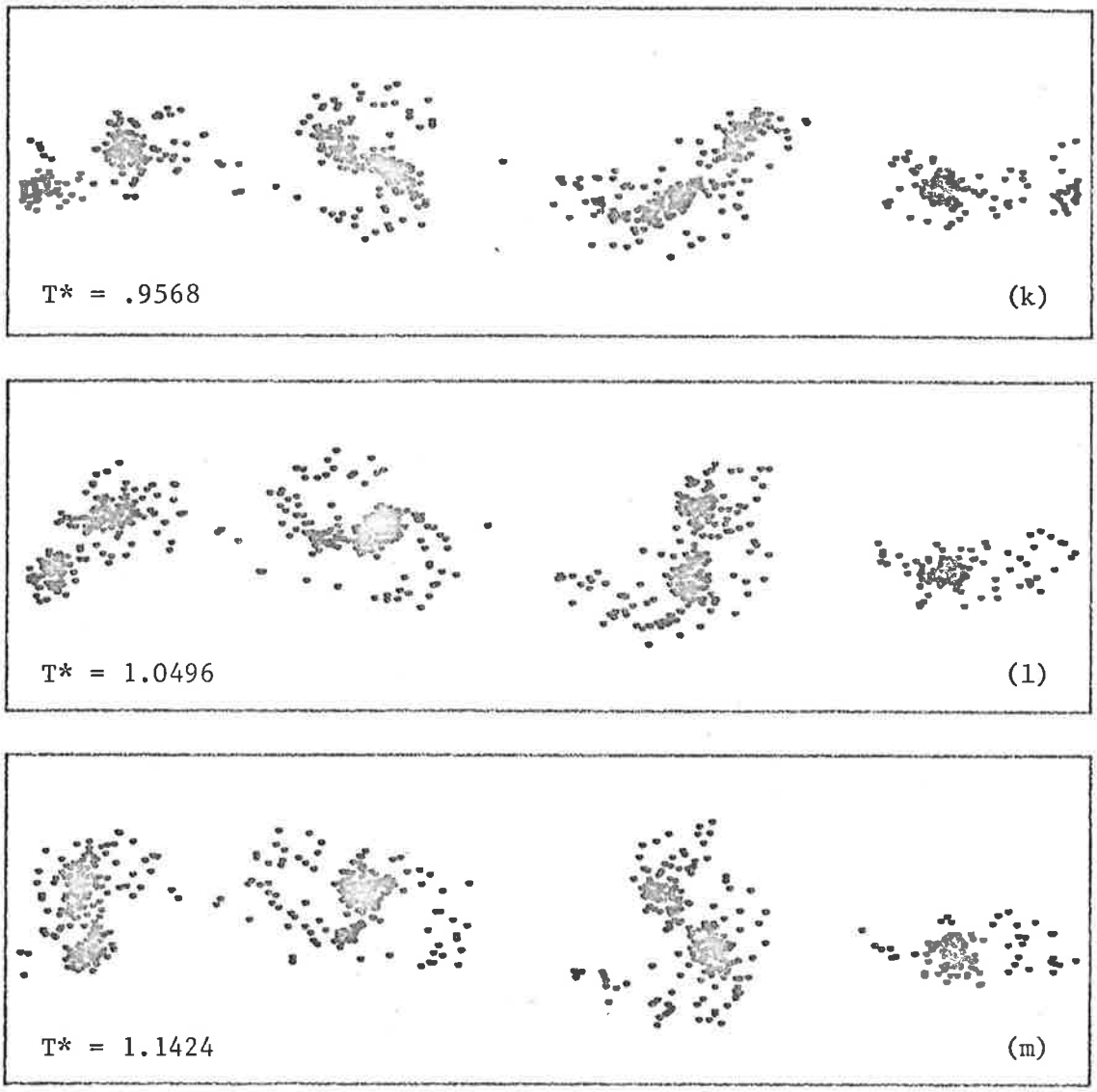

Figure 24: Evolution of type -I vorticity layer (continuation) (k)-(m) - ($t^* = t\Delta U/L$).

entrainment. In this context, it may be significant to mention that the only "tearing" event observed occurred for a particular initialization only, in an early Euler method - CTC computation, i.e., using a scheme that introduces spurious, larger "diffusion" effects (not shown in the figures).

A motion picture film, covering the complete evolution of a layer, was made using a digital colour display monitored by the PDP 11/34 computer facility in the Department of Mechanical Engineering. Plate 1 shows a reproduction of a photograph of the screen displaying simultaneously two frames of the evolution of the vorticity field. In this film, the development of the layer is seen as the repetitive occurrence of the pairing process (*), which eventually leads to the "wrapping up" of all vortices into a single cloud. The progressive disappearance of structures is clearly depicted in a "histogram-plot" of the type presented in Figure 25. These plots illustrate the temporal evolution of the function $h(x) = \sum_{\alpha} \kappa_{\alpha}(x)$ obtained by summing the circulation of all vortices having the same abscissa. For equi-strength vortices, the plots may be viewed as the frequency distributions of the abscissae of the vortices. The evidence of the amalgamations of vortices into distinct well separated clouds is unmistakable; the pairing process may also be inferred by inspection of these histograms. One of the interesting features of $h(x)$ is the development of large gaps; they indicate the absence of vortices in the regions linking adjacent vortical cores. The "braids" between structures are usually (but wrongly) present if Euler's integration scheme is employed.

(*) It is clear from the motion picture that interactions involving several structures and much more complex than pairings do occur in the flows; pairing, however, appears as the most frequent interaction mechanism in the layer.

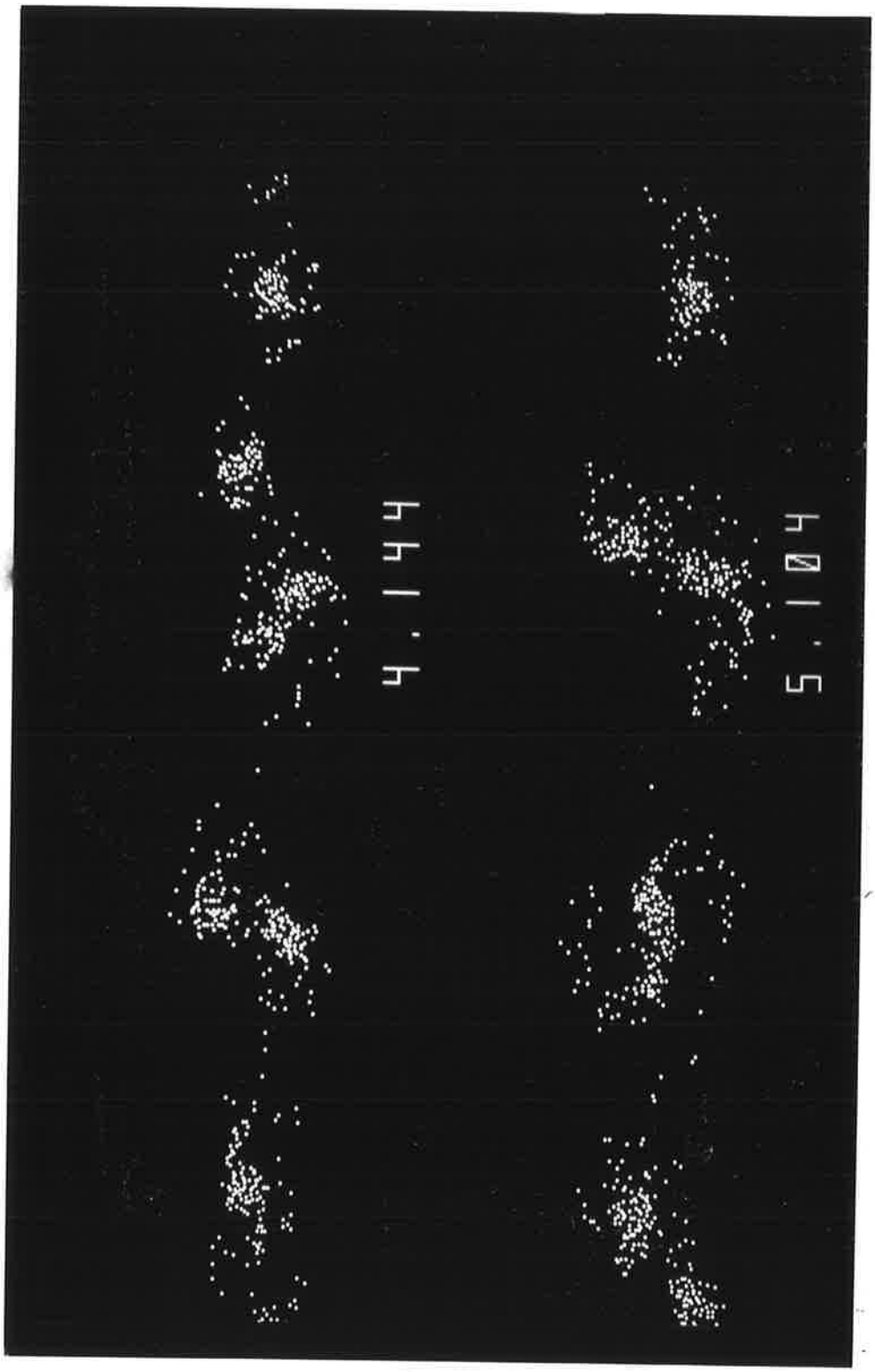

Plate 1 : Two late configurations in a type-I layer.
(Frames extracted from computer motion picture)

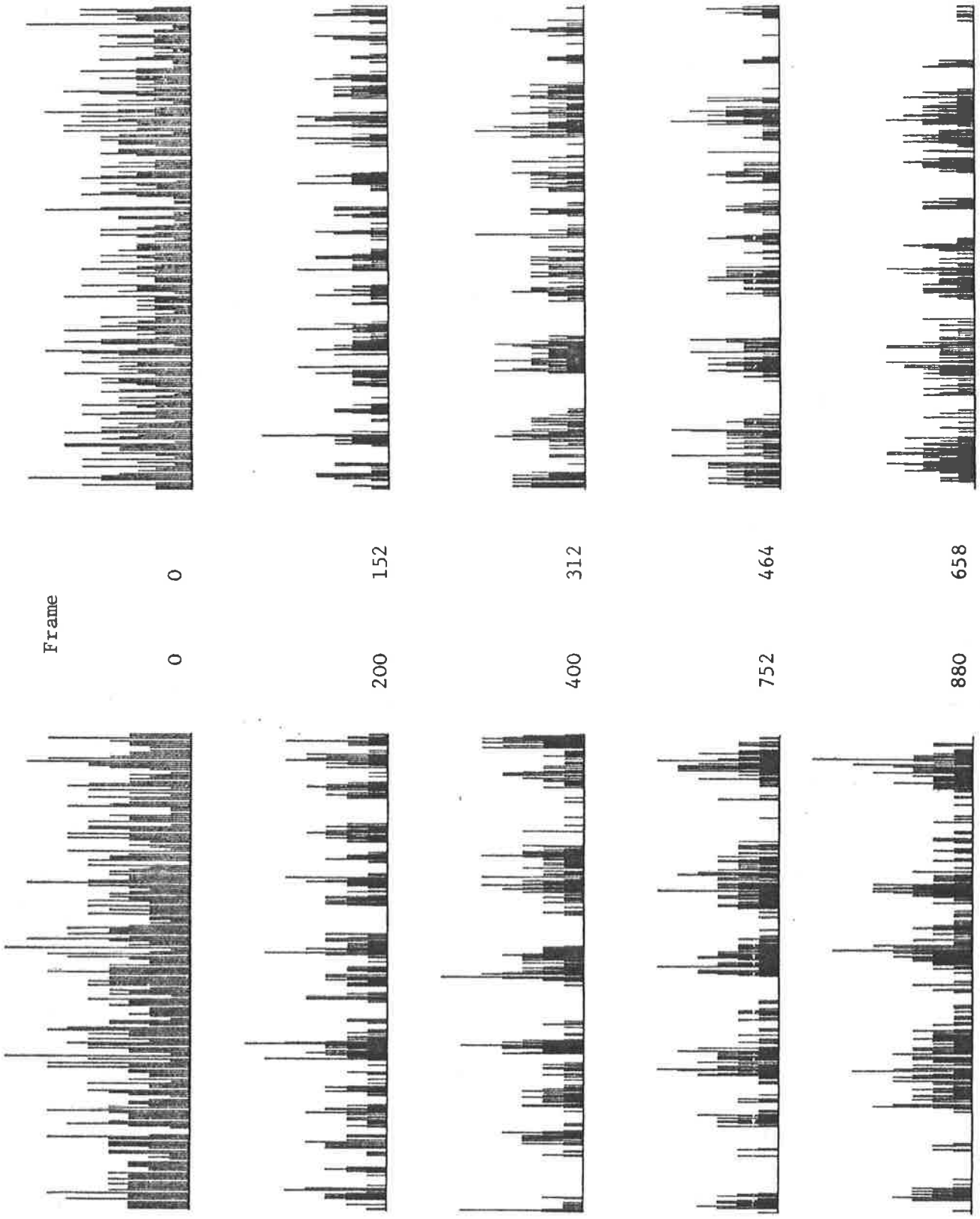

Figures 25a & b: Histogram plots showing the evolution of the distribution of the circulation along the interval L (type -I flows)

On the basis of the above discussion, the model appears to accurately predict qualitative aspects of the flow. Quantitative comparison between the model estimates and experimental evidence is the object of the following paragraphs, beginning with the growth histories of the sample flows.

III.4.2 The growth of the layers

III.4.2.1 Theoretical background

The self-preservation hypothesis, applied to inhomogeneous *spatial* mixing layers, asserts that, at sufficiently large values of $Re_x = xU_M/\nu$, the streamwise velocity distribution $U(y)$ and the density field $\rho(y)$ exhibit mean profiles of the form

$$\frac{U}{U_1} = F_u\ (\eta;\ r,s)$$
$$\frac{\rho}{\rho_1} = F_\rho\ (\eta;\ r,s) \qquad [3.10]$$

where $\eta = y/(x-x_o)$ is the similarity variable,

$r = U_2/U_1$ is the velocity ratio,

and $s = \rho_2/\rho_1$ is the density ratio.

Layers with mean velocity (density) profiles that scale like [3.10] must grow linearly as they develop downstream. Denoting by $\delta_u(x)$ $(\delta_\rho(x))$ an estimate of the layer thickness based on the velocity (density) profile, one predicts the dependence

$$\delta_u(x) = (x-x_o)\ C_u\ (r,s)$$
$$\delta_\rho(x) = (x-x_o)\ C_\rho\ (r,s)\ , \qquad [3.11]$$

where C_u and C_ρ are constants for any fixed choice of values of r and s. Examination of the layer spreading rate provides therefore a simple means of testing the relevance of the self-preservation arguments (note that a linear spreading is a necessary but not sufficient condition for self-preservation to be established). Knowledge of the functional dependence of the spreading rates $C(r,s)$ on the velocity and density ratios relies essentially on experimental investigation. The spreading rate function $C_\omega(r)$ for the vorticity thickness (*) of homogeneous layers (s=1) has been determined in various experimental situations. Presently available data suggest a possible linear dependence of $C_\omega(r)$ on the velocity difference parameter $\lambda = 2\Delta U/U_M$; at small values of λ, the Abramovich-Sabin relationship appears to hold:

$$C_\omega(r) = \left(\frac{1-r}{1+r} \right) K_\omega \quad , \qquad [3.12]$$

where K_ω is a constant. Data are well represented, at small λ, with $K_\omega = 0.181$. Alternative functional forms of the spreading function are discussed at length by Brown & Roshko (1974).

The spreading of spatial layers is perceived as a growth with time in the corresponding temporal problems. Dimensional considerations dictate that temporal layers grow according to the law

$$\delta_\omega(t) = (t-t_o)\ \Delta U\ K_\omega^T \qquad [3.13]$$

where K_ω^T is a constant. Using the Galilean transformation $(t-t_o) = (x-x_o)/U_c$ with $U_c = U_M = \frac{1}{2}(U_1+U_2)$ yields the equation

---

(*) The vorticity thickness δ_ω is defined as $\delta_\omega = \pm\Delta U/\left(\frac{\partial U}{\partial y}\right)_{MAX}$, the sign being selected according to that of the velocity gradient.

$$\frac{\delta_\omega}{x-x_o} = \left(\frac{1-r}{1+r}\right) 2K_\omega^T \quad , \qquad [3.14]$$

which is identified as the Abramovich-Sabin relationship. The expected value for K_ω^T is therefore $K_\omega^T = K_\omega/2 \approx .09$. Note that this Galilean transformation is only appropriate for $\Delta U/U_M$ small.

The growth of the computed layers was determined from the change with time of the vorticity thickness; this was preferred to the visual thickness whose determination appeared largely too subjective. The vorticity thickness was determined from the mean velocity profile, fitted with a high-order polynomial over its central portion (to avoid the long flat tails of the profile far from the layer). Typically, average values were computed over 75 stations uniformly distributed over the interval length; 7th-order polynomials were fitted to averaged data over an interval in the transverse direction equal to 120% of the visual layer thickness. This procedure was found to yield smooth velocity profiles and results fairly insensitive to changes in the parameters. Occasionally, for very thin layers, some uncertainty could not be avoided in the estimation of δ_ω.

The thickness may also be determined from the probability distribution, $p(y)$, of the number of vortices, using the relationship

$$\delta_\omega = \frac{1}{p(y)_{MAX}} \quad . \qquad [3.15]$$

Expression [3.15] may be established as follows. Consider a layer of period L, discretized by equi-strength point-vortices. Be $n(y)dy$ the number of vortices located in the strip $(y,y+dy)$; they carry a circulation $\gamma(y) = \gamma n(y)dy$, where γ is the individual vortex strength. Compute the circulation around a strip of height dy which covers the cyclic interval L. Clearly, one has $\gamma(y) = -L \frac{\partial u}{\partial y} dy$

and rearranging:

$$\frac{\partial u}{\partial y}\, dy = - \frac{\gamma}{L}\ NV\ p(y)dy\ , \qquad [3.16]$$

where $p(y) = n(y)/NV$ is the probability distribution function for the number of vortices, and $NV = \int_{-\infty}^{+\infty} n(y)dy$ is the total number of vortices. Integration of equation [3.16] yields directly

$$u(y) = - \frac{\Gamma}{L} \int_{-\infty}^{y} p(y)dy + u(-\infty)\ , \qquad [3.17]$$

where $\Gamma = \gamma\ NV$ is the total circulation. The quantity Γ/L may be expressed in terms of the velocities at infinity:

$$\frac{\Gamma}{L} = u(-\infty) - u(+\infty), \qquad [3.18]$$

and [3.17] may be recast as

$$u(y) = u(+\infty) \int_{-\infty}^{y} p(y)dy + u(-\infty) \int_{y}^{\infty} p(y)dy. \qquad [3.19]$$

Expression [3.19] indicates that the complete determination of the velocity profile requires, in addition to the shape of the function $p(y)$, that two independent constants be specified. Restricting the analysis to shear layers without overall mean motion, i.e. choosing

$$u(+\infty) = U_\infty \quad ; \quad u(-\infty) = - U_\infty\ , \qquad [3.20]$$

one obtains three equivalent forms for $u(y)$:

$$\begin{aligned} u(y) &= U_\infty \left[\int_{-\infty}^{y} p(y)dy - \int_{y}^{\infty} p(y)dy \right] \\ &= U_\infty \left[1-2 \int_{y}^{\infty} p(y)dy \right] = U_\infty \left[2 \int_{-\infty}^{y} p(y)dy - 1 \right] . \end{aligned} \qquad [3.21]$$

Expression [3.15] is a direct consequence of equations [3.21] and of the

definition of δ_ω; for all distributions tested, $p(y)_{MAX}$ is closely approximated by $p(0)$.

III.4.2.2 Computed growth rates

The growth histories of the computed layers are shown in Figures 26, which display the vorticity thickness ratio $\delta_\omega/\delta_\omega^\circ$ as a function of the dimensionless time $t\Delta U/\delta_\omega^\circ$. Recall that for type I and type II flows, the initial aspect ratio L/δ_ω° is close to 500 and 1000, respectively. From Figure 26a, it is apparent that the early growth rates for the two types of initial conditions are very different: type II flows grow nearly three times faster than type I flows. Despite different random initial conditions, growth rates of flows of the same type are remarkably consistent. Both flow families appear initially to have constant growth rates. For longer times, however, it is interesting that type I flows maintain an accurately linear growth until near the very end of the computations, where departures from linearity are connected with the small number of structures (which leads to oscillations in the computed thickness), and also, at longer times, with the effects from the periodic boundary condition. By comparison, it is obvious that type II flows slowly revert, over these longer times, to a reduced growth rate. In a primitive attempt to determine whether or not the growth rate of these flows approached that of type I flows at very large times, calculations were continued to a point where all 3 layers achieved the same aspect ratio (approximately 10); these layers were then placed end to end, two out of every three vortices removed, and the resulting configuration used as an initial condition for a further calculation. Apart from an initial adjustment in the thickness, this "compound" flow achieved a final growth rate only marginally different from

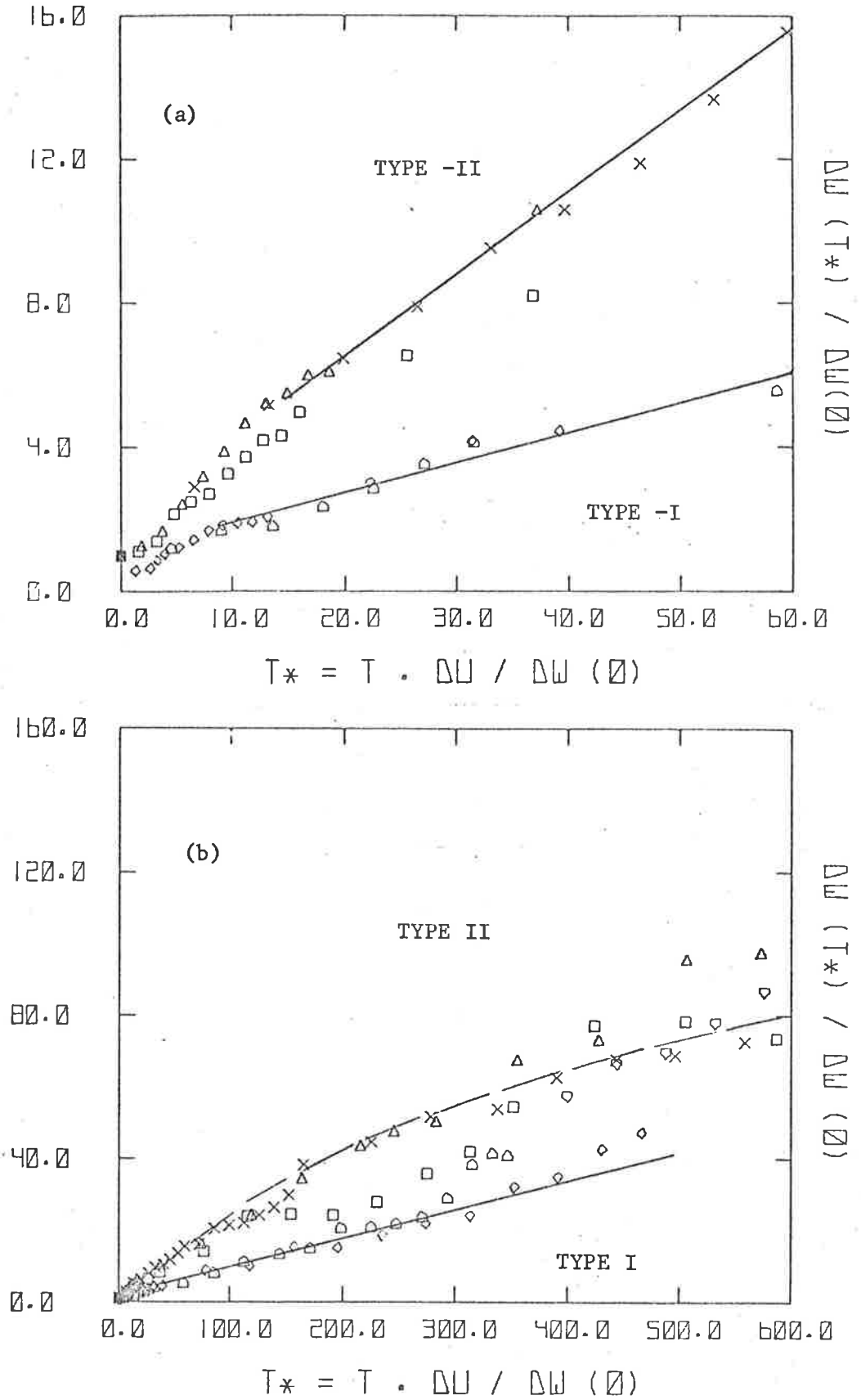

Figures 26(a)&(b): Growth histories of sample flows: vorticity thickness versus time.

that of the type I flows. By the time this calculation terminates, the thickness has reached 320 times its initial value (Figure 26c).

While the number of flows that were studied is very limited, it appears reasonable to conclude that the two types of flows are fundamentally different. The explanation may well be that, in the type II case, the random distribution of circulation per unit length on the initial sheet rapidly gives rise to vortical structures which have wider distributions of circulation and spacing than those of the type I family. The subsequent velocity of any structure normal to the sheet is determined by the nett balance of the opposing induced velocities due to all structures to the left and to all structures to the right. Now, if the initial distribution were exactly periodic - with a wavelength $\lambda = L/n$, then the sheet would presumably form n identical vortical structures which, in a sense, would form a final configuration with no further pairing; this periodic array, however, would be an *unstable* equilibrium configuration. Randomness seems crucial to pairing. Since the magnitude of the resultant of the opposing velocities will in general be greater for random circulation flows than for uniform circulation flows, the initial transverse velocity of the structures will also be greater and lead to the more rapid growth observed in type II flows. This is consistent with the experiment of Oster et al (1978), in which forcing the shear layer with a pure sine wave produced a *rapid initial* growth as the vortices develop and wrap up the shed vorticity, but a *subsequent limited* growth over a significant distance, as the closely similar neighbouring vortices convect downstream. These observations suggest that for the *infinite* vorticity layer, the growth rate depends on the probability distribution function for the circulation per unit length scaled by the vorticity thickness. This possibility is a plausible

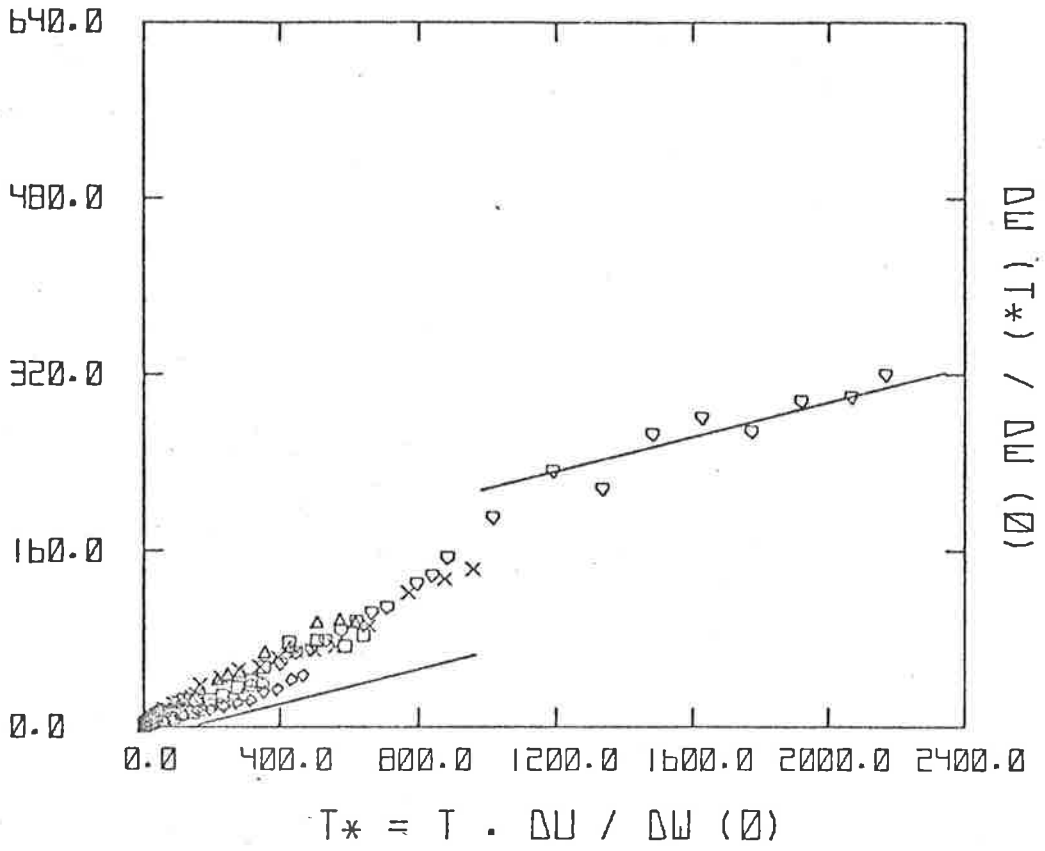

Figure 26(c): Growth histories of sample flows (continuation).

explanation for the behaviour of type II flows. For the infinite sheet, dimensional analysis predicts that the layer should grow linearly; that it does not for type II flows presumably reflects the significance of the periodicity in L. For these flows, the circulation per unit length will tend to become more uniform - δ_ω/L increasing - as the initially random strength, small-scale structures combine; a growth rate which decreases towards that of type I flows may then be expected.

The present results are consistent with the wide variation in the experimentally found growth rates of mixing layers, and particularly with the known sensitivity to a tripping device. Differences in growth rate as large as those between the two classes of flows studied here have not been found experimentally; yet, a trip will tend to introduce a randomness in the circulation about any small circuit near the splitter plate. This randomness - though not as large as that present in the calculations - may be responsible for the dramatic change in the spreading rate of tripped layers. In type I flows, the randomness in circulation is introduced "locally", i.e. on the scale of the spacing between two vortices; on a scale of several times the initial vorticity thickness, the circulation per unit length is uniform, and the randomness looks rather like a random displacement of the vorticity layer. This situation, one expects, models more closely the usual splitter plate condition at high Reynolds number. It is interesting to note that the asymptotic growth rate $\dot{\delta}_\omega/\Delta U$ of the type I flows is close to .08, over a very large increase of thickness (Figure 26b). This is to be compared with the value .09 inferred from experimental data and reported in the preceding section.

A prediction which would follow from these considerations is that a broad-band random fluctuation in *time* (*not* space) of the free-stream

velocity - for example, $U_1 = U_1(t)$ - would have a significant effect on the spreading rate of spatial layers. This may have interesting implications when considering the possible connection with the effects of mass flux variations in jets.

Whatever the explanation for the behaviour of the calculated growth histories, it is clear that different types of initial conditions have a persistent effect, in these effectively inviscid flows, over time intervals that appear surprisingly large. A measure of time in the spatial turbulent mixing layer, proposed by Dimotakis & Brown (1976), scales with the number of amalgamation (pairing) events undergone by the structures as they evolve downstream. The number of interactions $m(x)$ that take place over a downstream distance x is given by $m(x) = \log_2(x/\ell_o)$, where ℓ_o is the wavelength of the original disturbance. This estimate is based on the assumption that each pairing interaction doubles the spacing between the structures. According to this measure, 5 or 6 amalgamations have taken place during the history of the calculated flows; this is of interest if one notes that the same number of interactions have occurred by the time structures reach the farthest measuring station in the Dimotakis & Brown experiment; in most laboratory configurations, this number does not exceed 10 over the full length of the apparatus.

III.4.3 Correlation analysis of the velocity field

The evidence drawn from the analysis of the growth histories of the computed flows suggests that the large scale structure of random vorticity layers may evolve *asymptotically* towards a universal state, characterized by a unique, constant growth rate. This tendency is in agreement with conclusions drawn from dimensional arguments applied to the infinite vortex

sheet. It is important to collect additional information about the possible self-similar structure of these layers; it is also interesting to compare the characteristics of the structures that arise in two-dimensional computations with these observed in the turbulent mixing layer. This dual purpose may be fulfilled through the analysis of the correlation functions of the fluctuating velocity field, as described below.

The asymptotic evolution of mixing layers towards a fully *three-dimensional* self-preserving turbulent structure has been reported by various authors and is substantiated by a large amount of experimental data (Chandrsuda et al, 1978). The *uniqueness* of this asymptotic state appears, however, questionable in view of the evidence that an apparently distinct, essentially *two-dimensional* self-preserving state may also develop in turbulent mixing layers (Dimotakis & Brown, 1976). The possible connection between the latter type of flow evolution and the behaviour of the present numerical flows is without doubt an interesting one.

In their experimental investigation of a mixing layer in water, Dimotakis and Brown examine the behaviour of the autocorrelation function of the streamwise velocity fluctuations in terms of similarity properties and initial-conditions dependence. They report that the autocorrelation functions $R_{uu}(\tau) = \langle u'(t)\, u'(t+\tau) \rangle$ exhibit the fundamental periodicity that would be expected from similarity arguments. Their results indicate that the ratio τ_o/τ_c, where τ_c represents the downstream convection time of the structure $(\tau_c \approx x - x_o / \frac{1}{2}(U_1 + U_2))$, is effectively constant for all x, U_1 and U_2, for a given velocity ratio $r = U_2/U_1$. The average spacing between the structures inferred from their data is found to fall in the range $3.1 < \bar{\ell} / \delta_\omega < 5.$, δ_ω being the vorticity thickness of the layer.

The autocorrelation functions of the fluctuating velocities of the computed flows are defined by the expression

$$R_{\alpha\beta}\ (\xi;\ y,\ t) = <\ u'_{\alpha}\ (x,\ y,\ t)\ u'_{\alpha}\ (x + \xi,\ y,\ t)\ >_{x} \qquad [3.22]$$

where $u'_{\alpha} = u_{\alpha} - <\ u_{\alpha}\ >_{x}$ represents the velocity fluctuation in the x_{α} direction $(\alpha = 1,2)$; the angle brackets $<\ >_{x}$ denote the averaging operation that allows separation of the velocities into a mean value and a fluctuating part. Practically, the average $<q>_{x}$ of a quantity q (at a given ordinate and for a given flow configuration) is obtained as the arithmetic mean

$$<\ q\ (x,\ y,\ t)\ >_{x} = \bar{q}\ (y,\ t) = \frac{1}{N} \sum_{i}^{N} q\ (x_{i}, y,\ t) \qquad [3.23]$$

over samples evaluated at N stations x_{i} uniformly distributed over the computation interval.

Similarity scaling suggests that δ_{ω} be introduced as a characteristic length in expression [3.22]; the dependence of the functions $R_{\alpha\beta}$ on space and time is expressed as

$$R_{\alpha\beta}\ \left(\frac{\xi}{\delta_{\omega}}\ ;\ \frac{y}{\delta_{\omega}}\ ,\ t\right). \qquad [3.24]$$

The functions $R_{\alpha\beta}\ \left(\frac{\xi}{\delta_{\omega}}\ ;\ \pm 1,\ t\right)$ were computed for a number of flow configurations. The ordinate of the sampling line, relative to the position of the dividing line y^{*} defined by the condition $U(y^{*}) = 0$, was chosen as $y = \pm\ \delta_{\omega}$; this location corresponds to the observation stations in the experiment of Dimotakis and Brown. The velocity components $(u_{1},\ u_{2})$ were computed at N equidistant stations x_{α} distributed along the sampling line; average velocity values $<u>_{x}$, $<v>_{x}$ were then evaluated by formula

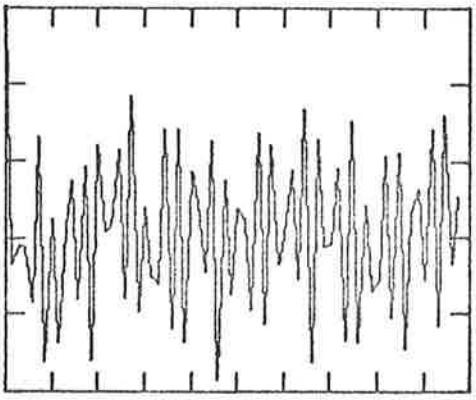

(a)

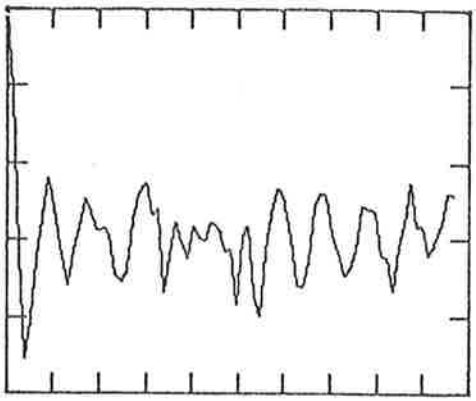

(d)

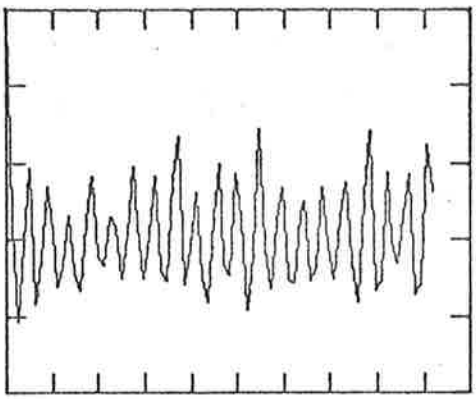

(b)

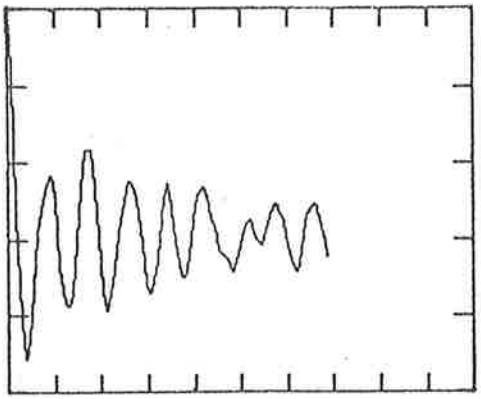

(e)

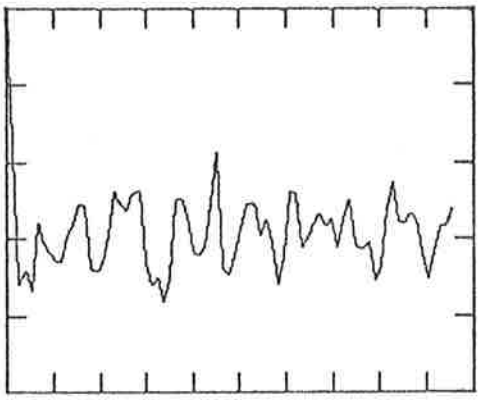

(c)

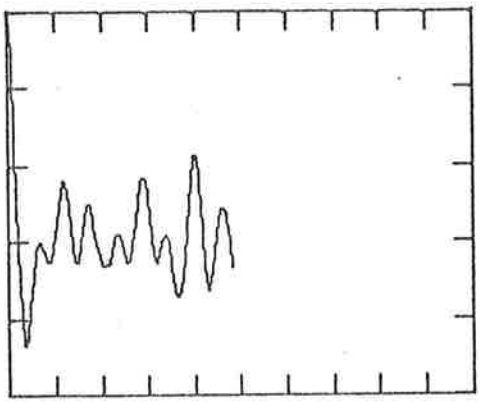

(f)

Figure 27: Typical instantaneous autocorrelation coefficients $r_{11}(\xi/\delta_\omega)$. Frames 1,2,6,10,16,22 of a sequence are shown. Each graduation of the abscissa scale corresponds to $4\delta_\omega$.

[3.23]. The correlation functions were approximated at M values of their argument ξ/δ_ω (0, $\Delta\xi$, $2\Delta\xi$, .., (M-1) $\Delta\xi$) by the formula

$$R_{\alpha\beta}(\ell) = \frac{1}{N}\sum_{i}^{N} u'_\alpha(i)\, u'_\beta(i+\ell) \qquad [3.25]$$

$$(\ell = 0,1,2,\ldots, M-1).$$

The interval $\Delta\xi$ and the number of estimates M were selected in order to limit $\xi_{MAX} = (M-1)\Delta\xi$ so as to avoid periodicity aliases due to folding (clearly $R(\xi) = R(\xi+L)$).

The salient features of this correlation analysis may be discussed in terms of the streamwise velocity autocorrelation function by plotting the ratio $r_{11}(\xi^*) = R_{11}(\xi/\delta_\omega) / R_{11}(0)$ as a function of the dimensionless spatial lag $\xi^* = \xi/\delta_\omega$. Figure 27 shows a sequence of frames that depicts the temporal evolution of $r_{11}(\xi^*)$ in a type-I flow. Each graduation on the abscissa scale represents an increment equal to 4 in the ξ/δ_ω values. It appears that the structures which emerge at the very early stages of the flow evolution tend to organize themselves in an array of spatial periodicity close to 3-4 vorticity thicknesses (frame 27b); this periodicity is not apparent in the initial conditions (frame 27a). It is remarkable that the structures seem to retain a similar periodic organization in the course of their interactions. To render the similarity behaviour more evident, an ensemble average was performed over a number of correlations $r_{11}(\xi^*, t_i)$ (i = 1,2,...NC), selecting the times t_i so as to scan uniformly the complete flow lifetime. Two representative average functions $\bar{r}_{11}(\xi^*) = \langle r_{11}(\xi^*, t) \rangle_t$ are shown in Figures 28a (type-I flow) and 28b (type-II flow); typically, NC was of the order of 25.

The behaviour of the ensemble correlation function does not show the clear periodicity that characterizes some of the instantaneous

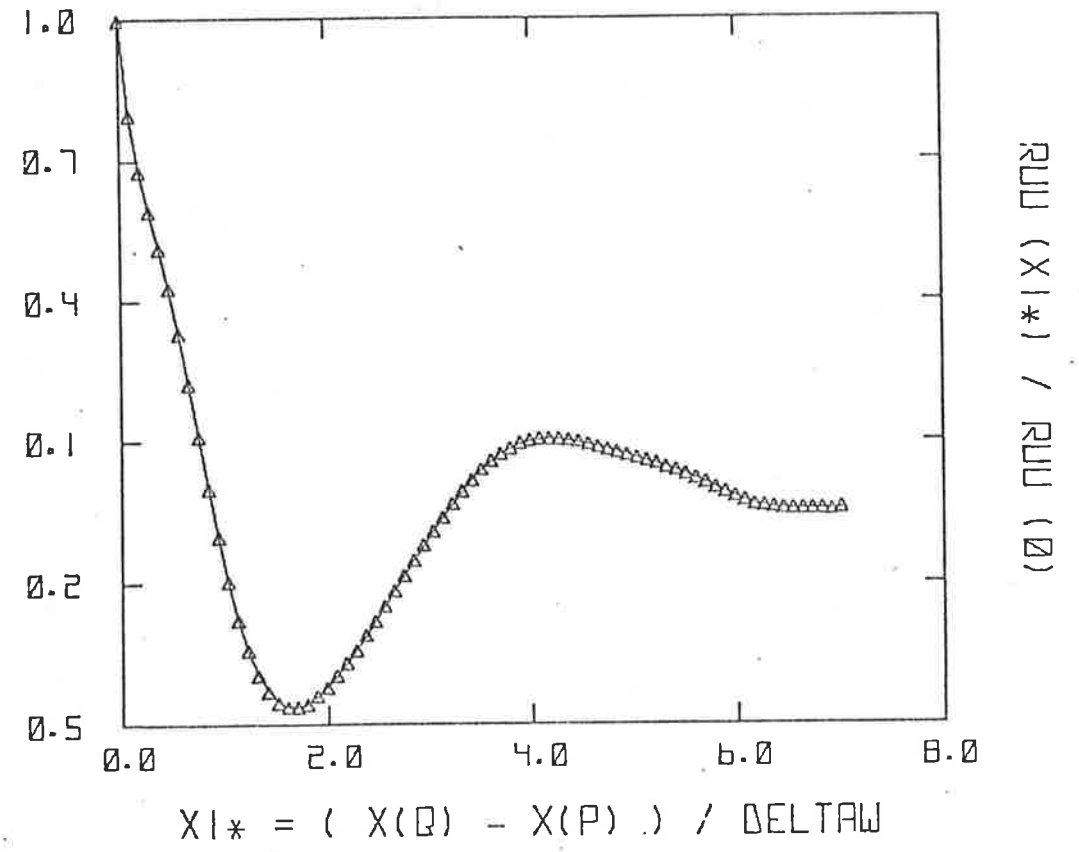

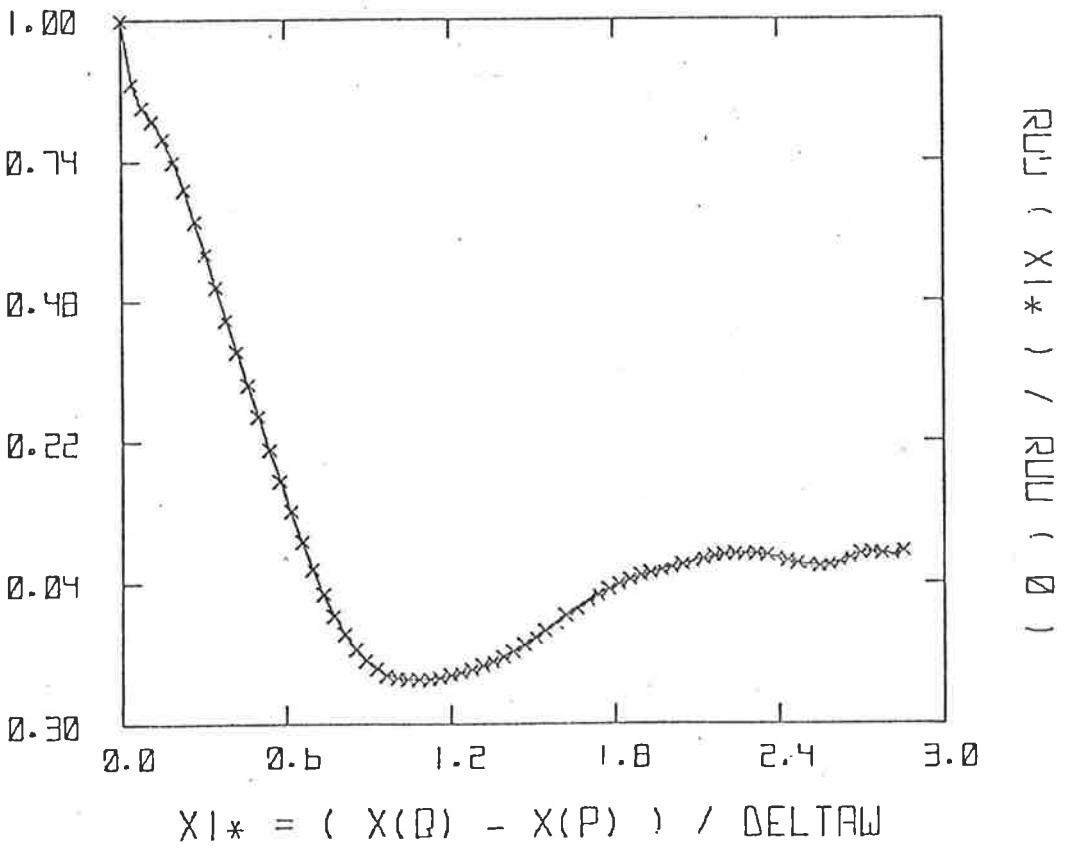

Figures 28a & b: Averages autocorrelation coefficients $\bar{r}_{11}$ (ξ/δ_ω) for type -I (top), type -II (bottom) flows.

correlations (e.g. that of Figure 27). This is probably due to the inclusion, in the averaging process, of correlation functions that relate to configurations in which only a few structures are left over the computation interval, and for which the ratio L/δ_ω is not an integer: for such configurations, periodic boundary conditions may distort the spontaneous organization of the structures. Nevertheless, the marked minimum of the ensemble correlations allows the determination of the fundamental period of the velocity fluctuations as twice the value of the spatial lag that corresponds to the minimum. The period defines the average distance $\bar{\ell}$ between structures; Figures 28 yields the estimates

$$\bar{\ell}_I \approx 3.2\ \delta_\omega \qquad \text{(type -I flows)}$$

and

$$\bar{\ell}_{II} \approx 2.0\ \delta_\omega \qquad \text{(type -II flows).} \qquad [3.26]$$

It is remarkable that type -I flows - which possess an asymptotic growth rate close to the rate observed in the laboratory - generate structures whose mean spacing agrees well with experimentally found values (i.e. $3.1 \leqslant \ell/\delta_\omega \leqslant 5.$).

On the other hand, it is not surprising, in view of the marked differences in the evolutions of the two types of flow, that the mean spacing of type -II flow structures would achieve a value substantially different from that of type -I structures. The *wide* distribution of circulation and *spacing* in type II structures, invoked in Section III.4.2 to account for the observed growth rate of type II layers, may also be responsible for the low value of $\bar{\ell}_{II}$. In any case, comparison of the estimate for $\bar{\ell}_{II}$ with the stability criterion of Moore & Saffman (1975) - according to which a vortical cloud resists disintegration in the distorting field of neighbouring structures if $\bar{\ell} \geqslant 3.5\ \delta_\omega$ - suggests

that type II structures are essentially unstable. The implications that this observation may have in relation with the growth mechanisms of the layer are interesting and open to further investigations, on the basis of additional data.

III.5 THE VISCOUS VORTICITY LAYERS

Results presented so far have shed some light upon the characteristics of the vortical structures that emerge spontaneously from random vorticity layers of *large* initial Reynolds numbers. Typically, these inviscid layers had an initial Reynolds number $\Delta U \delta_\omega^\circ / \nu$ of 1500, and were followed in their evolution until $\Delta U \, \delta_\omega / \nu$ reached a value of the order of 75,000.

A problem of considerable interest consists in investigating the dynamics of vorticity layers at much smaller Reynolds numbers, i.e. when the action of viscosity exerts a dominating influence on the flow. Experimental evidence suggests that the large-scale processes in the mixing layer are to a large extent unaffected by the action of viscosity, even at relatively small values of the Reynolds number; viscous effects are "felt" indirectly through the initial conditions of the layer, and not through direct action of viscosity on the large structures (Roshko, 1976). The possibility of including viscous effects in two-dimensional point-vortex models exists and has been discussed at length in a previous chapter (see Section II.6): molecular diffusion may be simulated by adding a Gaussian random walk to the hydrodynamical motion of the vortices. This simple device provides a convenient means of achieving very small initial Reynolds numbers. It seemed important to investigate the possible Reynolds number independence in the strictly two-dimensional conditions of the point-vortex model, and to determine the response of the coherent structure to the action of

relatively large viscosities. Extending these ideas further, it also seemed of interest to examine the diffusive action of a secondary small-scale motion on the large-scale structures. As pointed out in the introduction, this model of "turbular" fluid relies on simulating an enhanced viscosity, which scales with the flow but remains much smaller than the conventional "eddy" viscosity.

Following a different but connected line of thought, it appears that the study of the *transitional* properties of small initial Reynolds number layers is equally important. Here, the gist of the study is a verification that the layers exhibit an initial viscous growth, followed by the development of waves and the consequent formation of vortical structures, in the sequence of events expected from stability theory. That the numerical calculations would lead to the determination of a critical Reynolds number for two-dimensional transition is a possibility worth while considering.

This section presents a few preliminary comments and illustrations related to these ideas; a thorough investigation of the general stability problem falls beyond the scope of this thesis, and will be the subject of a separate work.

III.5.1 Viscous and turbular computations

The technique used to incorporate viscosity into the calculations has been extensively discussed in section II.6. According to equation [2.30], the magnitude of the viscosity ν is related to the root mean square amplitude σ of the Gaussian displacements and to the integration time step Δt by the expression, recalled here for convenience:

$$\nu = \frac{\sigma^2}{2\ \Delta t} \qquad [3.27]$$

A sequence of random numbers $(\zeta_\alpha, \eta_\alpha)$ normally distributed with zero mean and unit variance is generated and the equations of motion of the vortices are integrated under the form

$$x_\alpha(t+\Delta t) = x_\alpha(t) + \int_t^{t+\Delta t} u_\alpha(t)dt + \dot{\sigma}\ \zeta_\alpha(t) \ ,$$

$$y_\alpha(t+\Delta t) = y_\alpha(t) + \int_t^{t+\Delta t} v_\alpha(t)dt + \sigma\ \eta_\alpha(t) \ . \qquad [3.28]$$

The amplitude σ of the fluctuations is adjusted in order to achieve the desired value of viscosity; it is kept constant when simulating the effects of a molecular viscosity but varying linearly with time when modelling the "turbular" viscosity. The following discussion clarifies the physical significance of the "turbular" fluid concept.

It is known that the closure problem in classical turbulence theory is often bridged by the introduction of an "eddy"-viscosity model which assumes, that the turbulent shear stress and the mean shear are related through the simple expression

$$<-uv> \ = \nu_* \ \left(\frac{\partial U}{\partial y} \right) \ . \qquad [3.29]$$

Limitations of this model are severe, since turbulent transport of momentum is by no means a gradient-type mechanism; relation [3.29] is then regarded as providing a definition of ν_*, in general a function of position.

Dimensional arguments show that in developed mixing layers, the eddy viscosity is proportional to the velocity difference ΔU and to the size of the large-scale eddies, i.e. to the layer thickness δ_ω :

$$\nu_* \propto \delta_\omega \Delta U = C_* \ \delta_\omega \ \Delta U \qquad [3.30]$$

Experimental data confirm this expected behaviour and suggest the following expression for the turbulent viscosity:

$$\nu_* = \frac{\delta_\omega}{4} \left(\frac{<-uv>_{max}}{e} \right)^{1/2}$$

(Tennekes & Lumley, 1972). The value of the proportionality constant in [3.30] may be estimated as $C_* \approx .014$ if one uses for the maximum shear stress the typical value of $90\ 10^{-4}\ \Delta U^2$ (Wygnanski & Fiedler, 1970).

Turbular fluid effects are modelled by introducing in the point-vortex calculations a coefficient of viscosity ν_T which follows the same scaling law as ν_*, but which is characterized by a much smaller proportionality constant than C_*. Typical values of the ratio $C_T = \nu_T / \delta_\omega \Delta U$ of the order of 10^{-3} appear adequate, and still represent small-scale, diffusive processes of much larger intensity than those resulting from molecular action. The magnitude of the turbular viscosity is therefore computed from

$$\nu_T(t) = C_T \Delta U \delta_\omega^\circ \left[1 + \left(\frac{\dot{\delta}_\omega}{\Delta U} \right) \frac{\Delta U\ t}{\delta_\omega^\circ} \right] \quad ; \qquad [3.31]$$

in view of the exploratory nature of the modelling, the growth rate $\dot{\delta}_\omega / \Delta U$ needs not be computed exactly at each time step; its value is conveniently taken as a constant of the order of 0.1.

Figure 29 compares, at a given instant, the stages of development of the structures which have emerged from a type -I initialization in inviscid (top), viscous (middle) and turbular fluids (bottom). The turbular viscosity was characterized by a coefficient C_T equal to $5\ 10^{-3}$; the initial Reynolds number ($R\mathring{e} = \Delta U\ \delta_\omega^\circ / \nu$) in the viscous computation was close to 450. The coherent structure appears to withstand remarkably well the effects of the imposed diffusion. This insensitivity

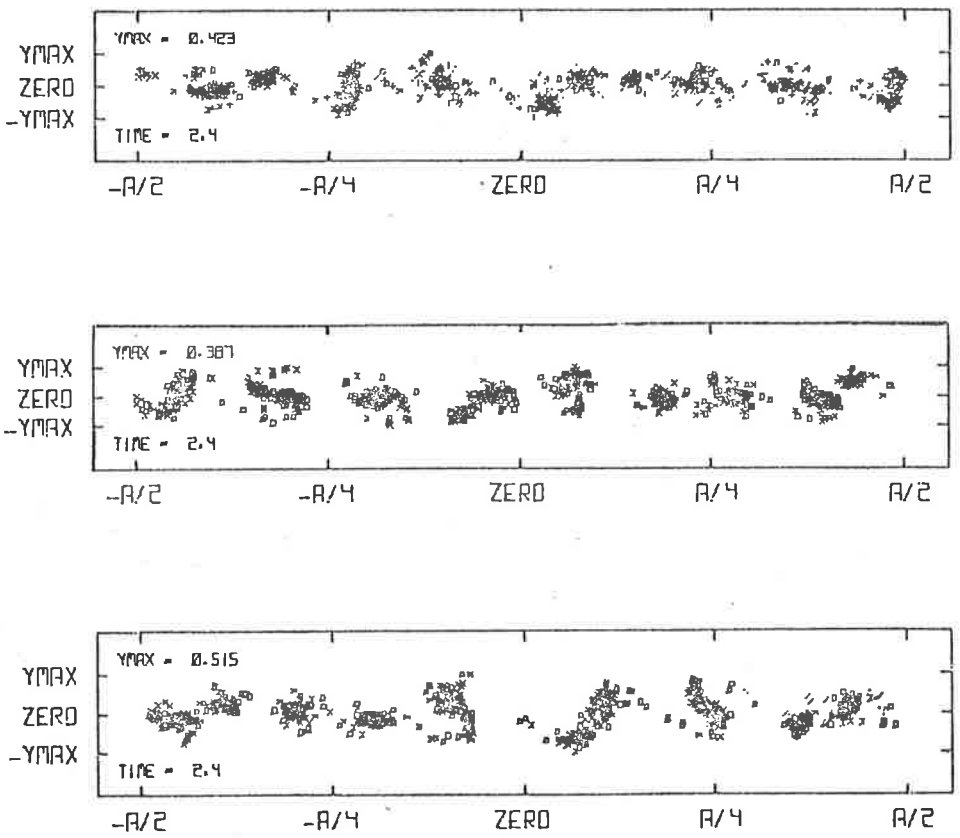

Figure 29: flow configurations in inviscid (top), viscous (middle) and turbular (bottom) computations for a type -I layer.

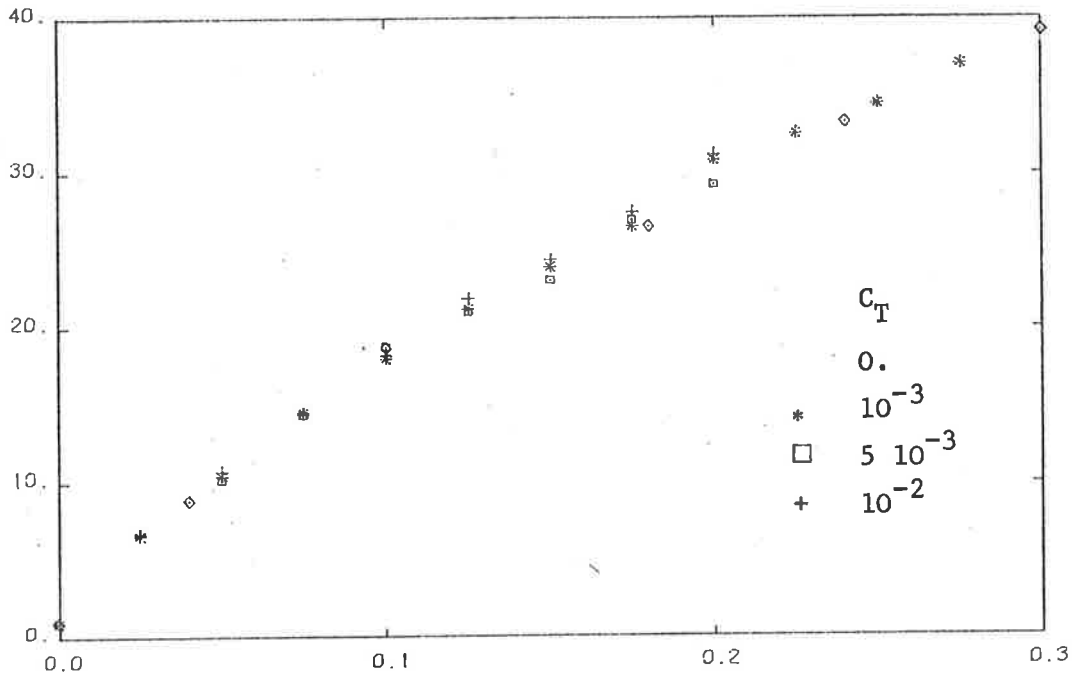

Figure 30: comparison of visual growth of type -II layers subject to "turbular" viscosities of various intensities.

to active diffusing mechanisms is also illustrated in Figure 30, which shows the growth histories of a type II layer subject to turbular diffusions of large intensities ($C_T = 10^{-3}$, $5\ 10^{-3}$ and 10^{-2}); departures from the growth of the inviscid reference flow, also shown on the figure, are surprisingly small. Further evidence of the lack of sensitivity of large vortical structures to molecular diffusion is put forward in Figure 31, which displays the average correlation coefficient $\bar{r}_{11}(\xi^*)$ of a type I viscous flow ($R\delta \approx 450$). It is remarkable to note how little the diffusive process has modified the similarity characteristic of the structure (compare with the correlation in Figure 28). All data suggest clearly a weak response of the coherent motion to the diffusive action of small-scale two-dimensional motions.

III.5.2 Low Reynolds number layers

It is of interest to mention here two results that were obtained in the analysis of low Reynolds number layers. Some "viscous" calculations were performed on layers initially defined by a *uniform* distribution of point-vortices (typically 3 superposed rows of 250 vortices each). In these configurations, the random displacements of the vortices provide the mechanism that displaces the system from its unstable equilibrium and triggers the motion of the layer.

The average autocorrelation coefficient $\bar{r}_{11}(\xi^*)$ that corresponds to a computation with an initial Reynolds number of the order of 450 is shown in Figure 32. Besides the well marked periodicity of the structure, one notes that the mean spacing between vortical clouds is extremely close to that of type -I layers (i.e. $\bar{\ell} \approx 3.6\ \delta_\omega$). This observation corroborates an earlier suggestion that the large-scale structure is strongly dependent on the distribution of circulation per unit length: it is clear that the

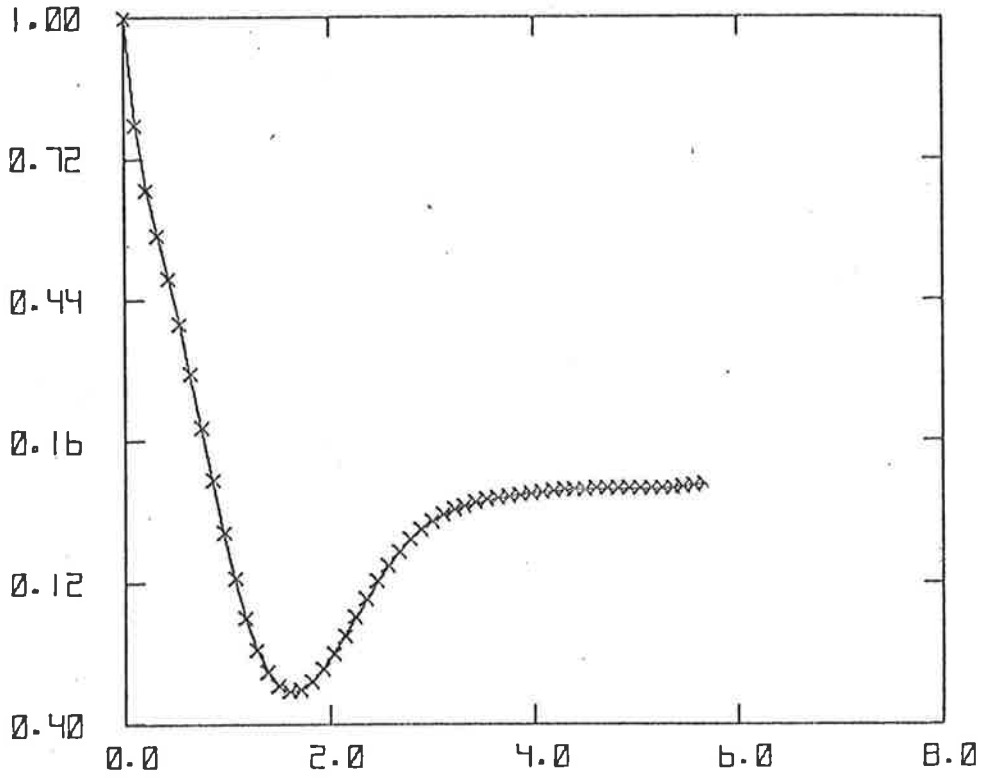

Figure 31: Average autocorrelation coefficient $\bar{r}_{11}$ (ξ/δ_ω) for type -I viscous flow ($R\mathring{e}$ ~ 450).

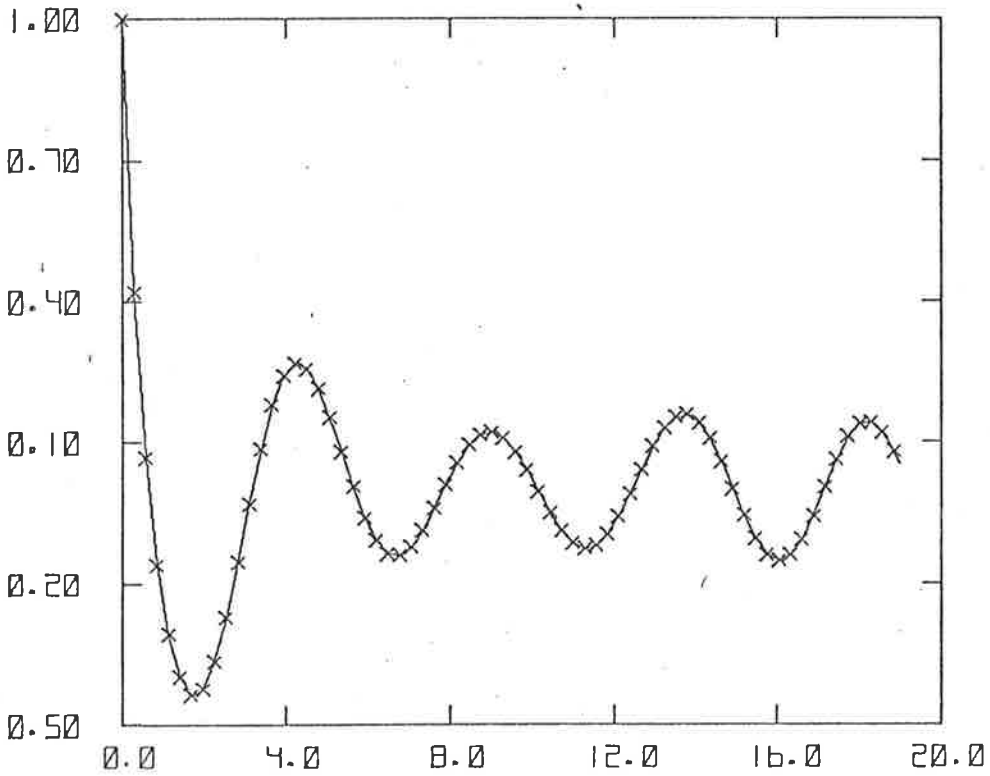

Figure 32: Average autocorrelation coefficient $\bar{r}_{11}$ (ξ/δ_ω) for initially uniform viscous layer ($R\mathring{e}$ ~ 450).

isotropic nature of the "viscous" random walk tends to generate an effective initialization analogous to a type -I layer.

Large values of the viscosity may be simply achieved by sufficiently large amplitudes of the Gaussian displacements. The typical evolution of a highly viscous layer ($R\mathring{e} \sim 1$) is depicted in Figure 33. It is known (see for example Batchelor, 1962, § 4.3) that the vorticity thickness of the layer grows linearly with the *square-root* of time as a result of viscous diffusion. The growth history of the layer represented here indicates clearly that the underlying growth mechanism is essentially a gradient-diffusion process. This is confirmed by the flow visualizations (not shown) where no tendency towards clumping into vortical clouds can be discerned. Efforts towards the precise determination of a critical Reynolds number for transition are presently undertaken and will be reported separetely.

III.6 SUMMARY

Broadly speaking, Chapter III presents a study of the motions which arise when an infinite perturbed vortex sheet deforms and evolves in its own induced velocity field. The vortex sheet is represented by thick periodic vorticity layers; attention is focused on the general properties of the large-scale structures which are found to emerge from the vorticity distributions. The relevance of these questions of vortex kinematics to the turbulent mixing layer is investigated, on the basis of a temporal problem which relates to the spatially developing flows through a Galilean transformation of coordinates.

Two specific types of vorticity distributions are considered. Type I distributions are characterized by a *uniform* distribution of circulation per unit length; these of type II have a *random* circulation

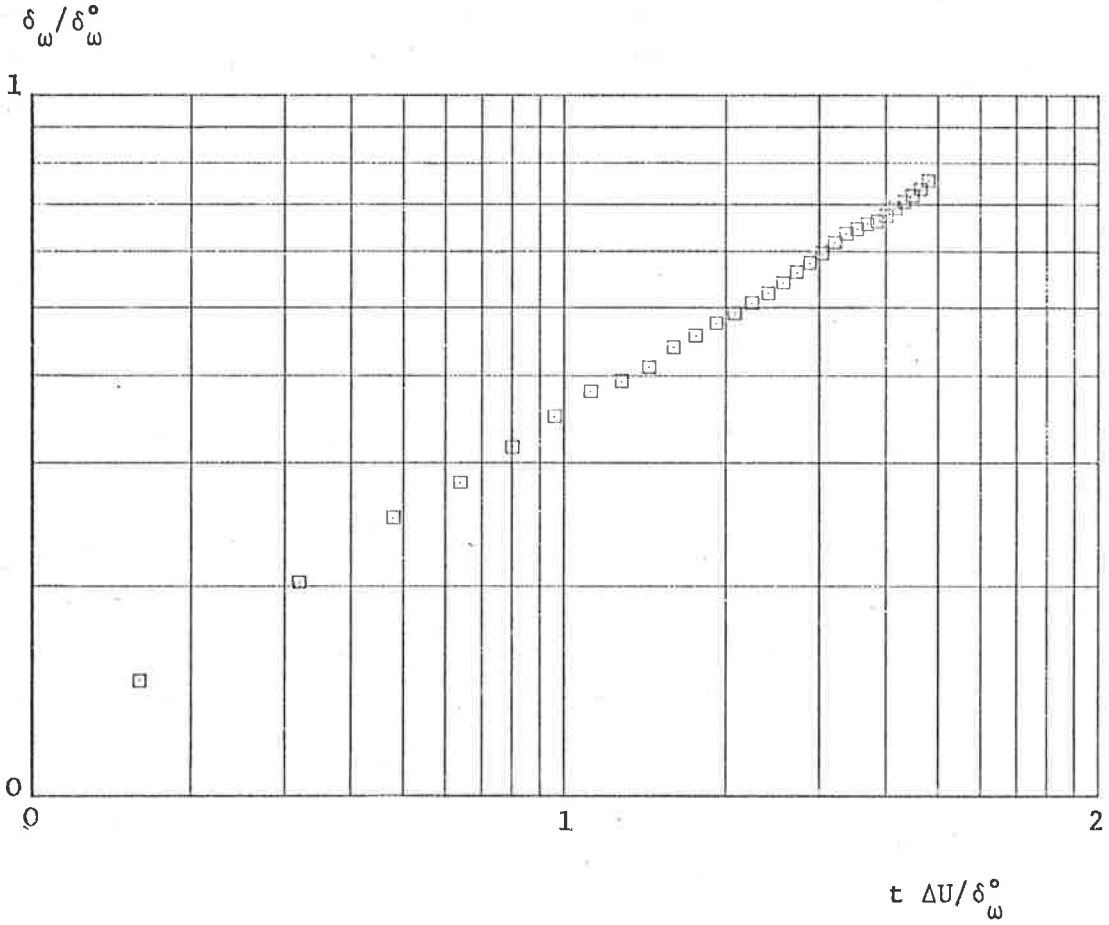

Figure 33: Growth of highly viscous ($R\mathring{e} \sim 1$), initially uniform layer. (Vorticity thickness ratio versus time).

per unit length. The vortex sheet is given a finite thickness by randomizing the coordinates of the point-vortices in the direction normal to the sheet. Use of the CTC method permits the tracking of a fairly large number of vortices (typically 750) at reasonable computing costs. Most computations are carried out in conditions where the fluid is very nearly inviscid. Several calculations are also performed to investigate the diffusive action of molecular viscosity and the effects of a small-scale motion on the larger flow structures; in these studies, diffusion is modelled by adding a Gaussian random component to the hydrodynamical motion of the vortices.

Inviscid calculations show in all cases the spontaneous emergence of arrays of vortical clouds that interact and amalgamate into larger, clearly identifiable structures. These interactions constitute the fundamental growth mechanism of the layers. The correlation analysis of the fluctuating velocity fields reveals the coherent character of the arrays of structures. All features of the computed flows appear strongly reminiscent of those observed in the large structure of the turbulent mixing layer.

Viscous computations at moderate initial Reynolds numbers (~500) indicate that the structure is remarkably insensitive to molecular and "turbular" diffusions. At very small Reynolds numbers (~10), viscous action "kills" the structure and the layer grows by a process of gradient diffusion.

CHAPTER IV : THE POINT-VORTEX APPROXIMATION OF NON-CIRCULATION PRESERVING FLOWS .

IV.1 INTRODUCTION

All vorticity layers studied in chapter III were characterized by a single parameter, the velocity difference ΔU across the interface between the two uniform streams. A more general class of shear layers is that characterized by a second parameter, $\Delta\rho$, which represents the density jump across the vortex sheet. Shear layers between fluids with different densities are the central subject of the present chapter; their study is relevant to problems as diverse as combustion, jet noise, pollutant dispersion control and weather prediction.

The lack of understanding of, and the general divergences about mixing, entrainment and transport processes in turbulent shear flows (see Roshko, 1976 & 1979) are a strong motivation for tackling certain aspects of the mechanics of simple shear flows by developing basic models; an attempt towards the modelling of density aspects on inviscid, non-uniform shear layers, based on a point-vortex, CTC calculation, is presented in the following pages. Although applied to a specific case, the scope of the modelling method proposed hereafter extends effectively to the broader class of "non circulation-preserving" motions. These flows possess the distinguishing property that the total rate of change of the circulation around a material curve is not necessarily zero; this is in contrast with all flows considered so far, for which $d\Gamma/dt$ did vanish identically. The general applicability of the present model will be implicit in many of the arguments to be developed.

Section IV.2 examines the origin and the nature of the mechanisms capable of modifying the distribution of vorticity in a fluid in motion; the source (sink) of circulation is identified in Bjerknes theorem as the interaction between the pressure gradient and the density gradient.

The modelling of vorticity regions by a point-vortex approximation in the presence of density inhomogeneities is considered in Section IV.3, for the case of *incompressible* fluids. It is argued that use of a suitable discretized form of Bjerknes theorem, coupled with a representation of the density field based on "density carriers" (i.e. particles that transport a density value), provides, in the spirit of the cloud discretization approach, a simple but adequate means of analysis. The model relies on the CTC algorithm as fundamental computational tool.

The proposed computation method is then applied to the study of the effects of density ratio (and to a lesser extent, of buoyancy) upon the structure developing from a sinusoidal vorticity layer of finite thickness. The results of various numerical experiments, presented in Section IV.4, suggest that the approach followed here, although of limited accuracy, provides a firm basis to comprehend and unveil the fundamental aspects of the physics of the problem.

IV.2 CREATION OF CIRCULATION IN A FLUID IN MOTION

Let us examine under which conditions the circulation around a material curve drawn in the fluid changes as the material loop is convected by the motion. The analysis is better understood if one bears in mind a theorem and an identity which belong to the study of the kinematics of continuous media, and which are recalled below.

IV.2.1 Vector flux across a material surface

Consider a vector field $\underset{\sim}{q}$ defined everywhere in the domain occupied by the fluid. By definition, the flux of this vector across a material surface S drawn in the fluid is instantaneously given by the expression

$$\phi(\underset{\sim}{q}) = \int_S \underset{\sim}{q} \cdot d\underset{\sim}{S} \qquad [4.1]$$

It is a theorem that the rate of change of this flux, as the motion evolves and entrains the surface of reference (always constituted of the same particles), is determined by the relation

$$\dot{\phi}(\underset{\sim}{q}) = \int_S [\, \dot{\underset{\sim}{q}} - (\underset{\sim}{q}.\nabla)\underset{\sim}{u} + \underset{\sim}{q}\theta \,] \cdot d\underset{\sim}{S} \qquad [4.2]$$

or equivalently by

$$\dot{\phi}(\underset{\sim}{q}) = \int_S [\, \frac{\partial \underset{\sim}{q}}{\partial t} + \nabla \times (\underset{\sim}{q} \times \underset{\sim}{u}) + \underset{\sim}{u}(\nabla.\underset{\sim}{q}) \,] \cdot d\underset{\sim}{S} \,, \qquad [4.3]$$

where $\underset{\sim}{u}$ is the velocity field, $\theta = \nabla.\underset{\sim}{u}$ the expansion (rate), and $\dot{\underset{\sim}{q}} = \frac{D\underset{\sim}{q}}{Dt}$ the rate of change of $\underset{\sim}{q}$ following the motion (see Truesdell, 1954).

IV.2.2 Acceleration, vorticity and expansion

The acceleration field $\underset{\sim}{a}$ is directly expressed in a Eulerian description of the motion as

$$\underset{\sim}{a} = \dot{\underset{\sim}{u}} = \frac{\partial \underset{\sim}{u}}{\partial t} + (\underset{\sim}{u}.\nabla)\underset{\sim}{u} \,, \qquad [4.4]$$

but can also be written in the form given by Lagrange:

$$\underset{\sim}{a} = \frac{\partial \underset{\sim}{u}}{\partial t} + \tfrac{1}{2}\nabla u^2 + \underset{\sim}{\omega} \times \underset{\sim}{u} \,, \qquad [4.5]$$

where $\underset{\sim}{\omega} = \nabla \times \underset{\sim}{u}$ represents the vorticity.

An expression for the quantity $\underset{\sim}{G} = \nabla \times \underset{\sim}{a}$ may be obtained by taking the curl of equation [4.5] ; this yields

$$\underset{\sim}{G} = \nabla \times \underset{\sim}{a} = \dot{\underset{\sim}{\omega}} + \theta\underset{\sim}{\omega} - (\underset{\sim}{\omega}.\nabla)\underset{\sim}{u} \,, \qquad [4.6]$$

an expression valid in any fluid and totally independent of the equations of motion. Note that the identity [4.6] simplifies to

$$\underset{\sim}{G} = \underset{\sim}{\nabla} \times \underset{\sim}{a} = \dot{\underset{\sim}{\omega}} + \theta\underset{\sim}{\omega} \qquad [4.7]$$

in the case of a two-dimensional motion.

IV.2.3 Rate of change of circulation

The previous theorem provides the starting point for classifying possible fluid flows into "circulation-preserving" and "non circulation-preserving" motions. Recalling that the flux of vorticity $\underset{\sim}{\omega}$ across a material surface S is the circulation Γ, one writes

$$\phi(\underset{\sim}{\omega}) = \int_S \underset{\sim}{\omega} \cdot d\underset{\sim}{S} = \int_S (\underset{\sim}{\nabla} \times \underset{\sim}{u}) \cdot d\underset{\sim}{S} = \oint_C \underset{\sim}{u} \cdot d\underset{\sim}{G} = \Gamma , \qquad [4.8]$$

where C is the base-contour or "support" of the material surface S. The rate of change of the circulation is then obtained from [4.2] as

$$\dot{\Gamma} = \dot{\phi}(\underset{\sim}{\omega}) = \int_S [\dot{\underset{\sim}{\omega}} - (\underset{\sim}{\omega}.\underset{\sim}{\nabla})\underset{\sim}{u} + \theta\underset{\sim}{\omega}] \cdot d\underset{\sim}{S} . \qquad [4.9]$$

In view of identity [4.6], this result is also expressed as

$$\dot{\Gamma} = \int_S (\underset{\sim}{\nabla} \times \underset{\sim}{a}) \cdot d\underset{\sim}{S} . \qquad [4.10]$$

One concludes that the rate of change of circulation in a moving fluid depends critically on the motion being/not being a motion for which $\underset{\sim}{\nabla} \times \underset{\sim}{a} = 0$. The existence of an acceleration potential characterizes circulation-preserving flow fields. The "source" of circulation arises from the configuration of the acceleration field; it is clear that further analysis requires the

inclusion of the dynamical aspects of the problem, that is, consideration of the equations of motion; this is done in the next section.

IV.2.4 Bjerknes theorem

Consider situations where the equations expressing the conservation of momentum take the form of Euler's equation

$$\rho \underset{\sim}{a} = - \underset{\sim}{\nabla} p + \rho \underset{\sim}{F} \; ; \qquad [4.11]$$

$\underset{\sim}{F}$ represents the external body force acting on the unit of mass of the fluid. The notation v will be introduced for the specific volume of the fluid ($v = \rho^{-1}$); it will also be assumed that the body forces are conservative, i.e. that there exists a scalar potential Ω such that $\underset{\sim}{F} = - \underset{\sim}{\nabla} \Omega$. Under this assumption, equation [4.11] becomes $\underset{\sim}{a} = - v \underset{\sim}{\nabla} p - \underset{\sim}{\nabla} \Omega$, and one obtains readily the expression for $\underset{\sim}{\nabla} \times \underset{\sim}{a}$:

$$\underset{\sim}{\nabla} \times \underset{\sim}{a} = \underset{\sim}{G} = \underset{\sim}{\nabla} p \times \underset{\sim}{\nabla} v \; . \qquad [4.12]$$

The rate of change of circulation obeys therefore the law

$$\dot{\Gamma} = \int_S (\underset{\sim}{\nabla} p \times \underset{\sim}{\nabla} v) \cdot d\underset{\sim}{S} \qquad [4.13]$$

Expression [4.13] discloses the nature of the mechanism responsible for the modification of the circulation in a non-homogeneous fluid, the interaction between the pressure and the density gradients; this relationship is known as the theorem of Bjerknes. This classical result is often presented in a different fashion. If the potential Ω exists, one may write [4.10] under the form

$$\dot{\Gamma} = - \int [\underset{\sim}{\nabla} \times (v \underset{\sim}{\nabla} p)] \cdot d\underset{\sim}{S} \; .$$

Applying Stokes theorem, one obtains

$$\dot{\Gamma} = -\oint_C v\nabla p \cdot d\underset{\sim}{C} \quad , \quad \text{i.e.} \quad \dot{\Gamma} = -\oint_C \frac{dp}{\rho} \quad , \qquad [4.14]$$

which is the conventional statement of the theorem. Note finally that in terms of the density, the theorem [4.13] is written

$$\dot{\Gamma} = \int_S \frac{1}{\rho^2} (\nabla\rho \times \nabla p) \cdot d\underset{\sim}{S} \, . \qquad [4.15]$$

Bjerknes theorem [4.15] applies whenever density gradients exist (or develop) in the fluid, irrespective of the origin of the corresponding inhomogeneities: the generation (destruction) of circulation arises from the same mechanism in compressible and incompressible inhomogeneous fluids.

In two-dimensional flow fields, the vector $\underset{\sim}{G}$ has only a non-zero component in the direction normal to the plane of motion; expression [4.15] simplifies in that case to

$$\dot{\Gamma} = \int_S \frac{1}{\rho^2} \left(\frac{\partial p}{\partial x}\frac{\partial \rho}{\partial y} - \frac{\partial p}{\partial y}\frac{\partial \rho}{\partial x}\right) dxdy \, . \qquad [4.16]$$

The above expression constitutes the basis of the study of two-dimensional, non circulation-preserving fluid motions; it is shown in Section IV.3 that the evolution of these flows may be computed by the method of discrete vortices. The success of the point-vortex approximation depends essentially on deriving a suitable discretized form of equation [4.16]; possible alternative choices for the numerical evaluation of [4.16] and a formula that appears well adapted to the point-vortex, CTC method are discussed in the following.

IV.3 POINT-VORTEX MODELLING OF NON-CIRCULATION-PRESERVING MOTIONS

IV.3.1 The fundamental approach

Point-vortex modelling of non circulation-preserving flows has not attracted a great deal of attention in the literature; two notable exceptions are the studies of Zalosh (1976) and Meng & Thomson (1978). Both papers examine flows in which the inhomogeneity arises at the interface between two *incompressible* fluids of *slightly* different densities. The present study is also restricted to the case of incompressible fluids (*), but removes the limitation of *small* density discontinuities: the possibility of large density ratios is included in the analysis.

The basis of the discrete vortex method, in the *homogeneous* case, consists of the equations of motion

$$\kappa_\alpha \dot{x}_\alpha = -\frac{\partial H}{\partial y_\alpha} \quad ; \quad \kappa_\alpha \dot{y}_\alpha = \frac{\partial H}{\partial x_\alpha} \qquad (\alpha = 1,2,\ldots,NV) \ , \qquad [4.17]$$

whose integration in time yields the trajectories of the NV vortices; H is the Kirchhoff function of the system of vortices (see Section I. .). In the *nonhomogeneous* case, the same equations of motion apply, complemented by the equations giving the rate of change with time of the strengths of the vortices:

$$\dot{\kappa}_\alpha = \dot{\kappa}_\alpha \ (\nabla p, \nabla \rho) \qquad (\alpha = 1,2,\ldots,NV) \qquad [4.18]$$

which are known (from [4.16]) to depend upon the pressure and density gradients, as explicitly indicated. Equations [4.17] and [4.18] form a set of 3 NV first-order differential equations for the variables x_α, y_α and κ_α

(*) Compressibility effects are not simply accounted for in a point-vortex approximation, as discussed in Section I.

($\alpha = 1,2,\ldots,NV$). The problem is fully determined if an initial configuration $(x^\circ_\alpha, y^\circ_\alpha, \kappa^\circ_\alpha)$ ($\alpha = 1,2,\ldots,NV$) is prescribed.

IV.3.2 Computation of $d\kappa_\alpha/dt$

Equation [4.18] is a discretized form of equation [4.16]; modified forms of [4.18] are obtained from [4.16] by eliminating the pressure-gradient term - a quantity not directly accessible to a point-vortex calculation - in terms of the local acceleration. Returning to equation [4.13], and noting that Euler's equation [4.11] reads $\nabla p = (F - a)/v$, one obtains

$$\dot{\Gamma} = \int_S [\,(a-F) \times \nabla(\log \rho)\,] \cdot dS \,. \qquad [4.19]$$

Use of the vector identity $\nabla \times (mc) = m(\nabla \times c) + (\nabla m) \times c$

yields immediately

$$\dot{\Gamma} = \int_S dS \cdot \{(\log \rho)\nabla \times (a-F) - \nabla \times [\log \rho (a-F)]\} \,,$$

and

$$\dot{\Gamma} = \oint_C \log \rho \,(F-a) \cdot dC + \int_S \log \rho \,(\nabla \times a) \cdot dS \,, \qquad [4.20]$$

after application of the theorem of Stokes and under the assumption of the existence of the potential Ω.

The discretized forms of equation [4.20] employed by Zalosh (who considered Rosenhead's problem, in the case of two fluids of different densities) and Meng & Thomson (in their study of the rise of a buoyant cylinder) stem from the same fundamental assumption: a distribution of point-vortices along the "line" of density discontinuity depicts faithfully

the geometry of the deforming interface. It is interesting to consider their formulae in some detail; they may be derived as follows.

IV.3.2.1 The classical formulation

Assume that vortices are distributed uniformly along the interface, a distance $\Delta\ell$ apart, as shown on Figure 34. The strength of vortex α is defined by the value of the circulation around a closed contour C_α of length $\Delta\ell$ and width ϵ encircling the vortex and "straddling" the interface (see Figure 34). For this contour, the contribution from the surface integral in [4.20] vanishes - the interface is the only site of vorticity changes -, and one obtains

$$\dot{\kappa}_\alpha = \oint_{C_\alpha} \log \rho \; (\underset{\sim}{F}-\underset{\sim}{a}) \cdot d\underset{\sim}{C}_\alpha \; . \qquad [4.21]$$

Letting ϵ tend to zero yields

$$\begin{aligned} \dot{\kappa}_\alpha &= \Delta\ell \; (\underset{\sim}{F}-\underset{\sim}{a}_\alpha) \cdot \{(\log \rho_2) \; \underset{\sim}{e}_{PQ} + (\log \rho_1) \; \underset{\sim}{e}_{RS}\} \\ &= (\log s) \; \Delta\ell \; (\underset{\sim}{F}-\underset{\sim}{a}_\alpha) \cdot \underset{\sim}{e}_\ell \; , \end{aligned} \qquad [4.22]$$

where $s = \rho_2/\rho_1$ is the density ratio and $\underset{\sim}{e}_\ell = d\underset{\sim}{\ell}/d\ell$ is the unit direction vector of the interface. An estimate for $\underset{\sim}{e}_\ell$ is obtained from the coordinates of the vortices adjacent to vortex α; clearly, from Figure 34, one has

$$\underset{\sim}{e}_\ell \simeq \underset{\sim}{e}_{AC} = \frac{1}{2\Delta\ell} \; (\delta x_{\alpha-1,\alpha+1}, \; \delta y_{\alpha-1,\alpha+1}) \; .$$

Substituting this estimate into [4.22] leads to the expression

$$\dot{\kappa}_\alpha = -\frac{\log s}{2} \; [a_x \, \delta x + (a_y + g) \, \delta y] \; , \qquad [4.23]$$

in which the subscripts α have been omitted for clarity; a_x and a_y

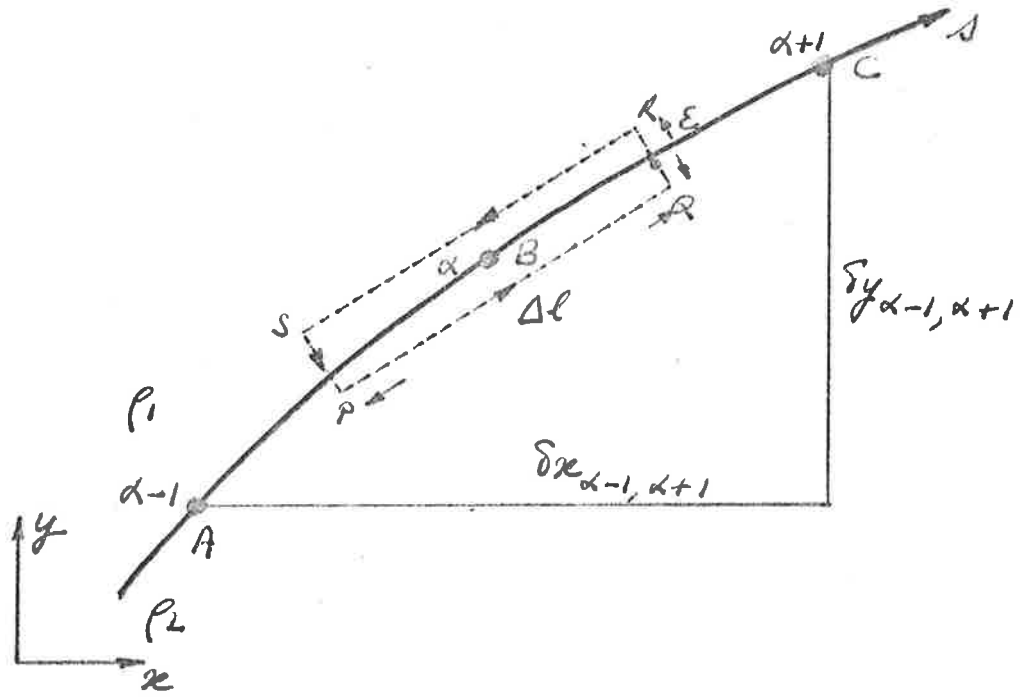

Figure 34: discretization of interface between fluids of different densities by a line distribution of point vortices.

represent the components of the acceleration of vortex α and g is the acceleration of gravity. With the additional assumption that the density ratio s is slightly different from unity, [4.23] writes (*)

$$\dot{\kappa}_\alpha = \left(\frac{1-s}{1+s}\right) [\, a_x\, \delta x + (a_y + g)\, \delta y\,] \quad ; \qquad [4.24a]$$

this is the approximation adopted by Zalosh (1976). In problems where no shear exists initially across the density interface and where the motion from rest is induced by buoyancy only, formula [4.24] reduces to

$$\dot{\kappa}_\alpha = \left(\frac{1-s}{1+s}\right) g\, \delta y \qquad [4.24b]$$

(Meng & Thomson, 1978).

IV.3.2.2 A "cloud discretization" formulation

Formulae [4.24] stem from the assumption that the evolution in time of a *single* row of point-vortices represents accurately that of the interface between the fluids. As observed in various studies (refer to the discussion in Section II. 7), the coincidence between the continuous vortex sheet and the line which connects the vortices tends to disappear as the flow evolves. This geometrical divergence destroys the validity of the approximations [4.24] at a stage of the computation that seems to depend on the number of vortices chosen for the discretization. Calculations of the motion of a sinusoidal vortex sheet in slightly non-uniform situations (density ratio close to unity), based on formula [4.24a], were performed; they were found to break down when the number of vortices was larger than 40, and sooner as this number was increased. These results are consistent

---

(*) Recall that $\log x = 2\left(\frac{x-1}{x+1}\right) + \frac{2}{3}\left(\frac{x-1}{x+1}\right)^3 + \ldots \quad (x > 0)$

with the observation that refining the single-row discretization of vortex sheets tends to trigger the occurence of random movements in the trajectories of the vortices (refer to Section II.2.2).

A possible solution to these problems, suggested and adopted in the early part of this work, is to represent the interface as a thin vorticity region of finite thickness, and use *several* rows of vortices in the discretization. The increase in definition of the vorticity distribution is then balanced by the loss in sharpness of the geometry of the interface; use of equations [4.24] is no longer warranted with this type of discretization. The rate of change with time of the strength of vortices used in a cloud approximation was computed on the basis of the formula derived in what follows.

Let us represent a vortex sheet by distributing (in a uniform or random fashion) NV vortices throughout a layer of finite thickness. Be ΔS_α the area of the material element associated with point-vortex α. Reverting to formula [4.19] written in terms of vector components, one obtains the time rate of change of the vortex strength as

$$\dot{\kappa}_\alpha = \int_{\Delta S_\alpha} \left(\frac{a_x}{\rho} \frac{\partial \rho}{\partial y} - \frac{a_y + g}{\rho} \frac{\partial \rho}{\partial x} \right) dxdy \ . \qquad [4.25]$$

Provided the number of vortices is sufficiently large (i.e. ΔS_α is suitably small), one may approximate the integral by considering local average values of the terms of the integrand; this leads to the estimate

$$\dot{\kappa}_\alpha (t) = \frac{\Delta S_\alpha}{\rho_\alpha} \left[a_{x\alpha} \left(\frac{\partial \rho}{\partial y}\right)_\alpha - (a_{y\alpha} + g) \left(\frac{\partial \rho}{\partial x}\right)_\alpha \right] . \qquad [4.26]$$

The values of ΔS_α and of ρ_α at time t are simply equal to the values taken at time $t = o$: in the incompressible case, one has

$$\frac{d\Delta S}{dt} = 0 \quad ; \quad \frac{d\rho}{dt} = 0. \qquad [4.27]$$

The acceleration terms in [4.26] are readily evaluated from the known motion of vortex α; the values of $a_{x\alpha}$ and $a_{y\alpha}$ at time t are given by the expressions

$$a_{x_\alpha} = \frac{u_\alpha(t) - u_\alpha(t - \Delta t)}{\Delta t} = \frac{\Delta u_\alpha}{\Delta t}$$
$$a_{y_\alpha} = \frac{v_\alpha(t) - v_\alpha(t - \Delta t)}{\Delta t} = \frac{\Delta v_\alpha}{\Delta t} \quad , \qquad [4.28]$$

using a simple first-order backward difference scheme (higher-order schemes could be used to improve the accuracy of these estimates; this is not justified, however, in view of the approximation made on the other terms and discussed below).

The evaluation of the local gradients of the density field is somewhat more delicate. Equation [4.27b] indicates that fluid particles retain their initial density value throughout the flow evolution. Vortices may then be "tagged" with a density value (defined by the shape of the density profile at flow initiation) which accompanies them during their motion. The salient idea for imbedding density effects in a point-vortex "cloud" computation is to estimate the values of the gradients $(\partial\rho/\partial x)_\alpha$ and $(\partial\rho/\partial y)_\alpha$ from the distribution $\rho(x_\beta, y_\beta)$ defined by the set of vortices β which surround vortex α. Fitting a surface $\rho(x,y)$ to the discretized field $\rho(x_\beta, y_\beta)$ yields estimates of the gradients as coefficients of the fit. The neighbourhood of vortex α at time t may be defined in two distinct ways: it may be constituted of those particles which are *initially* in the neighbourhood of the vortex, or made of the set of particles which *currently* happen to lie within a certain distance from the vortex. In

either case, the definition of the vicinity of a vortex involves some characteristic distance which fixes its spatial extent. The validity of the method rests on the implicit assumption that gradient estimates are not sensitive functions of this characteristic dimension; numerical tests showed a posteriori that this assumption is reasonably well founded (see Section IV.4). These arguments lead to the following formula for computing the change in circulation $\Delta\kappa$ of a point-vortex in an elementary time interval Δt:

$$\Delta\kappa = \frac{\Delta S\ \Delta u}{\rho}\ c_y - \frac{\Delta S\ \Delta v}{\rho}\ c_x - \frac{\Delta S\ g\ \Delta t}{\rho}\ c_x$$

$$= \Delta\kappa_x + \Delta\kappa_y + \Delta\kappa_g \ ; \qquad [4.29]$$

c_x and c_y are the values of the estimated density gradients in the x- and y- directions respectively, i.e. the relevant coefficients of the local polynomial fit. All quantities in this formula should be tagged with the index α that identifies the point-vortex.

In addition to the vortices, which constitute the active elements of the flow, passive "markers" may be distributed over the computation interval. Markers are effectively vortices that carry no circulation; their main function is to improve the definition of the density field. The presence of additional density carriers ensures that the estimates of the density gradients are computed in favourable conditions. They may be allocated "statically" or "dynamically" to the vortices in order to represent the local density distributions. Passive particles are also useful as an aid in visualizing the flow. The use of markers is computationally more advantageous than that of vortices: substitution of NM vortices by passive particles results in a saving of computation cost that scales like NM^2.

The suitability and performance of the computation method described in this section are discussed in the rest of the chapter, which is dedicated to a first analysis of the effects of (large) density ratios on the coherent structure of vorticity layers.

IV.4 DENSITY EFFECTS ON THE STRUCTURE OF VORTICITY LAYERS

IV.4.1 The temporal problem for two-density layers

The modelling of non-uniform density shear layers is based, as that of homogeneous layers, on a correspondence between the *spatially* developing flow and an idealized *temporal* problem. The principle of a Galilean transformation (see Section III.3.1) must be applied somewhat carefully in order to interpret the two-density layers results appropriately. Before examining this issue, let us recall a useful result of linear stability theory.

Consider a layer of fluid (density ρ_1) moving with a uniform velocity u relative to another layer of fluid (density ρ_2) which, without loss of generality, is assumed to be at rest. The movement of the upper layer is parallel to the interface between the fluids. The linear stability characteristics of this vortex sheet are obtained by considering perturbation quantities (pressure, velocities, interface displacement) of the form

$$q(x,y,t) = f(y)\ e^{i(\kappa x - \omega t)}$$

$$= f(y)\ e^{\omega_i t}\ \{\cos(\kappa x - \omega_r t) + i \sin(\kappa x - \omega_r t)\}\ ,$$

where $\omega = \omega_r + i\omega_i$ is a complex frequency.

It is found that disturbances whose complex velocity $c = \omega/\kappa$ is given by

$$c_{\pm} = \frac{u}{\rho_1 + \rho_2} \left[\rho_1 \pm i \sqrt{\rho_1 \rho_2} \right]$$

are solutions of the problem (Landau & Lifchitz, §30, 1971). The vortex sheet is absolutely unstable to infinitesimal perturbations of all wavelengths.

The phase velocity of the perturbation is given by

$$c_r = \frac{u\rho_1}{\rho_1 + \rho_2} = \frac{u}{1 + s} \quad ; \quad (s = \rho_2/\rho_1)$$

this expression shows that $c_r \to o$ for $s \gg 1$ (heavy fluid at rest) but that $c_r \to u$ for $s \ll 1$ (heavy fluid moving). One concludes that the instability wave tends to travel with a velocity approaching that of the *denser* fluid.

This important observation suggests that the following temporal problem be associated with spatially developing, two-density mixing layers (Brown, 1974). Suppose that the plane $z = 0$ separates two half spaces, one of fluid of density ρ_1 $(z > 0)$ and the other of fluid of density ρ_2 $(z < 0)$. At some initial time, both spaces are impulsively set into a uniform motion in which the velocities at infinity are equal but opposite in direction $(U(z \to +\infty) = -U(z \to -\infty) = U_\infty)$. The interface between the fluids is an unstable vortex sheet which will ultimately evolve towards a "turbulent" state by developing large scale vorticity structures. The emergence of the structures in the homogeneous case $(\rho_1 = \rho_2)$ is clearly established by the computer experiments described earlier in this work; that a (possibly distinct) structure develops in the two-density case $(\rho_1 \neq \rho_2)$ is suggested by the flow visualizations of the mixing layer between gases with different densities (Brown & Roshko, 1974). When $\rho_1 = \rho_2$, the structures do not move relative to the observer (i.e. to the computation interval). For $\rho_1 \neq \rho_2$, however, the observer will contemplate structures which travel with a velocity U_o in the same direction

as that of the heavier fluid. In a system of reference *moving with the structure*, the velocities at infinity will be

$$u_1 = U_\infty - U_o \quad ; \quad u_2 = U_\infty + U_o \qquad [4.30a]$$

if the heavier fluid is in the upper half-plane, and

$$u_1 = U_\infty + U_o \quad ; \quad u_2 = U_\infty - U_o \qquad [4.30b]$$

if the denser fluid fills the lower half-plane. Clearly, the translation velocity U_o depends on the density ratio $s = \rho_2/\rho_1$.

The apparent spreading angle $d\delta/dx$ of the temporally growing layer observed in a frame of reference translating relative to the structure may be shown to be

$$\delta' = .178 \; \frac{(1 + k(s))\;(1 - r)}{k(s) + r} \; , \qquad [4.31]$$

where $r = U_2/U_1$ is the ratio of the fluid velocities on either side (recorded in the moving axes) and where $k(s) = u_2/u_1$ (u_1 and u_2 are given by equations [4.30]). The function $k(s)$ may be related to the volume rates λ_1 and λ_2 at which the fluids are entrained on each side of the layer through the expression

$$\frac{\lambda_1}{\lambda_2} = \frac{1}{k(s)} \qquad [4.32]$$

(A full discussion of the model that leads to the predictions [4.31] and [4.32] may be found in Brown (1974).

Knowledge of the function $k(s)$ appears essential to the understanding of the growth and entrainment processes in non-uniform layers. The few available experimental data suggest a possible dependence of the type

$k(s) \approx s^{-n}$ $(n \approx 5)$. Preliminary calculations, showing the effects of the density ratio upon the vorticity structure for a simple flow geometry, are presented in the following section. The essential purpose of this investigation is to determine the *qualitative* behaviour of the structure in the presence of large density ratios; the analysis of the results in the light of the temporal problem defined above leads in addition to a *quantitative* prediction for the function $k(s)$ which appears reasonable in view of the simplicity of the model used.

IV.4.2 Effect of density ratio on the structure in a sinusoidal vorticity layer

In order to investigate the effects of large density ratios on the structure, it was decided to revert to the simplest initial configuration by considering the case of the sinusoidal vortex sheet of finite thickness. The vorticity layer was discretized into a number of superposed rows of point-vortices uniformly distributed over the layer thickness h and wavelength L. The rows were juxtaposed symmetrically on both sides of the mean layer position $\bar{y}(x) = A_o L \sin(2\pi x/L)$. A density value equal to ρ_1 is attributed to vortices located above $\bar{y}(x)$; those below this dividing line carry a density value $\rho_2 = s\rho_1$. Vortices were disposed uniformly along L by subdividing the computation interval into equal segments and placing the vortices at mid-length of each segment. Rows of markers (also located at mid-segment abscissae) were added on both sides of the layer along sinusoids of identical amplitude $A_o L$. Figure 35a shows the general arrangement of a layer defined with 3 rows of 50 vortices each and 2 rows of 50 markers. The initial strength of the vortices was modulated according to their position along the sinusoid, using the formula

$$\kappa(x) = \frac{L\Delta U}{NV} \left(1 - 2\pi A_o \cos (2\pi x/L) \right) ;$$

this expression accounts for the initial non-uniformity in the circulation of the displaced vortex sheet (Hama & Burke, 1960).

The accuracy of the computations was monitored by checking at each time step, the invariance of the total circulation ($\Gamma = L\Delta U$) of the layer. An upper limit of 10% was set on the allowable relative error $\Delta\Gamma/\Gamma_o$. The "quality" of the computations, measured in terms of $\Delta\Gamma/\Gamma_o$, was found to deteriorate with increasing density ratios; typically, values of $\Delta\Gamma/\Gamma_o$ of the order of 10^{-4} were recorded with $s = 1.1$, whilst values as large as 10^{-2} did occur for $s = 7.$ (all other computation parameters being identical). It is interesting to note that $\Delta\Gamma/\Gamma_o$ did not behave as a one-sided error; the device of resetting the total circulation to its initial value after each time step - by replacing the current vortex strength $\kappa_\alpha(t)$ by $\kappa'_\alpha(t) = \kappa_\alpha(t)\ \Gamma_o/\Gamma(t)$ - was found not to alter this behaviour and not to better the accuracy of the calculation: it was not retained as a significant improvement of the method. A series of tests showed that use of too low (5) or too high (>30) a number of particles for the "dynamic" definition of the local density field resulted in a poor overall accuracy; dynamic neighbourhoods containing an average number of 15 to 20 particles were retained as those yielding the "best" flows. In all calculations presented in the following, the local density field was approximated by fitting a least-square plane $\rho = c_o + c_x x + c_y y$ to the surface $\rho\ (x_i, y_i)$ defined by density carriers allocated dynamically to each point-vortex. Although the fundamental significance of these various approximations remains to be assessed, the consistency of the data obtained justifies at this stage the discussion of some of the salient features of the computed flows.

Figure 35 shows in parallel the evolution of the vorticity structure of a sinusoidal layer ($A_o = .05$) in the uniform-density case (left-hand side column) and in the case where the density ratio is 1/3 (right-hand side). The heavier fluid is, according to the definition of s, in the upper half space and travels from left to right on the pictures. The dissimilarities between the "uniform" and the "non-uniform" structures are striking. In the uniform flow, the structure emerges in the classical rolling-up sequence that leads to a perfectly symmetrical, spiral-like vortex cloud; the structure remains stationary relative to the computation interval. The non-uniform structure is, in contrast, essentially asymmetrical; it is also animated of a translating motion in the same direction as the stream of denser fluid. As it develops and moves from left to right, the rolling-up structure entrains a certain volume of fluid; the proportions in which the fluids are entrained depend clearly on their relative densities. It is interesting to estimate the entrainment ratio λ_1/λ_2 (i.e. ratio of volume of fluid entering the structure on side 1 to volume of fluid 2 entrained) on the basis of the areas limited on each side of the line $y = 0$ by the vorticity layer. A graphical evaluation of areas A and B in frame (f) yielded the value $\frac{A}{B} = \frac{1247}{710}$. The estimated entrainment ratio, $\lambda_2/\lambda_1 = 1.75$, agrees remarkably well with the value predicted by [4.32], namely $k\,(1/3) \approx \sqrt{3} = 1.7$.

A separate attempt was made to predict the dependence on s of the function $k(s)$ from estimates of the translation velocity U_o of the structure relative to the computation grid. Figure 36 shows the trajectories of the centre of mass of the structure on a x,t diagram, for several values of the density ratio (from $s = 1.1$ to $s = 5.$). The slope of a trajectory defines the instantaneous translation velocity of the structure, which

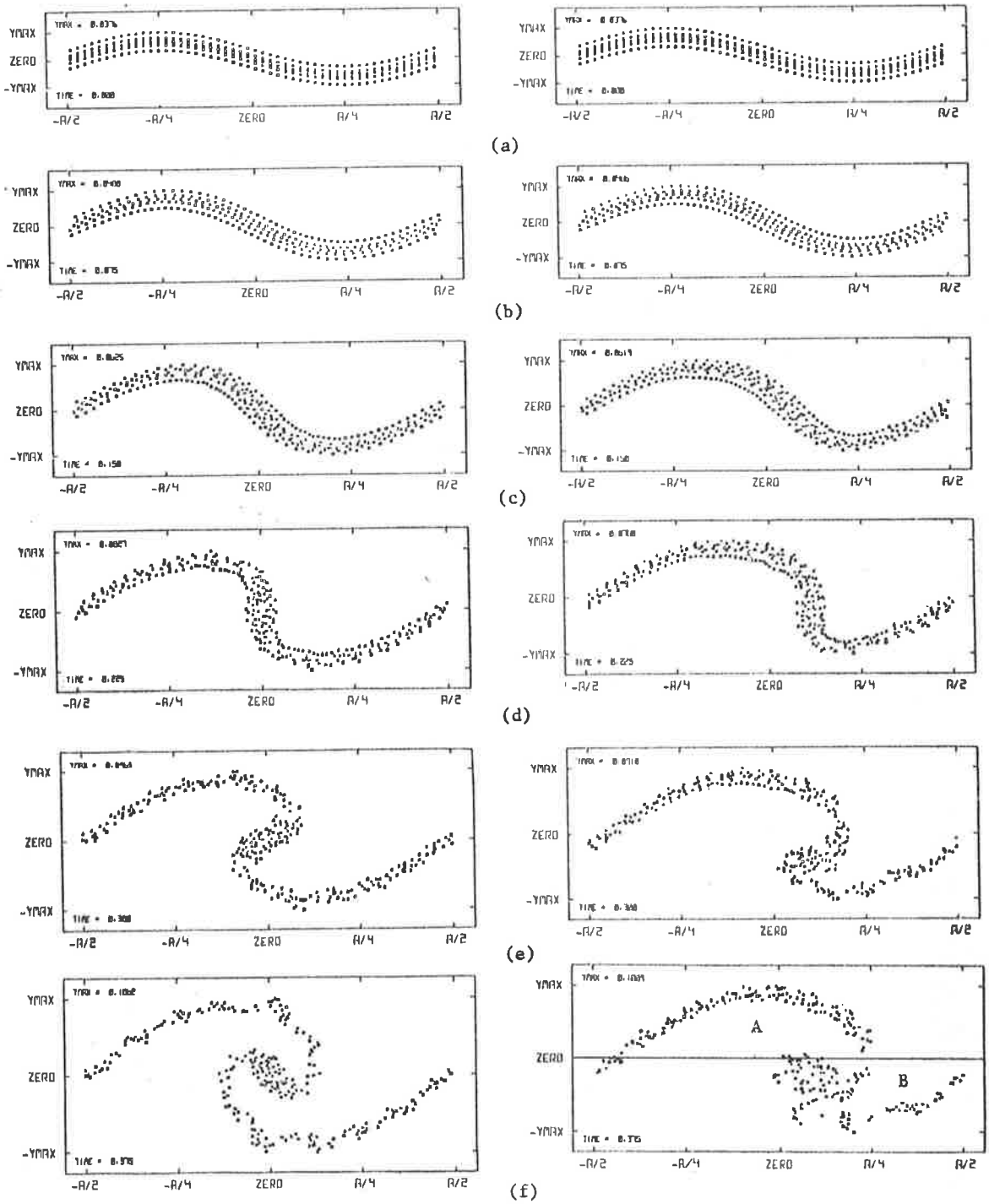

Figure 35: Evolution of a thick sinusoidal vorticity layer in the uniform (left hand side) and non uniform (s=3) cases.

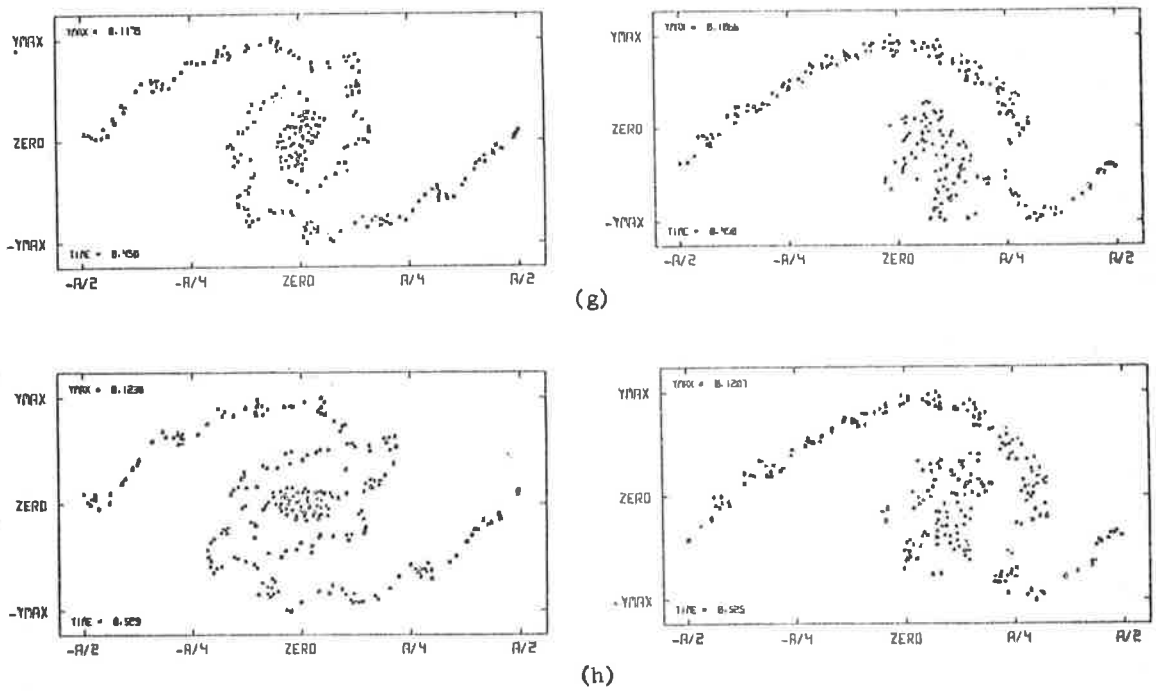

Figure 35: Evolution of a thick sinusoidal vorticity layer in the uniform and non uniform cases (continued).

appears to remain reasonably constant for a given density ratio. Data points displayed in Figure 36 correspond to the early stages of the flows where the error $\Delta\Gamma/\Gamma_o$ is smaller than 5%; the degradation in accuracy ($\Delta\Gamma/\Gamma_o$ increasing) observed at large times resulted in departures of the trajectories from their linear trend.

Estimates of U_o based on the data presented allowed to infer values of $k(s) = u_2/u_1$ based on equations [4.30]. Figure 37 shows the predicted behaviour (squares), which appears to be close to $s^{-0.4}$ (dashed line); the continuous line represents the function $s^{-\frac{1}{2}}$, suggested by available experimental data (Brown, 1974). In view of the simplified approach of the present model, the prediction in Figure 37 appears successful and an encouragement for further development.

IV.4.3 Froude number effects on the structure in a sinusoidal vorticity layer

All calculations presented so far did not take into account the effects of gravity which, according to equation [4.29], contributes to the modification of the circulation in the flow by its interaction with the density field. Inclusion of gravitational action into the computations involves a trivial modification of the computer code; it was thought interesting to conduct a few runs where $\Delta\kappa_g$ is not identically zero.

A first understanding of the phenomenon may be gained by a rough order of magnitude analysis of equation [4.29]. Assuming that changes in circulation are chiefly due to gravitational action, one infers from [4.29] that

$$\frac{\Delta\kappa}{\Delta t} \simeq \frac{\Delta\kappa_g}{\Delta t} \sim \frac{\Delta S}{\rho_M}\, g\, \frac{\Delta\rho}{\Delta x}\,, \qquad [4.33]$$

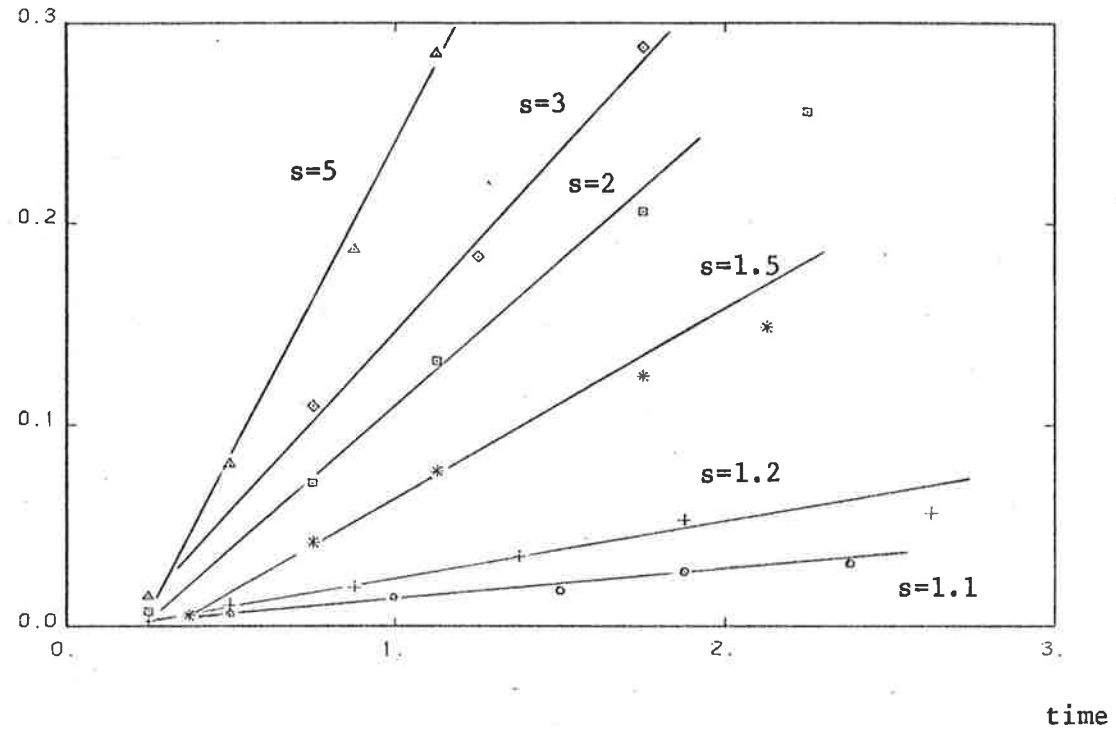

Figure 36: Trajectories of centre of mass of structure for various values of density ratio s

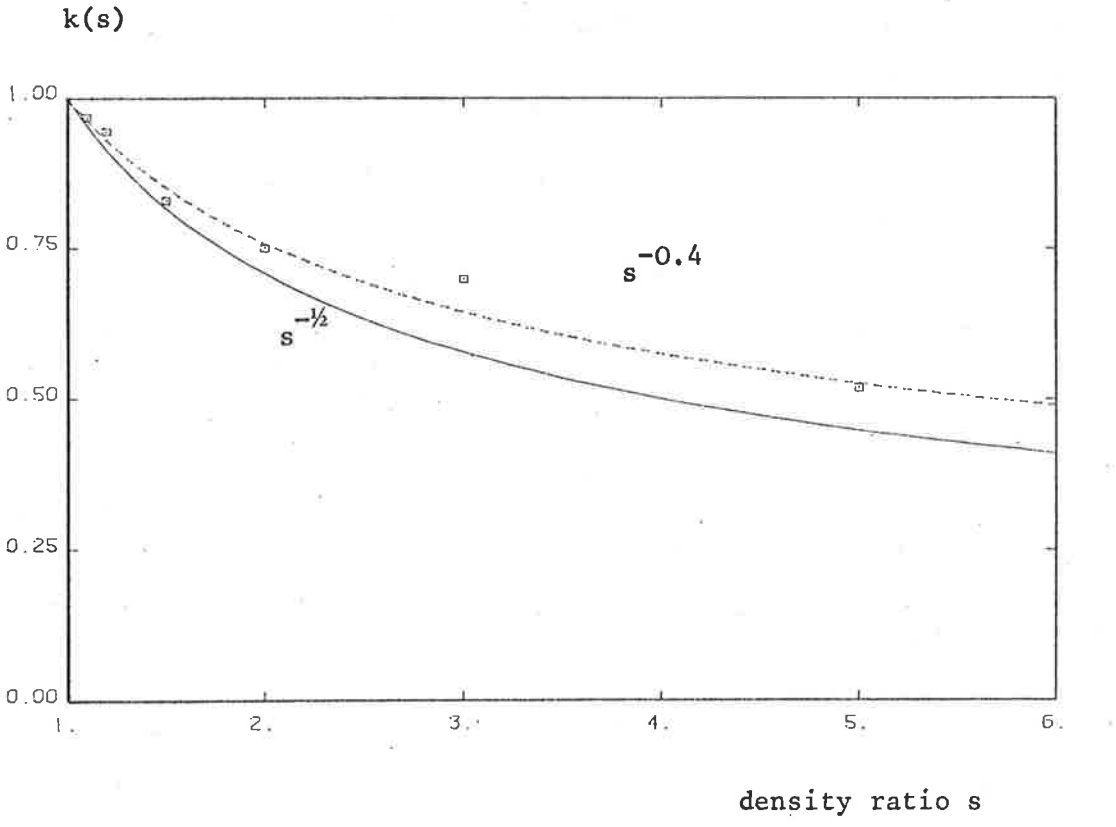

Figure 37: Estimated behaviour of entrainment ratio $k(s) = \lambda_2/\lambda_1$ as a function of density ratio.

where ρ_M denotes the average density value ($\rho_M = \frac{1}{2}(\rho_1+\rho_2)$). In terms of the vorticity ω, the above relation is rewritten

$$\frac{\Delta\omega}{\Delta t} = \frac{g}{\rho_M} \frac{\Delta\rho}{\Delta x} . \qquad [4.34]$$

For a layer of thickness δ and having a velocity jump ΔU, the quantities $\Delta\omega$, Δt and Δx are respectively estimated as $\Delta U/\delta$, $\delta/\Delta U$ and δ. One is then led to predict a marked gravitational influence when the ratio $g\delta\ \Delta\rho/\rho_M\ (\Delta U)^2$ is of the order of unity. Progressive disappearance of these effects are expected as the value of this ratio tends to zero. This criterion may be recast in terms of the Froude number of the problem

$$Fr = \frac{\Delta U}{\sqrt{gL}} \left(\frac{\rho_M}{2\,\Delta\rho}\right)^{1/2}$$

under the form

$$Fr^{-2} \left(\frac{\delta}{2L}\right) \begin{cases} \approx 1 & \text{(marked effect)} \\ \ll 1 & \text{(weak effect)} . \end{cases} \qquad [4.35]$$

Visualizations of flows characterized by different values of the Froude number are displayed in Figures 38 and 39. It is interesting to note that the response of the structure to gravity is in full agreement with prediction [4.35]. Figure shows in parallel the development of the structure in a flow where the density ratio is 3. The "aspect ratio" L/δ of the layer is of the order of 30. Gravity effects are practically inexistant for $Fr^{-2} \simeq 10^{-1}$ (left-hand side column) but are well marked for $Fr^{-2} \sim 1$: they provoke an important flattening of the structure. The structure disappears completely in the case $Fr^{-2} \sim 10$ (Figure 39), where one can observe the complete reversal of the flow behaviour.

It is understood that these preliminary results give a qualitative description of the phenomenon and must be accordingly given an indicative value only.

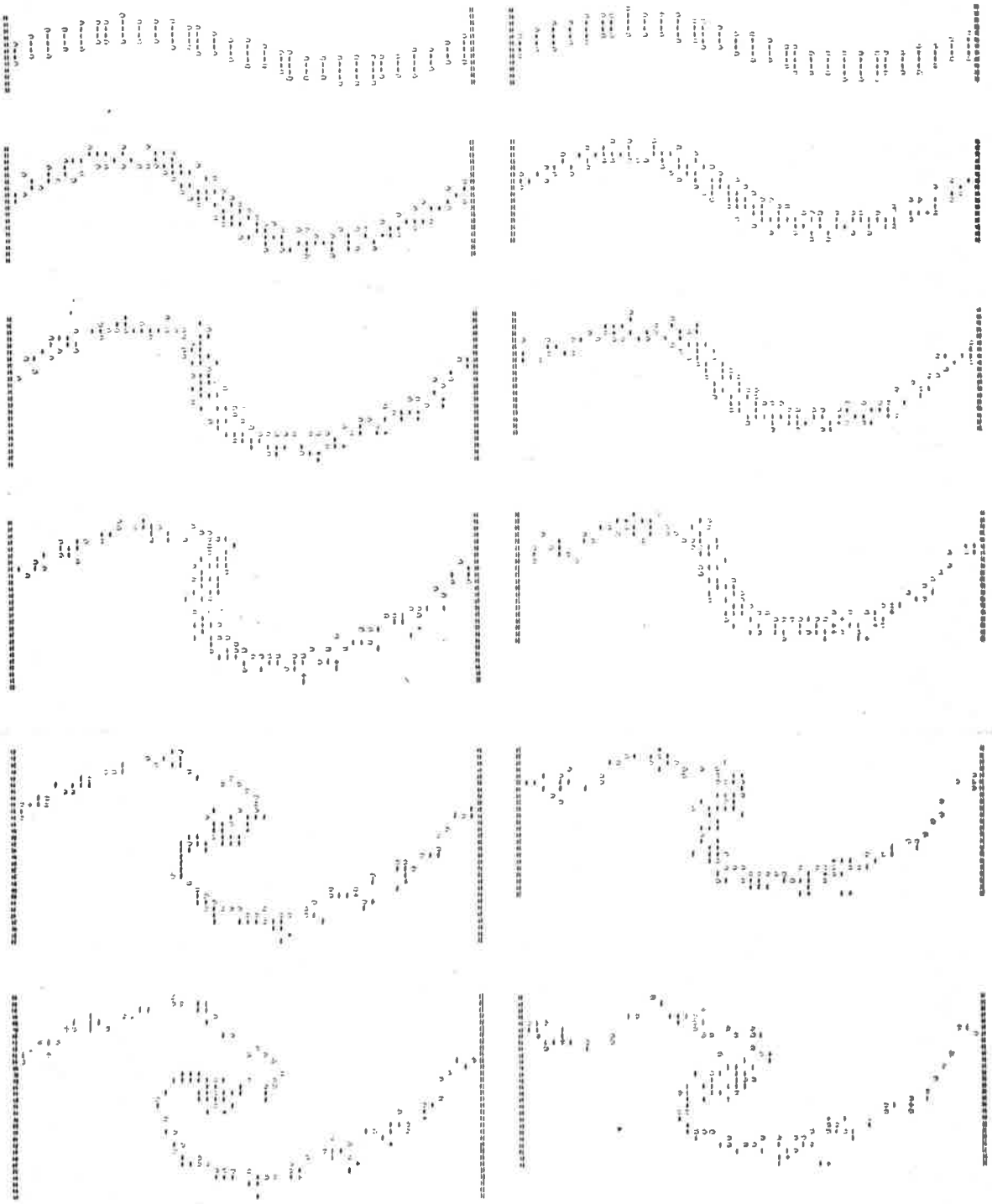

Figure 38a & b: Evolution of sinusoidal layer in presence of gravitational effects. Left-hand side patterns correspond to $Fr^{-2} \sim 10^{-1}$, right-hand side patterns to $Fr^{-2} \sim 1$.

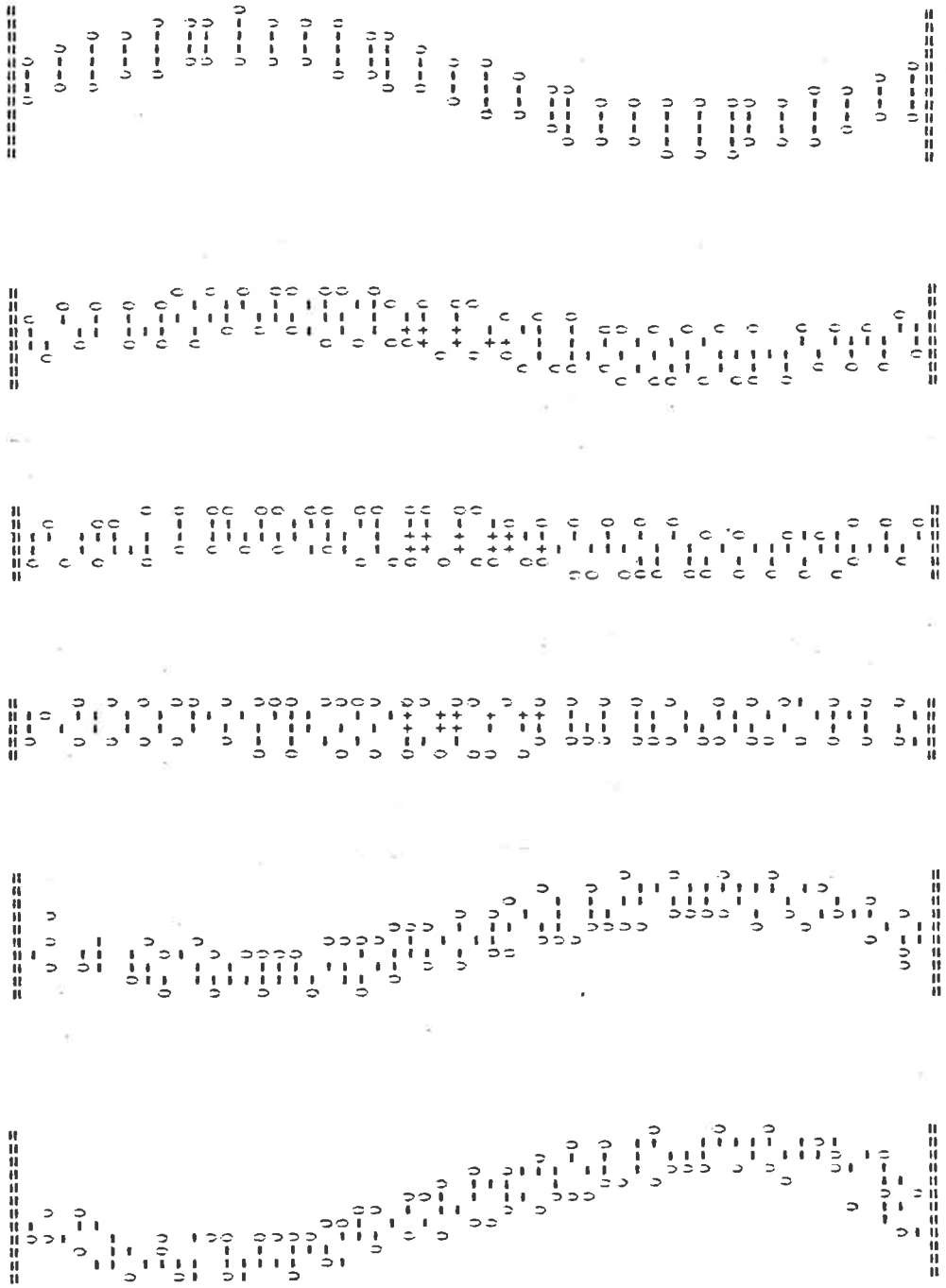

Figure 39: Evolution of sinusoidal layer under strong action of gravity ($Fr^{-2} \sim 10$).

IV.5 SUMMARY

The object of chapter IV is to discuss the extension of the point-vortex method to flows in which the material rate of change of the circulation is not identically zero.

The mechanisms which modify the distribution of circulation in non homogeneous fluids are examined for the general case of three-dimensional motions, and identified as resulting from the interaction between pressure and density gradients (Bjerknes theorem).

Two-dimensional flows of an inhomogeneous, incompressible fluid may be studied, in principle, by a generalized form of the point-vortex approximation. It is suggested that the success of the extended method depends critically on the use of a suitable discretization of Bjerknes theorem. Attention is focused on the specific problem of computing the change with time of the distribution of circulation at an interface between fluids with different densities. The need for a numerical procedure adapted to the discretization of the interface as a *thick* vortex sheet is demonstrated; a formula which appears to have the required properties is proposed. The novel approach relies essentially on the use of density "carriers" for representing the density field in a suitably defined neighbourhood of a point-vortex.

The generalized method is applied to study the effects of density ratio on the sinusoidal vorticity layer between two fluids of different molecular weights. This simple flow models the behaviour of non-uniform mixing layers provided the relationship between temporal and spatial problems is suitably formulated. Results indicate a strong distortion of the structure with fundamental modifications of the entrainment process. The model predicts a dependence of the entrainment ratio on the density

ratio that appears to agree with an analysis of Brown (1974). Qualitative results are presented which depict the effect of gravity (Froude number effect) on the structure.

REFERENCES

Abell, C.J. (1977)
Proceedings 6th Australasian Hydraulics and Fluid Mechanics Conference, Adelaide, p. 415.

Abernathy, F.H. & Kronauer, R.E. (1962)
The formation of vortex streets;
Journal of Fluid Mechanics 13, 1.

Acton, E. (1976)
The modelling of large eddies in a two-dimensional shear layer;
Journal of Fluid Mechanics 76, 3.

Acton, E. (1977)
A modelling of large eddies in an axisyimmetric jet; *Lecture Notes in Physics* 75, Structure and Mechanisms of Turbulence, Volume I, Springer Verlag.

Batchelor, G.K. (1967)
An introduction to fluid dynamics; Cambridge University Press.

Batt, R.G. (1975)
Some measurements on the effect of tripping the two-dimensional shear layer; *Aiaa Journal* 13.

Bernal, L.P., Breidenthal, R.E., Brown, G.L., Konrad, J.H. & Roshko, A. (1979)
On the development of three-dimensional small scales in turbulent mixing layers; *2nd Symp. on Turbulent Shear Flows*, London.

Birkhoff, G.D. & Fisher , J. (1959)
Do vortex sheets roll up ?; *Rc. Circ. mat. Palermo Ser.* 2, 8.

Birkhoff, G. (1962)
Helmholtz and Taylor instability;
Proc. Symp. in Applied Mathematics 13, Providence, R.I. : Ams.

Bradshaw, P. (1973)
Agardograph 169.

Browand, F.K. & Weidman, P.D. (1976)
Large scales in the developing mixing layer; *Journal of Fluid Mechanics*, 76, 1.

Browand, F.K. (1978)
Bulletin A.P.S. 23, p. 1007.

Brown, G.L. & Roshko, A. (1971)
The effect of density difference on the turbulent mixing layer; *Turbulent Shear Flows*, Agard - CP - 93.

Brown, G.L. & Roshko, A. (1979)
On density effects and large structure in turbulent mixing layers; *Journal of Fluid Mechanics* 64, 4.

Brown G.L. (1974)
The entrainment and large structure in turbulent mixing layers; *Fifth Australasian Conference on Hydraulics & Fluid Mechanics*, Christchurch, New Zealand.

Chandrasekhar, S. (1961)
Hydrodynamic and Hydromagnetic Stability; Oxford University Press.

Chandrsuda, C., Mehta, R.D., Weir, A.D. & Bradshaw, P. (1978)
Effect of free-stream turbulence on large structure in turbulent mixing layers; *Journal of Fluid Mechanics* 85, 4.

Chorin, A.J. & Bernard, P.S. (1972)
Discretization of a vortex sheet, with an example of roll up; Univ. Calif., *Berkeley Eng. Dept. Report* FM - 72 - 5.

Christiansen, J.P. (1973)
Numerical simulation of hydrodynamics by the method of point vortices; *Journal of Computational Physics* 13.

Clark, R.A., Verziger, J.H. & Reynolds, W.C. (1977)
Stanford University, Dept of Mech. Eng. Report JF - 9.

Clements, R.R. & Maull, D.J. (1975)
The representation of sheets of vorticity by discrete vortices; *Progress in Aerospace Sciences* 16, 2.

Delcourt, B.A.G. (1977)
Modelling plane turbulent flows with point vortices : a numerical experiment; *6th Australasian Hydraulics and Fluid Mechanics Conference*, Adelaide.

Delcourt, B.A.G. & Brown, G.L. (1979)
The evolution and emerging structure of a vortex sheet in an inviscid and viscous fluid modelled by a point-vortex method; *2nd Symp. on Turbulent Shear Flows*, London.

Dimotakis, P.E. & Brown, G.L. (1976)
The mixing layer at high Reynolds number : large-structure dynamics and entrainment; *Journal of Fluid Mechanics* 78, 3.

Fink, P.T. & Soh, W.K. (1974)
Calculation of vortex sheets in unsteady flow and applications in ship hydrodynamics; *Tenth Symposium Naval Hydrodynamics*, Cambridge, Mass.

Fink, P.T. & Soh, W.K. (1978)
A new approach to roll-up calculations of vortex sheets; *University of New South Wales Report* NAV/ARCH 78/1.

Friedrichs, K.O. (1966)
Special Topics in Fluid Dynamics; Gordon & Breach.

Hama, F.R. & Burke, E.R. (1960)
On the rolling-up of a vortex sheet; *Univ. Maryland Technical Note* BN-220.

Ho, C.M. & Nosseir, N.S. (1978)
The role of coherent structure in an impinging jet; *Bulletin of the American Physical Society*, II, 23.

Landau, L.D. & Lifshitz, E.M. (1971)
Mécanique des fluides; Editions Mir, Moscou.

Meng, J.C.S. & Thomson, J.A.L. (1978)
Numerical studies of some nonlinear hydrodynamic problems by discrete vortex element methods; *Journal of Fluid Mechanics* 84, 3.

Milinazzo, F. & Saffman, P.G. (1977)
The calculation of large Reynolds number two-dimensional flow using discrete vortices with random walk; *Journal of Computational Physics* 23.

Moore, C.J. (1977)
The discrete vortex approximation of a finite vortex sheet; *Journal of Fluid Mechanics* 63, 2.

Moore, D.W. & Saffman, P.G. (1975)
The density of organized vortices in a turbulent mixing layer; *Journal of Fluid Mechanics* 69, 3.

Kaden, H. (1931)
Aufwicklung einer unstabilen untstetigkeits fläche; *Ing. Arch.* 2.

Kadomtsev, B.B. & Kostomarov, D.P. (1972)
Turbulent layer in an ideal two-dimensional fluid; *The Physics of Fluids* 15, 1.

Kovasznay, L.S. (1977)
Coherent structures in turbulent shear flow; *Second Australasian Conference on Heat and Mass Transfer*, Sydney.

Kuwahara, K. & Takami, H. (1973)
Numerical studies of two-dimensional vortex motion by a system of point-vortices; *Journal of the Physical Society of Japan* 34, 1.

Oster, D., Wygnanski, I., Dziomba, B. & Fiedler, H. (1978)
Lecture Notes in Physics 75, p. 48, Structure and Mechanisms in Turbulence, Springler-Verlag.

Rosenhead, L. (1931)
Formation of vortices from a surface of discontinuity; *Proceedings Royal Society* A 134.

Roshko, A. (1976)
Structure of Turbulent Shear Flows : a new look; Dryden Lecture, *Aiaa 14th Aerospace Sciences Meeting*, Aiaa paper 76-78.

Saffman, P.G. (1977)
Lecture Notes in Physics 76, pp. 273-306, Springer-Verlag.

Takami, H. (1964)
Numerical experiment with discrete vortex approximation, with reference to the rolling-up of a vortex sheet; *Dept. Aero. and Astron. Stanford Univ. Report* Sudaer 202.

Truesdell, C. (1954)
The kinematics of vorticity; Indiana University Press.

Watson, G.N. (1922)
Theory of Bessel Functions; Cambridge University Press.

Westwater, F.L. (1935)
The rolling-up of a surface of discontinuity behind an aerofoil of finite span; *ARC R & M* 1962.

Winant, C.D. & Browand, F.K. (1974)
Vortex pairing : the mechanism of turbulent mixing-layer growth at moderate Reynolds number; *Journal of Fluid Mechanics* 63, 2.

Wygnanski, I. & Fiedler, H.E. (1970)
The two-dimensional mixing region; *Journal of Fluid Mechanics* 41.

Wygnanski, I., Oster, D., Fiedler, H. & Dziomba, B. (1978)
Tel Aviv Univ. Report SOE 488.

Zalosh, R.G. (1976)
Discretized Simulation of Vortex Sheet Evolution with Buoyancy and Surface tension Effects; *Aiaa Journal* II, II.

APPENDIX A:

INVARIANTS OF TWO-DIMENSIONAL CONTINUOUS VORTICITY DISTRIBUTIONS: AN ANALYSIS IN FOURIER SPACE

The purpose of this appendix is to present another aspect of the invariance properties of the differential equations that govern the motion of two-dimensional, inviscid vorticity distributions.

The analysis consists essentially in deriving evolution equations for the generalized moments

$$M(m,n) = \int_A x^m y^n \omega \, dA$$

$$H(m,n) = \int_A x^m y^n \omega\psi \, dA \, ,$$

and examining for which values of (m,n) the invariance property may be established. The method relies on the fact that the above quantities can be easily expressed in terms of the Fourier transforms of the vorticity field and of the stream function. The conditions of existence of the invariants may then be defined in all generality in terms of the existence of expressions involving Fourier transforms.

1. BASIC EQUATIONS

The two-dimensional vorticity field $\omega(x,y,t)$ in an inviscid fluid satisfies the system of equations

$$\frac{\partial \omega}{\partial t} + \frac{\partial \psi}{\partial x}\frac{\partial \omega}{\partial y} - \frac{\partial \psi}{\partial y}\frac{\partial \omega}{\partial x} = 0 \qquad [A.1]$$

$$\nabla^2 \psi = \omega \qquad [A.2]$$

where $\psi(x,y,t)$ is the stream function.

Defining the spatial Fourier transforms of ω and ψ as

$$W(\xi,\eta,t) = F[\omega] = \int_{-\infty}^{+\infty}\int_{-\infty}^{+\infty} \omega(x,y,t) e^{-2i\pi(x\xi+y\eta)} dxdy \qquad [A.3]$$

$$P(\xi,\eta,t) = F[\psi] = \int_{-\infty}^{+\infty}\int_{-\infty}^{+\infty} \psi(x,y,t) e^{-2i\pi(x\xi+y\eta)} dxdy, \qquad [A.4]$$

one obtains the inversion formulae as:

$$\omega(x,y,t) = F^{-1}[W] = \int_{-\infty}^{+\infty}\int_{-\infty}^{+\infty} W(\xi,\eta,t) e^{+2i\pi(x\xi+\eta y)} d\xi d\eta \qquad [A.5]$$

$$\psi(x,y,t) = F^{-1}[P] = \int_{-\infty}^{+\infty}\int_{-\infty}^{+\infty} P(\xi,\eta,t) e^{+2i\pi(x\xi+\eta y)} d\xi d\eta \; . \qquad [A.6]$$

Analysis of the problem in the wave number space can be pursued in terms of W and P - which will be assumed to exist, if necessary as generalized functions - by Fourier-transforming equations [A.1] and [A.2]. This leads to the equations

$$\frac{\partial W}{\partial t} = F\left[\frac{\partial \omega}{\partial x}\frac{\partial \psi}{\partial y}\right] - F\left[\frac{\partial \omega}{\partial y}\frac{\partial \psi}{\partial x}\right]$$

$$F[\nabla^2 \psi] = W.$$

Recalling the convolution theorem

$$F[fg] = F[f] * F[g] \quad ,$$

where $f * g$ denotes the two-dimensional convolution

$$h(x,y) = \int_{-\infty}^{+\infty}\int_{-\infty}^{+\infty} f(\alpha,\beta) g(x-\alpha, y-\beta) d\alpha d\beta \quad ,$$

one obtains

$$-\frac{1}{4\pi^2}\frac{\partial W}{\partial t} = (\eta P) * (\xi W) - (\xi P) * (\eta W), \qquad [A.7]$$

$$P = -\frac{1}{4\pi^2} W/(\xi^2+\eta^2) \ . \qquad [A.8]$$

The right-hand side of equation [A.7] is explicitly written as

$$\int_{-\infty}^{+\infty}\int_{-\infty}^{+\infty} d\alpha d\beta \ \beta(\xi-\alpha)P(\alpha,\beta)W(\xi-\alpha,\eta-\beta)$$

$$-\int_{-\infty}^{+\infty}\int_{-\infty}^{+\infty} d\alpha d\beta \ \alpha(\eta-\beta)P(\alpha,\beta)W(\xi-\alpha,\eta-\beta).$$

In the following, functions with shifted arguments will be denoted by the corresponding lower case letter, i.e.:

$$w = W(\xi-\alpha,\eta-\beta)$$

$$p = P(\xi-\alpha,\eta-\beta).$$

The previous expression, using this notation, is then rewritten

$$\int_{-\infty}^{+\infty}\int_{-\infty}^{+\infty} d\alpha d\beta \ \beta(\xi-\alpha)P_W - \int_{-\infty}^{+\infty}\int_{-\infty}^{+\infty} d\alpha d\beta \ \alpha(\eta-\beta)P_W \ .$$

Elimination of P between [A.7] and [A.8] leads finally to the evolution equation for W:

(*)

$$\frac{\partial W}{\partial t} = \int_{-\infty}^{+\infty} \frac{\beta\xi-\alpha\eta}{\alpha^2+\beta^2} \ W_W \ d\alpha d\beta \qquad [A.9]$$

which will be the basis of the invariance analysis for the quantities $M(m,n)$.

2. EVOLUTION EQUATION FOR M(m,n)

An evolution equation for $M(m,n)$ can be derived from [A.9] by observing that the high-order derivatives of the function $W(\xi,\eta)$,

---

(*) The double integration sign will be dropped for clarity.

evaluated at the origin $(\xi = 0, \eta = 0)$, are directly related to the moments $M(m,n)$.

From [A.3], one computes easily the quantity

$$W^{(m,n)} = \frac{\partial^{m+n} W(\xi,\eta)}{\partial\xi^m \partial\eta^n} .$$

One has successively

$$W^{(m,n)} = \int_{-\infty}^{+\infty} \omega\ (-2i\pi x)^m (-2i\pi y)^n\ e^{-2i\pi(x\xi+\eta y)} dxdy$$

$$= (-2i\pi)^{m+n} \int_{-\infty}^{+\infty} \omega\ (x,y) x^m y^n\ e^{-2i\pi(x\xi+\eta y)} dxdy$$

and evaluation of this expression at $\xi = \eta = 0$ yields immediately that

$$M(m,n) = W_0^{(m,n)} / (-2i\pi)^{m+n} \qquad [A.10]$$

where the notation

$$W_0^{(m,n)} = \frac{\partial^{m+n}}{\partial\xi^m \partial\eta^n} W(\xi,\eta)\Big|_{\xi=\eta=0}$$

has been employed.

Equation [A.9] may now be used to derive the rate of change with time of all quantities $W^{(m,n)}$, which will yield evolution equations for the quantities $M(m,n)$ when evaluated at $\xi = \eta = 0$. This is done as follows.

Equation [A.9] is rewritten

$$\frac{\partial W^{(0,0)}}{\partial t} = \dot{W}(0,0) = \int_{-\infty}^{+\infty} \frac{\beta\xi - \alpha\eta}{\alpha^2+\beta^2} wW\ d\alpha d\beta .$$

Now

$$\dot{W}^{(m,n)} = \frac{\partial^{m+n}\ \dot{W}(0,0)}{\partial\xi^m\ \partial\eta^n}$$

$$= \int_{-\infty}^{+\infty} \frac{W d\alpha d\beta}{\alpha^2+\beta^2} \frac{\partial^{m+n}\ (\beta\xi-\alpha\eta)w}{\partial\xi^m\ \partial\eta^n} . \qquad [A.11]$$

The derivative is evaluated as follows:

$$\frac{\partial^m}{\partial\xi^m}(\beta\xi-\alpha\eta)w = \frac{\partial^{m-1}}{\partial\xi^{m-1}}\left[\beta W + (\beta\xi-\alpha\eta)\frac{\partial w}{\partial\xi}\right]$$

$$= \frac{\partial^{m-2}}{\partial\xi^{m-2}}\left[2\beta\frac{\partial w}{\partial\xi} + (\beta\xi-\alpha\eta)\frac{\partial^2 w}{\partial\xi^2}\right]$$

$$= m\beta\frac{\partial^{m-1}w}{\partial\xi^{m-1}} + (\beta\xi-\alpha\eta)\frac{\partial^m w}{\partial\xi^m} \quad .$$

Now

$$\frac{\partial^{m+1}}{\partial\xi^m\partial\eta}(\beta\xi-\alpha\eta)w = m\beta\frac{\partial^m w}{\partial\xi^{m-1}\partial\eta} \quad \ldots$$

$$\ldots - \alpha\frac{\partial^m w}{\partial\xi^m} + (\beta\xi-\alpha\eta)\frac{\partial^{m+1}w}{\partial\xi^m\partial\eta}$$

and generally

$$\frac{\partial^{m+n}}{\partial\xi^m\partial\eta^n}(\beta\xi-\alpha\eta)w = m\beta\, w^{(m-1,n)} - n\alpha\, w^{(m,n-1)}$$

$$+ (\beta\xi-\alpha\eta)w^{(m,n)} \quad , \qquad [A.12]$$

if by definition

$$\frac{\partial^{m+n}w}{\partial\xi^m\partial\eta^n} = \frac{\partial^{m+n}W(\xi-\alpha,\eta-\beta)}{\partial\xi^m\,\partial\eta^n} = w^{(m,n)} \quad . \qquad [A.13]$$

Substitution of [A.12] into [A.11] yields the equation

$$\dot{W}^{(m,n)} = \int_{-\infty}^{+\infty}\frac{W\,d\alpha d\beta}{\alpha^2+\beta^2}\left\{m\beta\, w^{(m-1,n)} - n\alpha\, w^{(m,n-1)}\right.$$

$$\left. + (\beta\xi-\alpha\eta)w^{(m,n)}\right\} \quad . \qquad [A.14]$$

Evaluation of this expression at $\xi = \eta = 0$ yields the evolution equation for the moments $M(m,n)$:

$$(-2i\pi)^{m+n} \frac{\partial M(m,n)}{\partial t} = \int_{-\infty}^{+\infty} \frac{W \, d\alpha d\beta}{\alpha^2+\beta^2} \left\{ m\beta \, w_0^{(m-1,n)} - n\alpha \, w_0^{(m,n-1)} \right\} \qquad [A.15]$$

which is the expression required for the invariance analysis. Note that the notation

$$w_0^{(m,n)} (\alpha,\beta) = w^{(m,n)} (\xi = \eta = 0) \qquad [A.16]$$

$$= \frac{\partial^{m+n} W(\xi-\alpha,\eta-\beta)}{\partial\xi^m \, \partial\eta^n}\bigg|_{\xi=\eta=0}$$

which is consistent with that used in [A.10], has been introduced.

3. INVARIANCE PROPERTIES OF M(m,n)

Ley us now examine the right-hand side of equation [A.15] and establish the conditions for which it vanishes. In this connection, the following "symmetry" property is especially useful.

Let us show that in all cases,

$$W^{(m,n)} (\alpha,\beta) = w_0^{(m,n)} (-\alpha,-\beta) \quad . \qquad [A.17]$$

Clearly:

$$\frac{\partial^{m+n} W(\xi-\alpha,\eta-\beta)}{\partial\xi^m \, \partial\eta^n} = (-)^{m+n} \frac{\partial^{m+n} W(\xi-\alpha,\eta-\beta)}{\partial\alpha^m \, \partial\beta^n} \quad .$$

Therefore,

$$w_0^{(m,n)} (\alpha,\beta) = (-)^{m+n} \frac{\partial^{m+n} W(\xi-\alpha,\eta-\beta)}{\partial\alpha^m \, \partial\beta^n}\bigg|_{\xi=\eta=0} \quad .$$

Now by definition

$$W^{(m,n)}\ (\alpha,\beta) = \frac{\partial^{m+n} W(\alpha,\beta)}{\partial\alpha^m\ \partial\beta^n}$$

and hence

$$W^{(m,n)}\ (-\alpha,-\beta) = w_0^{(m,n)}\ (\alpha,\beta) \qquad [A.18]$$

which is equivalent to [A.17] .

The invariance of the lower order moments may now be proved as follows.

(a) $m = n = 0$.

Inspection of [A.15] shows that $\dot{M}(0,0)$ vanishes, so that

$$M(0,0) = \int_{-\infty}^{+\infty} \omega\ dxdy \qquad [A.19]$$

is invariant.

(b) $m = 1 \quad n = 0$

One obtains from [A.15]

$$(-2i\pi)\ \frac{\partial}{\partial t}\ M(1,0) = \int_{-\infty}^{+\infty} \frac{W\ d\alpha d\beta}{\alpha^2+\beta^2}\quad w_0^{(0,0)}\ .$$

Now from [A.16] one knows that

$$w_0^{(0,0)}\ (\alpha,\beta) = W^{(0,0)}\ (-\alpha,-\beta)$$

so that

$$(-2i\pi)\ \frac{M(1,0)}{\partial t} = \int_{-\infty}^{+\infty} \frac{\beta\ d\alpha d\beta}{\alpha^2+\beta^2}\ W(\alpha,\beta)W(-\alpha,-\beta)\ .$$

The integrand is an odd function in (α,β) and hence its integral vanishes identically. Therefore

$$M(1,0) = \int_{-\infty}^{+\infty} x\ \omega\ dxdy \qquad [A.20]$$

is invariant.

(c) $m = 0 \quad n = 1$

Repeating the argument developed for the case $(m = 1, n = 0)$ establishes the invariance of the moment

$$M(0,1) = \int_{-\infty}^{+\infty} y\, \omega\, dxdy. \qquad [A.21]$$

(d) $(m = 2, n = 0) + (m = 0, n = 2)$

The evolution equation for the combination $I = M(2,0) + M(0,2)$ is obtained from [A.15] as

$$\frac{(-2i\pi)^2}{2} \frac{d}{dt} [M(2,0) + M(0,2)]$$

$$= \int_{-\infty}^{+\infty} \frac{W\, d\alpha d\beta}{\alpha^2+\beta^2} [\beta\, w_0^{(1,0)} - \alpha\, w_0^{(0,1)}]$$

where, by definition

$$w_0^{(1,0)} = W^{(1,0)}\ (-\alpha,-\beta) = \frac{\partial W(-\alpha,-\beta)}{\partial \alpha}$$

$$w_0^{(0,1)} = W^{(0,1)}\ (-\alpha,-\beta) = \frac{\partial W(-\alpha,-\beta)}{\partial \beta} \qquad [A.22]$$

The invariance of I is proven if one establishes the identity

$$M_1 = M_2$$

where

$$M_1 = \int_{-\infty}^{+\infty} W\, d\alpha d\beta \frac{\partial}{\partial \beta} [\log\ (\alpha^2+\beta^2)] \frac{\partial W(-\alpha,-\beta)}{\partial \alpha}$$

and

$$M_2 = \int_{-\infty}^{+\infty} W\, d\alpha d\beta \frac{\partial}{\partial \alpha} [\log\ (\alpha^2+\beta^2)] \frac{\partial W(-\alpha,-\beta)}{\partial \beta}$$

where use has been made of the fact that

$$\frac{\beta}{\alpha^2+\beta^2} = \frac{1}{2}\frac{\partial}{\partial\beta}\log(\alpha^2+\beta^2)$$

$$\frac{\alpha}{\alpha^2+\beta^2} = \frac{1}{2}\frac{\partial}{\partial\alpha}\log(\alpha^2+\beta^2).$$

The expressions for Ml may be transformed as follows by carrying out the integration ω r. to β

$$Ml = \int_{-\infty}^{+\infty} d\alpha \int_{-\infty}^{+\infty} d\beta \frac{\partial}{\partial\beta}\log(\alpha^2+\beta^2)\, W \frac{\partial \bar{W}}{\partial\alpha}$$

$$= \int_{-\infty}^{+\infty} d\alpha \left\{\left[\log(\alpha^2+\beta^2)\, W \frac{\partial \bar{W}}{\partial\alpha}\right]_{\beta_0}^{\beta_1} - \int_{-\infty}^{+\infty} d\beta \log(\alpha^2+\beta^2) \frac{\partial}{\partial\beta}\left[W \frac{\partial \bar{W}}{\partial\alpha}\right]\right\}$$

$$Ml = [Ml] - \int_{-\infty}^{+\infty}\int_{-\infty}^{+\infty} d\alpha d\beta \log(\alpha^2+\beta^2)\left[\frac{\partial W}{\partial\beta}\frac{\partial \bar{W}}{\partial\alpha} + W\frac{\partial^2 \bar{W}}{\partial\alpha\partial\beta}\right]$$

where [Ml] represents the integrated term.

Identical manipulations on M_2 yield the expression

$$M_2 = \int_{-\infty}^{+\infty} d\beta\left\{\left[\log(\alpha^2+\beta^2)\, W \frac{\partial \bar{W}}{\partial\beta}\right]_{\alpha_0}^{\alpha_1} - \int_{-\infty}^{+\infty} d\alpha \log(\alpha^2+\beta^2) \frac{\partial}{\partial\alpha}\left[w \frac{\partial \bar{W}}{\partial\beta}\right]\right\}$$

$$= [M2] - \int_{-\infty}^{+\infty}\int_{-\infty}^{+\infty} d\alpha d\beta \log(\alpha^2+\beta^2)\left[\frac{\partial W}{\partial\alpha}\frac{\partial \bar{W}}{\partial\beta} + W\frac{\partial^2 \bar{W}}{\partial\alpha\partial\beta}\right].$$

Both integrated terms vanish provided the vorticity distribution vanishes sufficiently rapidly toward infinity. It is readily seen - with the change of

variables $\alpha \to -\alpha$; $\beta \to -\beta$ - that the identity M1 = M2 is verified in this case, which establishes the invariance of the expression

$$I = \int_{-\infty}^{+\infty} (x^2+y^2)\ \omega\ dxdy \qquad [A.22]$$

4. EVOLUTION EQUATION FOR H(m,n)

Define the function $\phi(x,y)$ as the product

$$\phi(x,y) = \psi(x,y)\ \omega(x,y) \qquad [A.23]$$

and its Fourier transform $F(\xi,\eta)$ by

$$F(\xi,\eta) = \int_{-\infty}^{+\infty}\int_{-\infty}^{+\infty} \phi(x,y)\ e^{-i2\pi(x\xi+y\eta)}dxdy \qquad [A.24]$$

with the corresponding inversion formula

$$\phi(x,y) = \int_{-\infty}^{+\infty}\int_{-\infty}^{+\infty} F(\xi,\eta)\ e^{2i\pi(x\xi+y\eta)}d\xi d\eta \quad . \qquad [A.25]$$

It is easily shown that one has

$$\left.\frac{\partial^{m+n} F(\xi,\eta)}{\partial\xi^m\ \partial\eta^n}\right|_{(0,0)} = (-2i\pi)^{m+n} \int_{-\infty}^{+\infty} x^m y^n\ \phi(x,y)dxdy \qquad [A.26]$$

so that

$$H(m,n) = F_0^{(m,n)} \int_{-\infty}^{+\infty} (-2i\pi)^{m+n} \quad . \qquad [A.27]$$

The invariance of the moments H(m,n) may be investigated by considering the evolution equation for the quantities $F_0^{(m,n)}$.

The equation giving $\frac{\partial F}{\partial t}$ is easily obtained from [A.7] and [A.8] by noting that $F = W * P$. Clearly then

$$\frac{\partial F}{\partial t} = -4\pi^2 \, P * \{(\xi W) * (\eta P) - (\eta W) * (\xi P)$$

$$= 16\pi^4 \, P * [(\xi^3+\xi\eta^2)P * \eta P - (\eta^3+\eta\xi^2)P * (\xi P)]$$

after repeated use of [A.8] .

The foregoing expression may be rewritten as

$$\frac{\partial F}{\partial t} = 16\pi^4 \, T(\xi,\eta) \qquad [A.28]$$

where $T(\xi,\eta)$ is given by

$$T(\xi,\eta) = \int_{-\infty}^{+\infty} \int_{-\infty}^{+\infty} (\alpha^2+\beta^2)P(\alpha,\beta) \, d\alpha d\beta \quad \ldots$$

$$\ldots \int_{-\infty}^{+\infty} \int_{-\infty}^{+\infty} dudv \, (\alpha u-\beta v)P(u-\alpha,v-\beta)P(\xi-u,\eta-v) \; . \qquad [A.29]$$

In particular,

$$\frac{\partial F_0^{(0,0)}}{\partial t} = 16\pi^4 \, T(0,0)$$

$$= 0$$

in view of expression [A.29]. This completes the proof that the quantity

$$H(0,0) = H = \int_{-\infty}^{+\infty} \int_{-\infty}^{+\infty} \psi \, \omega \, dxdy \qquad [A.30]$$

is an invariant of the vorticity distribution.

Intuitively, one suspects that the treatment of vortices in Fourier transform space should lead to economics in computer time requirements, but this approach has not been pursued further at the present time.

APPENDIX B:

STREAM FUNCTION AND INVARIANTS FOR THE DISK OF UNIFORM VORTICITY

The integral,

$$\psi(P) = -\frac{1}{4\pi} \int_{\mathcal{D}} \omega(Q) \log R_{PQ}^2 \, d\mathcal{D}(Q) \qquad [B.1]$$

defining the stream function associated with a distribution of vorticity $\omega(Q)$ over a bounded domain $\mathcal{D}$ can be explicitly evaluated for the particular case of the disk of uniform vorticity, for which one has

$$\omega(Q) = \text{constant} = \omega_0$$
$$\mathcal{D} \equiv \{(x,y) : x^2 + y^2 \leqslant a^2\} .$$

The positions of P (fixed) and Q (element of domain $\mathcal{D}$) are expressed in terms of polar coordinates (ρ,ϕ) and (r,θ) (refer to Figure B.1). One has

$$(x(P),y(P)) = (\rho \cos \phi, \rho \sin \phi)$$
$$(x(Q),y(Q)) = (r \cos \theta, r \sin \theta)$$
$$R_{PQ}^2 = r^2 - 2r\rho \cos(\theta - \phi) + \rho^2$$
$$d\mathcal{D}(Q) = r \, dr \, d\theta ,$$

and expression [B.1] is rewritten

$$\psi(P) = -\frac{\omega_0}{4\pi} \int_0^a r dr \int_0^{2\pi} d\theta \log [r^2 - 2r\rho \cos(\theta - \phi) + \rho^2] . \qquad [B.2]$$

It is easily shown that

$$\int_0^{2\pi} d\theta \log [r^2 - 2r\rho \cos(\theta - \phi) + \rho^2] =$$
$$2 \int_0^{\pi} d\theta \log [r^2 - 2r\rho \cos\theta + \rho^2] ,$$

so that [B.2] is rewritten

$$\psi(P) = -\frac{\omega_0}{2\pi}\int_0^a r\,dr \int_0^\pi d\theta \log\,[\,r^2 - 2r\rho\cos\theta + \rho^2\,]\,. \qquad [B.3]$$

This expression may now be evaluated on the basis of the formula

$$\int_0^\pi \log\,(A^2 - 2AB\cos\alpha + B^2)\,d\alpha = \begin{cases} 2\pi \log A & (A > B) \\ 2\pi \log B & (B > A) \end{cases} \qquad [B.4]$$

$(A,B > 0)$, taken from standard integral tables.

The integration with respect to θ in [B.3] must be carried out differently if $r \geqslant \rho$ or if $r < \rho$. This leads to distinct forms for the stream function depending on whether P lies inside or outside the disk. One finds easily the two forms:

$$\begin{aligned} \psi(P) &= -\frac{\omega_0 a^2}{2}\log\rho \quad (\rho \geqslant a) \qquad (P \text{ exterior}) \\ \psi(P) &= -\frac{\omega_0}{4}(\rho^2 - a^2) - \frac{\omega_0 a^2}{2}\log a \quad (\rho \leqslant a) \qquad (P \text{ interior}) \end{aligned} \qquad [B.5]$$

The invariants of the vorticity distribution are easily evaluated from their definition integrals [1.16], [1.20], [1.22] and [1.25]. Their values are:

(a) Total circulation Γ

$$\Gamma = \omega_0 \int_0^a 2\pi r\,dr = \pi\,\omega_0\,a^2 \qquad [B.6]$$

(b) Coordinates of vorticity centre (X,Y)

$$X = Y = 0 \qquad [B.7]$$

(c) Moment of inertia $G\ (= I^2)$

$$\Gamma G = \omega_0 \int_0^a \int_0^{2\pi} r^3\,dr\,d\theta$$

i.e. $$G = a^2/2 \quad \text{or} \quad I = a/\sqrt{2}\,. \qquad [B.8]$$

(d) Hamiltonian (Kirchhoff function)

$$H = -\frac{\omega_0^2}{8\pi} \int_0^a r\,dr \int_0^a \rho\,d\rho \int_0^{2\pi} d\theta \int_0^{2\pi} d\phi\ \log\ [\,r^2 + \rho^2 - 2r\rho\cos(\theta - \phi)\,]$$

Using formula [B.4] and proceeding in a manner similar to that used when evaluating $\psi(P)$ lead to the expression

$$H = \frac{\omega_0^2 a^4 \pi}{16}\ (1 - 4\log a)\ . \qquad [\,B.9]$$

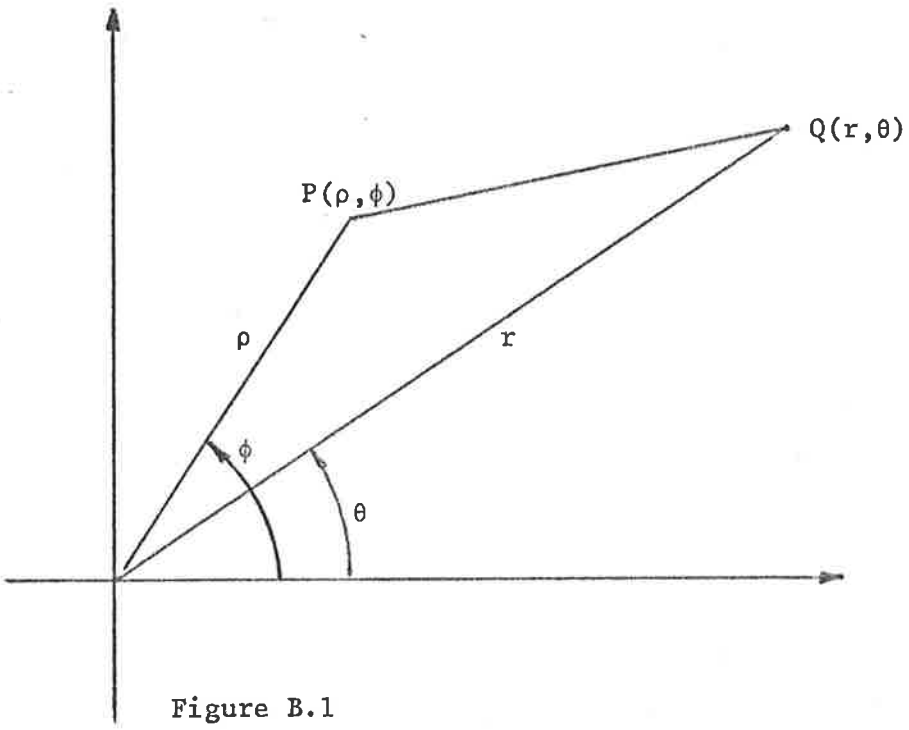

Figure B.1

APPENDIX C:

NUMERICAL EVALUATION OF $\Omega_\nu\ (\rho,\xi)$ AND OF 4 ASSOCIATED INTEGRALS

The solution for the problem of the viscous diffusion of the vorticity disk has been found to be

$$\Omega_\nu\ (\rho,\xi) = \frac{e^{-\rho^2/4\xi}}{2\xi} \int_0^1 e^{-\lambda^2/4\xi}\ \lambda\ I_o\ (\frac{\rho\lambda}{2\xi})\ d\lambda \qquad [C.1]$$

(Refer to [2.47]). Using the change of variables $u = \rho\lambda/2\xi$, one obtains the alternative form

$$\Omega_\nu\ (\rho,\xi) = \frac{2\xi}{\rho^2}\ e^{-\rho^2/4\xi} \int_0^{\rho/2\xi} e^{-\xi u^2/\rho^2}\ u\ I_o(u)\ du\ . \qquad [C.2]$$

Difficulties arise in the numerical evaluation of the function $I_o(u)$ for large values of its argument, due to a rapid increase in magnitude; overflow conditions are expected to arise for large values of $\rho/2\xi$.

A manner of avoiding computational problems is to base the calculation on the available polynomial approximations for the functions

$$I_o\ (x) \qquad (0 < x \leqslant 3.75)$$

and $G_o\ (x) = e^{-x}\ \sqrt{x}\ I_o\ (x)$ $(3.75 < x < \infty)$.

(see Abramovitch & Stegun, 1964, 9.8.1 & 9.8.2). This requires the modification of the above expression for Ω_ν as follows. Writing $A = 3.75$ and $F = \frac{2\xi}{\rho^2}$, one decomposes the integral in [C.2] in two parts, writing:

$$\Omega_\nu(\rho,\xi) = F(\Omega_1 + \Omega_2) \quad , \quad \text{with}$$

$$\Omega_1 = e^{-\rho^2/4\xi} \int_0^A e^{-\xi u^2/\rho^2} \; u\, I_o(u)\, du \qquad [C.3]$$

and $$\Omega_2 = \int_A^{\rho/2\xi} e^{-\xi u^2/\rho^2 - \rho^2/4\xi} \; u\, I_o(u)\, du \quad ,$$

i.e. $$\Omega_2 = \int_A^{\rho/2\xi} e^{u(1-\xi u/\rho^2) - \rho^2/4\xi} \; \sqrt{u}\, G_o(u)\, du \; . \qquad [C.4]$$

Ω_ν is then evaluated as $\Omega_\nu = F\Omega_1$ for $\frac{\rho}{2\xi} \leqslant A$ and as the sum $\Omega_\nu = F(\Omega_1 + \Omega_2)$ for $\frac{\rho}{2\xi} > A$. Both integrals are evaluated using the Gauss method, for which one has the approximation

$$\int_{-1}^{+1} f(u)\, du \simeq \sum_{\alpha=1}^{NG} f(x_\alpha) \cdot w(x_\alpha) \quad , \qquad [C.5]$$

for any function f. The weighting functions $w(x_\alpha)$ and the Gauss nodes x_α ($\alpha = 1,2,\ldots NG$) are available as tabulated values in various textbooks on numerical analysis (see for instance Abramovitch & Stegun, 1964, Table 25.4).

In all computations, 50 nodes were used; the convergence of the method was checked by varying the number of nodes; stabilization of the values was generally observed for as low a value as NG = 20.

The changes of variables required to scale the integration bounds down to the range [-1,+1] are readily found; one used:

(a) for Ω_1 : $v = \frac{2u}{A} - 1$, giving

$$\Omega_1 = \frac{A^2}{4} \int_{-1}^{+1} (v+1)\, e^{-\xi \left[\frac{A(v+1)}{2\rho}\right]^2} \; I_o\left[\frac{A(v+1)}{2}\right] \; dv \; ; \qquad [C.6]$$

(b) for Ω_2 : $v = \frac{u-N}{M}$ $(M = \frac{\rho}{4\xi} - \frac{A}{2}$; $N = \frac{\rho}{4\xi} + \frac{A}{2})$, giving

$$\Omega_2 = M \int_{-1}^{+1} e^{(Mv+N)} \left[1 - \frac{\xi (Mv+N)}{\rho^2} \right] G_o\ (Mv+N)\ \sqrt{Mv+N}\ dv. \qquad [C.7]$$

For $\rho=0$, Ω_ν may be computed from the simpler expression

$$\Omega_\nu = 1 - e^{-1/4\xi} \qquad [C.8]$$

(see [2.48]).

Having computed $\Omega_\nu\ (\rho,\xi)$, the evaluation of the related integral quantities

$$\Gamma = 2\pi \int_0^\infty r\ \omega(r,t)\ dr\ , \qquad [C.9]$$

$$H_\nu = -\frac{\Gamma}{2} \int_0^\infty r\ \omega(r,t)\ \log r\ dr + \pi \int_0^\infty u\ \omega(u,t) \int_u^\infty r\ \omega(r,t)\ \log \left(\frac{u}{r}\right) dr\ du\ , \qquad [C.10]$$

$$\chi = 2\pi \int_0^\infty r\ \omega^2(r,t)\ dr \quad \text{and} \qquad [C.11]$$

$$G_\nu = \frac{2\pi}{\Gamma} \int_0^\infty r^3\ \omega(r,t)\ dr \qquad [C.12]$$

may then be carried out using the same Gauss method. Here, the changes of variables required to map the infinite ranges of integration onto the $(-1,+1)$ interval are simply $r = tg\ u$ and $v = 4u/\pi - 1$.

APPENDIX D:

EVOLUTION IN TIME OF THE MOMENT OF INERTIA OF THE VORTICITY DISK IN A VISCOUS FLUID

By definition, the moment of inertia G_ν of a vorticity distribution is given by the expression

$$\Gamma G_\nu = \int_A \omega_\nu r^2 \, dA \, , \qquad [D.1]$$

where Γ is the total circulation. For the case of the uniform disk, one has

$$G_\nu = \frac{2}{a^2\omega_0} \int_0^\infty r^3 \, \omega_\nu(r) \, dr = 2 \, J/a^2\omega_0 \, ,$$

$$\text{where} \quad J = \int_0^\infty r^3 \, \omega_\nu(r) \, dr \qquad [D.2]$$

Let us evaluate $\frac{dG_\nu}{dt}$ by computing $\frac{dJ}{dt}$ from the differential equation

$$\frac{\partial \omega_\nu}{\partial t} = \frac{\nu}{r} \frac{\partial}{\partial r} \left(r \frac{\partial \omega_\nu}{\partial r} \right). \qquad [D.3]$$

Multiplying equation [D.3] by r^3 and integrating over the whole space with respect to r yields

$$\frac{dJ}{dt} = \nu \int_0^\infty r^2 \frac{\partial}{\partial r} \left(r \frac{\partial \omega_\nu}{\partial r} \right) dr. \qquad [D.4]$$

Successive integrations by parts may be carried out; one obtains:

$$\frac{dJ}{dt} = \nu \left[r^3 \frac{\partial \omega_\nu}{\partial r} \right]_0^\infty - 2\nu \int_0^\infty r^2 \frac{\partial \omega_\nu}{\partial r} \, dr$$

and

$$\frac{dJ}{dt} = \nu \left[r^3 \frac{\partial \omega_\nu}{\partial r} \right]_0^\infty - 2\nu \left[r^2 \omega_\nu \right]_0^\infty + 4\nu \int_0^\infty r \, \omega_\nu \, dr \, .$$

For $\omega_\nu(r)$ behaving at least like r^{-2} at infinity, this yields

$$\frac{dJ}{dt} = 4\nu \frac{\Gamma}{2\pi} = \text{constant} , \qquad [D.5]$$

since by definition $\Gamma = \int_A \omega_\nu \, dA = 2\pi \int_0^\infty r\omega_\nu dr.$

The time evolution of $G_\nu(t)$ is then given by

$$G_\nu(t) = G_\nu(o) + t\left(\frac{dG_\nu}{dt}\right)_0 \qquad [D.6]$$

so that $$G_\nu(t) = G_\nu(o) + t \frac{2}{a^2\omega_0} \frac{4\nu\,\Gamma}{2\pi}$$

i.e. $$G_\nu(t) = G_\nu(o) + 4\nu t , \qquad [D.7]$$

which is an exact relationship. In terms of the variable $\xi = \nu t/a^2$, it is rewritten

$$\frac{G_\nu(\xi)}{G_\nu(o)} = 1 + 8\,\xi \qquad [D.8]$$

since $G_\nu(o) = a^2/2.$